Machinability Studies of Machinable Glass-Ceramic Materials: Macor and Boron Nitride

By: Mohamed. A.Y. Dabnun (B.Sc.Eng)

A Thesis Submitted in Fulfilment of the Requirements for the Degree of Master of Engineering (M.Eng)

School of Mechanical and Manufacturing Engineering
Dublin City University

Name of Supervisors: Prof. Saleem Hashmi
Prof. M.A.El-Baradie

DECLARATION

I hereby certify that this material, which I now submit for assessment on the programme of study leading to the award of Master of Engineering is entirely my own work and has not been taken from the work of others save and to the extent that such work has been cited and acknowledged within the text of my work.

Signed: Yassin ID No: 52143848

Date: 22/09/04

ACKNOWLEDGEMENTS

I am extremely thankful to my thesis advisor, Professors, M.A. El-Baradie and M.S.J. Hashmi. Without their continuous help and advice this work would not have been possible.

I also would like to take this opportunity to extend my thanks to the academic staff of the school and the workshop technical staff Mr. Liam Domican and Mr. James Barry.

I am indebted to my mother, young brother Mr. Abdlkaader Dabnun, my sisters, and whole Dabnun family, who have given me the chance of discovering what I like, and of devoting myself to it.

Last but not least I would like to take this opportunity to extend my thanks to each one of my friends, here in the Ireland and back home, for their truthful and sincere concerns about my study and myself. If I forget some body please forgive me, I thank you as well.

ABSTRACT

Machinability assessment of two ceramic materials was carried out using uncoated carbide tool inserts under dry conditions. The materials investigated were Macor and Boron nitride and the machining operation was a continuous operation (turning). The objectives of this investigation were to generate reliable machining data in terms of surface finish, tool life and cutting force in relation to cutting speed, feed rate and depth of cut. The cutting tests were carried out using one-variable-at-a-time and design of experiments.

For one variable at-a-time experiment, surface finish, cutting forces and tool life were measured. In these tests the cutting variables i.e, cutting speed, feed rate, depth of cut and nose radius were varied to study their effects on the surface finish, tool life and cutting forces. With the design of experiments, the combined effects of the cutting variables were investigated on the machining responses.

The experimental data on the design of experiments were analysed by the response surface methodology.

Using the mathematical models for different responses, a computerized machinability data base system was developed to facilitate the optimum selection of cutting parameters.

TABLE OF CONTENTS

NOMENCLATURE

MGC	Machinable glass-ceramic
BN	Boron nitride
V	Cutting speed (m/min)
d	Depth of cut (mm)
DOC	Depth of cut (mm)
f	Feed rate (mm/rev)
f.p.m	Feed per minute
Fx	Axial (feed) force
Fy	Radial force
Fz	Tangential force
F	Resultant cutting force
Ra	Observed arithmetic average surface roughness (μm)
Rt	Maximum roughness
Rp	Smoothening depth
Rz,Rq	Roughness parameter
RMS	Root-mean-square
T	Tool life
KT	Crater depth (mm)
VB_B	Average width of flank wear (mm)
VB_N	Width of notch wear (mm)
e.m.f	Electromotive force
VB	Covariance matrix of (μ_B)
μ_B	Parameter vector known from prior information
ε	Experimental error
BHN	Brinell hardness number
HV	Vickers hardness
DAQ	Data acquisition system
PCMCIA	Personal computer memory card international association
ISA	Standard for I/0 buses
EISA	Extended ISA
PCI	Local bus system designed for higher-end computer system

T	Charge amplifier sensitivity
n	Number of observations
x	Matrix of independent machining variables
x_1	Coded variable (speed)
x_2	Coded variable (feed)
x_3	Coded variable (depth of cut)
X^T	Transpose of X
$(X^TX)^{-1}$	Inverse of the matrix (X^TX)
y	Observed logarithmic response (surface roughness, tool life, forces)
$\hat{y}$	Predicted response in logarithmic scale
$(y-\hat{y})$	Residuals
b	Matrix of the parameter estimates
Q	Metal removal rate (cm^3/min)
DF	Degrees of freedom
MS	Mean square
RSM	Response surface methodology
BUE	built up edge
ISO	International Standards Organisation

1 INTRODUCTION

Modern science and technology constantly require new materials with special properties to achieve breathtaking innovations. This development centres on the improvement of scientific and technological fabrication and working procedures. That means rendering them faster, economically more favourable, and better quality.
Ceramics make up one of three large classes of solid materials. The other main material classes are metals and polymers. The combination of two or more of these materials together to produce a new material whose properties would not be attainable by conventional means is called a composite. Examples of composites include steel reinforced concrete, steel belted tyres and glass or carbon fibre - reinforced plastics (so called fibre-glass resins) used for boats, tennis rackets, skis, and racing bikes. Ceramics can be defined as inorganic, non-metallic materials that are typically produced using clays and other minerals from the earth or chemically processed powders.
Most people, when they hear the word ceramics, think of art, dinnerware, pottery, tiles, brick and toilets. The above-mentioned products are commonly referred to as traditional or silicate-based ceramics. While these traditional products have been, and continue to be, important to society, a new class of ceramics has emerged that most people are unaware of. These advanced or technical ceramics are being used for applications such as space shuttle tile, engine components, artificial bones and teeth, computers and other electronic components, and cutting tools, just to name a few.

In the first sight, the definition of the term 'Machinability' presents little difficulty. It is the property of a material, which governs the ease or difficulty with which a material can be machined using a cutting tool. The term is in wide use by those concerned with engineering manufacture and production, yet detailed enquiries would expose a measure of vagueness about its precise definition, or even its general meaning. Unlike most material properties, there is no generally accepted parameter used for its measurement and it is evident that, in practice, the meaning attributed to the term 'Machinability' tends to reflect the immediate interests of the user. The engineer concerned especially with surface finish problems tends to think in terms of 'finishability', others may consider that the term can be used legitimately to indicate the consistency with which a material behaves in a particular machine tool set-up under a constant set of machining conditions, whilst some may consider it to be a determinant of the useful life of the cutting tool. In most fields of science and technology great care is devoted to the definition of relevant parameters, but, in machining, Machinability tends to remain a term, which means 'all things to all men'. The main reason for the continued interest in the definition and assessment of machinability is the problem of specifying the cutting conditions for an optimal economic utilization of resources.

The main goals of this machinability study are as follows:

1. Optimisation of the machined surface roughness under different cutting conditions.
2. Optimisation of the cutting forces produced under different cutting conditions.
3. Development of optimum conditions for the process, in terms of tool life.
   The process parameters include cutting speed, rate of feeds and depth of cut.

Chapter 2 surveys the literature in the area of machinability and covers a general introduction on machinability studies, ceramic materials and tool materials including high speed steel, cemented tungsten carbide cubic boron nitride, carbide ceramics, diamond inserts and ceramic tools. It also focuses on methods of assessing machinability such as surface finish, cutting force and tool life.

Chapter 3 gives a general overview of machinability and includes the factors, which influence machinability. It also described the workpiece materials, and the chemical and mechanical properties of the workpiece material used for the tests are discussed in this chapter.

Chapter 4 covers the different methods of assessing machinability. Mechanisms of tool wear, which occur during machining are discussed, as is the method of tool life testing that was carried out along the guidelines of ISO standard. Also in this chapter the method of assessing machinability by using both cutting force tests and surface finish tests are discussed.

In chapter 5, the experimental facilities that were used are presented. These include a description of surface roughness tests, Kistler 3-component dynamometer, and a toolmaker's microscope. The chemical composition of materials is covered. Also in this chapter, the operation of dynamometer with charge amplifiers, data acquisition system and experiment of material hardness is described.

Chapter 6 covers the experimental results from the one-variable-at-a-time tests for the ceramic materials. The surface roughness, tool life and cutting force results are presented and analysed. The effects of cutting speed, rate of feeds, and depth of cut on surface roughness; tool life and cutting force are discussed.

Chapter 7 the development of machinability models using the method of Response Surface Roughness Methodology is discussed. The experimental results of the design of experiment tests are presented. The influence of depth of cut and nose radius on surface roughness have been investigated and recorded. Mathematical models of surface roughness based on the response surface methodology are presented. Also in this chapter response contours of surface roughness are shown in different plots. Contour of metal removal rate are also shown. RSM can be used to optimize the efficiency or power output without large changes in the operating parameters, while continuing the operation without interruption. The main advantage of RSM is that it can be done "on the fly" and provides a large amount of information with a small amount of experimentation.

Finally, in chapter 8 the conclusions and recommendations from this research have been discussed.

CHAPTER TWO: LITERATURE SURVEY

2 LITERATURE SURVEY

2.1 Introduction

A review of literature pertaining to machinability assessment of advanced materials can be distributed in to several sections as follows:

2.2 Machinability
2.3 Ceramic Materials
2.4 Tool Materials
2.5 Machinability Tests
2.6 Surface Finish
2.7 Cutting Forces
2.8 Tool Life
2.9 Tool Geometry
2.10 Experiment Design

2.2 Machinability

The term machinability is used to describe the ease with which a work material is machined under a given set of cutting conditions. If a material *x* is more machinable than material *y*, it can mean that higher tool life is achievable with material *x*, or less power is required to machine that material and it could be that a better surface finish is produced when machining that material. Moreover, ease of chip disposal, cutting temperature, operator safety, etc, are other criteria of machinability [1].

It is important to mention that the machinability is only applicable to a particular set of circumstances under which the observations can be made. Machinability of a material *x* may be better than material *y* with respect to surface finish under a set of cutting conditions while machinability of material *y* may be better than that of *x* with respect to tool life under a different set of cutting conditions.

According to Ernst [2] the term machinability means a complex physical property of a metal, which involves true machinability, finishability, or ease of obtaining a good surface finish and abrasiveness or the abrasion undergone by the tool during cutting. Boston [3] has defined machinability as the response of a metal to machining which gives long tool life under otherwise equal conditions when compared with other materials, provides good surface finish, produces well broken chips, gives uniform dimensional accuracy of successive parts, produces each part at the lowest overall cost, and requires lower power consumption in removing a given quantity of chips.

According to Boccaccini et al [4] the relationship between the machinability and the brittleness of glass-ceramic materials is investigated. It was found that good machinability occurs when the brittleness index of the material is lower than $B \approx 4.3\mu m^{-1/2}$. Baik and Chun [5] says the change in the microhardness and machinability of mica glass-ceramic is related closely to its microstructural parameters. The aspect ratio of the crystals, the volume crystallinity and the spatial arrangement of the particles must be considered in order to be able to estimate the characteristics of the material. With a high aspect ratio and crystallinity, the microhardness decreases because of high connectivity. By introducing the effective crystallinity, indicating the effectiveness of disk-like crystals in forming a connected structure of crystals, the variation in microhardness can be explained. A steep decrease in the microhardness of mica glass-ceramics occurs due to the connection of the mica crystals, leading to good machinability.

Reen [6] stated that the three most important factors to be considered are surface finish, tool life and power consumption. Trent [7] concluded that cutting force, chip formation, surface finish, and tool life are all important factors to be considered when rating materials for machinability. Sandvik [8] define machinability as the ability of a work material to be machine. Base on Choudhury and Baradie [9] Nickel-base super alloys responsible for its poor machinability. They have an austenitic matrix, and like stainless steels, work harden rapidly during machining. Song and Evan [10] argued that machinability is not only indirectly dependent on compact strength but is dependent directly on the initial defect size and cutting parameters. Boulger [11] has defined machinability as the removal of chips with satisfactory tool life and surface finish.

According to [12] Macor MGC can be machined with high-speed steel tools, however carbide tools are recommended for longer wear.

In general machinability of a material can be considered as a combination of small cutting force, high metal removal rate, longer tool life, better surface finish/integrity, well-broken chips, and uniform dimensional accuracy. The different factors influencing machinability of a material are (i) machining operations, (ii) cutting conditions, (iii) workpiece properties, (iv) tool properties, and (v) machine tool-tool-workpiece dynamics [12].

The machining operation may be a continuous cutting operation (turning) or a discontinuous cutting operation (milling). The cutting conditions that influence the machinability parameter are cutting speed, feed rate, depth of cut, and cutting fluid. The higher the cutting speed, the lower the tool life. This is true for the feed as well. Moreover, as the feed rate increases, the power consumed during cutting also increases. The higher the depth of cut is, the greater the power requirements.

2.3 Ceramic Material

The word ceramic comes from the Greek term Keramos, which means burnt matter. This term was coined by ancient civilizations that found that clay could be mixed with water, shaped, dried and placed in a fire to harden. The present definition of ceramics is broader. It includes not only the traditional material made by heating naturally occurring substances but also the highly refined and synthesized materials engineered for modern chemical, electrical, magnetic, optical and mechanical applications.

It is a common causation that a ceramic is brittle, has a high melting, is non conducting (of both heat and electricity) and is nonmagnetic. It is also a common causation that metals have opposite properties. These stereotyped viewpoints are not necessarily true for either ceramics or metals. In fact, there is no clear-cut boundary that separates the two. Rather, there are intermediate compounds that have some aspects typical of ceramics and others typical of metals. The nature of a material is largely controlled by the type of bonding between its constituent atoms, which in turn is controlled by the electron configuration of the atoms. Elements with unfilled outermost electron shells interact with other atoms, such that electrons are shared or exchanged between these atoms to achieve full shells. Pure metals consist of atoms of a single size and electron configuration in a close-packed arrangement. All the atoms in the structure freely share the outer electrons. This mutual sharing of electrons provides the bond force that holds the atoms together into a metal crystal. It also provides the basis for most of the properties that we associate with a metal: ductility, high electrical conductivity, thermal conductivity and thermal expansion [13].

a) **Properties of ceramics**

The properties of ceramics and metals result from a combination of the effects of atomic bonding and microstructure. The effects of bonding are primarily reflected in the intrinsic properties chemical, physical, thermal, electrical, magnetic and optical. Microstructure can also affect some of the intrinsic properties, but it's major effect is on mechanical properties and on the rate of chemical reaction.

b) **Thermal expansion**

The rate of thermal expansion of metals and ceramics is determined by the bond strength and the atomic structure. The greater the bond strength, the lower the expansion. Metals and ionic ceramics have close-packed atomic structures and a relatively high thermal expansion. When each atom within the structure expands due to thermal vibration, it pushes against surrounding atoms. The total expansion of the structure is the sum of the expansion of all the individual atoms. On the other hand, covalent bonding is directional and produces structures having large open spaces. When a covalent ceramic is heated, a portion of the expansion can be absorbed by the open space within the structure or by bond angle shifts, resulting in low expansion. Ceramic materials such as lithium aluminium silicate, fused silicate and magnesium aluminium silicate have very low thermal expansion rates.

c) **Thermal conductivity**

Thermal conductivity is controlled by the amount of heat energy present, the nature of the heat carrier in the material and the amount of heat dissipation. The carriers in metals are electrons. These are relatively free to move throughout the structure and result in high thermal conductivity. The primary ways to carry heat in ceramics are by lattice vibrations and radiation. Ceramic materials such as diamond, graphite, BeO, SiC and B_4C, which have simple structures made up of atoms of similar atomic weight, transfer heat readily by lattice vibrations and have high thermal conductivity. More complex structured ceramics have greater scattering or attenuation of lattice vibrations and lower thermal conductivity. Porous ceramics, ceramic powders and ceramic fiber aggregates contain dead-air space and have very low thermal conductivity.

d) **Melting temperature**

Many ceramics are used in applications that require a high melting temperature and chemical stability. Melting temperature is a function of the strength of the atomic bond. Weakly bonded alkali metals (Na) and monovalent ionic ceramics (NaCl) have low melting temperatures. More-strongly-bonded transition metals (Fe, Ni, Co) and multivalent ionic ceramics (BeO, Al_2O_3, ZrO_2) have much higher melting temperatures. Very strongly bonded metals (W) and covalent ceramics (TiC, HfC) have the highest melting temperatures [13].

e) **Ductility**

Dislocation movement along planes of atoms accommodates ductility. For this to occur, a dislocation must: (i) be present or be easily initiated; (ii) have activation energy below the fracture initiation energy for the material and (iii) have an unobstructed path for movement. These conditions are satisfied ideally in a pure metal having a close packed structure. Not all metals have high ductility. Addition of secondary atoms as either alloying agents or a secondary dispersion blocks the movement of dislocations and increases the energy required for slip. The highly alloyed super alloys only have elongations at room temperature in the range of 5 to 20%, compared with 40-60% for some pure metals. Ionic bonded ceramics have close-packed structures similar to the pure metals and thus have many potential slip planes. However, due to the opposite electrical charge of adjacent ions, each ion is stable only in a certain equilibrium position and coordination (number of nearest neighbours). A higher activation energy than is required for metals is necessary to move oppositely charged ions and cause slip. In most cases this activation energy is higher than the energy required to initiate fracture through stress concentration at a surface or internal material flaw. This situation is similar for covalent ceramics. The directionality of bonding will place atoms in equilibrium positions that require high activation energy for slip. Metals typically fail in a ductile mode due to the presence of imperfections that allow slip along atomic planes at relatively low shear stress. Ceramics fail in a brittle mode due to the presence of fabrication and structural flaws that result in stress concentration and fracture at a load well below the theoretical strength. Most ceramics fracture at an applied load of less than 100,000 P.S.I. However, because of their brittle nature, ceramic components must be designed differently and more carefully than metals to avoid localized stress concentration resulting from impact, attachment, notches, thermal gradients or other sources.

f) **Chemical resistance**

The major characteristic that makes ceramics appealing to chemical processing plants is chemical stability over a broad temperature range. Ceramics having strong ionic and covalent bonding and high purity are most resistant to chemical attack. These ceramics generally do not occur in quantity in the earth's crust but instead must be either synthesized or carefully processed e.g., aluminium oxide. Some ceramics are basic and others are acidic, which strongly affects the nature of their reaction with solutions and melts. Al_2O_3 and ZrO_2, however are amphoteric. Spinel ($MgAl_2O_4$), BeO and MgO are weakly basic. Zircon ($ZrSiO_4$), SiO_2, SiC, and Si_3N_4 are slightly acidic. In general, the more basic oxides are resistant to attack by basic solutions and melts but are susceptible to acidic ones. A recent material that has excellent corrosion resistance is Si_3N_4. Si_3N_4, is not attacked by strong acids (except HF). The material is reportedly not corroded by 900°C Cl_2 gas or 1,000°C H_2S gas [13].

2.4 Tool Material

The tool material and its geometry also have an influence on the machinability of a material. The main factors that affect of a good cutting tool is (i) high hardness (ii) wear resistance (iii) chemical inertness and (iv) fracture toughness. Rake angle of a cutting tool has an affect on the cutting force. As the rake angle becomes positive, the cutting force decreases [14]. To cut effectively and provide acceptable tool life, the cutting-tool material must of course be harder than the material being cut. Also high temperature hardness is very important because during the cutting process the very high temperatures developed tend to soften tool materials and cause failure of the cutting edge. Figure (2.1) shows the hot hardness of various tool materials [28]. With the introduction of sialon materials, it is possible to increase the cutting speed by a factor of five, and more recently silicon carbide whisker-reinforced alumina tools have made it possible to machine at cutting speeds of up to ten times those used with cemented carbide. Ceramic tools are suitable with regard to the first three properties even at high cutting speeds. However, their fracture toughness is much lower than that of the other widely used tool materials such as high-speed steel and carbides.

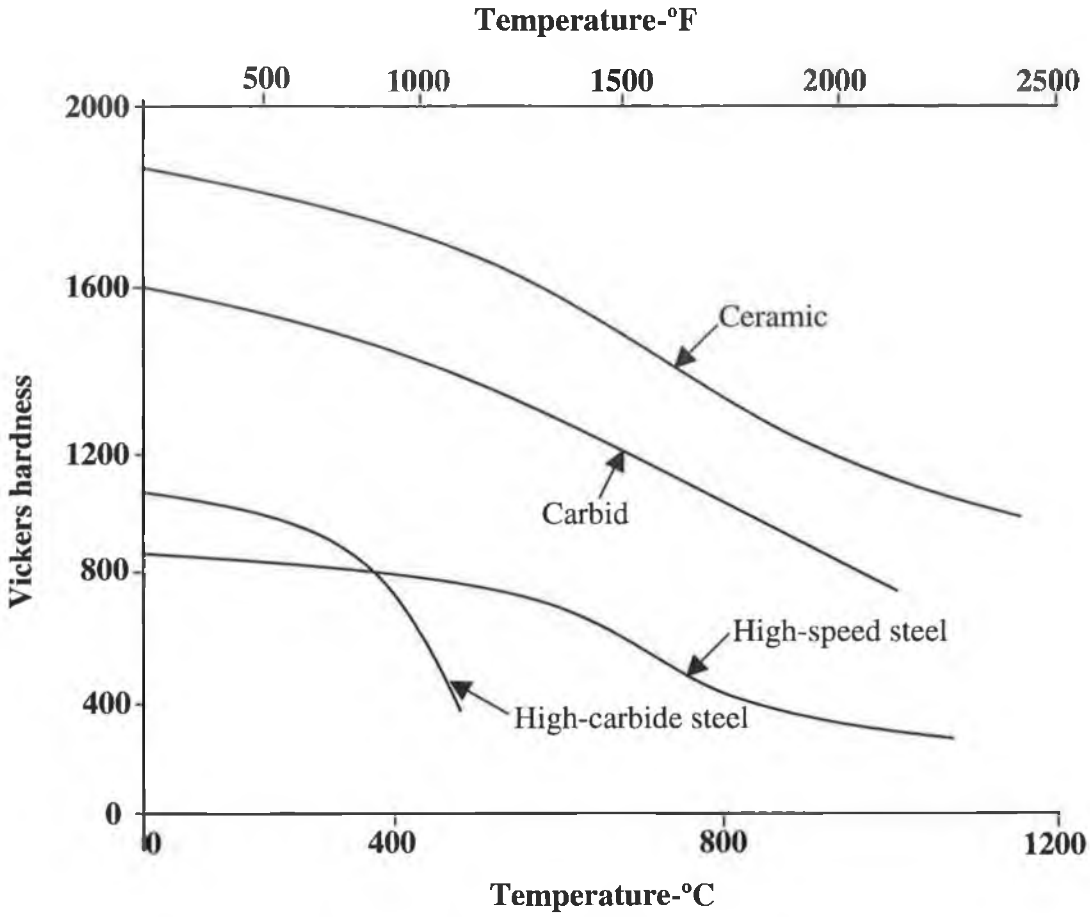

Figure 2.1 Variation of hardness with temperature, for various tool materials [28].

2.4.1 High Speed Steel (HSS)

This class of tool steel was developed just before 1900, the incentive being increased productivity of the machine shop. The low speed at which steel could be machined had become a severe handicap to its rapidly expanding use in engineering. The tool material available for metal cutting since the beginning of the industrial revolution had been carbon tool steel and before the high speed steels the only significant innovation had been the self-hardening steel initiated by Robert Mushet in the 1860s. [7] For use in metal cutting, carbon tool steel was hardened by quenching it in water from a temperature between 750°C and 835°C followed by a tempering treatment between 200°C and 350°C. The self-hardening tool steels were heated in the same temperature range for hardening but did not need to be quenched in water, air cooling sufficed and this was an advantage, particularly for large tools. Mushet's introduced steel in England having approximately the composition: carbon 2%, manganese 1.6%, tungsten 5.5%, and chromium 0.4%. This steel was air hardening and retained its hardness to high cutting temperature. As a result it could be used to speeds of about 25 f.p.m. (0.13m s^{-1}).

F.W. Taylor and M. White (1901) produced tools of greatly increased stability, which allowed cutting speeds of about 60 f.p.m. and consequently this material became known as high-speed steel (HSS). Contrary to common belief this was not the development of new steel but rather a new heat treatment for the existing material. Taylor and White found that if tools were heated quickly through the brittle temperature range of 845°C to 930°C to a temperature just short of the melting point of the steel before quenching, a steel of improved hot-hardness resulted. It was also found that a higher Tempering temperature improved such tools. The composition of the steel used by Taylor and White in 1901 was approximately 1.9 percent carbon, 0.3 percent manganese, 8 percent tungsten and 3.8 percent chromium. This is seen to differ from the original Mushet steel mainly in the increased amount of tungsten and the replacement of manganese by chromium. Taylor also found that improved tools were produced by using less carbon and more tungsten (the carbon decrease was necessary to make the steel forgeable when tungsten was increased to improve hot-hardness). In 1912 it was found that the red-hardness of HSS could be improved by additions of from 3 to 5 percent cobalt. Current HSS tools enable steel to be machined at speeds that are often in excess of 300 f.p.m. It is well known that the hardness and wear resistance of HSS depends on the composition, size and distribution of the carbides in the steel and upon the stability of the matrix at high temperatures. The lather is increased by addition of cobalt. Harder mixed carbides are provided by increased vanadium and carbon content. A major development in the HSS area in the 1950s was the discovery that steels of increased hardness (R_c 70 instead of the R_c 65 for the more conventional HSS) and reasonable toughness may be produced by use of compositions such as: -

1.4 % C, 4 % V, 9 % W, 4 % Mo, 12 % Co

These steels have a large concentration of finely and uniformly divided carbides in a rather refractory matrix. During the 1970s there have been two additional significant developments in the HSS area [15]. High-speed steel tools revolutionised metal cutting practice, vastly increasing the productivity of machine shops and requiring a complete revision of all aspects of machine tool construction. It was estimated that in the first few years, engineering production in the USA had been increased by $8000 M through the use of $20 M worth of high-speed steel.

However, cast HSS tools have in general not produced tools as shock-resistant as wrought HSS tools. Originally these steels were made with 0.7 % carbon together with about 18% tungsten, 4 % chromium and 1 % vanadium. The need for better hot hardness and abrasion resistance has led to the introductions of carbon and other alloying elements. Table (2.1) gives compositions for a number of commercially available high-speed steels.

2.4.2 Cemented Tungsten Carbide Tool

Carbide cutting tools are the oldest amongst the hard cutting tool materials. Tungsten-based carbides can be used in high feed-rate cutting and severe interrupted cutting, but because of their poor thermo chemical instability, they cannot be used at high speed. Coated carbides on the other hand have good wear resistance and strength [4]. However, carbide tools cannot be used for high-speed machining because they cannot withstand the high temperature and stresses in the cutting zone encountered during such machining.

2.4.3 Cubic Boron Nitride (CBN)

CBN is one of the hardest materials available after diamond and does not occur in nature. Synthesis of polycrystalline CBN is composed of about 50% - 90% CBN and ceramic binders such as titanium carbide and titanium nitride. A high CBN content is better in cutting super alloys. Compared to ceramics, CBN has better hardness and resistance to fracture but poorer chemical resistance. These tools are used to machine nickel or cobalt-base alloys of hardness equal to or greater than 340 HV. CBN inserts can increase productivity in many difficult metal cutting operations – up to 10 times better than carbide or ceramics in terms of longer tool life and/or higher metal removal rates. CBN is primarily used in finishing of steel, grey cast iron and heat resistant alloys. The unique multi-corner CBN inserts improve tool life and give lower costs per edge than conventional CBN inserts.

Table 2.1 Composition (w %) of some commercially available high-speed steels

*AISI designation	Weight percent C	W	Cr	V	Mo	Co
M1	0.80	1.75	3.75	1.15	8.75	-----
M2, Class1	0.85	6.25	4.00	2.00	5.00	-----
M3, Class1	1.05	6.25	4.00	2.50	5.75	-----
M4	1.30	5.50	4.00	4.00	4.75	-----
M6	0.80	4.25	4.00	1.50	5.00	12.00
M7	1.02	1.75	3.75	2.00	8.75	-----
M8	0.80	5.00	4.00	1.50	5.00	(1.25 Cb)
M10, Class1	0.89	0.70	4.00	2.00	8.00	------
M15	1.50	6.50	4.00	5.00	8.50	5.00
M30	0.80	1.80	4.00	1.20	8.25	5.00
M34	0.90	1.75	3.75	2.10	8.75	8.25
M36	0.85	6.00	4.00	2.00	5.00	8.25
M41	1.10	6.75	4.25	2.00	3.75	5.25
M42	1.08	1.60	3.75	1.15	9.60	8.25
M43	1.20	2.70	3.75	1.60	8.00	8.20
M44	1.15	5.25	4.25	2.00	6.50	11.75
M45	1.27	8.25	4.20	1.60	5.20	5.50
M46	1.24	2.10	4.00	3.20	8.25	8.25
T1	0.73	18.00	4.00	1.00	-----	-----
T2	0.85	18.00	4.00	2.00	-----	-----
T3	1.05	18.00	4.00	3.00	0.60	-----
T4	0.75	18.00	4.00	1.00	0.60	5.00
T5	0.80	18.00	4.25	2.00	0.90	8.00
T6	0.80	20.50	4.25	1.60	0.90	12.25
T7	0.75	14.00	4.00	2.00	-----	-----
T8	0.80	14.00	4.00	2.00	0.90	5.00
T9	1.20	18.00	4.00	4.00	-----	-----
T15	1.55	12.50	4.50	5.00	0.60	5.00

* The American Iron and Steel Institute (AISI) has introduced symbols for the two major classes of HSS: the symbol T designates a tungsten-base steel while the symbol M a molybdenum-HSS.

2.4.4 Carbide Ceramics

In some applications where carbide tips wear too rapidly but ceramics suffer from chipping the most satisfactory tool materials are the carbide ceramics. They are mixtures of oxides (usually aluminium oxide) and carbide; their transverse rupture strength is higher than that of ceramics but lower than carbides. They are most commonly used for cast iron and lower-grade Nimonics.

2.4.5 Diamond Inserts

Diamond is the hardest material known which allows non-ferrous metals and non-metallic to be machined faster and at lower costs than with cemented carbide tools. Diamond is used to get excellent surface finish and semi-finishing operations under stable conditions.

2.4.6 Ceramic Tool

There are two basic ceramic materials that are used as cutting tools. These are aluminium oxide (Al_2O_3) and silicon nitride (Si_3N_4). The pure ceramics is based on Al_2O_3 but contains a small amount of zirconia (ZrO_2) for added bulk toughness. Whilst the mixed ceramic is based on Al_2O_3 but contains titanium carbide (TiC), which gives it better thermal properties. The reinforced ceramic is based on Al_2O_3 but contains silicon carbide (SiC) whiskers, which gives it better thermal considerably. The silicon nitride (Si_3N_4) based ceramic known as sialon has better thermal properties and toughness than Al_2O_3 based ceramic, these tools are used widely to machine super alloys. Sialon ceramics have a low coefficient of thermal expansion compared to that of alumina-based ceramics. Table (2.2) shows the properties of different tool material [16].

Table 2.2 Properties of different tool

Material Property	Tool material					
	Tungsten carbide (K10) 94% WC + 6% Co(wt.%)	Alumina 90-95 % Al_2O_3 + 5-10% ZrO_2	Mixed alumina Al_2O_3+30% TiC+5-10% ZrO_2, Al_2O_3+30% TiN+5-10% ZrO_2	Whisker-reinforced alumina 75% Al_2O_3+25% SiC	Sialon 77% Si_3N_4+13% Al_2O_3+1%Y_2O_3	Cubic boron nitr-ide 50-90% CBN +50-10%TiN-TiC
Grain size (μm)	1-2	1-2	1-2	------	1	1-3
Density (g cm^{-3})	14.8	3.9-4.0	4.2- 4.3	3.7	3.2	3.1
Hardness (HV) at 20°C	1700	1700	1900	2000	1600	3000-4500
Hardness (HV) at 1000°C	400	650	800	-----	900	1800
Fracture toughness ($MNm^{-3/2}$)	10	1.9	2	8	6	10
Young's modulus (KN mm^{-2})	630	380	420	390	300	680
Thermal conductivity (W m^{-1} °C)	100	8 –10	12-18	32	23	100
Coefficient of thermal ex-Pansion ($\times 10^{-6}$ -°C)	5.6	8.5	8	-----	3.2	5

2.4.6.1 Alumina and alumina-tic ceramics

Aluminium oxide (Al_2O_3) ceramic has high hardness and high compressive strength. It is chemically stable at very high temperature with respect to nickel and iron. However, it has low fracture toughness and low thermal shock resistance. This white ceramic is chemically very stable and inert to most environments, which makes it suitable for high-temperature applications. However it has worse thermal and mechanical shock resistance properties compared to tungsten carbides. The fracture toughness of alumina ceramics can be improved by the adding of titanium carbide or titanium nitride.

2.4.6.2 Silicon nitride ceramics (Si_3N_4)

Silicon nitride is known to be one of the toughest ceramic materials. Silicon nitride ceramics are two-phase materials consisting of silicon nitride crystals in an inter-granular bonding phase. This material is yttria-stabilized silicon aluminium oxynitride. A mixture of Alumina (~ 13%), Silicon nitride (~ 77%), yttria (~ 10) and Aluminium nitride is used as the sintering material to produce sialon ceramics. The main advantage of this ceramic is its high toughness see Table (2.2). The silicon materials have a low coefficient of thermal expansion. The silicon nitride grades CC6090 is a tough grade with very good wear resistance and notch wear performance. This is recommended for high speed machining of grey cast iron.

2.4.6.3 Whisker-reinforced alumina ceramics (Al_2O_3 + Sic_w)

The recent development of this ceramic tool is to improve toughness by mechanical means instead of chemical means. Fibres or whiskers of silicon carbide are added (25% by vol.) for reinforcement of an alumina matrix. The whiskers have an average diameter of approximately 0.6μm and a length of from 10 to 80μm. The whisker-reinforced alumina ceramics have a low coefficient of thermal expansion in addition to resistance to high temperature. The high thermal conductivity and low thermal expansion coefficient of the whiskers also improve the thermal shock resistance [9].

2.5 Machinability Tests

A range of machinability tests have been developed often to specific to cutting conditions, whilst others are used for more general machining assessment. Sometimes machinability data is expressed in the form of a single index such as a "standard" material being rated as 100%, with others materials having values, which are in relation to it [17]. The ratings can be dependent on the type of test such as the Volvo "fly cutting" milling test. Here the tests have index values on a "100 scale".

In general a machinability test assesses the speeds and feeds which are varied by trial and error and with specified constraints [1].

Groover et al [18] show a series of tool life tests is conducted on two work materials under identical cutting conditions, varying only speed in the test procedure. The first material, defined as the base material, yields the Taylor tool life equation:

$$VT^{0.28} = 1050$$

The other material (test material) yields the Taylor equation:

$$VT^{0.27} = 1320$$

Determine the machinability rating of the test material using the cutting speed that provides a 60-min tool life as the basis of comparison. This speed is denoted by υ_{60}.

Solution: the base material has a machinability rating = 1.0. Its υ_{60} value can be determined from the Taylor tool life equation as follows:

$$V_{60} = \frac{1050}{60^{0.28}} = 334 \text{ ft/min}$$

The cutting speed at a 60-min tool life for the test material is determined similarly:

$$V_{60} = \frac{1320}{60^{0.27}} = 437 \text{ ft/min}$$

Accordingly, the machinability rating can be calculated as:

$$\text{MR (for the test material)} = \frac{437}{334} = 1.31 \quad \text{(or 131\%)}$$

Many work material factors affect machining performance. Mechanical properties of a work material affecting machinability include hardness and strength. As hardness increases abrasive wear of the tool increases so that tool life is reduced. Strength is usually indicated as tensile strength even though machining involves shear stresses. As work material strength increases cutting forces, specific energy, and cutting temperature increase, making the material more difficult to machine.

Nevertheless, the three main parameters of machinability assessment are (i) cutting force (ii) Tool life and (iii) surface finish. Figure (2.2) shows different machinability parameters in the form of an input/output model of turning operation.

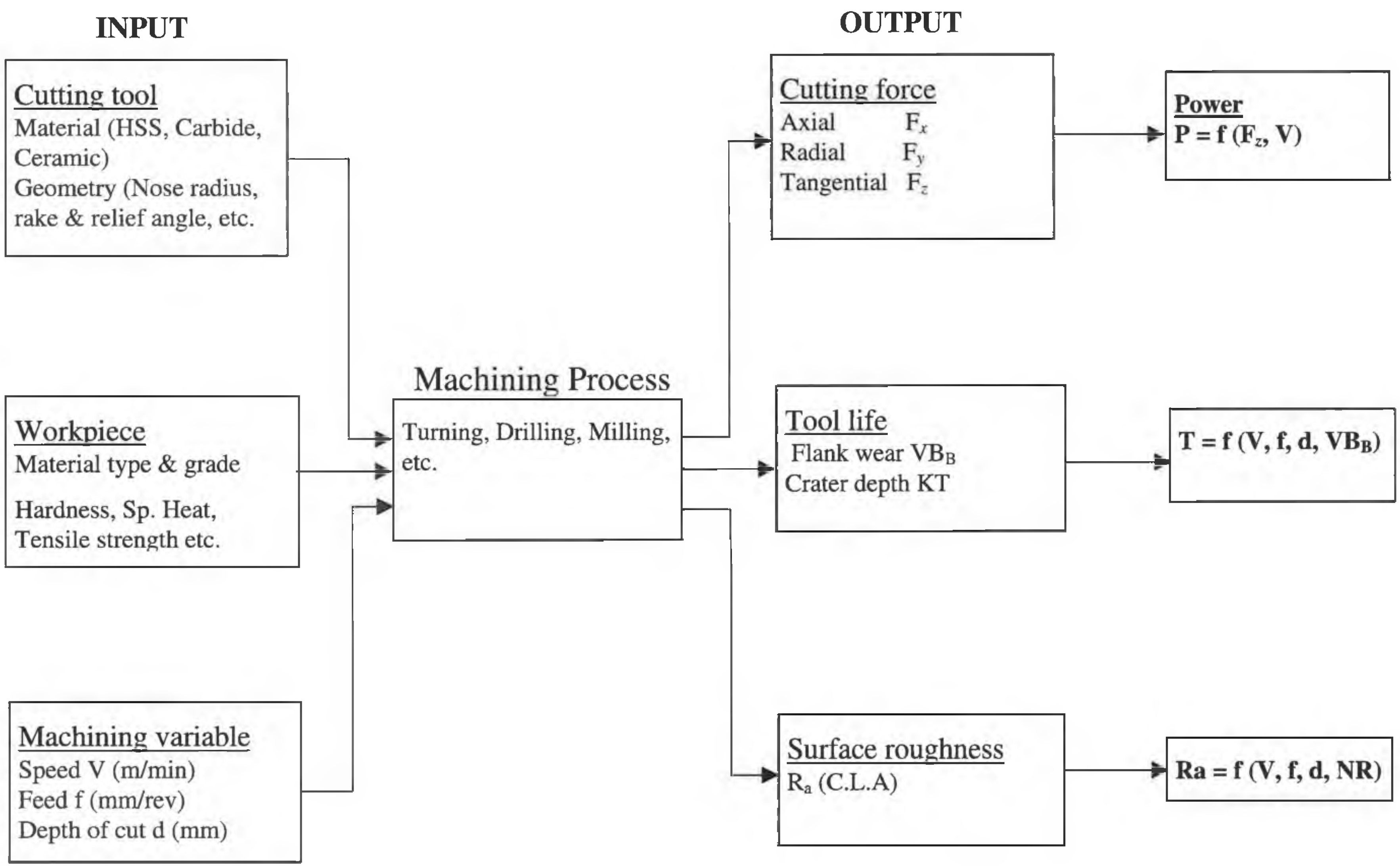

Figure 2.2 Various machinability parameters in a machining process.

2.6 Surface Finish

In any machined surface, the term used to describe its geometrical quality is know as surface roughness. The machinability of a material can be assessed by measuring the surface finish produced during a cutting operation. The surface finish is an extremely important functional quality of many components. Surface finish is a factor of great importance in the evaluation of machining accuracy. Although many factors affect the surface condition of a machined part, cutting parameters such as speed, feed rate, depth of cut and tool nose radius have a significant influence on the surface roughness for a given machine tool and workpiece set-up [19]. Based on [20] a variation of 500 % in the depth of cut will increase the roughness by only 20 %.

In light of the Fang and Jawahir study [21] the surface finish is an important machining parameter, which is greatly influenced by the input machining conditions (work material, tool geometry, chip-breaker type and cutting conditions)

According to Haron et al. [22] surface finish tends to become rougher toward the end of tool life. This is probably due to deformation on the flank face or adherence of the workpiece material at tool nose. Increasing the cutting speed led to higher roughness values. However, the roughness values recorded were unstable during the intermediate cutting process.

Based on [23] the surface finish is improved with the increasing cutting speed at the same feed rate eventually reaching the ideal surface finish. It is interesting to note that the best surface finish is obtained with a slightly worn tool. This is likely due to the stabilisation of the nose and cutting edge radii.

According to M. Rahman et al. [19] the surface roughness of the specimens using tungsten carbide and ceramic inserts at various depths of cut does not vary much at lower cutting speeds. However, the surface roughness of the specimens using ceramic is significantly higher than that of specimens using tungsten carbide and CBN insert at higher speeds. The reason for the poor surface finish is that the ceramics are prone to poor mechanical shock resistance, since the inserts may alternately encounter resin and fiber in CFRP specimens.

According to Groover [18] the roughness of machined surface depends on many factors that can be grouped as follows: (i) geometric factors, (ii) work material factors, and (iii) vibration and machine tool factors.

- **Geometric factors**

Geometric factors determine the geometry of the surface on a machined part. They include (i) type of machining operation, (ii) cutting tool geometry, most importantly nose radius, and (iii) feed. The surface geometry that would result form these factors is referred to as the ideal or theoretical surface roughness, which is the finish that would be obtained in the absence of work material, vibration, and machine tool factors. Type of machine operation refers to the machining process used to generate the surface. For example, peripheral milling, facing milling and shaping all produce a flat surface, however the geometry of the surface is different for each operation because of differences in tool shape and the way the tool interacts with the surface.

- **Work material factors**

Work material factors that affect finish include (i) bult-up edge effects (as the BUE cyclically forms and breaks away, particleas are deposited on the newly created work surface causing it to have a rough, sandpaper texture), (ii) damage to the surface caused by the chip curling back into the work, (iii) tearing of the work surface during chip formation when machining ductile materials, (iv) cracks in the work surface caused by discontinuous chip formation when machining brittle material, and (v) friction between the tool flank and the newly generated work surface. These work material factors are influenced by cutting speed and rake such that an increase in cutting speed or rake angle generally improves surface finish [18].

- **Vibration and machine tool factors**

These factors are related to the machine tool, tooling, and set-up in the operation. They include chatter or vibration in the machine tool or cutting tool, deflections in the fixturing, often resulting in vibration; and backlash in the feed mechanism, particularly on older machine tools. If these machine tool factors can be minimized or eliminated, the surface roughness in machining will be determined primarily by the geometric factors and work material factors described previously. Chatter or vibration in a machining operation can result in pronounced waviness in the work surface. When chatter occurs a distinctive noise is made that can be recognised by any machinist. It is very desirable to eliminate chatter by taking steps to reduce its occurrence. Possible steps to reduce or eliminate vibration include (i) adding stiffness and/or damping to the set-up, (ii) operating at speeds that do not cause cyclical forces whose frequency approaches the natural frequency of the machine tool system, (iii) reducing feeds and depths to reduce forces in cutting and (iv) changing the cutter design to reduce forces. Workpiece geometry can also sometimes play a role in chatter.

2.7 Cutting Force

Cutting force tests are used as a method to assess the machinability of a given work material. These forces are measured by a dynamometer. It has been shown by researchers that cutting forces are insignificant in affecting machining parameters such as the temperature produced, power required, vibration in the cutter and the surface finish that is produced.

In the light of Cherry's study [14] rake angle of a cutting tool has an effect on the cutting force. As the rake angle becomes positive, the cutting force decreases. Yellowley [24] used an analogy force model by considering both flank and rake force conditions to express the average values of force, torque and specific power. He stated that specific power is a unique function of mean chip thickness.

Koplev et al. [25] observed the difference between cutting parallel and perpendicular to the fibre axis. This represents two basic cutting mechanisms, one shearing in perpendicular direction and the other buckling in the parallel direction, hence different cutting forces are required.

Rahman et al. [19] observed that the cutting forces do not exhibit a particular trend. However, the radial component of the cutting force is consistently the largest of the three forces. This is due to the opposing motion of the tool and the workpiece. The cutting force encountered when machining short fiber composites fluctuate with respect to both the cutting speed and the depth of cut. This is due to fibers being oriented at different angles throughout.

The total force F can be divided into three components. Tangential force, axial force and radial force as shown in Fig (2.3). The tangential force F_z acts along the direction of the cutting speed i.e., it is tangential to the turned surface. This is main component of cutting force, which together with the cutting speed determines the power required for the main spindle drive.

The axial force F_x acts along the direction of the tool feed. The feed force together with the feed velocity determines the power required for the feed drive. The radial force F_y acts perpendicular to the turned surface. The net resultant force F becomes:

$$\mathbf{F} = \sqrt{F_x^2 + F_y^2 + F_z^2}$$

During the turning operation only two cutting forces can be considered, the force between the tool face and the chips (R) and the force between the workpiece and the chip along the shear plane ($R^{/}$), these must be as follow.

$$R=R^{/}$$

The forces R and $R^{/}$ are expediently resolved into three sets of components as indicated in Figure (2.4).

I). In the horizontal and vertical direction, F_P and F_Q.
II). Along and vertical to the shear plane F_S and N_S.
III). Along and perpendicular to the tool face, F_C and N_C [26].

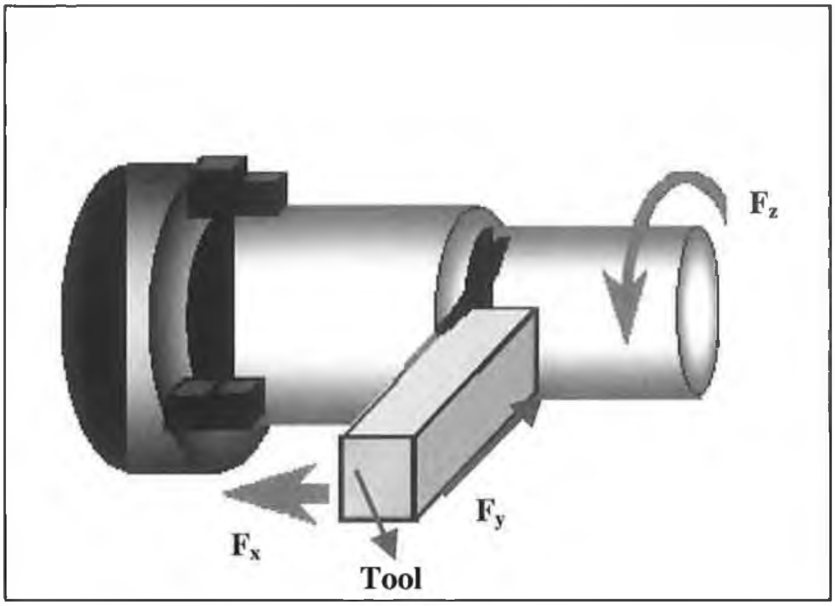

Figure 2.3 Three components of measurable cutting forces acting on single- point turning tool.

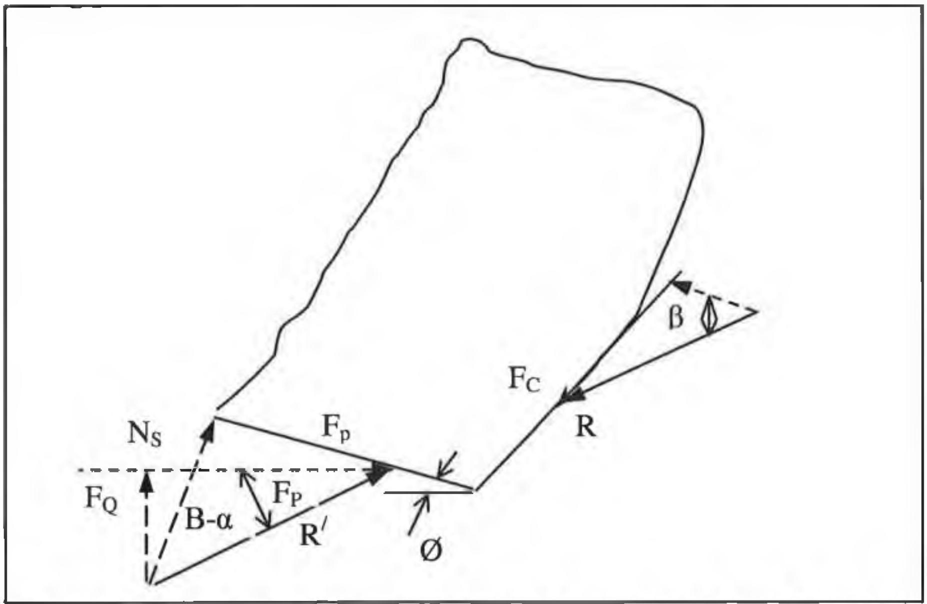

Figure 2.4 Free body diagram of chip and two cutting force R and R/

2.8 Tool Life

In metal cutting operation, the tool life is one of the most important economic considerations. Any tool or work material improvements that increase tool life is desirable. Cutting tools are in metal-to-metal contact with the chip and workpiece under conditions of very high stress at high temperature. The existence of extreme stress and temperature gradients near the surface of the tool further aggravates the situation.

Tool life was significantly influenced by temperature generated and forces exerted at or near the cutting edge of the tools. Therefore, changes in cutting speeds and feed rates will directly influence the cutting force and temperature generated, especially during dry cutting and hence the tool life [22].

In the light of Haron and Ginting's study [27] it has been observed that the tool life of coated and uncoated carbide tools decreases quickly at higher speeds, although the tool life of coated carbide tools was much longer than the uncoated carbide tools in magnitude. For this reason it can be concluded that the behaviour of tool life against cutting speed for coated and uncoated carbide tools was similar in nature. According to Moor Lane [28] some of the standards for judging tool life are (i) Volume of metal removed between regrinds, (ii) Cutting time between regrinds, (iii) Number of work pieces machined between regrinds, (iv) Cutting speed (the maximum speed at which the metal can be removed-known as the Taylor speed), for given tool life. (v) Relationship of cutting-tool life to that of other tools (say drills and taps) in the production cycle. Cutting speed is the variable with has by far the greatest influence on tool life. F.W.Taylor, after a great number of experiments, showed that the approximate relationship between tool life and cutting speed could normally be represented by the empirical equation [28].

$$\mathbf{VT^n = C}$$

Where **V** = cutting speed,

T = cutting time between tool regrinds in minutes.

C = a constant whose value depends on workpiece material and variables.

n = exponent whose value varies with tool and work materials and with other machine variables.

If a series of turning tests were carried out on a metal in which all parameter is except cutting speed V were held constant, a definite value of tool-life T at failure would be obtained at each speed. These points plotted on Cartesian co-ordinates generate a hyperbolic curve, Fig (2.5). If the points are plotted on a log-log scale they produce a straight line, Fig (2.6).

The term "tool wear" refers to the degradation of the cutting and/or clearance surface of the tool, fracture and a reduction of the tool mechanical properties due to high temperature [54]. Tool wear is a product of a combination of four load-factors, which continually attempt to change the geometry of the cutting edge [8]. These four factors are chemical, mechanical, thermal and abrasive which result in five basic wear mechanisms; (i) adhesive wear, (ii) abrasive wear (iii) fatigue wear (iv) diffusion wear (v) oxidation wear. Acting in isolation or in combination, these mechanisms cause two distinct wear modes [54].

Colding [29] states that crater wear is also important in determining tool life when a work material produces long and continuous chips. The tougher the material the more important is the rake wear in determining the life of the tool. The rake wear is also considered important when high cutting speeds and feed rates are used in machining the tough material.

Yellowley was of the opinion that in general cutting tools wear steadily on both their flank and rake faces. He stated that while crater wear has often been used as a criterion for tool life it has been realized in both the areas of industry and research that the stipulation of reliable limits for crater wear and measurement of actual crater wear are difficult. Also, the advent of higher alloyed tool material has meant that even at high cutting speeds the mechanism of tool failure is attributable to flank wear and not to crater wear [24].

McGoldrick and Hijazi assessed the tool life in end milling by investigating the amount of weight loss of the tool occurring during machining. This is a measure of the total wear of the tool that occurs. However, this method is not that practical as it cannot distinguish between flank wear and rake wear on the tool [30].

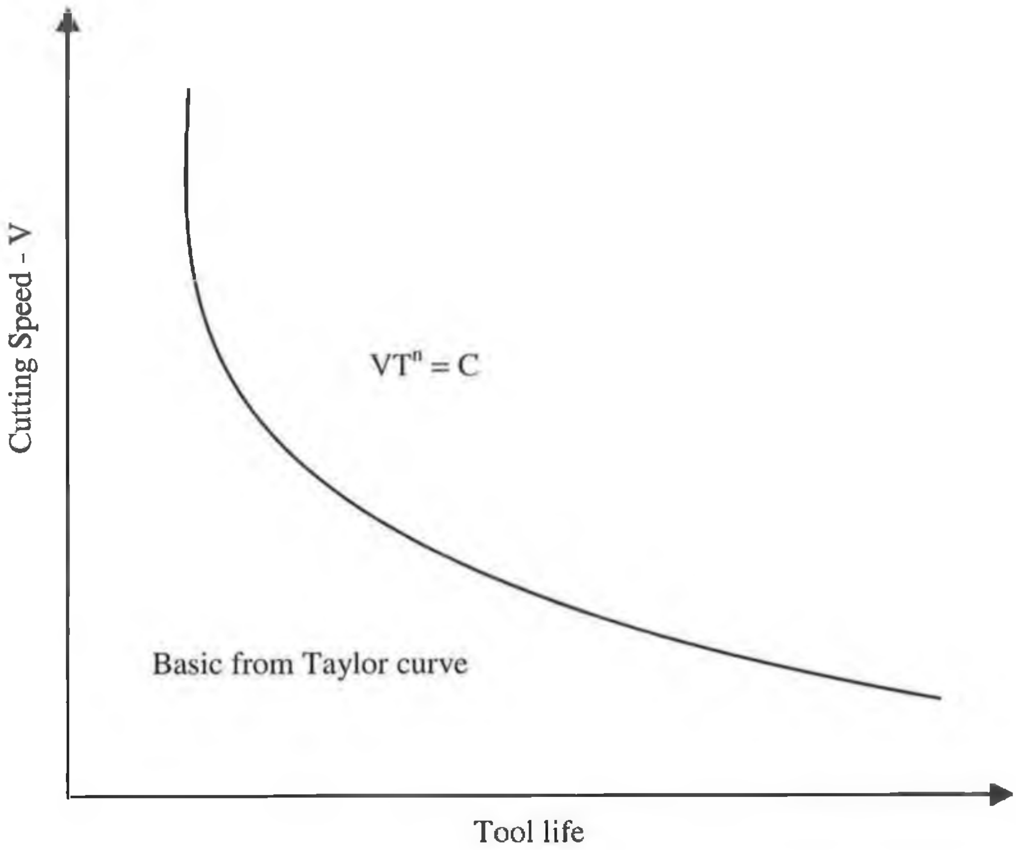

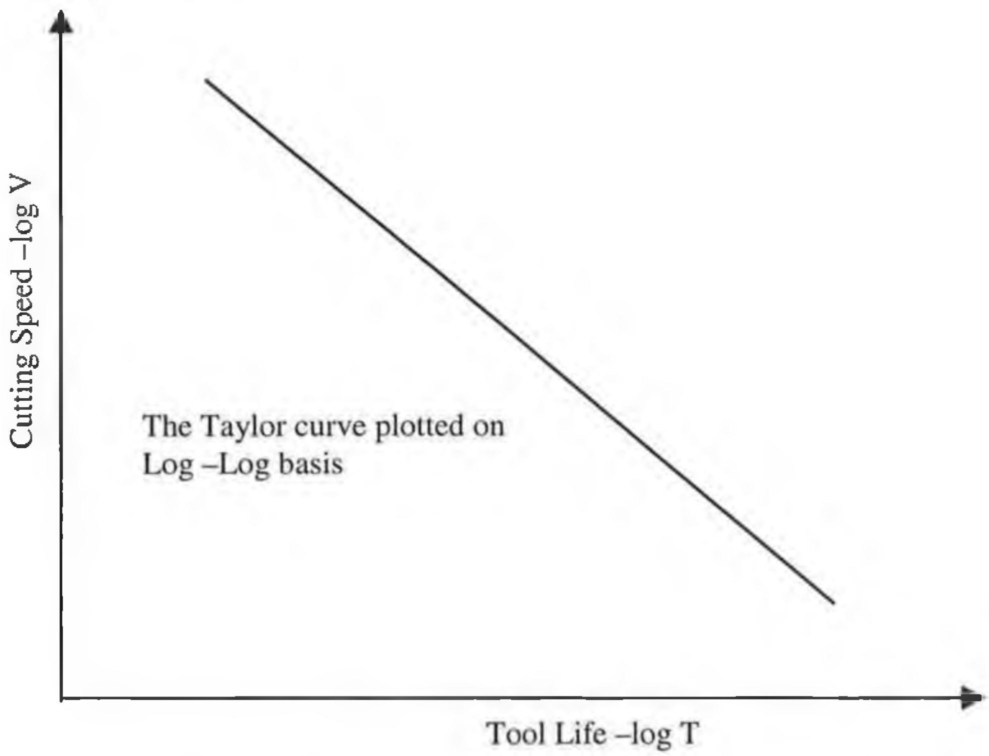

Figure 2.5 & Figure 2.6 Taylor Tool Life Curves [17]

2.9 Tool Geometry

A cutting tool must possess a shape that is suited to the machining operation. One important way to classify cutting tools is according to the machining process. Thus we have turning tools, milling cutters, drill bits, reamers, taps, and many other cutting tools that are named for the operation in which they are used, each with its own unique geometry. Cutting tools can be divided into two categories: single-point tools and multiple-cutting –eadge tools. Turning tools generally represent the first type, while drills and milling cutters represent the second.

Single-point tool gemetry: the general shape of a single-point tool is illustrated in figure 2.7; we have previously treated the rake angle of a cutting tool as one parameter. In a single-point tool, the orientation of the rake face is defined by two angles, back rake angle (α_b) and side rake angle (α_s). Together, these angles are influential in determining the direction of chip flow across the rake face. The flank surface of the tool is defined by the end relief angle (ERA) and side relief angle (SRA).These angles determine the amount of clearance between the tool and the freshly cut work surface. The cutting edge of a single-point tool is divided into two

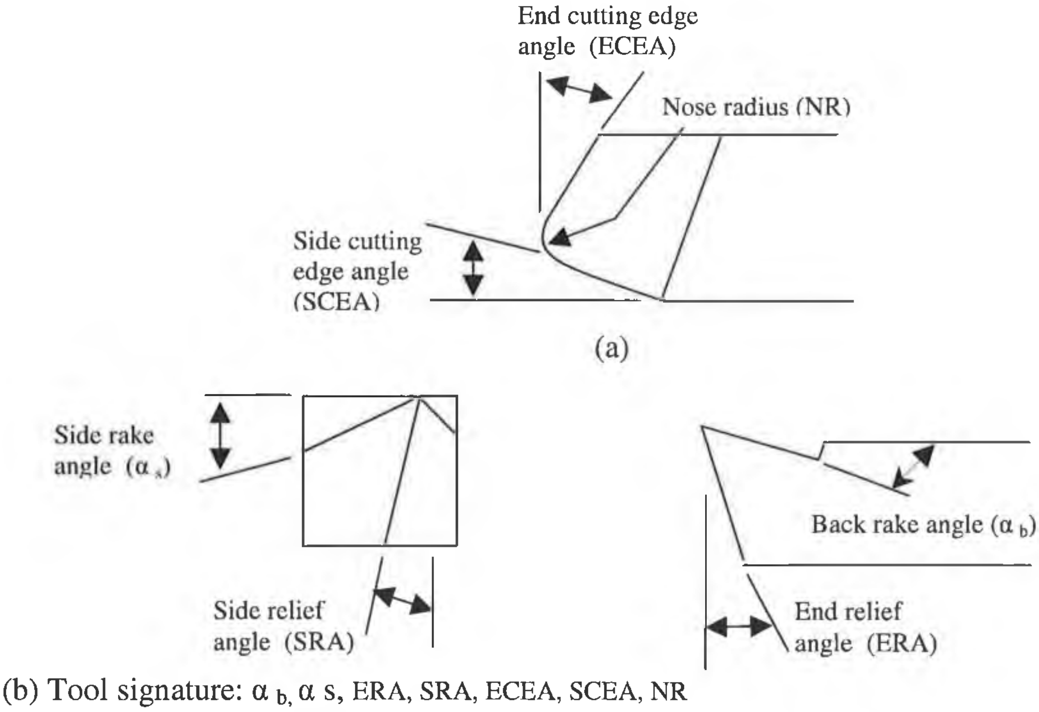

Figure 2.7; (a) seven elements of single point tool geometry and (b) the tool signature convention that defines the seven elements.

sections, side cutting eadge and end cutting edge. These two sections are separated by the tool point, which has a certain radius, called the nose radius. The side cutting edge angle (SCEA) determines the entry of the tool into the work and can be used to reduce the sudden force the tool experiences as it rnters a workpart. Nose raduis determines to a large degree the texture of the surface generated in the operation. A small nose radius results in very pronounced feed marks on the surface. End cutting edge angle (ECEA) provides a clearance between the trailing edge of the tool and the newly generated work surface, thus reduceing rubbing and friction against the surface [18].

2.10 Design of Experiments

To establish an adequate functional relationship between the machining response (surface finish, tool life and cutting force) and the cutting parameters (feed rate, cutting speed, and depth of cut) a large number of cutting tests are necessary. It requires a separate set of tests for each and every combination of cutting tool and workpiece material. This increases the total number of tests and as a result experimentation cost also increases.

The design of experiment takes into account the simultaneous variation of cutting speed, feed rate and depth of cut and the predicts the response. This approach is known as response surface methodology where the response of the dependent variable (tool life, surface roughness or cutting force) is viewed as a surface and was first pioneered by Wu [53]. Factorial designs are widely used in experiments involving several factors where it is necessary to study the combined effect of these factors on a response. The meaning of the factorial design is that each complete trial or replications of the all-possible combinations of the levels of the factors are investigated. By using the response surface methodology and 2^3 factorial design of experiment, first and second order models have been developed with 95% confidence level. These model equations have been used to develop the response contours for different cutting conditions.

The functional relationship between response (surface roughness) of the cutting operation and the investigated independent variables can be represented by the following equation:

$$R_a = CV^k f^l d^m \qquad (2.1)$$

Where R_a is the surface roughness (μm), while V, f and d are the cutting speed (m/min), feed rate (mm/rev) and depth of cut (mm) respectively. Equation (2.1) may be written as follow:

$$\ln R_a = \ln C + k \ln V + i \ln f + m \ln d \qquad (2.2)$$

Which may represent the following linear mathematical model:

$$y = b_0 x_0 + b_1 x_1 + b_2 x_2 + b_3 x_3 + \varepsilon \qquad (2.3)$$

Where y is the measured surface roughness on a logarithm scale, ε is the experimental error and, $x_0 = 1$ (dummy variable), $x_1 = \ln V$, $x_2 = \ln f$, $x_3 = \ln d$, and b_0, b_1, b_2 and b_3 are the model parameters to be estimated. The a values are b_0, b_1, b_2 .... etc, are to be estimated by the method of least squares. The basic formula is:

$$b = (X^T X)^{-1} X^T y \qquad \mathbf{(2.4)}$$

Where the calculation matrix is X and the variance matrix is $(X^T X)^{-1} \cdot b$. Values for b are now calculated by using equation (2.4).

The 12 experiments were performed in two blocks to develop the first-order model. The first block consisted of experiments 1,4,6,7,9 and 10, while the second block consisted of experiments 2,3,5,8,11 and 12, as shown in Fig (2.8).

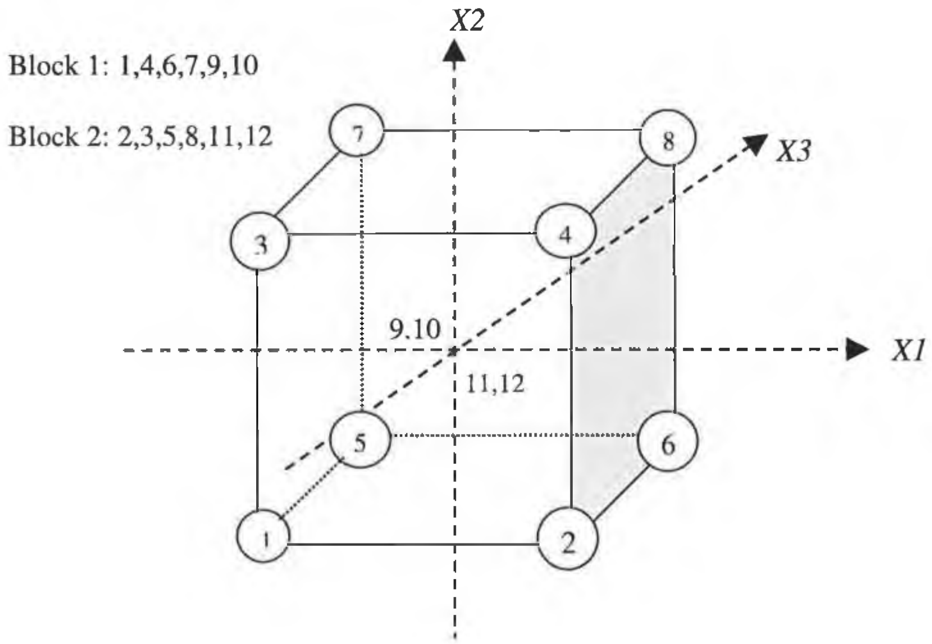

Figure 2.8 Representation of a 2^3 central composite design.

The central composite design with 12 experiments provided three levels for each independent variable. The independent variables were coded as follows:

$$x_1 = \frac{\ln V - \ln(v)_{centre}}{\ln(v)_{high} - \ln(v)_{centre}} \qquad (2.5)$$

$$x_2 = \frac{\ln F - \ln(f)_{centre}}{\ln(f)_{high} - \ln(f)_{centre}} \qquad (2.6)$$

$$x_3 = \frac{\ln D - \ln(d)_{centre}}{\ln(d)_{high} - \ln(d)_{centre}} \qquad (2.7)$$

The rate of metal removal Q (cm^3/min) is given by:

$$Q = dfV \qquad (2.8)$$

Where d is the depth of cut (mm), f is the feed (mm/rev) and V the cutting speed (mm/min). Equation (2.8) can be written as:

$$\ln Q = \ln d + \ln f + \ln V \qquad (2.9)$$

Based on [31] the surface finish was observed to improve with increase of cutting speed or depth of cut. Noticeably, the effect of depth of cut on the improvement of surface finish was more than the effect of the speed. Perhaps with greater depth of cut the material becomes more rigid and the surface finish improves. However, surface finish decreases with the increase of feed rate. It has also has been observed that the cutting force decreases with increase of speed, whilst it increases with increase of feed rate or depth of cut. The depth of cut is found to have the maximum influence on the cutting force.

Choudhury and El-Baradie [32] have developed first and second-order tool-life models at 95% confidence level for turning high strength steel. The tool life models were developed in terms of cutting speed, feed rate and depth of cut using response surface methodology and design of experiment. The effects of the main cutting variables (cutting speed, feed rate and depth of cut) on tool life were investigated by the application of the factorial design method. All of the cutting tests were performed using uncoated carbide tools under dry conditions. The relationship between the machining response (tool life) and machining independent variables can be represented by the following:

$$T = C\left(V^{l} f^{m} d^{n}\right)\varepsilon \qquad (2.10)$$

Where T is the tool life in minutes, *V*, *f*, and d are the cutting speeds (m/min), feed rate (mm/rev) and depth of cut (mm) respectively and *C, l, m, n* are constants while ε is random error. Equation (2.10) can be written in the following logarithmic form:

$$\ln T = \ln C + l \ln V + m \ln f + n \ln d + \ln \varepsilon \qquad (2.11)$$

The linear model of equation; (2.11) is:

$$y = b_0 x_0 + b_1 x_1 + b_2 x_2 + b_3 x_3 + \varepsilon \qquad (2.12)$$

The proposed relationship between tool life and independent machining variables can be described by the following equation:

$$T = 4564 V^{-1.7903} f^{-0.4883} d^{-0.1924} \qquad (2.13)$$

The equation of metal removal rate Q (cm^3/min) in logarithmic form is given by:

$$\ln Q = \ln d + \ln f + \ln V$$

The metal removal rate for specific depth of cut (0.75 mm) becomes:

$$\ln Q = 2.5004 + 0.5878 x_1 + 0.47 x_2 \qquad (2.14)$$

However the equation shows that tool life decreases with the increase of cutting speed, feed rate, and depth of cut. The cutting speed has the most effect on tool life, followed by the depth of cut and feed rate.

Summary

The definition of the term 'Machinability' presents little difficulty. It is the property of a material, which governs the ease or difficulty with which a material can be machined using a cutting tool. The literature contains work examining the effect of the workpiece material, tool geometry, tool material and other process parameters (feed rate, depth of cut and cutting speed) on the surface finish, tool life and cutting forces.

Techniques for a "Design of Experiments" approach are widely used to produce efficient experimental programmers. Response surface methodology techniques have been used to model the inter-relationship of the variables. These methods will all be used in the present study.

CHAPTER THREE:
MACHINABILITY OVERVIEW

3 MACHINABILITY OVERVIEW

3.1 Introduction

Machinability is the characteristic or behaviour of a material when it is being cut. It has been suggested that the word "machinability" was first used in the 1920s and referred specifically to the speed/tool life relationship. Now machinability is defined in a number of different ways. In general machinability can be defined as an optimal combination of following factors;

- Small cutting forces
- High tool life
- Good surface finish
- High metal removal rates
- Good surface integrity
- Good breakdown of chip
- Accurate and consistent workpiece geometrical characteristics

Although machinability generally refer to the work material, it should be recognized that machining performance depends on more than just material. The type of machining operation, tooling, and cutting conditions are also important factors, as are material properties. In addition, the machinability criterion is also a source of variation. One material may yield a longer tool life while another material provides a better surface finish. All these factors make evaluation of machinability difficult. Some of the characteristics that influence machinability are discussed in the following sections.

3.2 Factors Influencing Machinability

The machinability characteristics are defined by a number of independent factors such as the cutting conditions, workpiece properties and the tool properties.

3.2.1 Cutting Conditions

3.2.1.1 Cutting speed

Cutting speed is the important variable in the cutting operation as it directly affects the tool wear rate, surface finish cutting forces and the type of chip formed. At low speeds the material behaves in a brittle manner, with discontinuous chips and low tool wear rates, however it also results in a poor surface finish. High speeds result in continuous chips and improved surface finish but can cause high tool wear rates and low tool life. Therefore there has to be a trade off between good tool life surface finish and chip formation. The major effect of speed is on tool wear rates so efforts must be balance these factors to attain the most desired conditions.

3.2.1.2 Feed rate

Feed rate is similar to cutting speed in that it influences cutting forces, tool wear rates and to a lesser extent surface finish. An increase in feed rate results in an increase in cutting forces, tool wear rates and a poor surface finish. The surface finish produced is a direct function of the feed rate.

3.2.1.3 Depth of cut

Depth of cut has a significant affect on the cutting forces produced. A small increase in the depth of cut results in a significant increase in the cutting forces produced but only has a small effect on the tool wear rate and insignificant effect on the surface finish. Moreover the higher the depth of cut is, the greater is the power requirements.

3.2.1.4 Cutting fluid

Cutting fluid has two effects as it acts as both a coolant and a lubricant. In continuous operations its presence results in increased tool life as it removes the swarf and reduces the temperature in the cutting zone. In intermittent operations it can cause thermal cyclic loading, which can result in thermal fatigue failure [33].

3.2.2 Workpiece Factors

Machinability is all about efficient ways and means of machining a workpiece. The workpiece is the central figure of a machinability study. The workpiece factors, which influence machinability, are;

3.2.2.1 Microstructure

Microstructure refers to the arrangement of the crystals or grain structure of a metal. Metals of similar microstructure generally have similar machining properties, but small changes in microstructure can greatly affect machinability. Sections of the same bar, or of metal produced from the same 'melt' often display very wide differences in machinability owing to inclusions (particles of foreign matter) or to variations in grain structure. For good tool life the grain structure of a given batch of metal must be uniform.

3.2.2.2 Grain size

Grain size cannot be taken to indicate the likely machinability of a metal, except that a regular intermediate sized grain gives the best results. Ductile metals may have fine or coarse grain-structures, but they cut easily. However a good finish cannot easily be obtained because the chip tears away from the parent metal. Brittle material can vary in grain size and are difficult to cut but relatively easy to finish.

3.2.2.3 Metallurgical condition due to manipulation

Production operations such as drawing, rolling and forging which sometimes call for per-heating have an important influence on the final structure of a metal and therefore on its physical characteristics. The user must know the physical and thermal treatment a metal has undergone before deciding on the method of machining.

3.2.2.4 Metallurgical condition due to heat-treatment

During manufacture most metals pass through cycles of heating and cooling. Many of these cycles from an essential part of production processes, but others are carried out to refine the microstructure or to modify it to the form necessary for its eventual purpose. For instance, electrical properties can be changed, the metal can be made ductile or tough and machinability can be influenced.

3.2.2.5 Hardness

The hardness of a metal depends on many factors. For example its composition, structure and the treatment it has undergone before machining. Hardness is usually defined as a metal's resistance to indentation. An indenter made of diamond or hardened steel is pressed into the prepared surface of a metal specimen under specified conditions of load, rate of application and time. The depth or area of indention is compared with that of similar metals, to give relative hardness. The probable machinability can then be deduced. The hardness and ductility of similar metals are related, so it possible to predict from data obtained whether a metal machines easily and whether it can take a good finish. Hardness is related to strength, and therefore the hardness number also gives some indication of the cutting pressures required.

3.2.2.6 Chemical composition

The structure and mechanical properties of an alloy are determined basically by its chemical composition. Alloying elements in a metal have a strong influence on its machinability, the following are examples of some elements.

a) **Carbon** (C): Carbon steels with the best machinability have a carbon content of 0.3 to 0.6 %. Below this range the steels are too ductile and good finish is difficult to obtain. Above it they are hard and brittle and difficult to machine.

b) **Sulphur** (S): Sulphur improves the machinability of steels, and is added in controlled quantities to give free-machining steels. Normally the quantity of sulphur added is from 0.1 to 0.3 %, according to the required characteristics of the alloy, but in special cases it may be as high as 0.6%.

c) **Silicon** (Si): Machinability decreases as silicon content increases.

d) **Lead** (Pb): Lead in steels, form 0.15 to 0.35 %, gives a very good free-machining metal without affecting the basic mechanical properties.

e) **Phosphorus** (P): This element improves machinability if the content is between 0.02 and 0.06%, but the benefit is not very great.

f) **Manganese** (Mn): The effect of manganese on steel is similar to that of carbon. High manganese-content steels are hard and are difficult to machine because they work-harden. For the best machining properties the manganese content should be 0.7 % to 1.3 %. Where the carbon content is high, the manganese content should be restricted to the lower end of this range. Conversely if the carbon content is low, the manganese content may be higher.

Other elements such as chromium, vanadium, nickel and molybdenum are added to steel to improve heat-resistance, corrosion-resistance, hardness, toughness and other mechanical properties. All these elements reduce machinability, so in some cases alloys containing them must be softened by heat treatment [28].

3.2.3 Tool Properties

The requirements of a good cutting tool is it's high hardness and toughness, good wear resistance, mechanical and thermal shock resistance and the ability to maintain these properties at very high temperatures encountered during metal cutting operation [17].

Tool material and geometry must be carefully chosen in relation to the workpiece material to be machined. The main factors that affect a good cutting tool material is (i) high hardness (ii) cast alloys, (iii) cemented tungsten carbide, (iv) coated cemented carbides, (v) TiC-TiN based cermets, (vi) ceramics, (vii) polycrystalline diamond and cubic boron nitride, and (viii) single crystal diamond [14].

3.3 Workpiece Material

Modern science and technology constantly require new materials with special properties to achieve breathtaking innovations. This development centres on the improvement of scientific and technological fabrication and working procedures. That means rendering them faster, economically more favourable, and better quality. At the same time, new materials are introduced to improve our general quality of life, especially in human medicine and dentistry and daily life (housekeeping). Among all these new materials one group plays a very special role:

➢ **Glass-ceramic materials**.

Glass-ceramics offer the possibility of combining the special properties of conventional sintered ceramics with the distinctive characteristics of glasses. It is however possible to develop modern glass-ceramic materials with features unknown thus far in either ceramics or glasses or in other material such as metals or organic polymers. Furthermore, developing glass-ceramics demonstrates the advantage of combining various remarkable properties in one material [34].

Glass-ceramics are a class of ceramic material produced by conversion of glass into a polycrystalline structure through heat treatment. The proportion of crystalline phase in the final product typically ranges between 90% and 98%, with the remainder being unconverted vitreous material. Grain size is usually between 4μin and 40μin (0.1 to 1.0μm), significantly smaller than the grain size of conventional ceramics. This fine crystal microstructure makes glass-ceramics much stronger than the glasses from which they are derived. Also, due to their crystal structure, glass-ceramics are opaque (usually grey or white) rather than clear. The processing sequence for glass-ceramics is as follows: (1) The first step involves heating and forming operations used in glass working to create the desired product geometry. Glass-shaping methods are generally more economical than pressing and sintering to shape traditional and new ceramics made from powders. (2) The product is cooled. (3) The glass is reheated to a temperature sufficient to cause a dense network of crystal nuclei to form throughout the material. It is the high density of nucleation that inhibits grain growth of individual crystals, thus leading ultimately to the fine grain size in the glass-ceramic materials. The key to the intensity for nucleation is the presence of small amounts of nucleating agents in the glass composition. Common nucleating agents are TiO_2, P_2O_5, and ZrO_2. (4) Once nucleation is initiated, the heat treatment is continued at higher temperature to cause growth of the crystalline phases [17].

Several examples of glass-ceramic systems and typical compositions are listed in Table (3.1). The Li_2O-AlO_3-SiO_2 system is the most important commercially; it includes corning ware (pyroceram), the familiar product of the corning Glass Works.

Table 3.1 Several Glass-ceramic systems [17].

	Typical composition (to nearest %)							
Glass-ceramic system	**Li_2O**	**MgO**	**B_2O_3**	**K_2O**	**Al_2O_3**	**SiO_2**	**TiO_2**	**F**
Li_2O-Al_2O_3-SiO_2	3	-	-	-	18	70	5	-
MgO-Al_2O_3-SiO_2	-	13	-	-	30	47	10	-
Macor (MGC)	-	17	7	10	16	46	-	4

Mica type

MACOR	$K_{1-x}Mg_3Al_{1-x}Si_{3+x}O_{10}F_2$

Note: x <0.2

Significant advantages of glass-ceramics are (1) efficiency of processing in the glassy state, (2) close dimensional control over the final product shape, and (3) good mechanical and physical properties. Properties include high strength (stronger than glass), absence of porosity, low coefficient of thermal expansion, and high resistance to thermal shock. These properties have resulted in applications in cooking ware, heat exchangers, and missile radomes. Certain systems (for example, MgO-Al_2O_3-

SiO_2 system) are also characterized by high electrical resistance, which leads to electrical and electronics applications.

Glass-ceramics are inorganic material, generally but not necessarily silicate-based materials, which are initially prepared as glass and which, in bulk from are shaped by glass-forming techniques. They are then processed further by suitable heat-treatment to develop, firstly, nuclei in the glass and subsequently crystal phases (Mc Millan, 1979) [35].

Figure (3.1) illustrates a typical heat-treatment cycle for such a glass-ceramic with nucleation and crystallization temperature holds (more holding stages may be included as necessary to develop the required structure and properties). The heat-treatment process is so designed that the microstructure of the resultant body is one in which one or more crystal phases exist (together with a residual glassy phase) in a closely interlocking structure with mean crystal size generally in the region of 1μm. Although in some cases the mean crystal size can be considerably less (Partridge 1982).

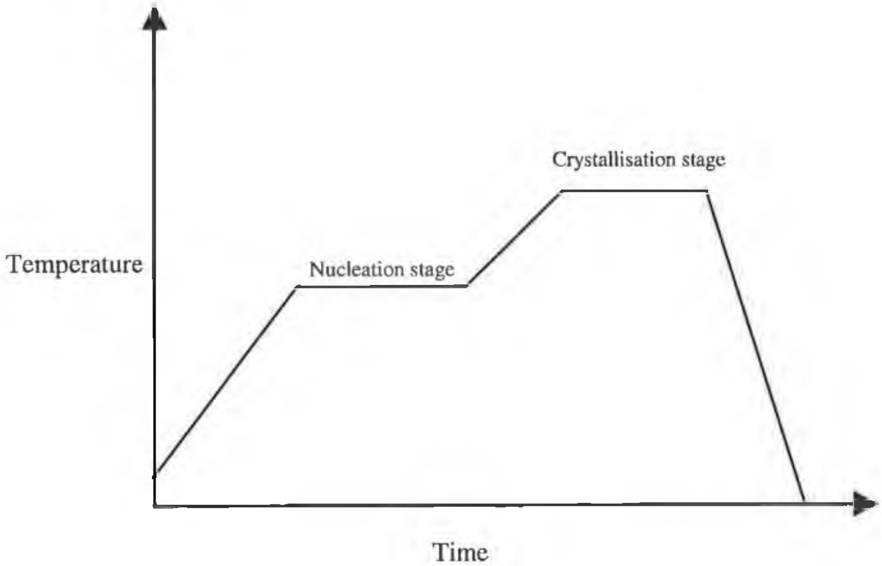

Figure 3.1 Typical heat-treatment schedules for the production of glass-ceramics showing nucleation and crystallization holding stages [35].

3.3.1 Advantages of Glass-ceramic

Glass-ceramics demonstrating particularly favourable properties were developed on the basis of two key advantages. The variation of the chemical composition and of the microstructure. These properties are listed briefly below:

3.3.1.1 Processing properties

The research on the discovery of suitable base glasses revealed that the technology used in the primary shaping of glass could also be applied to glass-ceramics. Therefore, bulk glasses are produced by rolling, casting, spin casting, or by press-blowing a glass melt or by drawing a glass rod or ring from the melt. The thin-layer method they also be used to produce thin glass sheets. In addition glass powder or grains are transformed into glass-ceramics.

3.3.1.2 Thermal properties

A particular advantage in the production of glass-ceramics is that products demonstrating almost zero shrinkage can be produced. These specific materials are produced on a large scale for industrial, technological and domestic applications (e.g., kitchenware) [34].

3.3.1.3 Optical properties

Since glass-ceramics are nonporous and usually contain a glass-phase they demonstrate a high level of translucency and in some cases even high transparency. Furthermore, it is also possible to produce very opaque glass-ceramics, depending on the type of crystal and the microstructure of the material. Glass-ceramics can be produced in virtually every colour. In addition, photo induced processes may be used to produce glass-ceramics and to shape high precision and patterned end products. Fluorescence, both visible and infrared and opalescence in glass-ceramics are also important optical characteristics.

3.3.1.4 Chemical properties

Chemical properties, ranging from resorbability to chemical stability, can be controlled according to the nature of the crystal, the glass phase or the nature of the interface between the crystal and the glass phase. As a result resorbable or chemically stable glass-ceramics can be produced. The microstructure in particular also permits the combination of resorbability of one phase and chemical stability of the other phase [34].

3.3.1.5 Biocompatibility

Biocompatible glass-ceramics have been developed for human medicine and for dentistry in particular. Furthermore, bioactive materials are used in implantology.

3.3.1.6 Mechanical properties

Although the highest flexural strength values measured for metal alloys have not yet been achieved in glass-ceramics, it has been possible to achieve flexural strengths of up to 500MPa. The toughness of glass-ceramics has also been considerably increased over the years. As a result, K_{IC} values of more than 3 $MPa.m^{0.5}$ have been reached. No other material demonstrates these properties together with translucency and allows it to be pressed or cast, without shrinking or pores developing, as in the case of monolithic glass-ceramics.

The fact that glass-ceramics can be produced as machinable materials represents an additional advantage. In other words, by first processing the glass melt, a primary shape is given to the material. Next, glass-ceramic is provided with a relatively simple final shape by drilling, milling, grinding or sawing. Furthermore, the surface characteristics of glass-ceramics, for example, roughness, polishability, lustre or abrasion behaviour can also be controlled.

3.3.1.7 Electrical and magnetic properties

Glass-ceramics with special electrical or magnetic properties can also be produced. The electrical properties are particularly important if the material is used for isolators in the electronics or microelectronics industry. It must also be noted that useful composites can be formed by combining glass-ceramics with other materials. For example, metal. In addition, glass-ceramics demonstrating high ion conductivity and even superconductivity have been developed. Furthermore, magnetic properties in glass-ceramics were produced similarly to those in sintered ceramics. These materials are processed according to methods involving primary shaping of base glasses followed by thermal treatment for crystallization [34].

3.3.2 Advanced Glass-ceramic Materials

The advanced glass-ceramic materials division category deals with advanced ceramic materials including:

- Macor (MGC)

Machinable glass-ceramic (Macor) is an outstanding engineering material and is machinable with ordinary metalworking tools. Macor is also a problem solving material combining the performance of a technical ceramic with the versatility of high performance plastic. We say sometimes 'ceramic-like' because Macor is neither a glass nor a ceramic, but has properties similar to each family of materials, being an electrical and thermal insulator, a material which is good at high temperature and in corrosive environments, being of relatively low density while being brittle rather than ductile [36].

- Shapal

Shapal is a machinable form of Aluminium nitride ceramic with excellent mechanical strength and thermal conductivity. Shapal has unique characteristics. It is suitable for a wide range of applications, particularly in the vacuum and nuclear industries. It has zero porosity, good abilities to seal under vacuum, low thermal expansion coupled with a high heat resistance. Shapal also offers excellent machinability with conventional machine tools.

- Boron Nitride

Boron Nitride is a unique material. It offers outstanding thermal conductivity, excellent dielectric strength, and very good thermal shock resistance and is easily machinable. This material is an advanced synthetic ceramic available in powder solid, liquid and aerosol spray forms. In an oxidizing atmosphere it can be used up to 900°C. However, in an inert atmosphere some grades can be used as high as 3000°C. Grades are available with a very low porosity and ultra high strength for use in semiconductor processing applications.

- Alumina

Alumina is a very hard material, which is suitable for use in a great deal of applications. Alumina is a very popular material, one of the most common ceramics and is available in a range of purities to suit individual applications. Alumina is very hard wearing, has excellent electrical properties and zero porosity. Alumina is used for high temperature, wear resistant components. It is very suitable for use in a vacuum environment. Alumina has very low out gassing and is stable at high temperatures. It can be machined with diamond grinding and laser cutting and can be printed using thin or thick film technology which makes it ideal for use in the electronic industries. It can also be hermetically sealed with pin connectors using a glass frit [36].

- Zirconia

Zirconia is the strongest and toughest of all the advanced ceramic materials at room temperature. It has similar properties to Alumina, however Zirconia is a much tougher material with greater wear capabilities. Zirconia is suitable for applications including pistons, knife blades, bearings and pump shafts etc.

- Silicon Carbide

Silicon carbide is an extremely hard material with the highest corrosion resistance of all advanced ceramic materials. It retains its strength at temperatures as high as 1400°C. The material has a high level of resistance to wear and excellent resistance to thermal shock. This material is suitable for use as mechanical seals, nozzles, silicon wafer polishing plates and in particular pump parts due to its ability to be machined to high level of accuracy achieving very good surface finishes [36].

- Silicon Nitride

Silicon Nitride has excellent resistance to thermal shock. It also offers a good combination of low density, very high strength, low thermal expansion and good corrosion resistance. The material also has a high level of fracture toughness. With this combination of properties, Silicon nitride is very suitable for use in the molten metal industry for use as riser tubes, processing parts, various aerospace and automotive engine components, papermaking machine wear surfaces and burner nozzles [36].

Silicon Nitride is available in both reaction-bonded form and sintered form. These materials are lightweight, have very high strength, toughness and resistance to fatigue. They have superior thermal shock behaviour and excellent wear resistance. The offer a low coefficient of friction against steel which makes the materials particularly good for bearing applications. The materials both offer good resistance to oxidation at high temperatures and exceptional chemical corrosion resistance to acid or alkaline solutions and non-ferrous molten metals [36].

➢ Quartz

Quartz is a hard glassy like material that can be joined together to make complex shapes and components. It has a very high working temperature and commonly is used in vacuum applications as view ports, bell jars and wafer holders. Quartz is transparent and colourless when pure. Quartz is a very important industrial material and many useful applications exist for it. It's piezoelectric properties are widely used in electronics as pressure sensors and oscillators. Quartz is the raw material used in the manufacture of silicon carbide, a widely used industrial abrasive. The material is resistant to most materials and easy to clean after deposition processes.

➢ Sapphire

Sapphire offers excellent mechanical properties, chemical stability and light transmission. These characteristics make it an ideal material for applications such as POS scanner windows, microwave plasma tubes, thin-film substrates and various opto-electronic and mechanical components [36].

In this work Macor and Hot Pressed Boron Nitride will be the workpiece materials, therefore more information will be presented in details.

3.3.3 Machinable Glass-ceramics; Macor®

Machinable glass-ceramics are based on internally nucleated fluoromica crystals in glass (Beall 1971a). One commercial product has been marketed for 20 years under the trademark MACOR® and has found wide application in such diverse and speciality areas as precision electrical insulators, vacuum feed-through, windows for microwave-type parts, samples holders for field-ion microscopes, seismograph bobbins, gamma-ray telescope frames and boundary retainers on the space shuttle. The precision machinability of the MACOR® material with conventional metalworking tools, combined with high dielectric strength (~40 KV/nm) and very low helium permeation rates are particularly important in high-vacuum applications.

Although the MACOR® glass-ceramic is based on the fluorine-phlogopite phase ($KMg_3AlSi_3O_{10}F_2$) this stoichiometry does not form a glass. The bulk composition had to be altered largely through additions of B_2O_3 and SiO_2 to form a stable although opalized glass (Table 3.1). The parent glass is composed of a dispersion of aluminosilicate droplets in a magnesium-rich matrix (chyung et al., 1974). The crystallization begins near 650°C when a metastable phase chondrodite, ($2Mg_2SiO_4{\cdot}MgF_2$) forms in the magnesium-rich matrix at the interfaces to norbergite, ($Mg_2SiO_4{\cdot}MgF_2$) which finally react with the components in the residual glass to produce fluorphlogopite mica and minor mullite [34].

$$\underset{}{Mg_2SiO_4{\cdot}MgF_2} + \underset{\text{(Glass)}}{KAlSi_2O_6} \rightarrow KMg_3AlSi_3O_{10}F_2$$

$KAlSi_2O_6$ represents the glassy droplet phase having near leucite composition.
The mica grows in a preferred lateral direction because the residual glass is fluidised by the B_2O_3 flux and is also designed to be deficient in the cross-linking species potassium. The thermal, electrical, mechanical and chemical properties of the glass-ceramic (Macor) are shown in Table (3.2). These properties are particularly important for applications in the manufacture of equipment and installations, as well as in the very demanding aerospace and aeronautical industries. In particular the following industrial applications of MACOR® glass-ceramics in high-performance fields must be mentioned.

- **Aerospace industry**

More than 200 special parts of the U.S. space shuttle orbiter are made of this glass-ceramic. These parts include rings at all hinge points, windows and doors.

- **Medical equipment**

The accurate machinability of the material as well as it's inert character is particularly important in the production of specialized medical equipment.

- **Ultrahigh applications**

MACOR® glass-ceramics make excellent insulators. They are widely used to manufacture equipment for vacuum technology. Compared with sintered ceramics, glass-ceramics are pore-free.

- **Welding**

MACOR® is used in welding equipment as the material exhibits excellent no wetting properties with regard to oxyacetylene.

- **Fixtures**

MACOR is used as an electrode support and burner block in several industrial high heat, electrical cutting operations due to its low thermal conductivity and excellent electrical properties.

- **Nuclear-related experiments**

MACOR® is not dimensionally affected by irradiation. As a result, applications in this field are possible.
This wide spectrum of application as a high-performance material demonstrates the importance of MACOR® glass-ceramics in technology and medicine. Further potential applications must be considered.

- **Machining**

Machining tolerances are up to 0.13mm. MACOR MGC can be machined to a surface finish of less than 0.5 micron and polished to a smoothness of 0.013 micron. Configurations are limited only by available equipment and the experience of the machinist. Key factors for successful machining are proper machine speeds and coolant.
MACOR MGC can be machined with high-speed steel tools, but carbide tools are recommended for longer wear. For very fine pitch work, diamond tools may be more suitable. A water-soluble coolant especially formulated for cutting and grinding glass or ceramics should be used. No post firing is required after machining.

- **Sealing, joining and metalising**

MACOR can also be joined or sealed-both to itself and to other materials-in a number of ways. Metalised parts can be soldered together and brazing has proved to be effective method of joining the material to various metals. Epoxy produces a strong joint and sealing glass create a vacuum tight seal. Even a straightforward mechanical joint is possible. It can be thick film metalised using metal inks or thin film metalised by sputtering [36].

Table 3.2 MACOR® Specifications

Composition	Glass-ceramic, 55% mica crystal, 45% matrix glass
Density	2.52 g/cm^3
Porosity	0
Hardness	144 HB
Maximum use temperature	1000° C, 1832° F, no load
Coefficient of thermal expansion	94×10^{-7} in/in ° C, 52×10^{-7} in/in ° F
Compressive strength	50,000 psi
Flexural strength	15,000 psi
Dielectric strength	1000 volts-mil
Volume resistively	> 10^{16} ohm-cm

3.3.4 Hot Pressed Boron Nitride; BN

Boron nitride is a synthetic material, which although discovered in the early 19th century was not developed as a commercial material until the latter half of the 20th century. Boron and Nitrogen are neighbours of carbon in the periodic table. In combination boron and nitrogen have the same number of outer shell electrons and the atomic radii of Boron and Nitrogen are similar to that of Carbon. It is not surprising therefore that boron nitride and carbon exhibit similarity in their crystalline structure.

Boron nitride is a unique engineering material. It is a soft, machinable ceramic, which can be combined with other refractory ceramics including Aluminium oxide, Silicon nitride and Aluminium nitride. It offers outstanding thermal conductivity, excellent dielectric strength and very good thermal shock resistance and is easily machinable. This material is advanced synthetic ceramic available in powder, solid, liquid and aerosol spray forms. In an oxidizing atmosphere it can be used up to 900°C. However, in an inert atmosphere Boron nitride can be used as high as 3000°C. Most molten metals do not wet Boron nitride, which makes it suitable for use in the metal processing industry. The thermal, electrical, mechanical and chemical properties of Boron nitride are shown in Table (3.3).

3.3.4.1 Preparation and manufacturing processes

Boron nitride is manufactured using hot pressing or pyrolytic deposition techniques. These processes cause orientation of the hexagonal crystals resulting in varying degrees of anisotropy. There is one pyrolytic technique that forms a random crystal orientation and an isotropic body, however the density is only 50% to 60% of theoretical. Both manufacturing techniques yield high purity (greater than 99%) Boron nitride. The major impurity in the hot pressed materials is Boric oxide, which tends to hydrolyse in the presence of water degrading dielectric and thermal shock properties. The addition of CaO to tie up the borate minimizes the water absorption. Hexagonal hot pressed BN is available in a variety of sizes and shapes while the pyrolytic hexagonal material is currently available in thin wall, generally less than 1mm geometry only [37].

3.3.4.2 Chemical properties

- Boron nitride will oxidize above 1100°C, forming a thing boric acid layer on its surface that prevents further oxidation as long as it coats the BN.
- BN is stable in reducing atmospheres or up to 1650°C. However, it starts decomposing at above 1500°C.
- BN has high thermal conductivity, ease of machining, excellent electrical insulating characteristics, inertness and non-toxicity.

Table 3.3 Hot Pressed Boron Nitride (BN) Specifications

Chemical Composition (wt %)	
Boron + Nitrogen	> 99.0
Boron	> 42.6
Nitrogen	> 55.9
Oxygen	< 0.5
Boric Acid (sol.)	< 0.1
Carbon	<0.05
Metallic Impurities	<0.1 total
Physical Properties	
Density	2.21 g/cm^3
Bending Strength (4 point)	44Mpa
Compressive Strength	120Mpa
Young's Modulus	50Gpa
Poisson's Ratio	0.23
Thermal Properties	
Coefficient of Thermal Expansion	
20°C - 500°C	4.6×10^{-6}/K
500°C - 1000°C	6.7×10^{-6}/K
Thermal Conductivity	
20°C	49 W/mK
800°C	28 W/mK
Specific Heat	1.96 J/gK
Max. Recommended Operating Temperature	
In Air	1000°C
In Nitrogen	2900°C
In Vacuum	2200°C
Electrical Properties	
Specific Electrical Resistivity	
20°C (Ω. cm)	5×10^{12} .cm

3.3.4.3 Typical applications of Boron nitride

- Electronic parts – heat sinks, substrates, coil forms, prototypes
- Boron doping wafers in silicon semiconductor processing
- Nuclear applications (has a high neutron capture cross section)
- Vacuum melting crucibles
- CVD crucibles
- Microcircuit packaging
- High precision sealing, brazing, and metallizing fixtures
- Microwave tubes
- Horizontal caster break rings
- Plasma arc insulators
- High temperature furnace fixtures and supports.

3.3.5 Future Direction

Since the discovery of glass-ceramics in the 1950s the major applications have been in fields where thermo mechanical properties (strength, low CTE, thermal stability) are most critical. These include missile nose cones (radomes), then cookware, tableware, stovetops and electronic packaging. Each of these applications also required secondary properties of considerable diversity. For example, radomes must be transparent to microwaves, kitchenware must be chemically durable, stovetops are transparent to aenear-infrared radiation and electronic packaging materials must have low dielectric constants and losses.

In recent years there has been an increasing interest in glass-ceramic applications where optical properties are key. A parallel but unrelated trend involves the use of glass-ceramics as dental and surgical prostheses. In the optical area the most significant properties are luminescence in the near infrared range in combination with excellent transparency. Efficient broadband luminescence in crystallites is the basis of applications such as tuneable lasers and optical amplifiers, both of which can be made in both bulk and fiber form as glass-ceramics.

Dental biomaterials and surgical implants require different properties. Aesthetic appearance, good durability and good mechanical properties at ambient temperatures are critical to the former, while biocompatibility and flexural strength are essential to the latter. Dental biomaterials are continually developed to satisfy the demands of patients, dentists and dental technicians.

We foresee a dramatic increase in technical interest and applications in both optical and biological areas over the next few decades. There will also be continual application of glass-ceramics in traditional areas, although with less growth. Then there are always unexpected applications, which may surface and require an entirely new combination of material properties. In any event the wide range of potential properties combined with the flexibility of high-speed hot glass forming and the intricacy of shape associated with powder and extrusion processing will ensure the continued growth of glass-ceramic technology [34].

Summary

This chapter covered a general overview of machinability and includes the factors, which influence Machinability such as cutting conditions (cutting speed, feed rate, depth of cut and cutting fluid) and workpiece factors such as (microstructure, hardness and chemical composition). It also described the workpiece materials, and the chemical and mechanical properties of the workpiece material used for the tests are discussed in this chapter.

CHAPTER FOUR:
MACHINABILITY ASSESSMENT

4 MACHINABILITY ASSESSMENT

Generally the Machinability of a material is assessmed by investigating one or all of the following parameters:

1. **Tool life**
2. **Tool wear**
3. **Cutting force**
4. **Surface finish**

4.1 Tool Life

Tool life is one of the most important factors in the assessment of Machinability. Specifically, the manufacturing engineer needs to know the relation of tool life to cutting speeds, feeds of rate and the other pertinent machining parameters. For production operations, tool life is usually expressed as the number of pieces machined per tool grind. In machinability testing, tool life is generally defined as the cutting time in minutes to produce a given wear-land for a set of machining conditions. This cutting time can be converted to cubic inches of metal removed for a given depth of cut.

Turning tests usually are used for evaluating the Machinability of a material in terms of tool life. This operation is used because of the simplicity of the cutting tool. In addition, all of the machining conditions, such as cutting speed, feed rate, tool geometry, tool material and cutting fluid, can be readily controlled. By varying one of the machining conditions and keeping the others constant, it is possible to determine the effect of such a change on tool life [38].

4.1.1 Tool life Criteria

The type of wear and the tool life criterion should be reported. If it is not clear which type of wear will preponderate, all relevant wear measurements should be taken. In some circumstances the criterion will change with changes in cutting speed and this will result in a broken cutting speed-tool life curve as shown in Figure (4.1).

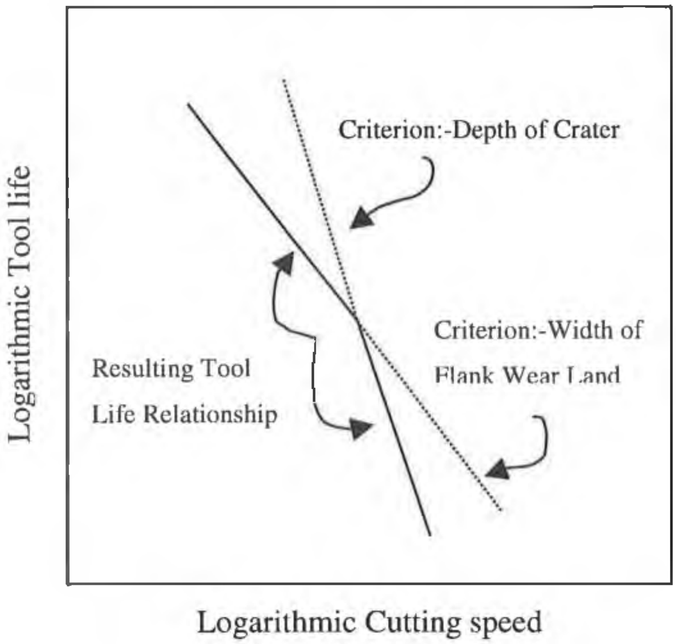

Figure 4.1 Cutting speed-tool life curves for combined flank and crater wear [39].

For high speed-steel tools three criteria of tool failure are usually used and these are:

1. Catastrophic failure.
2. If the flank wear is even the average flank wear land width is 0.3 mm.
3. If the flank wear land is irregular, scratched, chipped or badly grooved, the maximum flank wear land width is 0.6 mm.

Of these, by far the most common criterion is that of catastrophic failure. For cemented carbide cutting tools three criteria of tool failure are usually used and these are:

1. If the flank wear is even the average flank wear land width is 0.3 mm.
2. If the flank wear land is irregular, scratched, chipped or badly grooved the maximum flank wear land width is 0.6 mm.
3. A crater depth of $(0.06 + 0.3f)$ mm where f is the feed rate in millimetres per revolution.

Of these, by far the most general criterion is flank wear and usually an average wear land of 0.3 mm. The general exception to this is machining cast irons at high speed when, often, the tool failure mode is cratering. For ceramic tools three criteria of tool failure are normally used and these are:

1. Catastrophic failure.

2. If the flank wear is even the average flank wear land width is 0.3 mm.
3. If the flank wear land is irregular, scratched, chipped or badly grooved the maximum flank wear land width of 0.6 mm.

The various types of wear are illustrated in Figure (4.2)

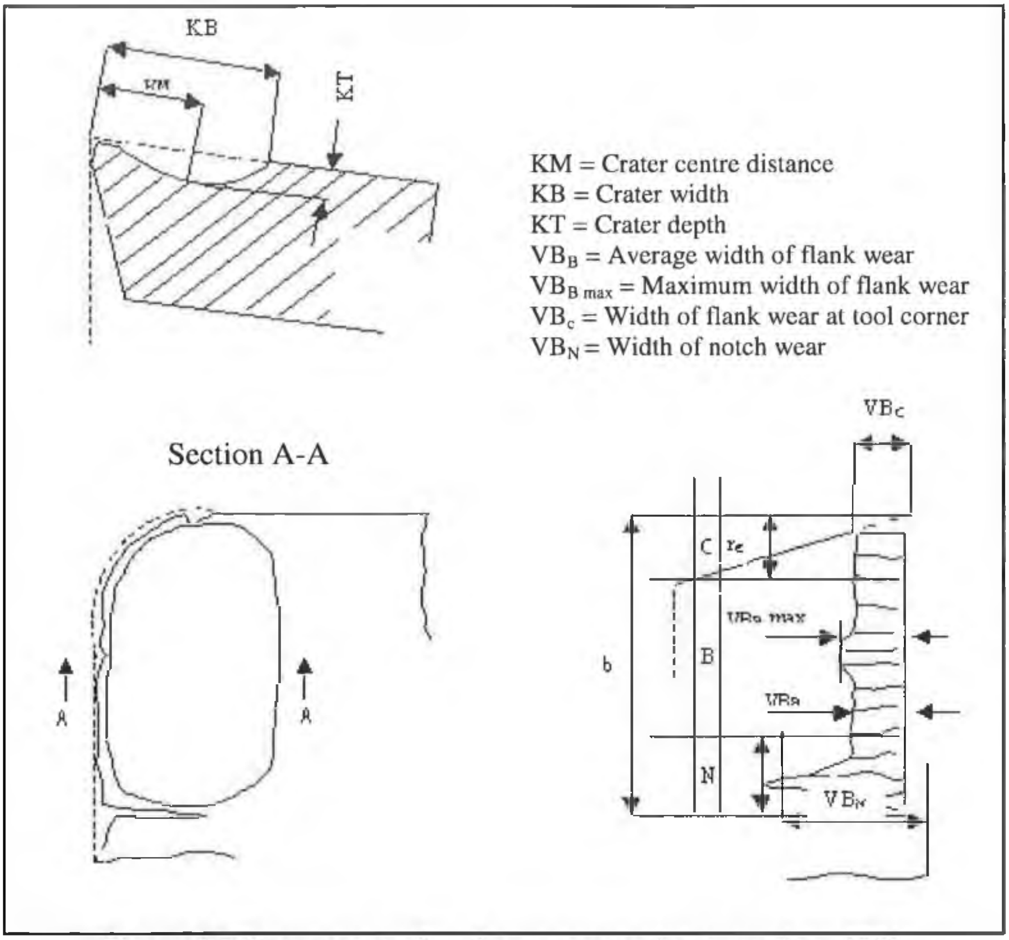

Figure 4.2 Some types of tool wear on turning operations [39].

Other wear phenomena such as notch wear, wear of the minor flank, plastic deformation of the tool corner, and edge chipping may occur in practise but all of these eventually result in one of the preferred criteria being valid and this criterion should be used. In the unusual case of premature failure of the tool which is invariably caused by a 'hard spot' in the workpiece material, a machine malfunction or unduly severe cutting conditions, tool failure is unpredictable and values obtained should never be used to determine the tool life [39].

4.1.2 Tool life and Temperature Relationship

It has been known for many years that as the tool temperature increases, the tool life reduces. The relationship between the tool life and temperature is of the form

$$\theta\, T^n = C_3$$

Where θ is some measure of tool temperature; and n and C_3 are constants for the tool-workpiece combination. The temperature can be measured in a variety of ways but the most common method uses a work-tool thermocouple, i.e. a device that uses the dissimilar material junction between the tool and the workpiece as a means of generating an e.m.f. Which is proportional to the temperature of the junction, but since the junction temperature will vary considerably from place to place along the junction it is not easy to say exactly what is being measured. However, it has been found that the temperature as recorded by a work-tool thermocouple when used to plot a θ-T relationship gives good results. Typically, the exponent n in this relationship is between 0.05 and 0.1 and this indicates how critically cutting temperature affects tool life [39].

4.2 Tool Wear

The wear mechanisms include abrasive and adhesive wear, diffusion wear, wear arising from electrochemical action, and surface fatigue wear. Section 4.2.1 gives a brief summary of these wear mechanisms.

4.2.1 Mechanisms of Wear

1. Wear by Abrasion

The most common type of tool wear is that of abrasion where the relative motion between the underside of the chip and the face and the newly cut surface and the flank causes the tool to wear even though the newly cut workpiece surface and the chip may be very much softer than the tool material. In many cases, however, even though the workpiece and the chip may be relatively soft, hard inclusions or precipitates arising from the manufacturing process or from heat treatment will be present in the workpiece. Hard particles may also result from the breaking down of heavily work-hardened, unstable built-up-edges. Abrasive wear normally causes the improvement of a flat on the flank face and a crater on the face of the tool. Hard inclusions having sharp edges produce micro cutting and give higher wear rates than hard, smooth, spherical inclusions which tend to groove the surface by plastic deformation rather than produce abrasive wear particles as shows in figure (4.3)

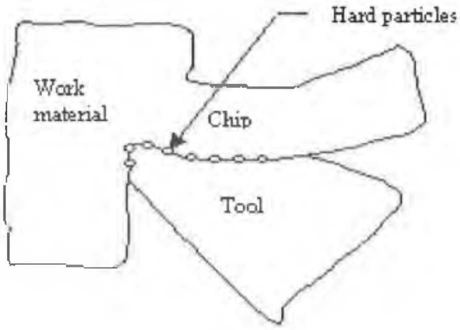

Figure 4.3 Abrasive Wear

2. Wear by Adhesion

As has already been mentioned, pressure welding exists between the face of the tool and the underside of the chip under all cutting conditions. For those conditions where only a built-up-layer or a stable built-up-edge is present, although adhesion will occur, it will not result in the removal of tool material. However, when an unstable built-up-edge occurs, as well as particles of built-up-edge causing abrasive wear, it is likely that when the built-up-edge detaches itself from the face it will carry with it small quantities of tool material if strong bonding occurs between the built-up-edge and the tool material. Thus adhesive wear is primarily a wear mechanism on the face of the tool and usually occurs at low cutting speeds when an unstable built-up-edge is likely to be present as shows in figure (4.4).

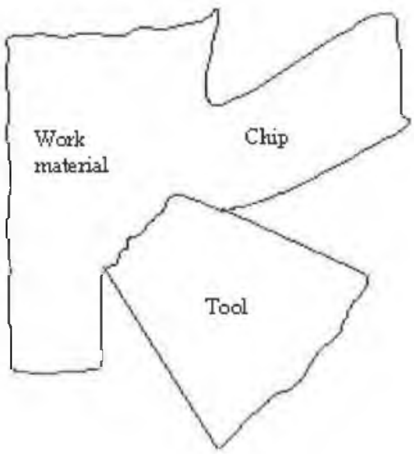

Figure 4.4 Adhesive wear

3. Wear by Diffusion

Diffusion between cemented carbides and steel workpiece materials occurs at high cutting speeds and is a strongly temperature-dependent process in which atoms diffuse in the direction opposite to the concentration gradient (Fick's first law).
Opitz and Konig [40] have shown that under the static conditions which occur in the seizure region on the face of a cutting tool, cobalt will diffuse into the steel. With the binding element removed a low shear strength layer exists on the surface of the tool, which is transported from the tool by the underside of the chip.
Trent [7] has shown that additions of titanium carbide (TiC) and tantalum carbide (TaC) reduce cratering wear by diffusion since they modify the structure of the tungsten carbide (WC) grains and this lowers their solubility in the workpiece.

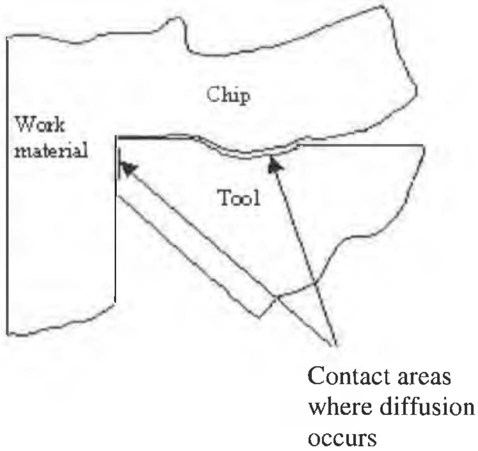

Figure 4.5 Shows wear by diffusion

4. Wear by Electrochemical Action

Under appropriate conditions, normally caused by the presence of a cutting fluid, it is possible to set up an electrochemical reaction between the tool and the workpiece, which result in the formation of a weak low shear strength layer on the face of the tool. While this is usually a desirable effect because it reduces the friction force acting on the tool, which results in a reduction in the cutting forces and hence cutting temperatures, it will also typically result in small amounts of tool material being carried away by the chip. If the overall wear pattern is studied it is probably that the reduction in abrasive and, to some extent, adhesive wear which result from the action of the cutting fluid in reducing temperature and friction, respectively, will more than compensate for the small amounts of wear which occur due to electrochemical action. In addition to the wear processes described above, tool material is sometimes removed by other mechanisms- the three most common being brittle fracture, edge chipping, and plastic deformation of the tool. Brittle fracture and edge chipping cause relatively large amounts of tool material to be removed whereas plastic deformation of the tool results in an adverse change in tool geometry which causes severe wear, usually on the tool flank [39].

Brittle fracture often causes a large portion of tool material to become detached from the tool this results in instantaneous tool failure. This type of failure is normally associated with either extremely high forces acting on the tool due to the use of excessive feeds rate and /or depths of cut, or is due to the complex stress distribution set up in the tool under certain cutting conditions. If good metal cutting practice is adopted, the former should never result in failure since it should be possible to reduce the feed rate and/or depth of cut or to suitably strengthen the tool. The latter is normally associated with the cutting of high strength materials with carbide cutting tools and it has been shown in Ellis and Barrow study [41] that as the flank wear land starts to develop the stress pattern in the tool is modified until, even with a relatively small flank wear land, tensile stresses are set up within the tool. Since the tool is weak in tension this will often result in tool failure. Edge chipping is a common wear phenomenon in intermittent cutting operations where cyclic mechanical and thermal stresses are applied to the tool; this results in fine cracks developing near to the cutting edge and flaking of tool material. Plastic deformation of the cutting edge, particularly the tool corner, is caused by high temperatures and stresses and is therefore primarily a high cutting speed effect in which high tool temperatures are generated.

5. Wear by fatigue

Fatigue wear is only an important wear mechanism when adhesive and abrasive wear rates are small. Surfaces, which are repeatedly subjected to loading and unloading, may gradually fail by fatigue leading to detachment of portions of the surface. This condition can arise in intermittent cutting, which may also cause edge chipping. Nucleation of subsurface fatigue cracks may be initiated at subsurface defects such as non-metallic inclusions. Fatigue cracking does not normally occur if the stress is below a certain limit. Since the contact pressures are determined by the yield properties of the workpiece material, using cutting tools, which are appreciably harder than the workpiece, can reduce fatigue [39].

4.2.2 Tool Wear and Time Relationship

For progressive flank wear the relationship between tool wear and time follows a fixed pattern. Initially, with a new tool, the tool wear rate is high is referred to as primary wear. The time for which this wear rate acts is dependent on the cutting conditions but, typically, for a given workpiece material, the amount of primary wear is approximately constant but the time to produce it decreases as the cutting speed is increased. This wear stage is followed by the secondary wear stage where the rate of increase of flank wear is sensibly constant but considerably less than the rate of primary wear in the practical cutting speed range. At the end of the secondary wear stage, when the flank wear is usually considerable and far greater than that recommended as the criterion for tool failure, the conditions are such that a second rapid wear rate phase commences (tertiary wear) and this, if continued, rapidly leads to tool failure. The three stages of wear are illustrated in figure (4.6). It is often suggested that the high rate of wear in the primary wear stage is due to edge crumbling and is not typical of a 'worn-in' tool. However, it has been suggested in the Redford study [42], that it is not the primary wear rate, which is large for the tool-workpiece combination, but that the reduced secondary wear rate is a consequence of the protection afforded to the tool by the small stable built-up-edge, which forms as the edge is removed from the tool.

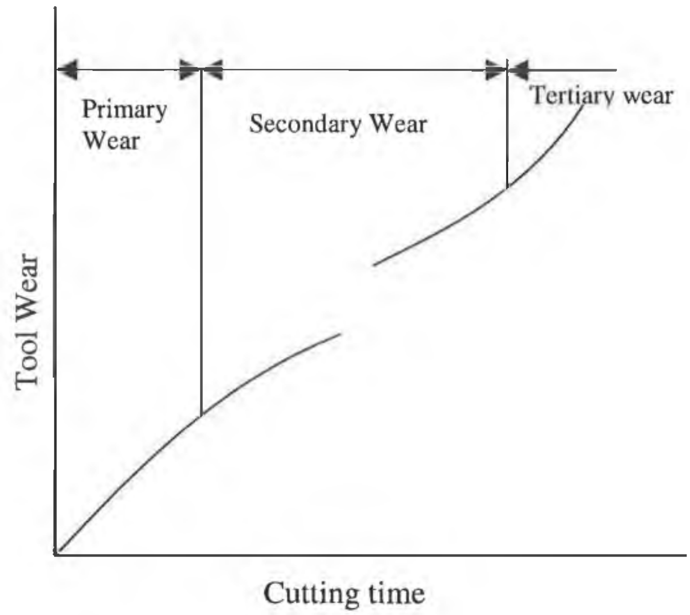

Figure 4.6 Typical relationship between flank wear and cutting time [39].

Crater wear, normally measured in terms of the depth of the crater, increases progressively with time until a point is reached when the crater weakens the tool sufficiently for the forces acting on the tool to fracture it. Thus the criterion for tool failure due to crater wear is based on a crater depth of a constant amount plus a further amount, which is proportional to the feed. Catastrophic failure of high-speed-steel tools is merely an extension of the flank wear criterion for carbides and follows the same type of relationship with time. All other forms of wear which result in rapid deterioration of the tool are often difficult to relate to time in a meaningful manner since the tool can fail when there is little or no wear and this can often be due to a transient condition in what is basically a steady-state operation.

4.2.3 Tool Wear and Cutting Conditions Relationship

F.W. Taylor in his study [43] suggested that for progressive wear, the relationship between the time to tool failure for a given wear criterion and cutting speed was of the form:

$$VT^{-1/k} = C_1$$

Where V is the cutting speed T is the tool life k and C_1 are constants for the tool workpiece combination. This basic relationship has been tested repeatedly for a wide range of tool and workpiece materials and cutting conditions and, except at very low or very high cutting speeds and provided the tool failure criterion does not change, has been found to be valid. The equation was later extended to the more general form

$$T = \frac{C_2}{v^p f^q d^r}$$

Where f is feed d is the depth of cut and p, q, r and C_2 are constants for the tool workpiece combination.

Considering the major variables of speed, feed rate and depth of cut, in general, by far the most significant is cutting speed where for modern carbide cutting tools p will be of the order of 2 to 4 and for high-speed-steel cutting tools will lie between 4 and 7. In contrast to this, q will usually be unity or less and r, the constant associated with depth of cut, will often be vary small and negative, i.e. as the depth of cut is increased, the tool life tends to increase slightly.

4.2.4 Tool Wear Measurement

Parts adhering to the flank directly under the wear land can give the appearance of a large width to the wear land. Also, a deposit in the crater results in lower values of the crater depth. Loose material should be removed carefully but chemical etchants should not be used except at the end of the test. For the purpose of the wear measurements the major cutting edge is considered to be divided into three regions as shown in figure (4.2).

Region C is the curved part of the cutting edge at the tool corner region N is the quarter of the worn cutting edge length b farthest away from the tool corner and region B is the remaining straight part of the cutting edge between region C and region N.

The width of the flank wear land VB_B should be measured within region B in the tool cutting edge plane perpendicular to the major cutting edge. The width of the flank wear land should be measured from the position of the original major cutting edge. The crater depth KT should be measured as the maximum distance between the crater bottom and the original face in region B [39].

4.3 Cutting Force

Another method of determining the machinability characteristics of a given work material is to carry out cutting force tests. Knowledge of these forces is useful for a variety of reasons. For example, knowledge of the power requirement and the forces acting on a cutting tool is desirable in both the design and selection of machine tools. In the general case, the force system acting on a cutting tool is three-dimensional. With the resultant force on the tool being made up of three components (one component per axis). However, it must be noted that the magnitude of the forces in metal cutting is small when compared to those encountered in metal-forming processes such as extrusion, wire drawing or forging. This is due to the small area being cut at any one instant. The forces measured are normally in the magnitude of a few hundred Newton's [44].

An understanding of the forces and velocities, which occur during the various cutting processes, is the essential basis for determining the size and material of load transmitting elements together with the required driving power.

The total force involved in a single-point turning operation can be divided into three components: tangential force, feed force (axial) and radial force (thrust) figure (2.2) chapter (2). Tangential force, the largest, is the one normally used in calculations of power consumption. This force tends to deflect the tool vertically. If the toque by the machine fluctuates, the tangential force also fluctuates, and these sets up tool vibrations, which cause chatter marks and in turn spoil the surface, finish and militate against accuracy. Vibration is especially undesirable when carbide or ceramic tools are used because these extremely brittle materials can shatter. Although some vibration will always be present it can be virtually eliminated by minimizing overhang of the tool. If vibration persists despite all practical efforts at elimination, tangential force must be reduced. This can be done by removing less metal per unit of time by reducing the feed rate, depth of cut or cutting speed. The feed force (axial) acts along the direction of the tool feed. This force is usually about 15% to 50% of the tangential force but accounts for only a small percentage of the power required. The feed force together with the feed velocity determines the power required for the feed drive.

The radial force acts perpendicular to the turned surface. This force is about 30% to 50% of the feed force and contributes very little to power requirements because the velocity in the radial direction is negligible.

4.3.1 Effect of Rake on Cutting Force

Tangential force is greatly influenced by rake angle. Negative rake imposes a penalty in terms of higher tangential force, so almost invariably it is better to use the maximum positive rake consistent with tool strength. Exceptions to this recommendation occur in instances such as the machining of Nimonics and where ‘throw-away’ carbide tips are used [28].

4.3.2 Effect of Feed on Cutting Force

Increased feed rate has a better effect on tangential cutting force, in terms of metal removal, than increased depth of cut or cutting speed. If the depth of cut or the speed is doubled, the power required is doubled, but if the feed rate is doubled, the power required is increased by only 60-70%. When speed is increased, however, the tangential force on the tool decreases but the tendency to vibration and chatter may rise [28].

4.4 Surface finish

In every machined surface, the term used to define its geometrical quality is known as surface roughness. Surface roughness refers to a property of machined surface. Roughness of surface is that part of surface finish (surface texture) which can be defined as the marks left by the action of the production process used, such as turning operation.

Roughness of surface consist of relatively closed-speed or fine surface irregularities usually in the form of feed marks left by the cutting tool on the machined surface. It is measured by the heights of the irregularities with respect to a reference line. The surface texture of a machined surface consists of primary texture (roughness) and secondary texture. The primary texture can be measured by various constants as shown in figure (4.7) such as average arithmetic roughness height Ra, smoothening depth Rp, maximum roughness Rt, and root-mean-square RMS height [45].

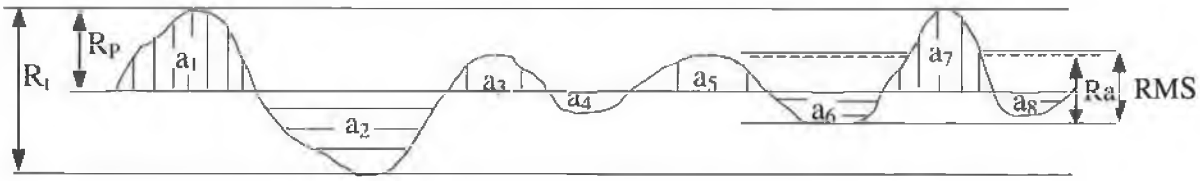

Figure 4.7 The various parameters R_a, R_p, R_t and RMS are illustrated [17].

With the exception of RMS these various constants (Ra, Rp, Rt) are commonly used. The index most commonly used is the arithmetic roughness height Ra. The secondary texture is that part of the surface texture which underlies the roughness. All types of machine vibrations, occurrence of built-up-edge and inaccuracies in the machine tool movement may contribute to secondary texture.

The smoothening depth Rp, is the distance between the highest point and the mean line. Rp generally results from the condition of the cutting tool such as a lathe tool or grinding wheel. The maximum peak to valley height within the tracing stroke of a surface profile is known as Rt. The RMS is average geometric roughness and is an American standard. Its numerical value is some 11% higher than that of Ra.

Turning: when chip formation occurs without a built-up edge the tool profile is etched or reproduced on the machined surface figure 4.8. The geometry of feed-marks depends on feed rate, side-cutting edge angle, nose radius and end-cutting edge angle. In Figure (4.8) the tool has a sharp corner i.e. nose radius is nearly zero.

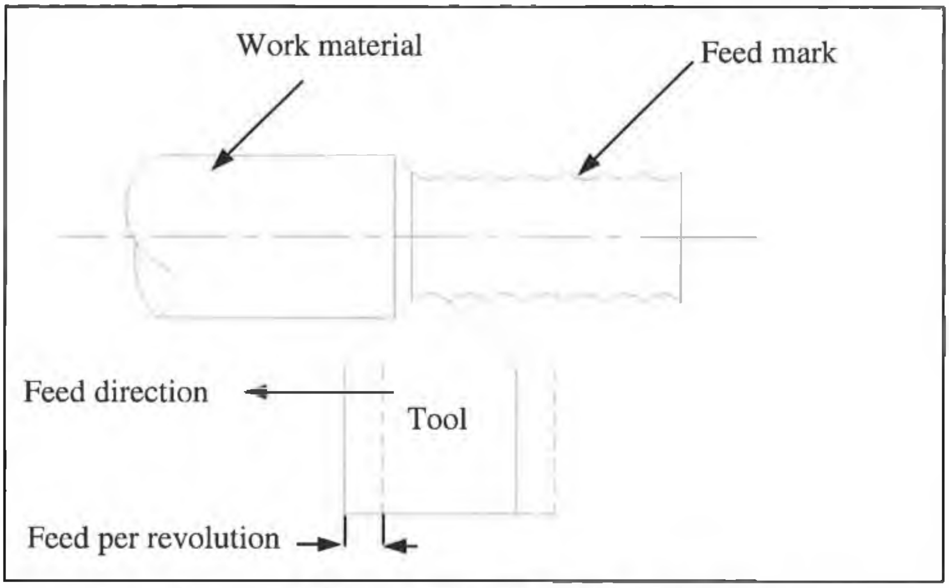

Figure 4.8 Shows feed-marks during Turning

The feed-marks corresponding to three different tool geometry and feed combinations. In (Figure 4.9.a) the geometrical relationships is:

$$f = AD + DC = BD \tan\theta_s + BD \cot\theta_e$$

$$f = h(\tan\theta_s + \cot\theta_e)$$

$$h = \frac{f}{\tan\theta_s + \cot\theta_e} \qquad (4.1)$$

$$h_{CLA} = \frac{f}{4(\tan\theta_s + \cot\theta_e)} \qquad (4.2)$$

The centreline roughness is h_{CLA}=h/4. Centreline average roughness is defined as the mean height of peaks or means depth of valleys with respect to the mean surface.
In the case of a radiuses tool it can be shown that the peak-to-valley roughness is given by the following expression [27].

$$h = (1-\cos\theta_e)r_n + f\sin\theta_e\cos\theta_e - \sqrt{2fr_n\sin^3\theta_e - f^2\sin^4\theta_e} \qquad (4.3)$$

When the feed rate is so small that cutting takes place totally on the nose radius (figure 4.9,c) it was found that:

$$h = r_n - r_n\cos\phi$$

$$h = r_n(1-\cos\phi) = r_n(1-\sqrt{1-\sin^2\phi})$$

$$\sin\phi = \frac{f}{2r_n}$$

$$h = \frac{f^2}{8r_n} \qquad (4.4)$$

Where f is feed rate, r_n is nose radius and h is higher roughness. From equation (4.4) it can seen that the surface roughness depends on the feed rate and nose radius.

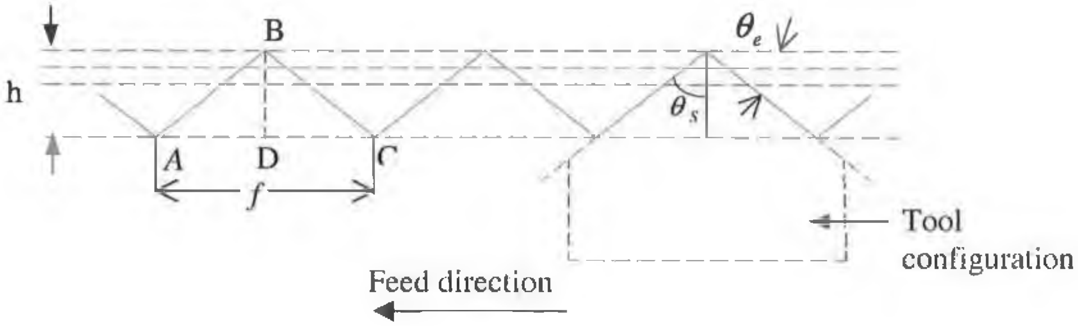

(a) Tool without a nose radius

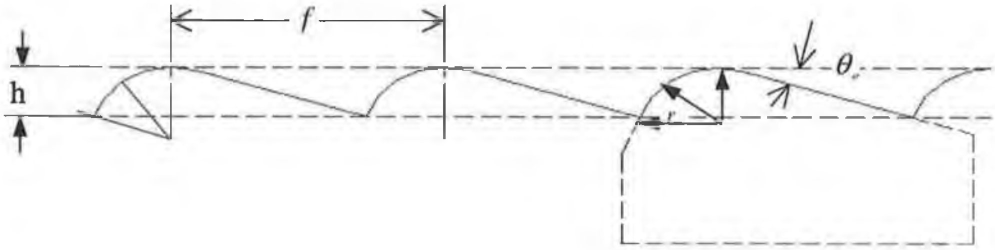

(b) Tool with a nose radius-larger feed rate

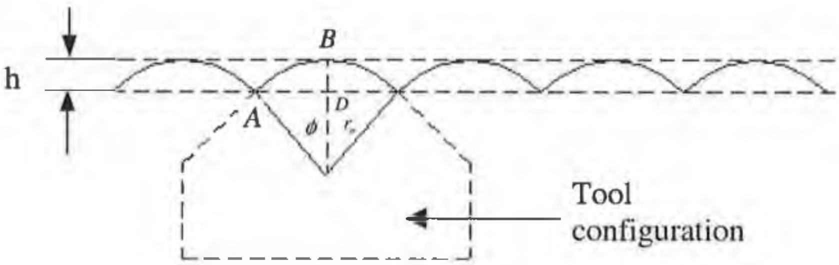

(C) Tool with a nose radius-small feed rate Figure

Figure 4.9 Different types of feed-mark

4.4.1 Factors which Influence Surface Finish

4.4.1.1. The basic geometry of the cut surface is influenced primarily by the tool geometry and the feed. It is unusual for this contributor to surface finish to present any technical problems in practice but in general it could be said that there is a cost penalty, in time, which has to be paid for improving the quality of the geometric surface. This condition only applies for a given process. Clearly some cutting processes inherently produce a better surface finish per unit cost than others.

4.4.1.2. Under normal cutting conditions, when cutting most materials, unstable built-up-edge production will not usually present a severe problem and the effect of built-up-edge fragments on the workpiece will be small particularly if carbide or ceramic cutting tools are used at economic cutting speeds. Thus, in practice degradation of the surface from the geometric surface due to adverse cutting conditions is caused by factors, which can be controlled, and it should therefore be possible to eliminate most of the problems. If the cutting speed can be set high than the adverse effect of small tool rake angles becomes much less critical and as a consequence, for practical rake angles and common ferrous workpieces it would be unusual to produce significant extra surface roughness when cutting at high speed. However, when cutting ductile materials, even at high speed, the choice of rake angle is very important and, from the surface finish aspect only, increasing the rake angle tends to improve the machining conditions and improve surface finish. Even when cutting at high speed, however, many non-ferrous ductile materials produce conditions where an irregular and often unstable built-up-edge is formed and this can have a marked adverse effect on surface finish. Invariably, the only way that a good surface finish can be produced when machining these materials is by using a cutting fluid, which will prevent built-up-edge formation. A badly adjusted obstruction-type chip former or a poor geometry groove-type chip former will often lead to a poorer surface finish if cutting results in severely 'overbroken chip' i.e. chips which are too tightly curled. To maintain the cutting conditions would require that the obstruction be moved further away from the cutting edge in the case of an obstruction-type former or that the groove width be increased for a groove-type chip former. If neither of these actions is possible, then a similar effect could be achieved by reducing the feed [39].

4.4.1.3. Machine tool vibrations particularly the phenomenon of chatter have been thoroughly investigated in the past yet, unfortunately, the methods by which chatter is eliminated are still often not predictable. Clearly, increasing or decreasing the stiffness of the tool mounting structure will, for a given severe chatter condition, tend to reduce the effect and usually it would be appropriate to stiffen the tool mounting structure. In a particular situation where, within reason, the stiffness of the tool mounting structure is fixed, other solutions have to be found. One possible solution is to increase the stiffness of the workpiece by utilising a better clamping arrangement, e.g. if, in turning, a chuck-mounted workpiece is chattering, it may be possible to reduce the overhang of the bar, mount the bar between centres, mount the bar between chuck and centres or use a fixed or travelling steady.

If the workpiece geometry and clamping are fixed then changes in cutting condition will be necessary and it is most common to first investigate the effect of changes in cutting speed. If these changes do not produce the desired effect than a change in feed may be beneficial, particularly an increase in feed. Unfortunately of course, this action would also produce a rougher geometric surface. A further alternative, which can have a beneficial effect, is to use or change the cutting fluid [39].

Summary

This chapter covered the different methods of assessing machinability. Mechanisms of tool wear such as "wear by abrasion, wear by adhesion, wear by diffusion, wear by electrochemical and wear by fatigue" which occur during machining are discussed, as is the method of tool life testing specified by the guidelines of the ISO standard. Also in this chapter the method of assessing machinability by using both cutting force tests and surface finish tests including the machining parameters which affect the surface finish of the material are discussed.

CHAPTER FIVE:
EXPERIMENTAL FACILITY

5 EXPERIMETAL FACILITY

5.1 Introduction

In this chapter the experimental facilities and procedures used for assessing the machinability have been discussed. The details of the machines, equipments, cutting tool inserts and workpiece materials used are described.

5.2 Experimental set-up

The three-component dynamometer in conjunction with the charge amplifiers, and a computer were used to measure and record the cutting forces. Surface finish was measured by a Surftest while the tool wear was measured under a Toolmakers microscope. A schematic diagram of the set-up for force measurement is shown in figure (5.2). The following machines, equipments, cutting tool inserts and workpiece materials comprised the experimental set-up.

5.2.1 Machine and Equipments

(1) Lathe machine engine 10HP. Colchester/Mascot 1600, minimum spindle speed 65 rpm, maximum spindle speed 1600 rpm and feed range of 0.06-1.0 mm/rev.

(2) Surface roughness tester (Mitutoyo Surftest 402 series 178).

(3) Kistler three-component dynamometer (type 92625A1, calibrated range: F_x = 0-15000 N, F_y = 0-15000 N and F_z = 0-30000 N) with three Kistler charge amplifiers is employed.

(4) Tool wear was measured under a Toolmakers microscope.

(5) Hardness; was measured by Rockwell hardness tester.

5.2.1.1 Surface roughness tester

Surface roughness can be expressed numerically in a number of ways, but the most widely used is the arithmetical mean deviation designated as R_a. The different parameters used to express surface roughness are Rq, R_z, and RMS values. In this experimental programme, R_a values have been used to express surface roughness. The range of R_a values were selected at 10 and 50 (μm). It depends on values of roughness being measured. If values of roughness are small, the range of 10μm is selected. If values of roughness are high 50μm is selected. Five sample measurements over the diameter were taken at each observation point to ensure that the values obtained are representative of the whole surface area. The average of the five readings were taken as the roughness value. Figure (5.1) shows a Surftest instrument. The specification details and technical information on the Mitutoyo Surftest – 402 are given in the operation manual [46]

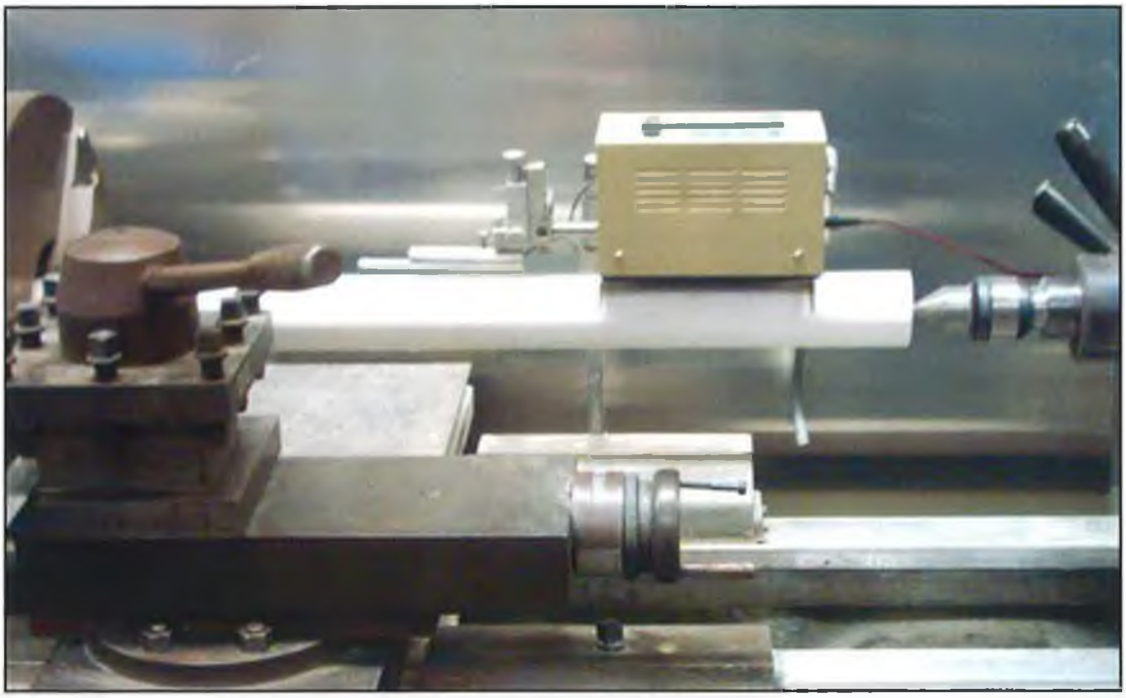

Figure 5.1 Mitutoyo Surftest is measuring workpiece

Detector:

Detecting method:	Differential inductance type
Stroke:	0.3mm
Linearity:	0.2mm
Stylus tip:	Diamond
Tip shape:	Conical of 90º
Tip radius:	5μm
Force variance ratio:	8μN/1μm
Curvature of radius of skid:	30mm

Driving/Display unit:

Displayable parameters:

R_{a}, Rq (RMS), Rz and R_{max}.

Displayable range:

R_{a}, Rq (0.01-2), (0.1-10), (0.2-50)

R_{z}, R_{max} (0.1-10), (0.2-50), (1-250)

Displayable: Liquid crystal display

Operation range:

Driving speed:

0.5 mm/s during measurement and 1 mm/s during return.

Detector elevation:

Coarse range ~ 40 mm and fine rang ~10 mm.

Cut-off value 0.25, 0.8 and 2.5 mm.

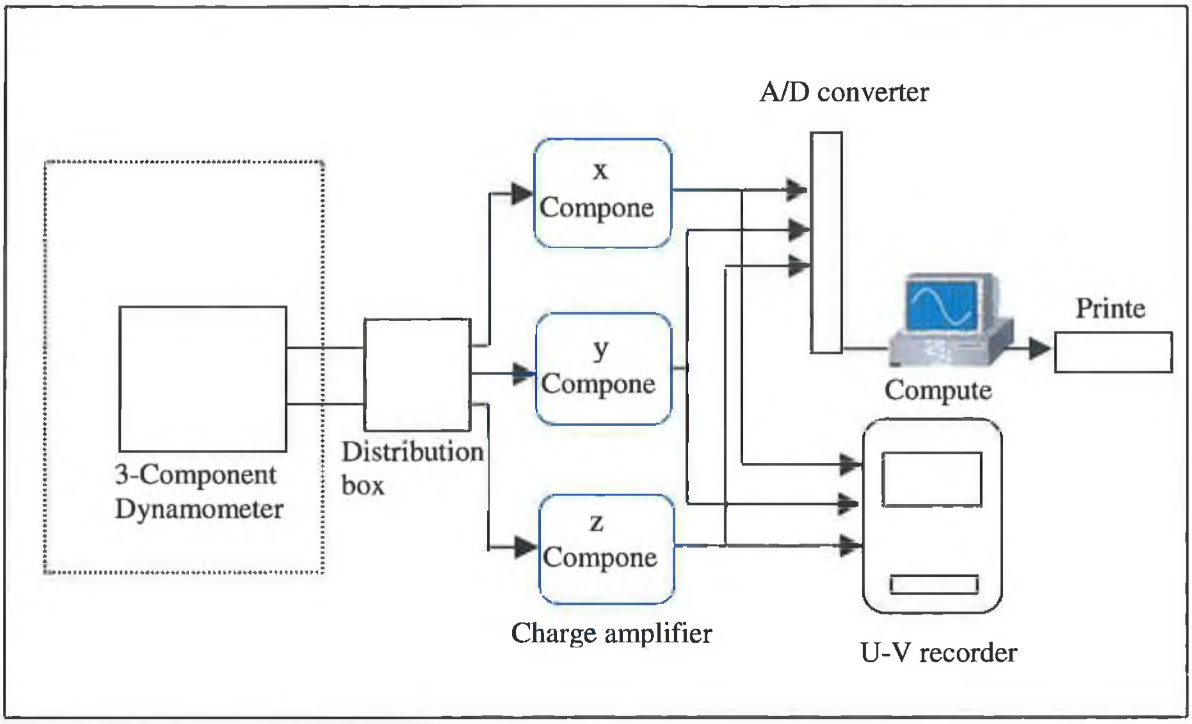

Figure 5.2 Diagram of force measuring set-up

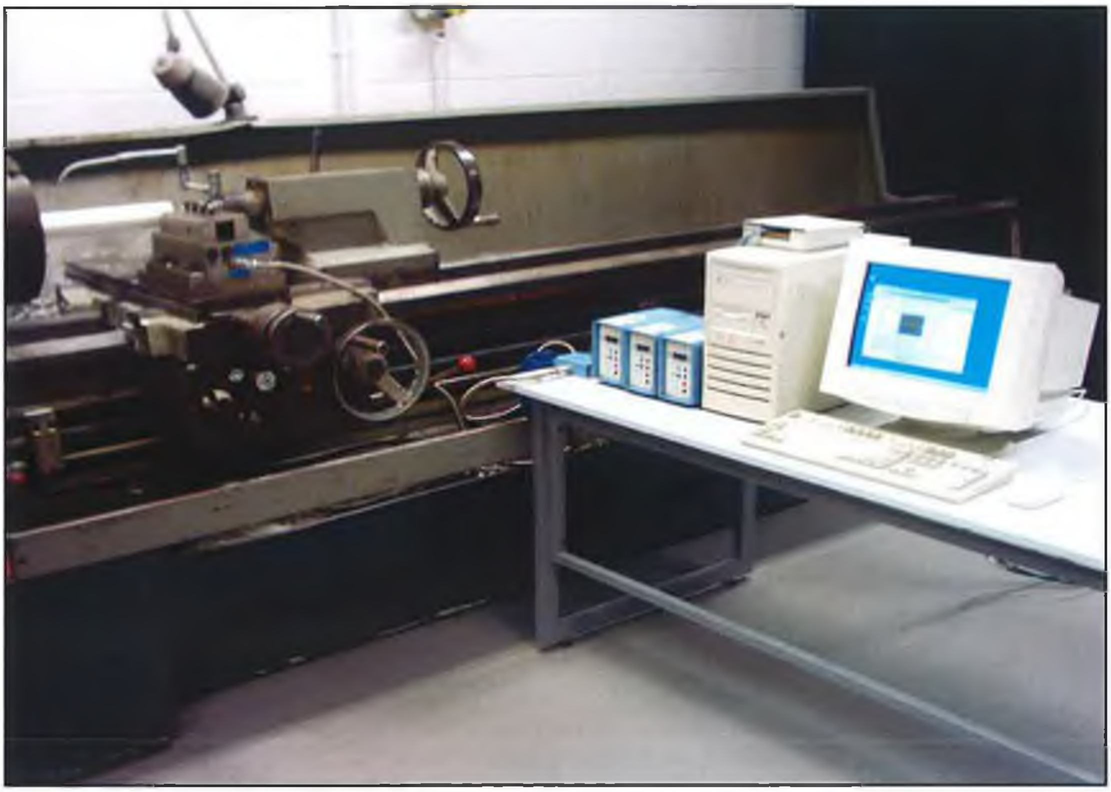

Figure 5.3 Shown the experiment set-up

The dynamometer consists of three components, distribution box, three charge amplifiers, an analog to digital (A/D) converter and a computer with printer facility.

5.2.1.2 Three-component dynamometer

The three-component dynamometer is a piezoelectric transducer that measures the three orthogonal components of a cutting force and consists of a basic unit and a fixture for lathe. This is procured from Kistler piezo-instrumentation, type 9265A1 for turning. The basic unit is the main component and consists of a stainless steel base plate, a mounting plate with a cooling system, and transducers. The base plate has mounting flanges and on one side, it has a 9-pin Fischer flanged socket. The four three-components transducers are held under high preload in between the base-plate and the mounting plate, where they are shielded both thermally and mechanically. The pre-load is necessary in order to enable tensile forces in the z-direction and cutting forces to be transmitted by frictional contact [47]. A proportional electric charge corresponding to each of the three-force component is generated in the dynamometer and converted by the charge amplifiers into proportional voltage. The technical details are given in kistler manual [47].

The calibrated range of F_x and F_y are from 0 to 1.5 KN and that F_z is from 0 to 30 KN. An isometric view of the dynamometer is shown in Figure (5.4).

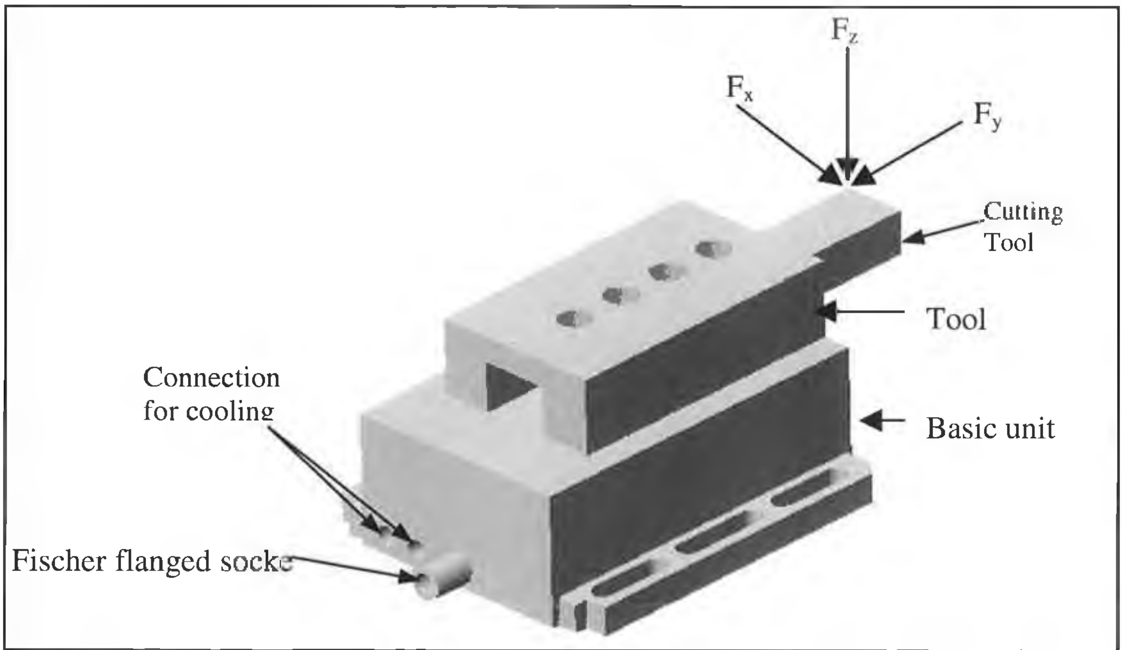

Figure 5.4 Three-component dynamometer

5.2.1.3 Charge amplifier

This is a mains operated microprocessor controlled one-channel amplifier, type 5011. Figure (5.5). Three of these types were used for three component forces. It converts the electric charge yielded by the pizo-electric transducers into a proportional voltage signal. The continuous range setting as well as the microprocessor-controlled electronics allow for a simple and clearly arranged manipulation. The technical details are given in Kistler charge amplifier manual [48].

Depending on the magnitude of the cutting forces, the measuring range could be set up in the amplifier through a combination of transducer sensitivity T and scale S. every channel was adjusted to the number of KN per volt output corresponding to the range. From the charge amplifiers, the output is parallely connected to a computer and UV recorder.

Figure 5.5 Three charges amplifiers for F_x, F_y, F_z

Operation of Dynamometer with Charge Amplifiers

1. Set the dynamometer and cutting tool on the lathe.
2. Connect the shielded cable from the dynamometer output to the signal splitter box input.
3. The signal splitter box has 3 outputs marked *X*, *Y*, and *Z*. connect these to the corresponding charge amplifier input. Charge amplifiers are also labelled *X*, *Y* and *Z*.
4. Charge amplifier operation: The manufacturer recommends powering these on at least 1 hour before measurements are taken to allow the units to warm up.

   The charge amplifier has four setting which are controlled from the menu on the front panel. The sensitivity (T) refers to the transducer and informs the amplifier of the relationship between the charge and the mechanical unit (force).

   The scale (S) relates the output voltage to the mechanical unit (force), multiplying the output voltage by the value set will give the value of the force. The other settings deal with the dynamic components of the signal. The time constant setting (TC) (short, medium or long) limits the decay of the signal over time. The low pass filter (LP) limits the high frequency elements of the signal. For machinability studies, probably 10 Hz is fine for this.
5. Charge amplifier sensitivity set-up: The sensitivity settings required for each charge amplifier is written on top of the instrument. This value can be checked from the on screen display. They should read as follows:

   X: 7.89 pC/N

   Y: 7.87 pC/N

   Z: 3.65 pC/N
6. Charge amplifier scale set-up: This is best done with 1 person operating the lathe and another checking the scale setting on the charge amplifier display. Connect a coax cable from the charge amplifier output to an oscilloscope. It may be necessary to set the zero adjust pot at the rear of the instrument so that the scope display reads 0v before continuing. This requires a suitable pot trimmer. The cursor must be locked and the operation switch pressed. Operate the lathe. Adjust the scale setting until the scope display shows a reading within the range of +/- 8 values. This will allow the signal to be read into Labview without distortion.

7. If there are problems with the signals it may be due to moisture in the connections and cables. The manufacturer recommends baking the dynamometer and cables at 50° C for 24 hrs to drive out the moisture if the unit has been unused for a long period.
8. Use the coax cables supplied to connect from the outputs of the charge amplifiers to the SCB-68 breakout box. Each channel will correspond to *X*, *Y* and *Z* forces.

5.2.1.4 Data acquisition system and Labview software

Today, most scientists and engineers are using personal computers with ISA, EISA, PCI, PCMCIA, Macintosh Nubus, or parallel or serial ports for data acquisition in laboratory research, test and measurement, and industrial automation. Many applications use plug-in boards to acquire data and transfer it directly to computer memory. Others use DAQ hardware remote from the PC that is coupled via parallel or serial port. Obtaining proper results from a PC-based DAQ system depends on each of the following system elements [49].

Labview software

Software transforms the PC and DAQ hardware into a complete DAQ, analysis, and display system. DAQ hardware without software is of little use-and without proper controls the hardware can be very difficult to program. The majority of DAQ applications use driver software is the layer of software that directly programs the registers of the DAQ hardware, managing its operation and its integration with the computer resources, such as processor interrupts, DMA, and memory. Driver software hides the low-level, complicated details of hardware programming, providing the user with an easy-to-understand interface [49].

Labview is programmed with set of icons that represents controls and functions, available in the menu of the software. Such a programming is called visual programming and national instruments calls it G. the user interface which is called a *vi* consists of two parts-a front panel and a diagram. This is similar to that of an instrument where a front panel is used for an input, output controls, and to display the data whereas the circuit resides on the circuit board. Similarly you can bring the buttons, indicators and graphing and display functions on the front panel [50].

5.2.1.5 Computer

The computer used is a Pentium MNX 128 M.HZ 8 GB hard disk was used to measure cutting force data. Data acquisition was achieved using Labview software. The DAQ card-6062E, PCI-MIO-16E-4 777383-01 was used.

5.2.1.6 Toolmakers microscope

The toolmaker microscope was used for flank wear measurement. The microscope is shown in Figure (5.6). The details of the microscope are as follows:

Type: Mitutoyo Corporation, and COD No: 176-941

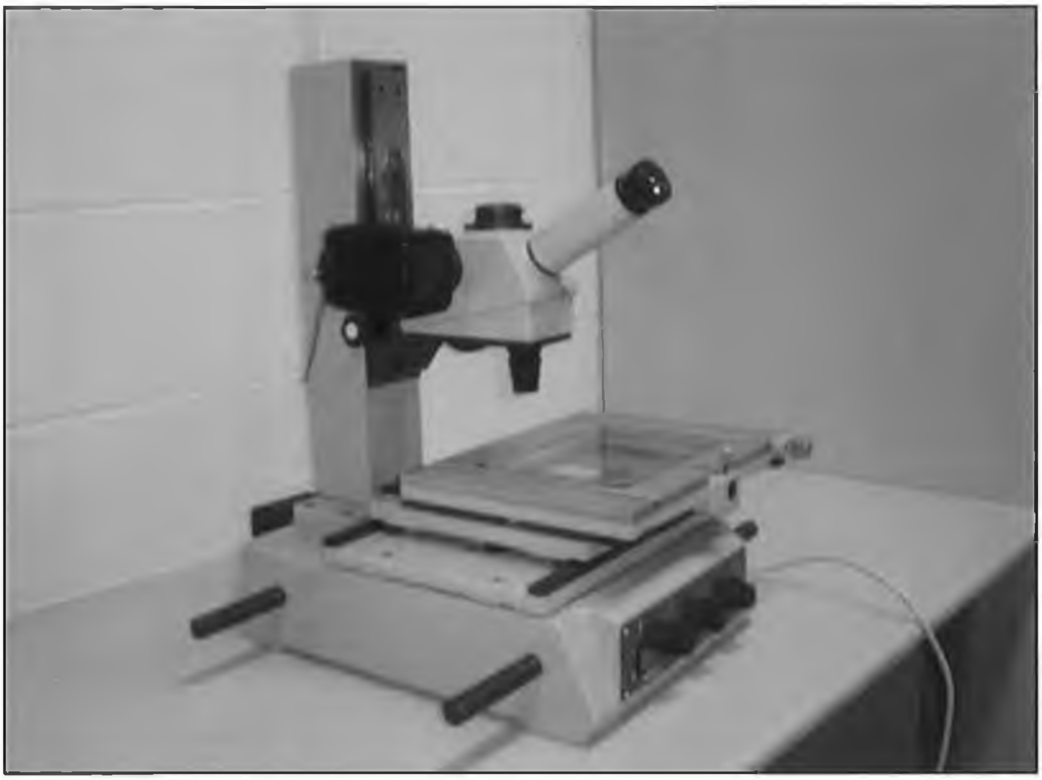

Figure 5.6 Mitutoyo toolmakers microscope

5.2.2 Workpiece Material

The workpiece materials used as the test specimen were Macor and Boron Nitride Machinable glass-ceramics (MGC), 50.8 mm diameter and 305mm long.

Table 5.1 Chemical Composition (%), of Macor and Boron Nitride ceramic

Macor	MgO	B_2O_3	K_2O	Al_2O_3	SiO_2	F
	17	7	10	16	46	4
Boron Nitride	BN	Boron	Nitrogen	Oxygen	Boric Acid	Carbon
	99.0	42.6	55.9	0.5	0.1	0.05

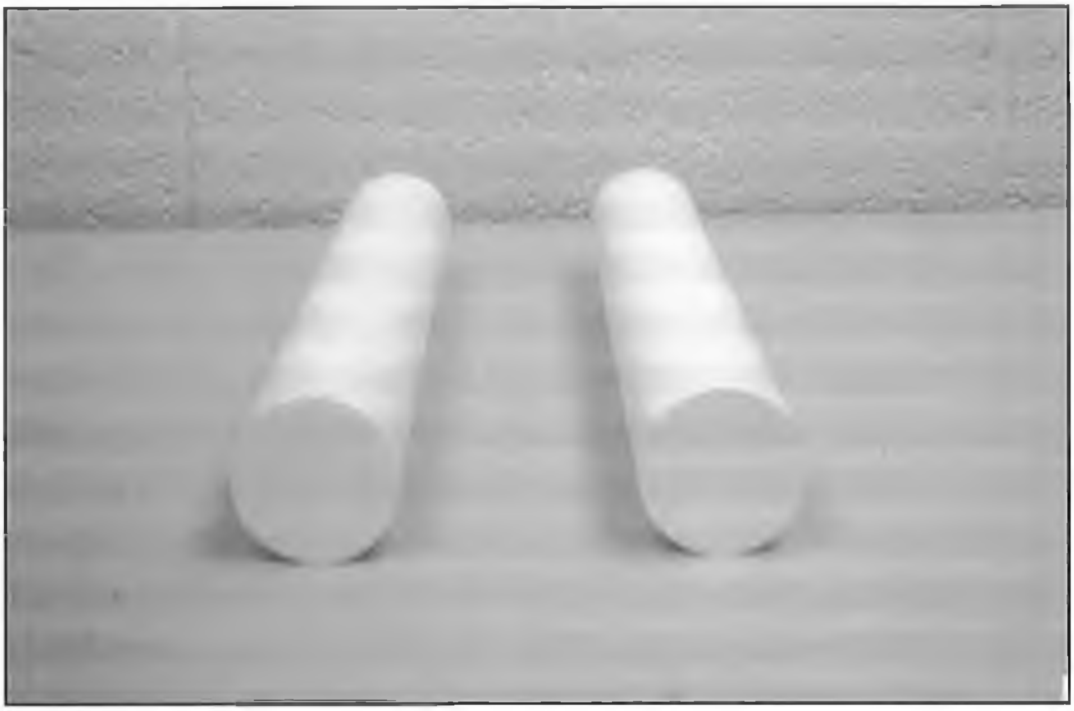

Figure 5.7 Macor and Boron nitride machinable glass-ceramics, (MGC).
(50.8 mm diameter and 305mm long)

5.2.3 Tool Material

The tool material and its geometry also have an influence on the machinability of a material. The main factors that affect of a good cutting tool is (i) high hardness (ii) wear resistance (iii) chemical inertness and (iv) fracture toughness. Uncoated carbide Tools specification: TNMG 16 04 04 – QM, TNMG 331 – QM was used for the turning tests. This is uncoated grade that can withstand high temperatures without being deformed.

5.2.4 Experiment of Material Hardness

The hardness of material is defined as its resistance to permanent indentation. Good hardness generally means that the material is resistant to scratching and wear. For many engineering applications, including most of the tooling used in manufacturing, scratch and wear resistances are important characteristics. As we shall see later in this section, there is a strong correlation between hardness and strength.

Hardness tester

Hardness tests are commonly used for assessing material properties because they are quick and convenient. However, a variety of testing methods are appropriate due to differences in hardness among different materials. The most well-known hardness tests are Brinell and Rockwell.

Brinell Hardness Test

The Brinell hardness test is widely used for testing metals and non-metals of low to medium hardness. It is named after the Swedish engineer who developed it around 1900. In the test, a hardened steel (or cement carbide) ball of 10-mm diameter is pressed into the surface of a specimen using a load of 500, 1500, or 3000 kg. The load is then divided into the indentation area to obtain the Brinell hardness number (*HB*). In equation form,

$$HB = \frac{2F}{(\eta D_b)\left(D_b - \sqrt{D_b^2 - D_i^2}\right)}$$

Where F = indentation load (kg), D_b = diameter of the ball (mm), and D_i = diameter of the indentation on the surface (mm). The resulting Brinell hardness number has units of kg/mm^2. But the units are usually omitted in expressing the number. For harder materials (above 500 HB), the cemented carbide ball is used, since the steel ball experiences elastic deformation that compromises the accuracy of the reading. Also, higher loads (1500 and 3000 kg) are typically used for harder materials. Because of differences in results under different loads, it is considered good practice to indicate the load used in the test when reporting HB readings [18].

Rockwell Hardness Test

The Rockwell tester has the capability of testing metals having a wide range of hardness. This capability is obtained by using different combinations of load and penetrator. The tow most common combinations are 100 kg major load applied to a 1/16-diameter ball to give B hardness number and a 150 kg major load applied to a shaped diamond (brale) penetrator to give a C hardness number. The C test is used for the harder materials such as cold worked or heat-treated steel and B test for low carbon hot rolled steel and softer materials [51]. As shown in table (5.2).

Table 5.2 Rockwell (R) Regular Scale applications

Rockwell (R) Regular Scale applications			
Scale symbol	Penetrator	Major(Minor) Load	Typical application
A	Brale	60 kgf (10 kgf)	Cemented carbides Thin steel Shallow case hardened steel
B	1/16" Ball	100 kgf (10 kgf)	Cooper alloys Soft steel Aluminium alloys Malleable iron

Vickers Hardness test

This test, also developed in the early 1920s, uses a pyramid-shaped indenter made of diamond. It is based on the principle that impressions made by this indenter are geometrically similar regardless of load. Accordingly, loads of Vickers hardness (*HV*) is then determined from the formula

$$HV = \frac{1.854F}{D^2}$$

Where F = applied load (kg) and D = the diagonal of the impression made by the indenter (mm). The Vickers test can be used for all metals and has one of the widest scales among hardness tests.

Calibration of Tester

1. Load flat anvil into base of tester
2. Load either diamond or ball indenting tool, depending on type of tester required
3. Set load required for test using the allen key on top of tester
4. Select calibrated specimen from wallet and place on anvil
5. Ensure handle position is forward of tester-on load applied
6. Raise base of tester and anvil until specimen just touching indenting tool
7. Carefully raise anvil while watching the small clock dial until it hs rotated 3 cycles and sits in the red spot
8. Zero outer clock dial
9. Gently pull handle to its back position applying the spring load
10. Leave dial to settle for 20 seconds
11. Release load by pulling handle forward and real off scale.

The hardness tester that was used in this study can directly measure Rockwell, Brinell hardness and can measure Vickers hardness by exemplifying tables.
The results of the hardness experiments carried out at different points as shows in figure (5.8). The straight line from the centre edge to the outer point of the work material at different locations is shown in table (5.3).

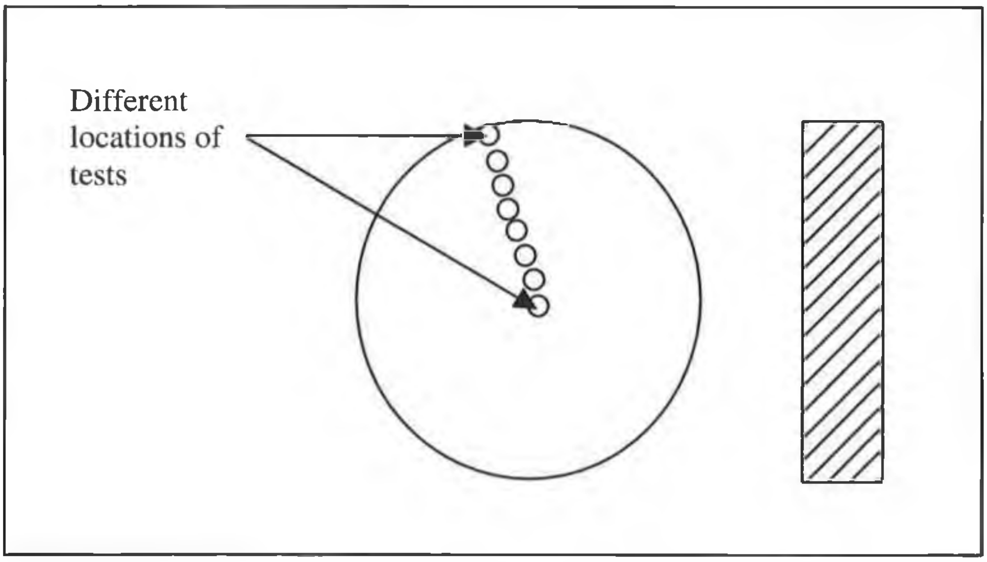

Figure 5.8 Shows experiment hardness test on the section of the work material

Table 5.3 shows the results of the Experiment of hardness Macor ceramic material

Test 1 No.	60kg Diamond Rockwell A	Hardness of material (Brinell)	Test 2 No.	60kg Diamond Rockwell A	Hardness of material (Brinell)
1'center	57.5	201	1	53.5	173
2	54	176	2	52	164
3	52	164	3	49	148
4	48	144	4	48	144
5	48	144	5	49	148
6	48	144	6	49.5	151
7	46	135	7	50.5	156
8 'outer	46	135	8	49	148

The average for these points is:

$$\text{Experiment 1 } Bhn = \frac{201+176+.........+135}{8} = 155.375\,\text{BHN}$$

$$\text{Experiment 2 } Bhn = \frac{173+164+.........+148}{8} = 154\,\text{BHN}$$

The same hardness experiments carried out for the Boron nitride and the results of the hardness were as shown in table 5.4.

Table 5.4 shows the results of the Experiment of hardness Boron Nitride material

Test 1 No.	60kg Diamond Rockwell A	Hardness of material (Brinell)	Test 2 No.	60kg Diamond Rockwell A	Hardness of material (Brinell)
1'center	42	114	1	41	110
2	41.5	112	2	42	114
3	41	110	3	41.5	112
4	40	108	4	41	110
5	39.5	106	5	40	108
6	40	108	6	39	106
7	39	106	7	39	106
8 'outer	39	106	8	38	102

The average for these points is:

$$\text{Experiment 1 } Bhn = \frac{114 + 112 + \dots\dots\dots + 106}{8} = 108.75 \text{ BHN}$$

$$\text{Experiment 2 } Bhn = \frac{110 + 114 + \dots\dots\dots + 102}{8} = 108.5 \text{ BHN}$$

Figure 5.8 Shows Rockwell Hardness Tester

Summary

This chapter the experimental facilities that were used are presented. These include a description of surface roughness tests, Kistler 3-component dynamometer, and a toolmaker's microscope. The chemical composition of materials is covered. Also in this chapter, the operation of dynamometer with charge amplifiers, data acquisition system and experiment of material hardness is described.

CHAPTER SIX:
EXPERIMENTAL RESULT & DISCUSSION
ONE VARIBLE AT-A-TIME

6 EXPERIMENTAL RESULT AND DISCUSSION ONE-VARIBLE-AT-A-TIME

6.1 INTRODUCTION

The surface roughness, tool life and cutting forces tests were carried out in this chapter, by using the one-variable-at-a-time method. Uncoated carbide tool was use in the conditions.

The experimental variables were considered are:

1. Cutting speed
2. Feed rate
3. Depth of cut
4. Nose radius

In conducting the experiments two of the machining parameters out of the three (cutting speed, feed rate and depth of cut), are kept constant. The third parameter was varied from one end of its operating range to the other.

6.2 Surface Finish

High quality products are obtained from good process. Surface roughness is a result of cutting conditions. Experiment are performed to analyze the effect of cutting speed, feed rate, depth of cut and also nose radius on the average surface roughness of machinable glass-ceramic (Macor & Boron nitride), that were machined used uncoated carbide tool under dry turning conditions. In the following sections, the machining results will discussed in the terms of each of the cutting conditions.

6.2.1 Cutting Speed

In this section the surface finish (Ra) is measured when the cutting speed is varied but depth of cut and feed rate are fixed to find out the effect of process parameters on surface finish. The experimental work for both materials used at a depth of cut 0.4, 0.8, 1.2, and 1.4 (mm), and feed rates were carried out at 0.08, 0.12, 0.2 and 0.25 (mm/rev), as shown in Figures. (6.1, 6.2, 6.3, 6.4) & (6.22, 6.23, 6.24, 6.25). The test results show that the value of surface roughness (Ra) is low at high cutting speed and comparatively high at low cutting speed within the experimental rang at constant feed rate and depth of cut. The same experiments work was carried out at feed rate 0.08, 0.12, 0.2 and 0.25 (mm/rev) as shown in Figures. (6.5, 6.6, 6.7, 6.8) & (6.26, 6.27, 6.28, 6.29).

6.2.2 Feed Rate

Figures. (6.9, 6.10, 6.11, 6.12, 6.13, 6.14) & (6.30, 6.31, 6.32, 6.33), show the effect of feed rate on surface roughness for the both materials, it can be seen that machined average surface roughness increases gradually with an increase in feed rate. As well known that increasing feed rate will increase the volume of material removed from the workpiece in the form chips, produces an increase in the surface damage and roughness. So the roughness increasing with increases the feed rate. It happened at each depth of cut, so that means the feed rate has a significant effect on the surface finish. The reason for that the feed marks is proportional to the square of the feed per revolution. Any way the surface finish can be improved by decreasing feed rate.

6.2.3 Nose Radius

The nose radius of an insert has a great influence in the metal cutting process. The primary function of the nose radius is to provide strength to the tip of the tool. Most of the other functions and the size of the nose radius are just as important. The choice of nose radius will affect the results of the cutting operation; however, a large radius causes more contact with the work surface and can cause chatter. One of the most important influences of a large radius is those of surface finish. However as shown in Figures. (6.15, 6.16, 6.17, 6.18, 6.19, 6.20) & (6.34, 6.35, 6.36, 6.37), the larger nose radius produces better surface finish.

6.2.4 Depth of cut

The depth of cut should never exceed half the insert's leg length, and the feed should not exceed half of the nose radius. These precautions will reduce the likelihood of fracture of the cutting edge and poor surface finish on the workpiece. The effects of depth of cut on the average surface roughness (Ra) are shown in Figures. (6.21) & (6.38). It can be seen that machined average surface roughness (Ra) increases with increasing depth of cut.

Results of Macor ceramic material

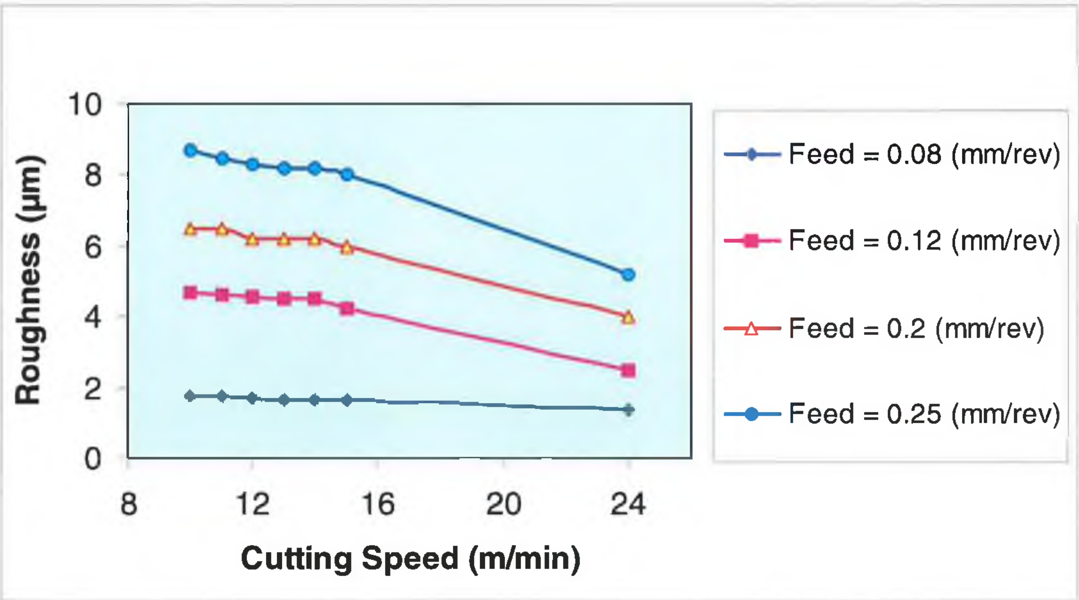

Figure 6.1 The Relationship between Cutting speed & Roughness at DOC 0.4 mm

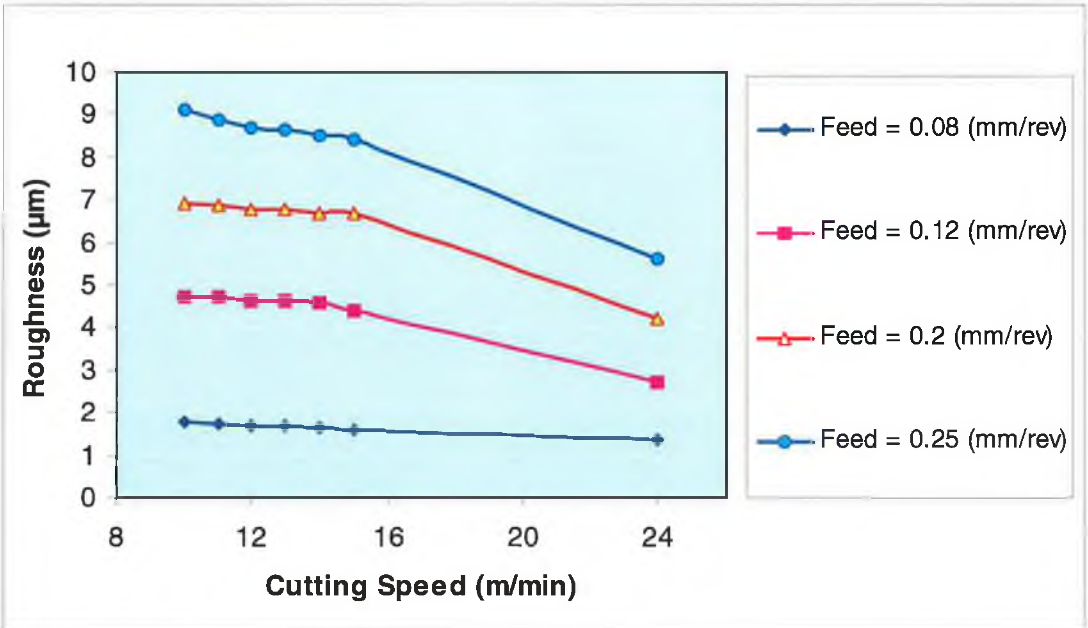

Figure 6.2 The Relationship between Cutting speed & Roughness at DOC 0.8 mm

Figures; (6.1, 6.2) shows that the value of surface roughness (Ra) is low at high cutting speed and comparatively high at low cutting speed within the experimental rang at constant feed rate and depth of cut.

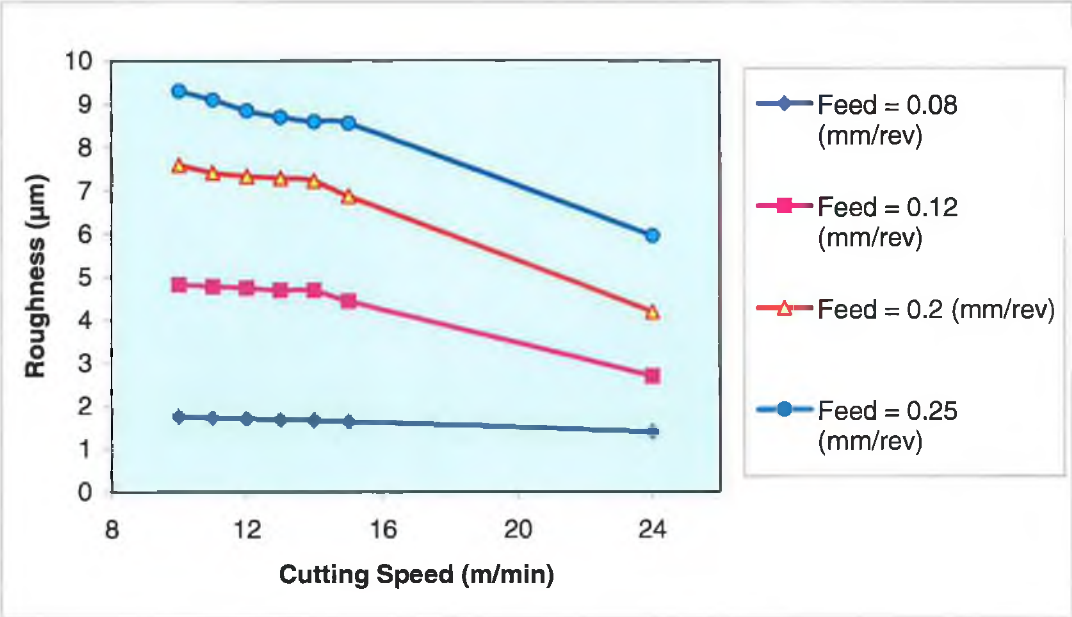

Figure 6.3 The Relationship between Cutting speed & Roughness at DOC 1.2 mm

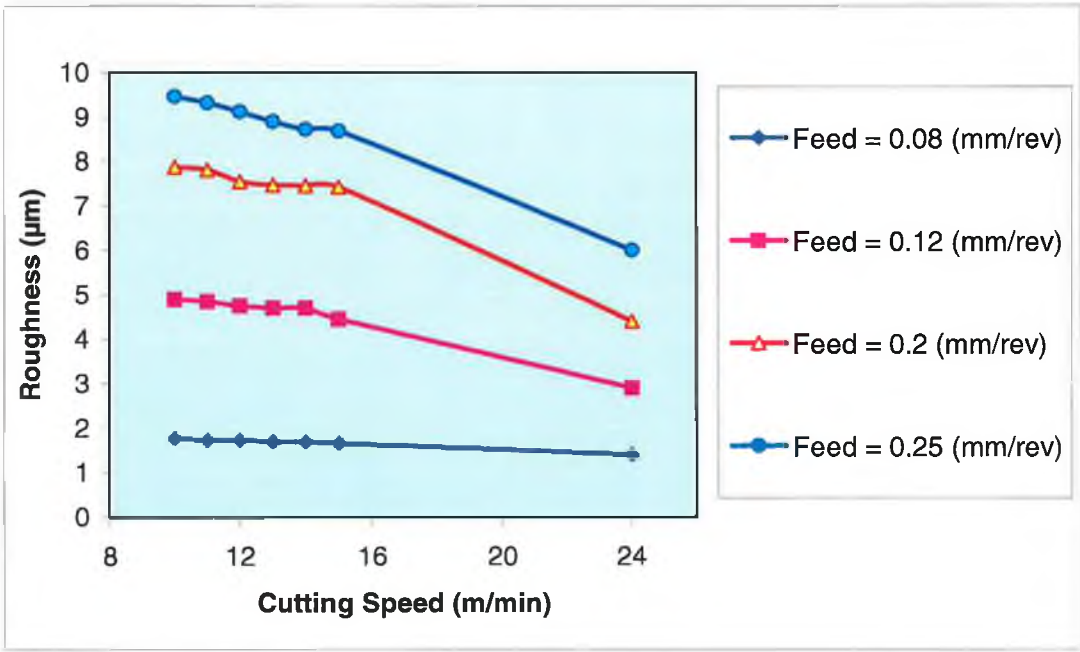

Figure 6.4 The Relationship between Cutting speed & Roughness at DOC 1.4 mm

Figures; (6.3, 6.4) shows that the value of surface roughness (Ra) is low at high cutting speed and comparatively high at low cutting speed within the experimental rang at constant feed rate and depth of cut.

The experiment in second part was carried out when the feed rate was fixed at 0.08, 0.12, 0.2 and 0.25 (mm/rev), at each depth of cut as shown in figures (6.5), (6.6), (6.7), and (6.8), so by this way we found out the affect of depth on surface finish.

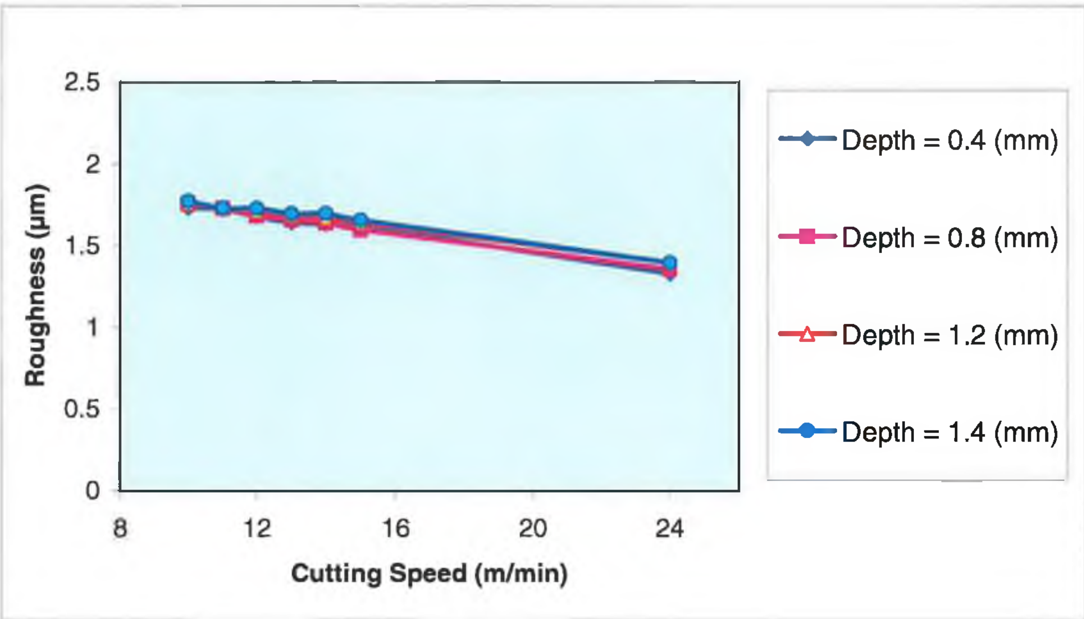

Figure 6.5 Relationship between Cutting speed & Roughness at Feed 0.08 (mm/rev)

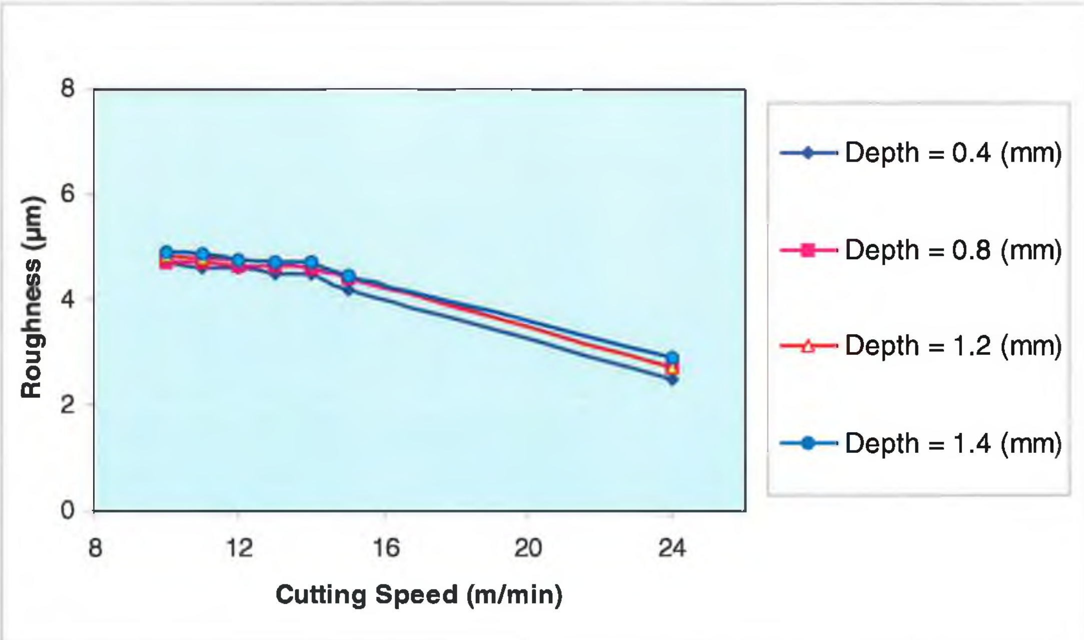

Figure 6.6 Relationship between Cutting speed & Roughness at Feed 0.12 (mm/rev)

Figures; (6.5, 6.6) shows that the value of surface roughness (Ra) is low at high cutting speed and comparatively high at low cutting speed within the experimental rang at constant feed rate and depth of cut.

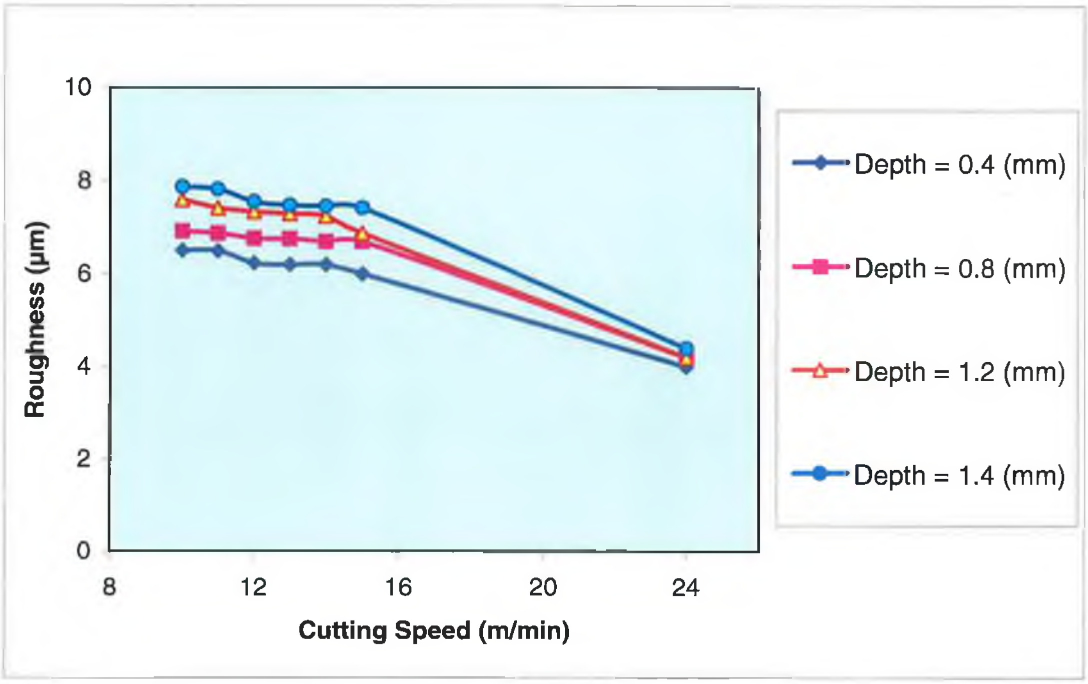

Figure 6.7 Relationship between Cutting speed & Roughness at Feed 0.2 (mm/rev)

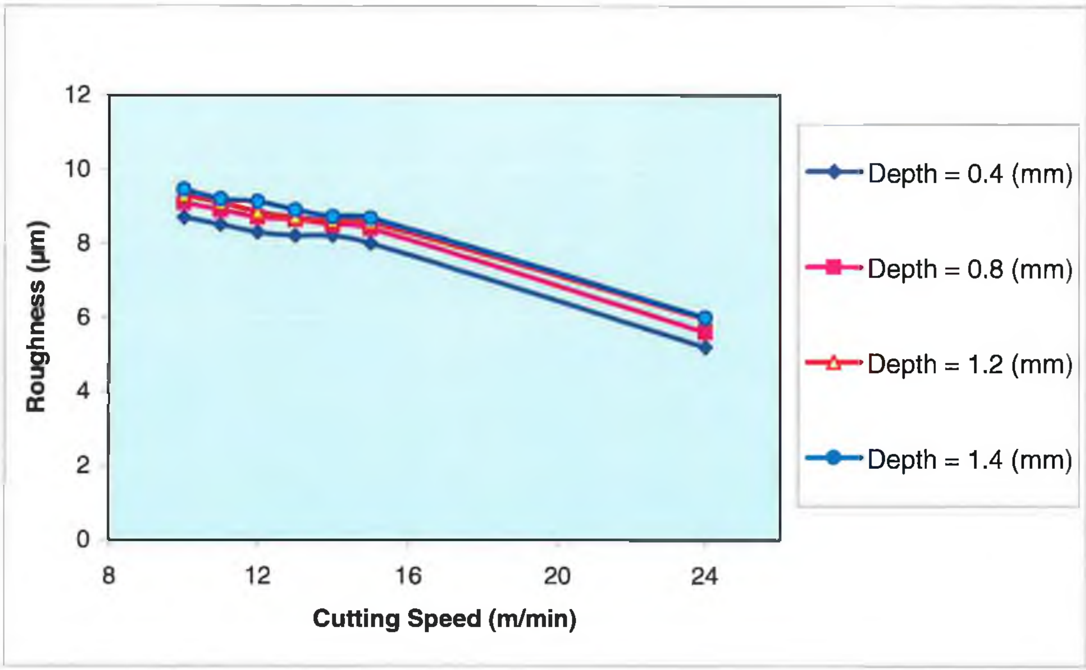

Figure 6.8 Relationship between Cutting speed & Roughness at Feed 0.25 (mm/rev)

Figures; (6.7, 6.8) shows that the value of surface roughness (Ra) is low at high cutting speed and comparatively high at low cutting speed within the experimental rang at constant feed rate and depth of cut.

In this section the measurement of surface finish (Ra) is measured when the feed rate are varied but depth of cut and cutting speed are fixed to find out the affect of process parameters on surface finish.

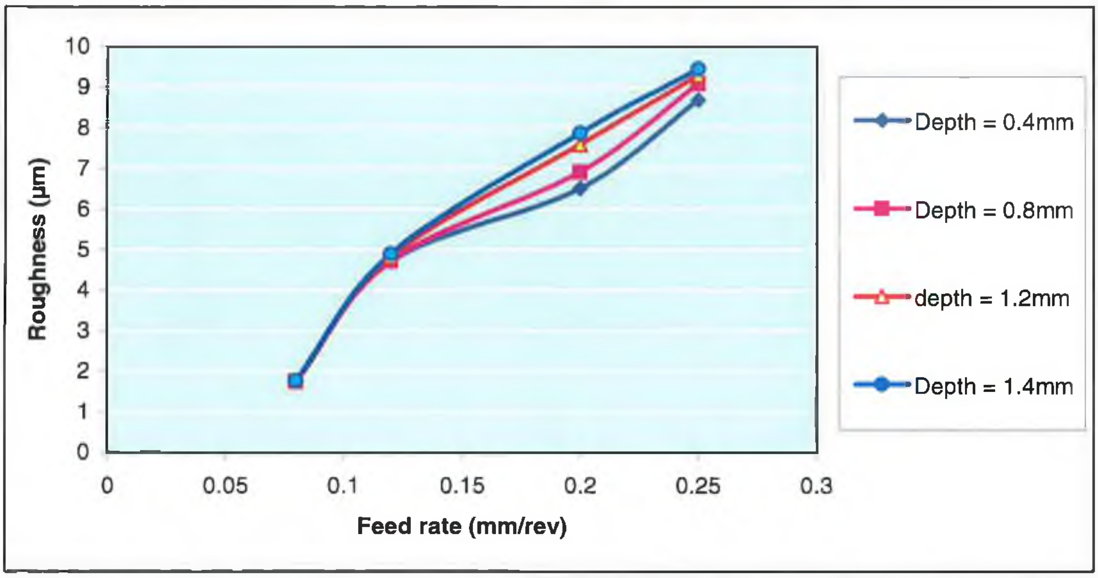

Figure 6.9 Shown the Relationship between Feed & Roughness at Speed 10(m/min)

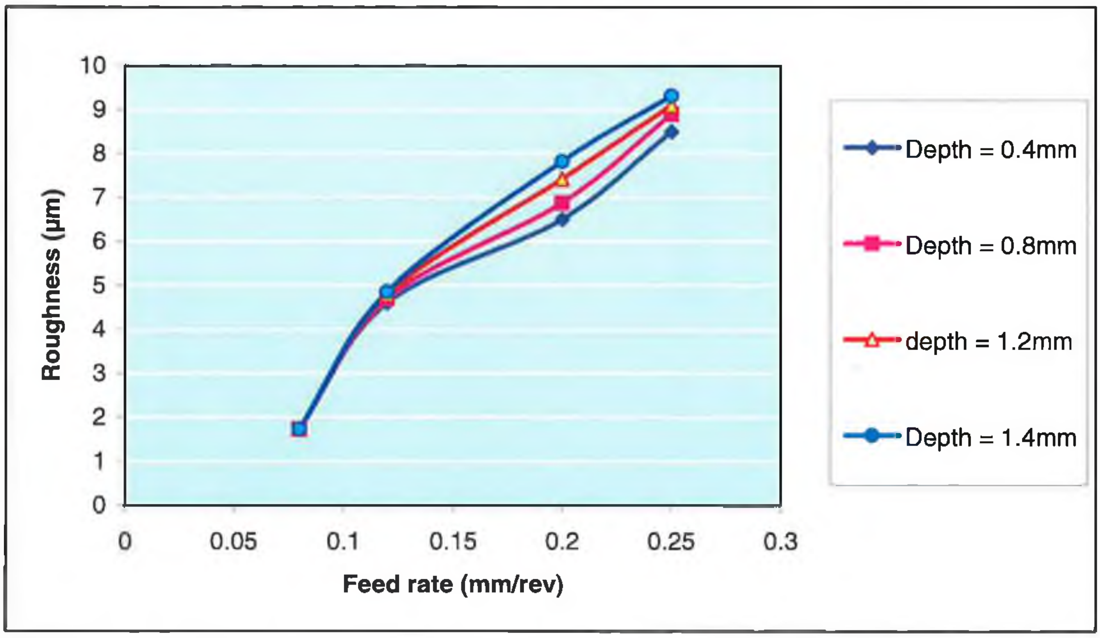

Figure 6.10 Shown the Relationship between Feed & Roughness at Speed 11(m/min)

Figures; (6.9, 6.10) shows that the value of surface roughness (Ra) increases gradually with an increase in feed rate, it happened at each depth of cut.

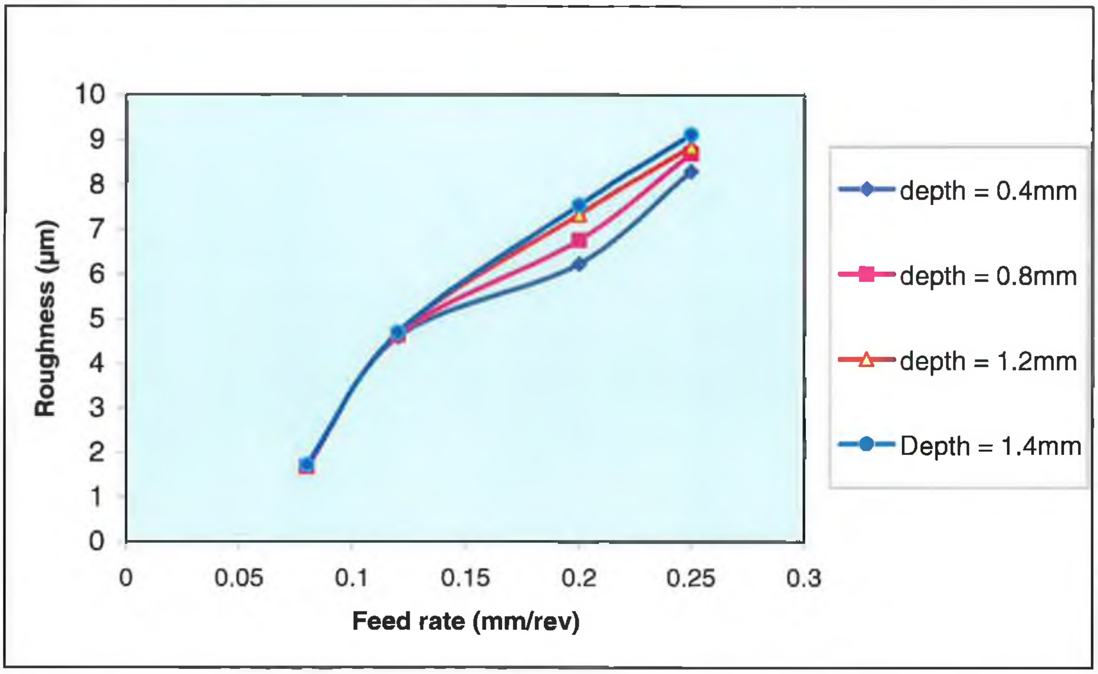

Figure 6.11 Shown the Relationship between Feed & Roughness at Speed 12 m/min

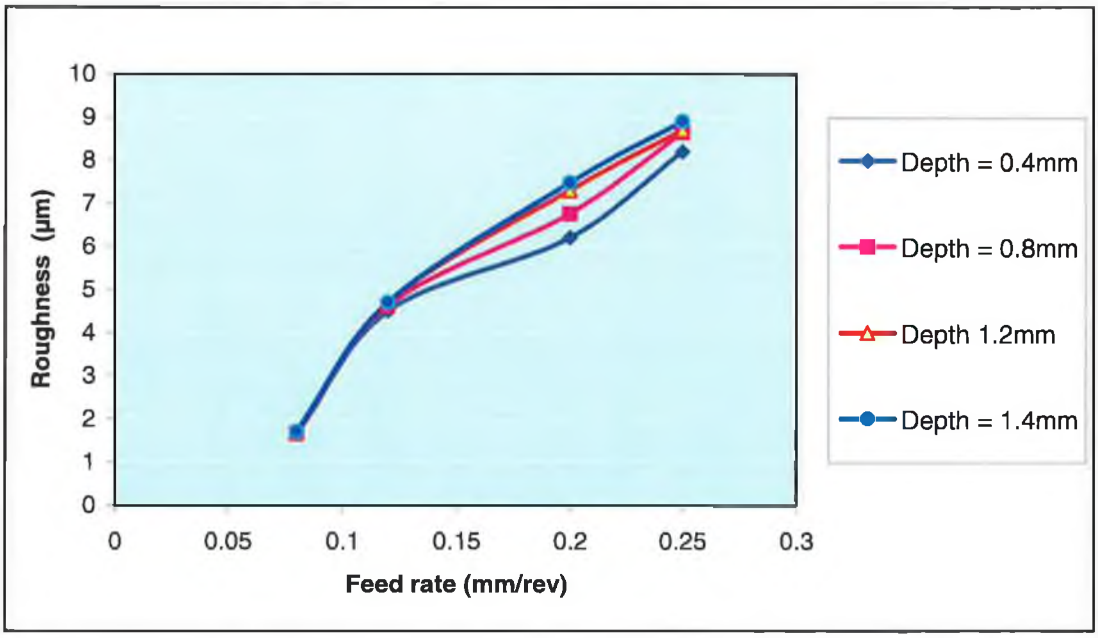

Figure 6.12 Shown the Relationship between Feed & Roughness at Speed 13 m/min

Figures; (6.11, 6.12) shows that the value of surface roughness (Ra) increases gradually with an increase in feed rate, it happened at each depth of cut.

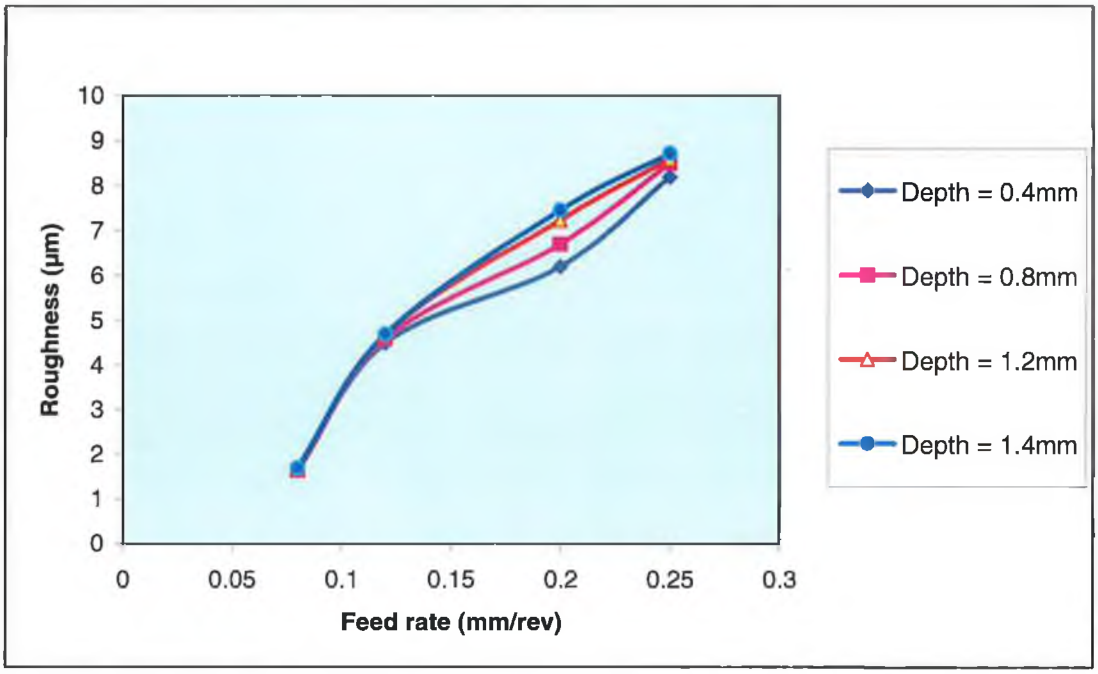

Figure 6.13 Shown the Relationship between Feed & Roughness at Speed 14 m/min

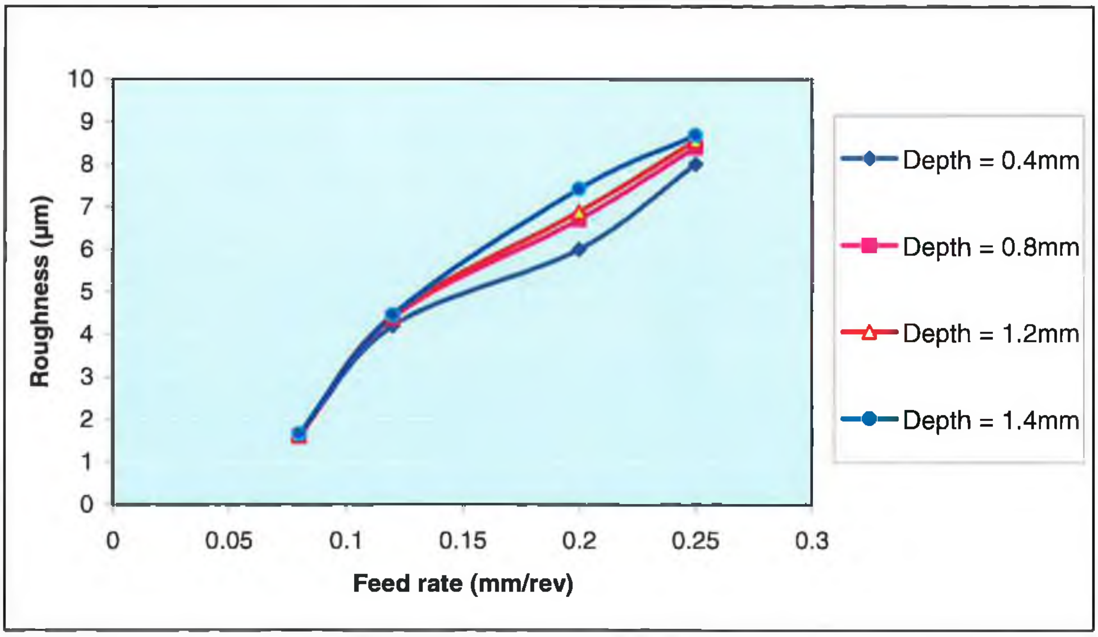

Figure 6.14 Shown the Relationship between Feed & Roughness at Speed 15 m/min

Figures; (6.13, 6.14) shows that the value of surface roughness (Ra) increases gradually with an increase in feed rate, it happened at each depth of cut.

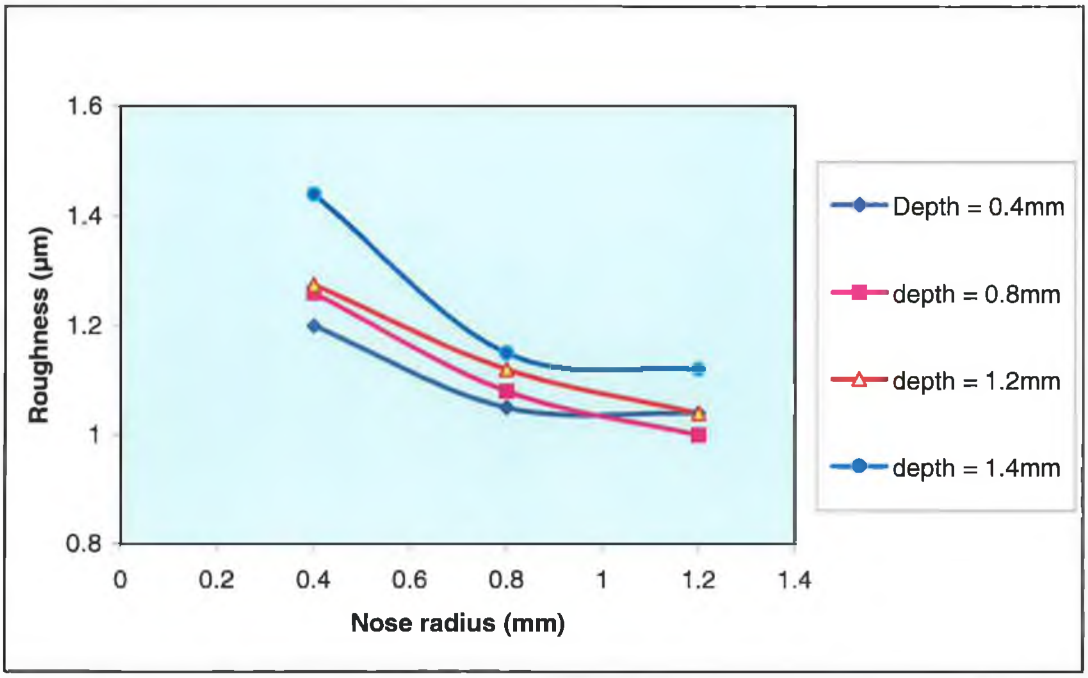

Figure 6.15 Shown the Relationship between Nose radius & Roughness at Feed 0.08 (mm/rev) and Speed 10 (m/min).

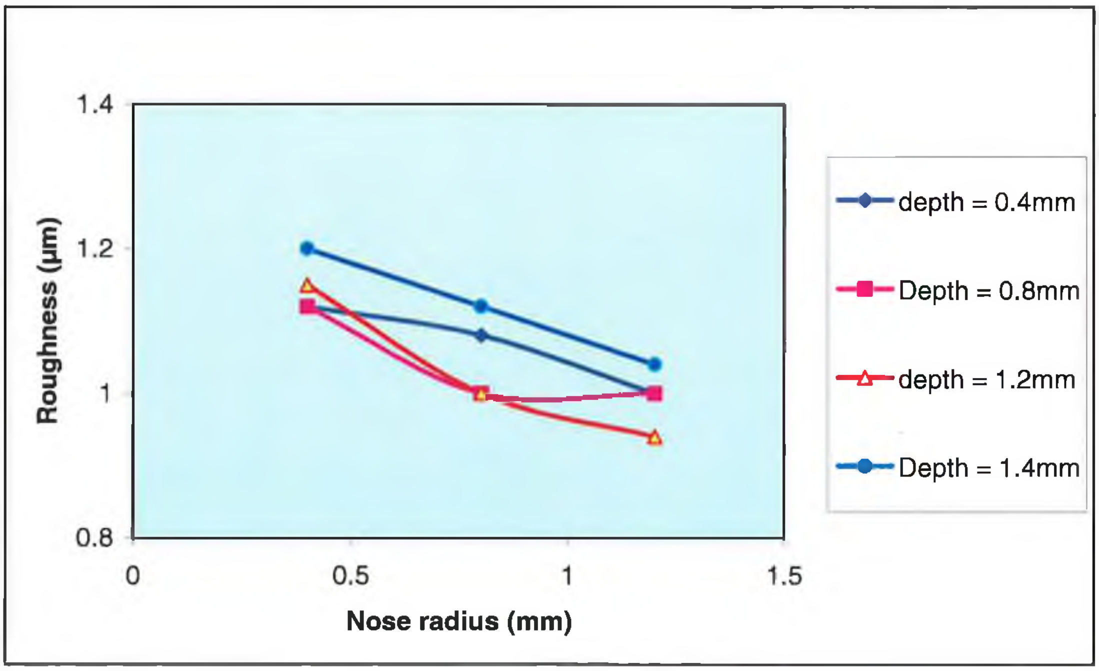

Figure 6.16 Shown the Relationship between Nose radius & Roughness at Feed 0.08 (mm/rev) and Speed 11 (m/min).

Figures; (6.15, 6.16) shows that the larger nose radius produces better surface finish.

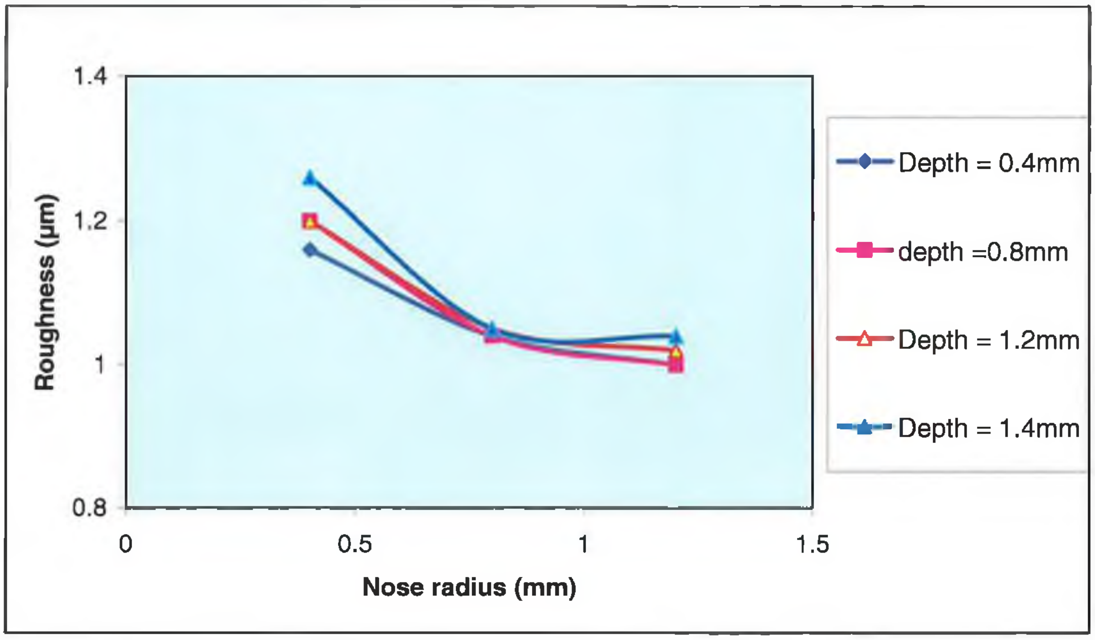

Figure 6.17 Shown the Relationship between Nose radius & Roughness at Feed 0.08 (mm/rev) and Speed 12 (m/min).

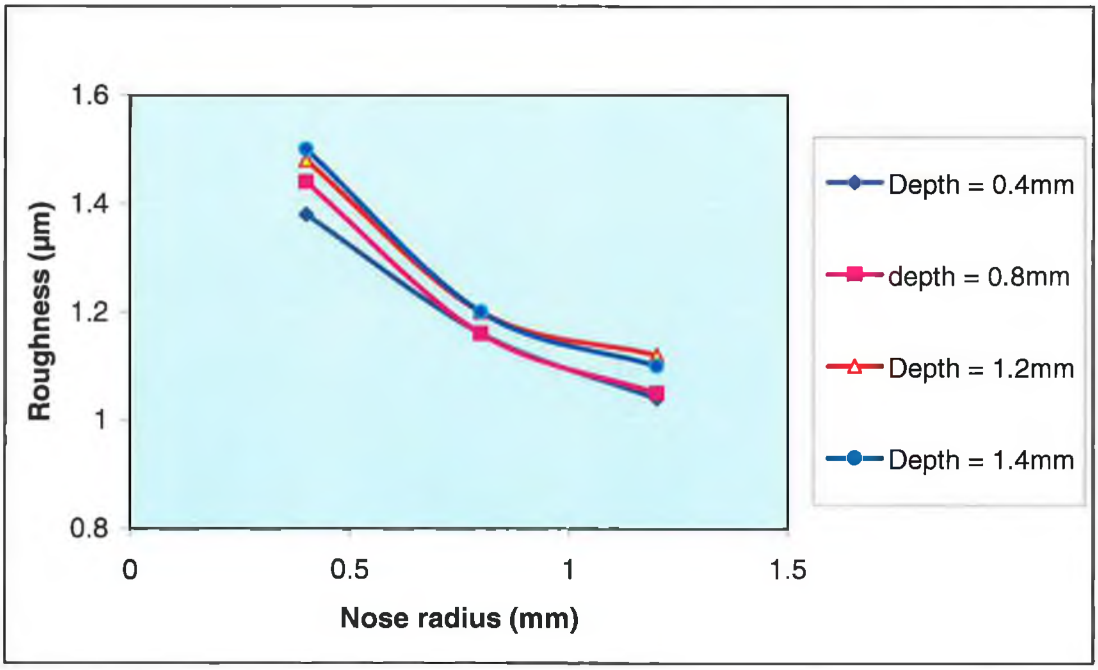

Figure 6.18 Shown the Relationship between Nose radius & Roughness at Feed 0.08 (mm/rev) and Speed 13 (m/min).

Figures; (6.17, 6.18) shows that the larger nose radius produces better surface finish.

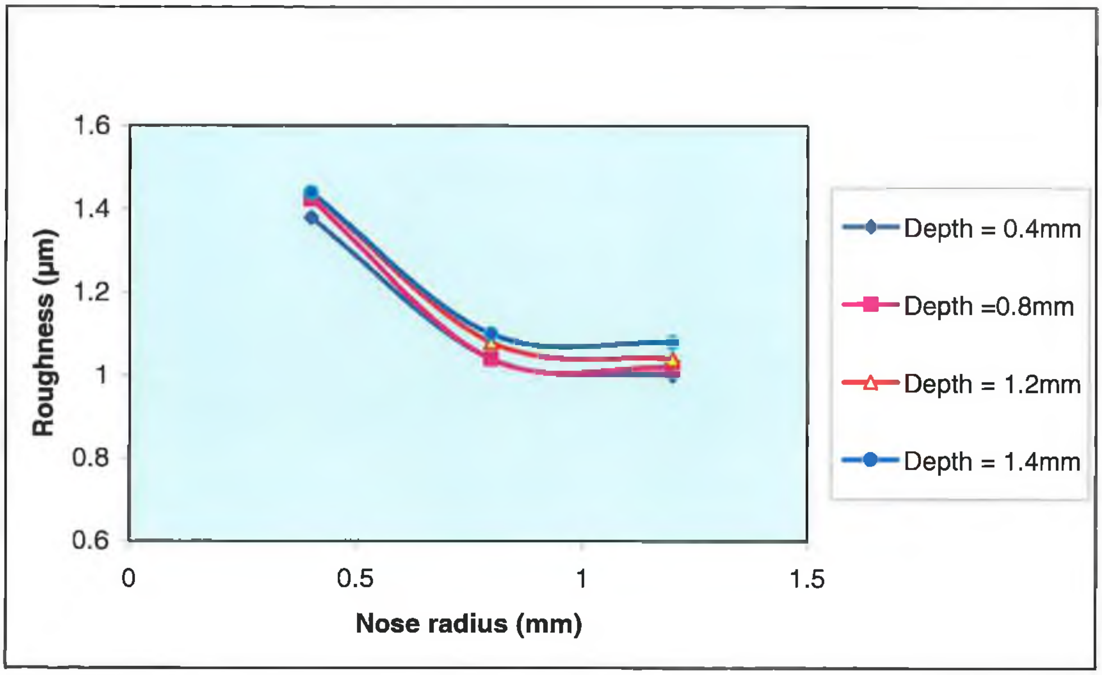

Figure 6.19 Shown the Relationship between Nose radius & Roughness at Feed 0.08 (mm/rev) and Speed 14 (m/min).

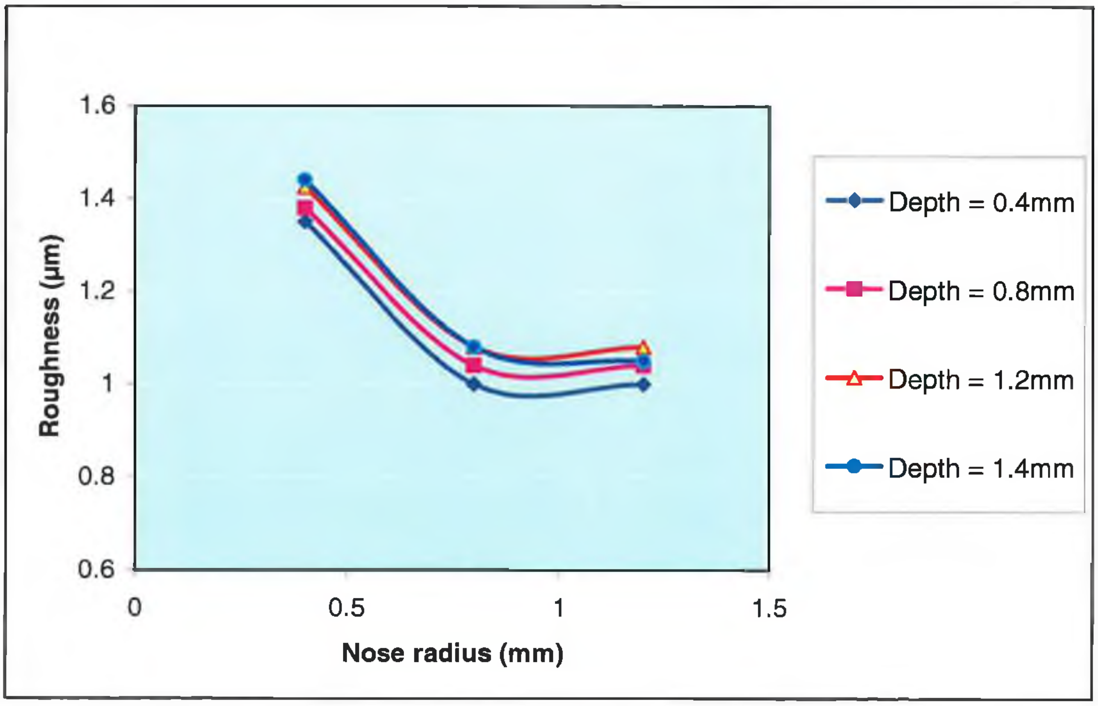

Figure 6.20 Shown the Relationship between Nose radius & Roughness at Feed 0.08 (mm/rev) and Speed 15 (m/min).

Figures; (6.19, 6.20) shows that the larger nose radius produces better surface finish.

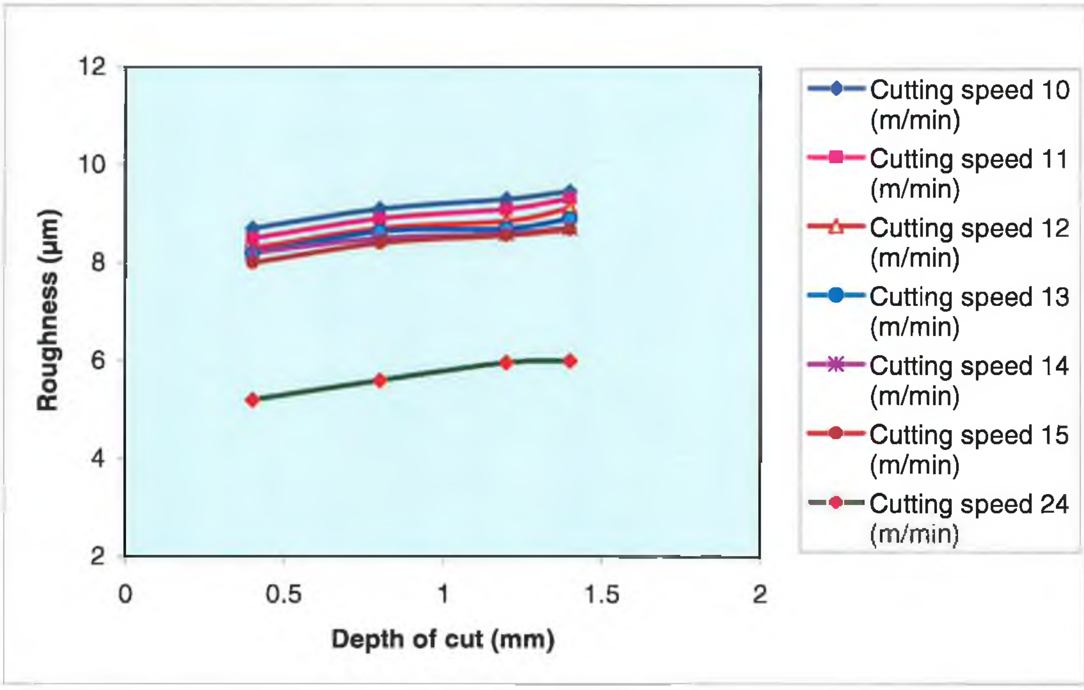

Figure 6.21 Relationship between Depth of cut & Roughness at Feed 0.25 (mm/rev)

Figures. (6.21) Shows that the machined average surface roughness (Ra) increases with increasing depth of cut.

Results of Boron nitride ceramic material

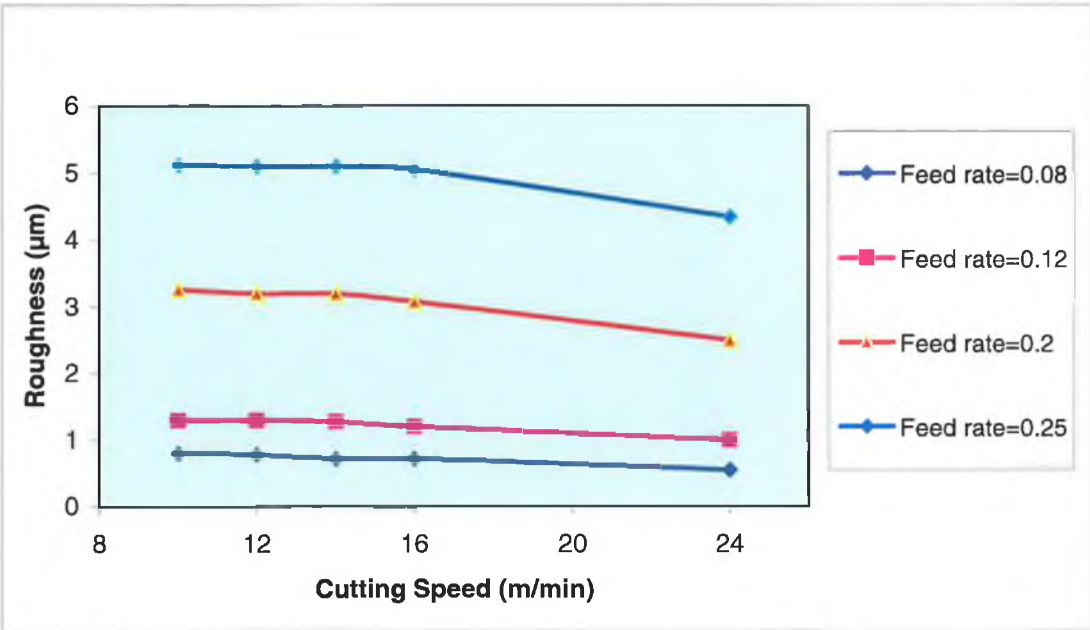

Figure 6.22 Relationship between Cutting speed & Roughness at DOC 0.4 mm

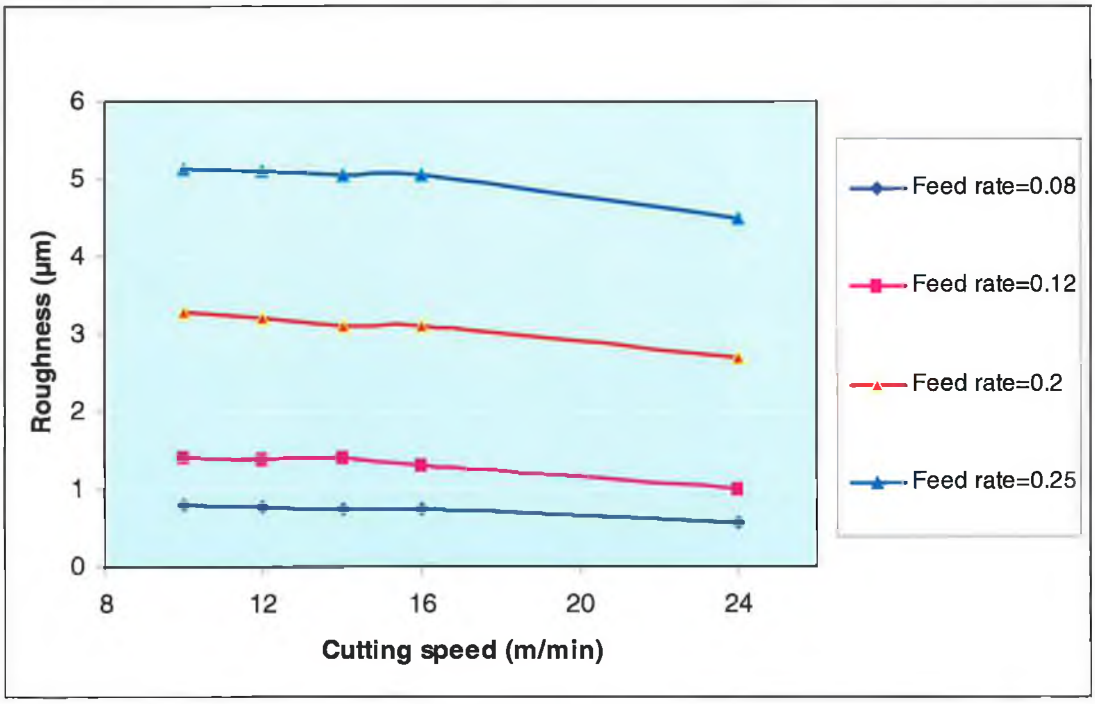

Figure 6.23 Relationship between Cutting speed & Roughness at DOC 0.8 mm

Figures; (6.22, 6.23) shows that the value of surface roughness (Ra) is low at high cutting speed and comparatively high at low cutting speed within the experimental rang at constant feed rate and depth of cut

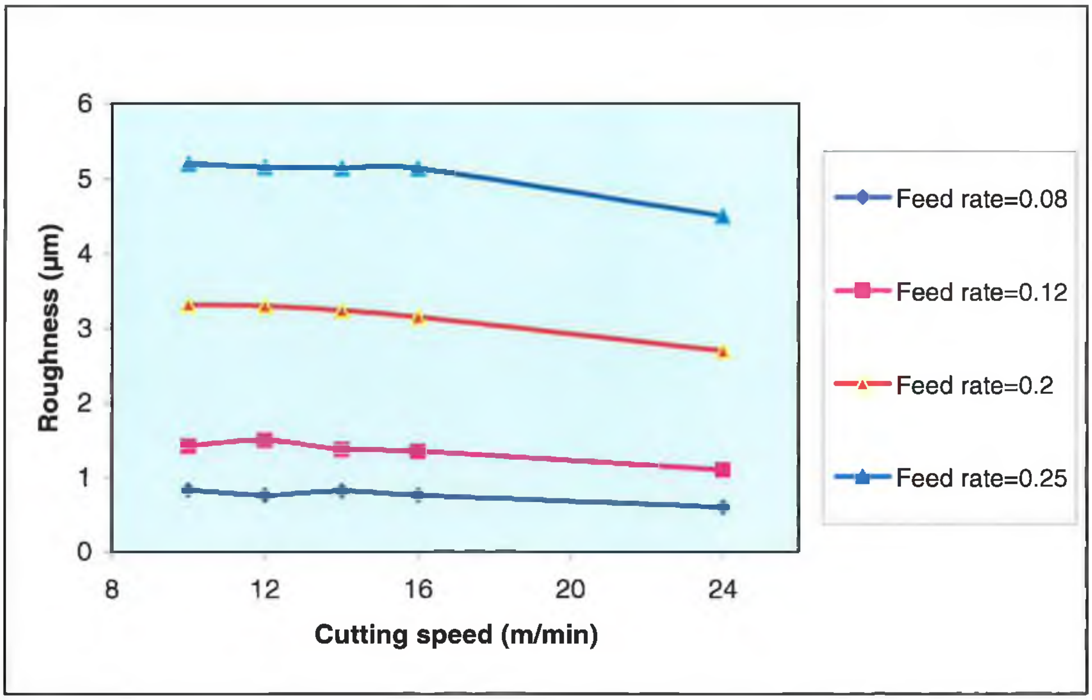

Figure 6.24 Relationship between Cutting speed & Roughness at DOC 1.2 mm

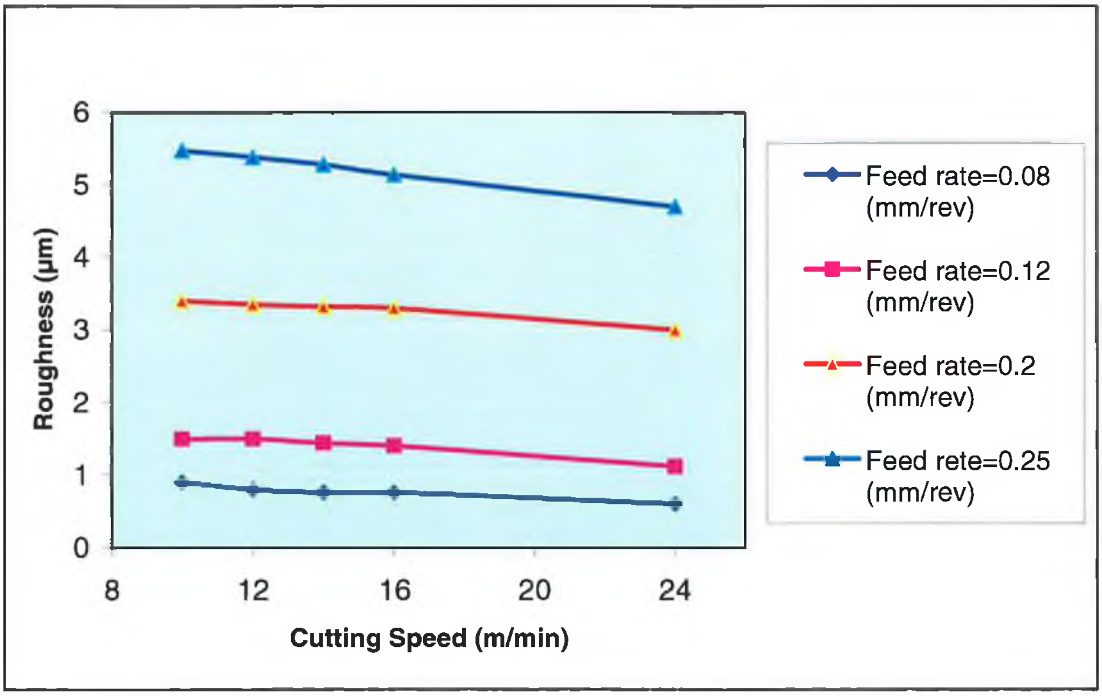

Figure 6.25 Relationship between Cutting speed & Roughness at DOC 1.4 mm

Figures; (6.24, 6.25) shows that the value of surface roughness (Ra) is low at high cutting speed and comparatively high at low cutting speed within the experimental rang at constant feed rate and depth of cut.

The experiment in this part was carried out when the feed rate fixed at 0.08 0.12, 0.2 and 0.25 (mm/rev), at each depth of cut as shown in figures (6.26), (6.27), (6.28) and (6.29) so by this way we found out the affect of depth of cut on surface finish.

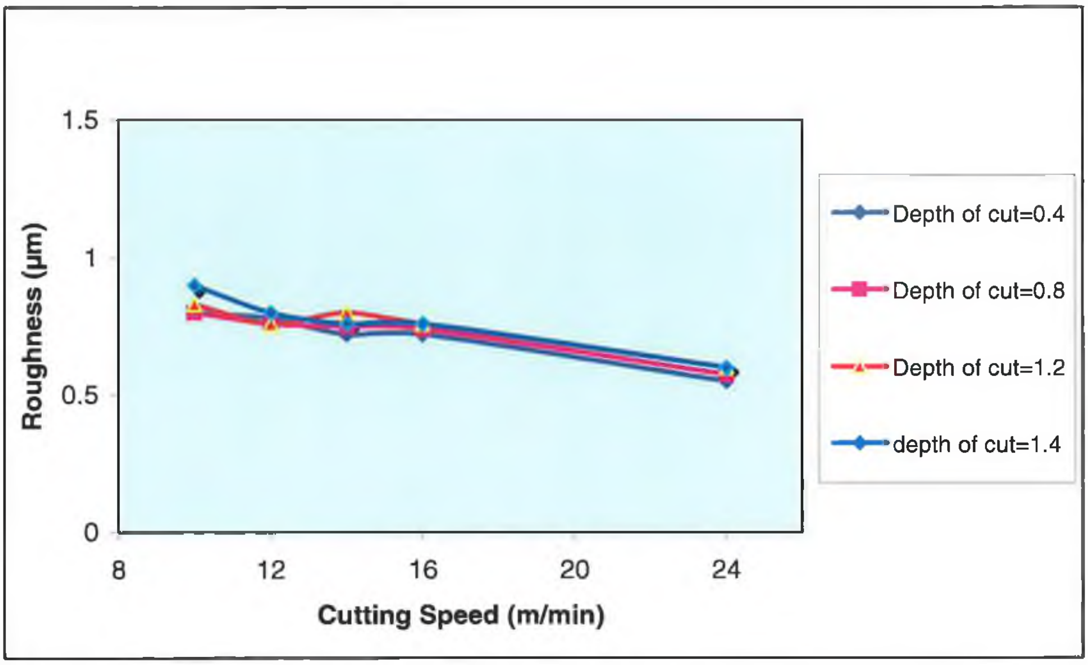

Figure 6.26 Relationship between Cutting speed & Roughness at Feed 0.08(mm/rev)

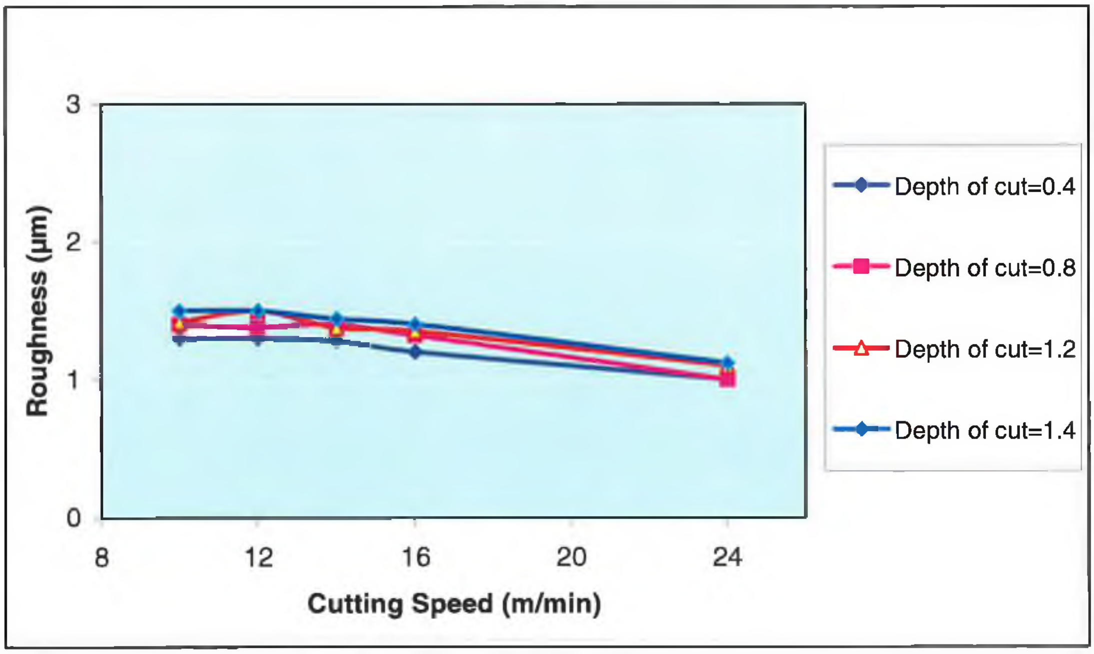

Figure 6.27 Relationship between Cutting speed & Roughness at Feed 0.12(mm/rev)

Figures; (6.26, 6.27) shows that the value of surface roughness (Ra) is low at high cutting speed and comparatively high at low cutting speed within the experimental rang at constant feed rate and depth of cut.

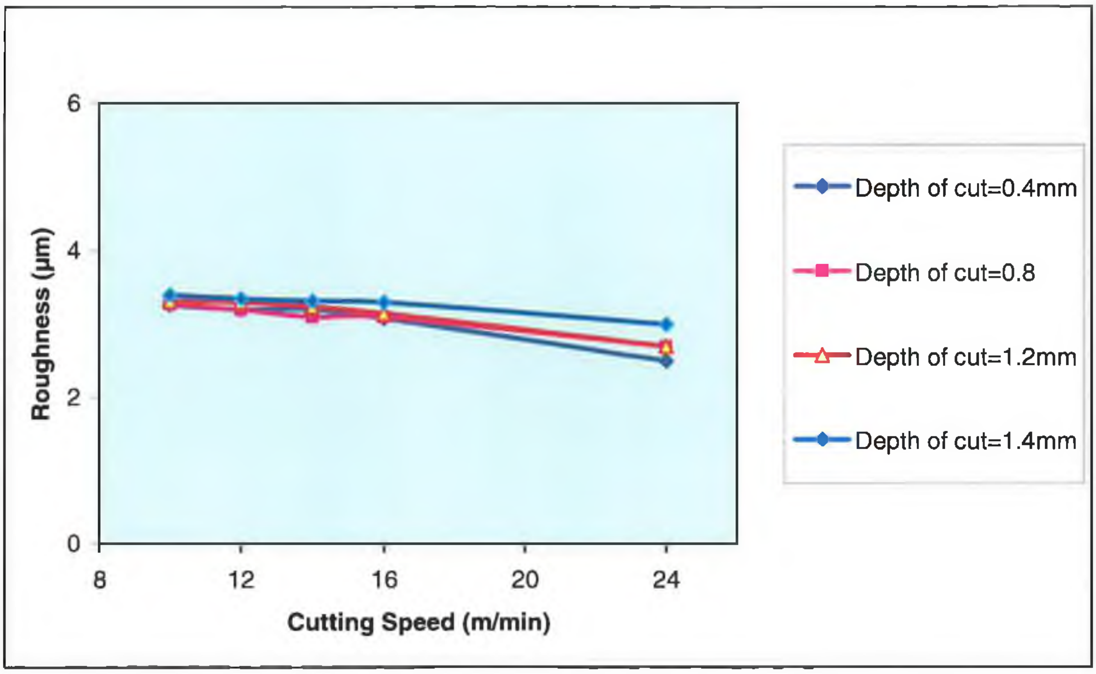

Figure 6.28 Relationship between Cutting speed & Roughness at Feed 0.2 (mm/rev)

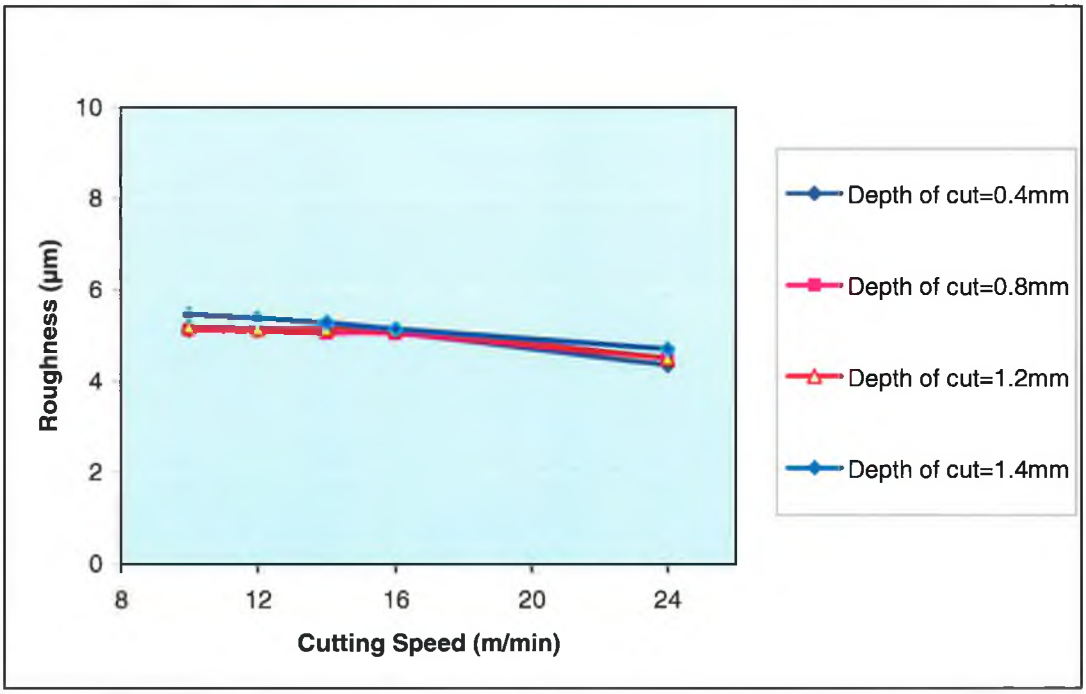

Figure 6.29 Relationship between Cutting speed & Roughness at Feed 0.25(mm/rev)

Figures; (6.28, 6.29) shows that the value of surface roughness (Ra) is low at high cutting speed and comparatively high at low cutting speed within the experimental rang at constant feed rate and depth of cut.

In this section the measurement of surface finish (Ra) is measured when the feed rate are varied but depth of cut and cutting speed are fixed to find out the affect of process parameters on surface finish.

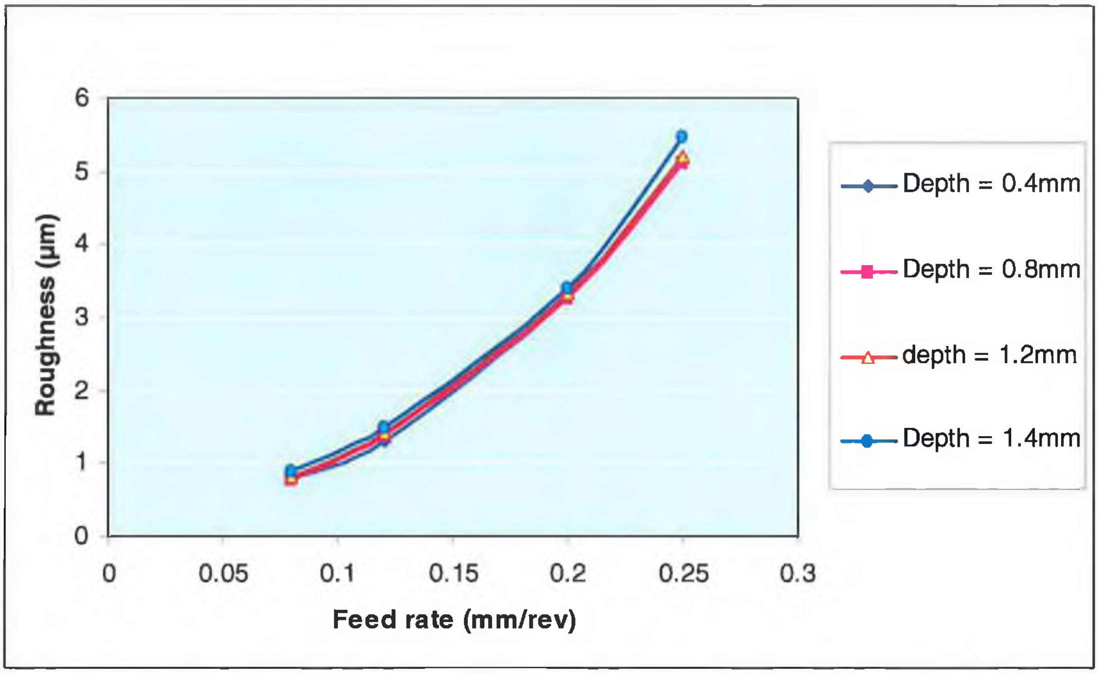

Figure 6.30 Shown the Relationship between Feed & Roughness at Speed 10(m/min)

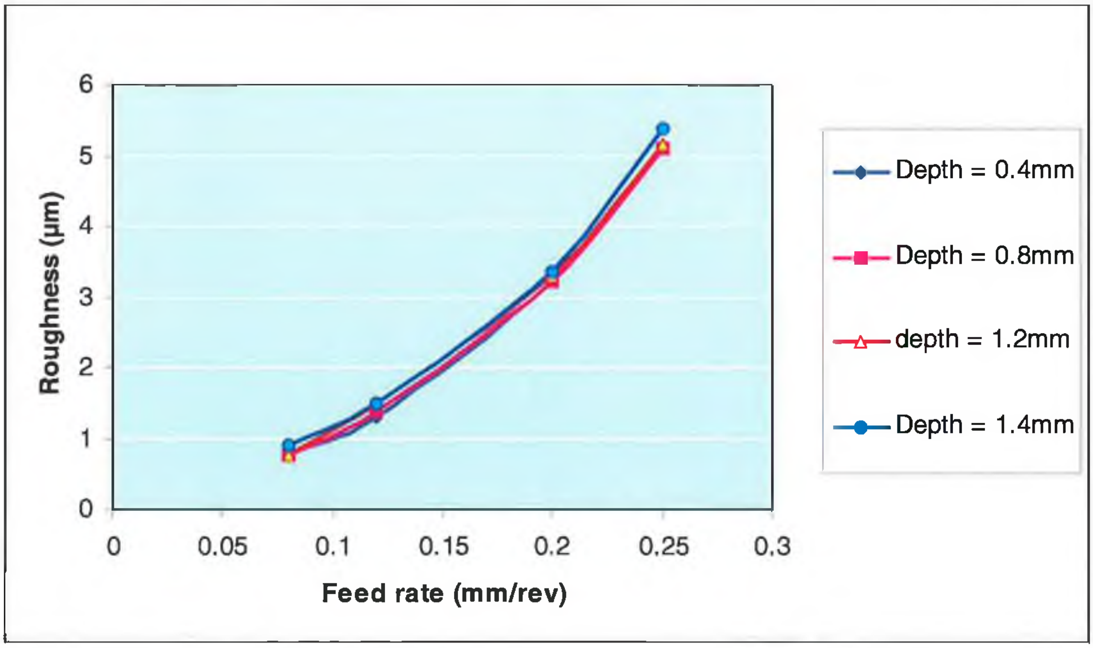

Figure 6.31 Shown the Relationship between Feed & Roughness at Speed 12 m/min

Figures; (6.30, 6.31) shows that the value of surface roughness (Ra) increases gradually with an increase in feed rate, it happened at each depth of cut.

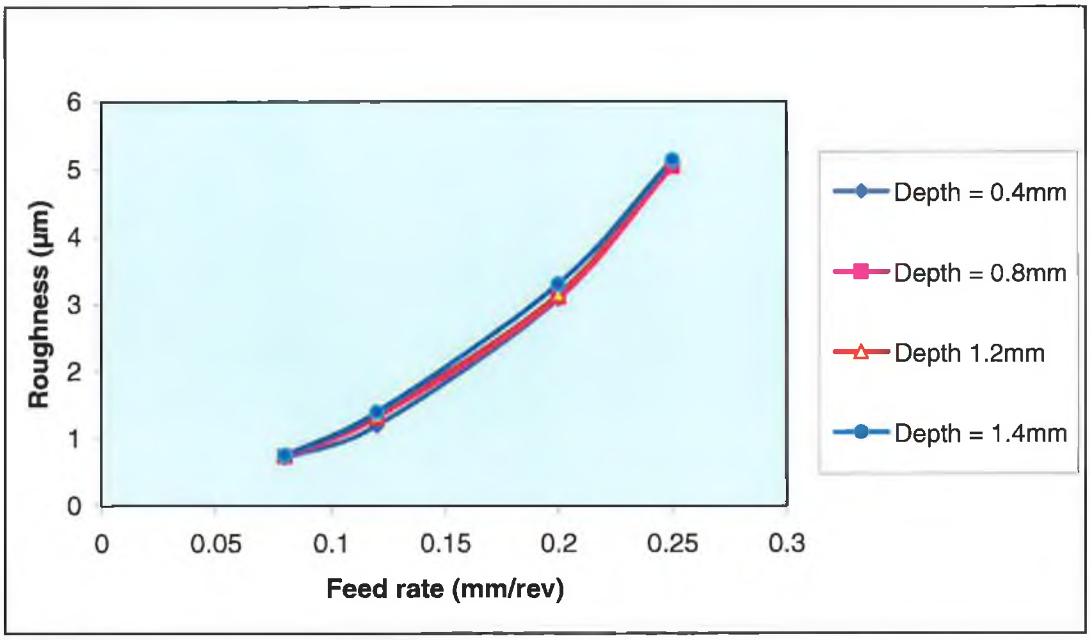

Figure 6.32 Shown the Relationship between Feed & Roughness at Speed 14 m/min

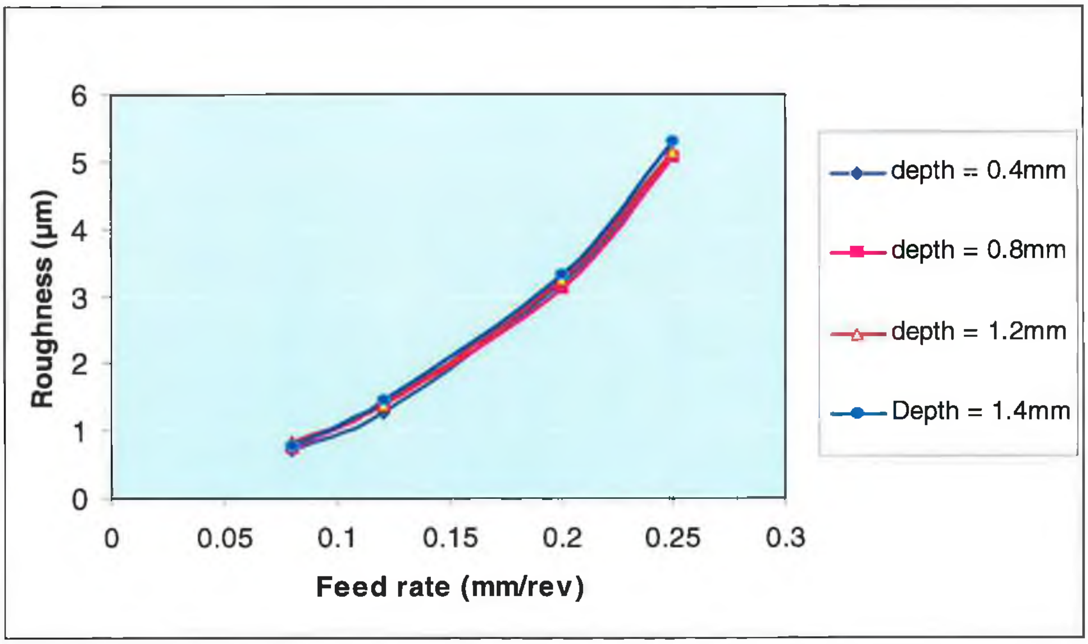

Figure 6.33 Shown the Relationship between Feed & Roughness at Speed 16 m/min

Figures; (6.32, 6.33) shows that the value of surface roughness (Ra) increases gradually with an increase in feed rate, it happened at each depth of cut.

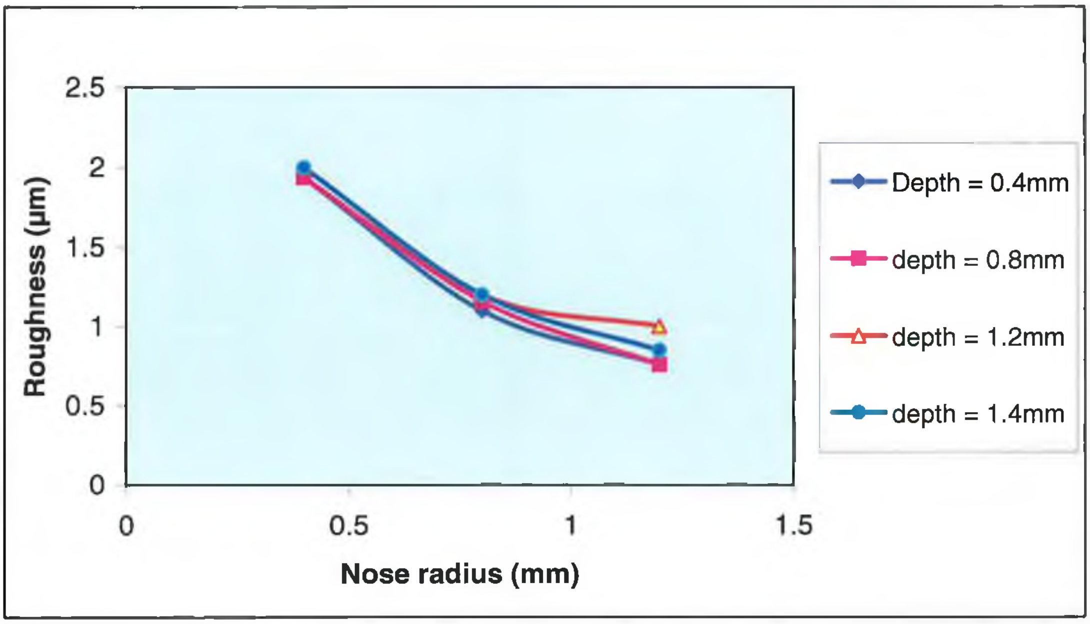

Figure 6.34 Shown the Relationship between Nose radius & Roughness at Feed 0.08 (mm/rev) and Speed 10 (m/min).

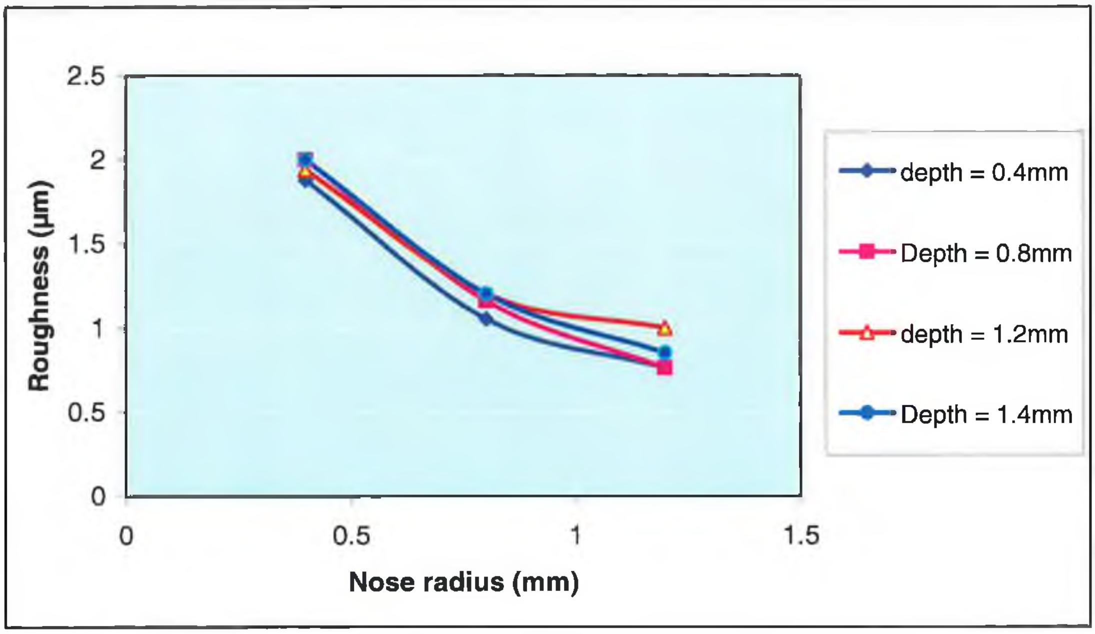

Figure 6.35 Shown the Relationship between Nose radius & Roughness at Feed 0.08 (mm/rev) and Speed 12 (m/min).

Figures; (6.34, 6.35) shows that the larger nose radius produces better surface finish.

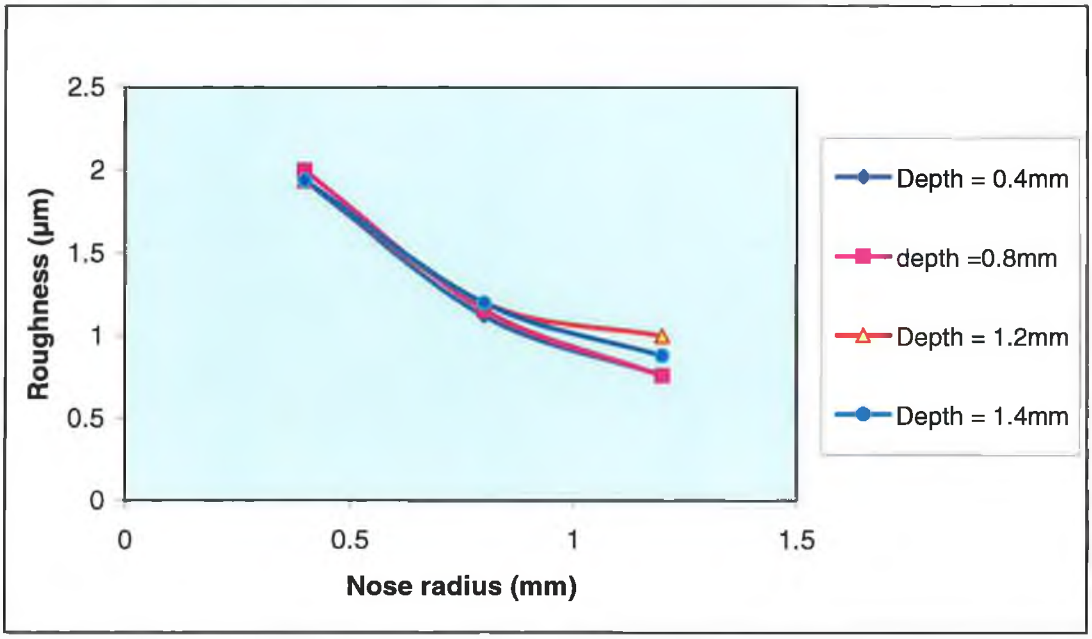

Figure 6.36 Shown the Relationship between Nose radius & Roughness at Feed 0.08 (mm/rev) and Speed 14 (m/min).

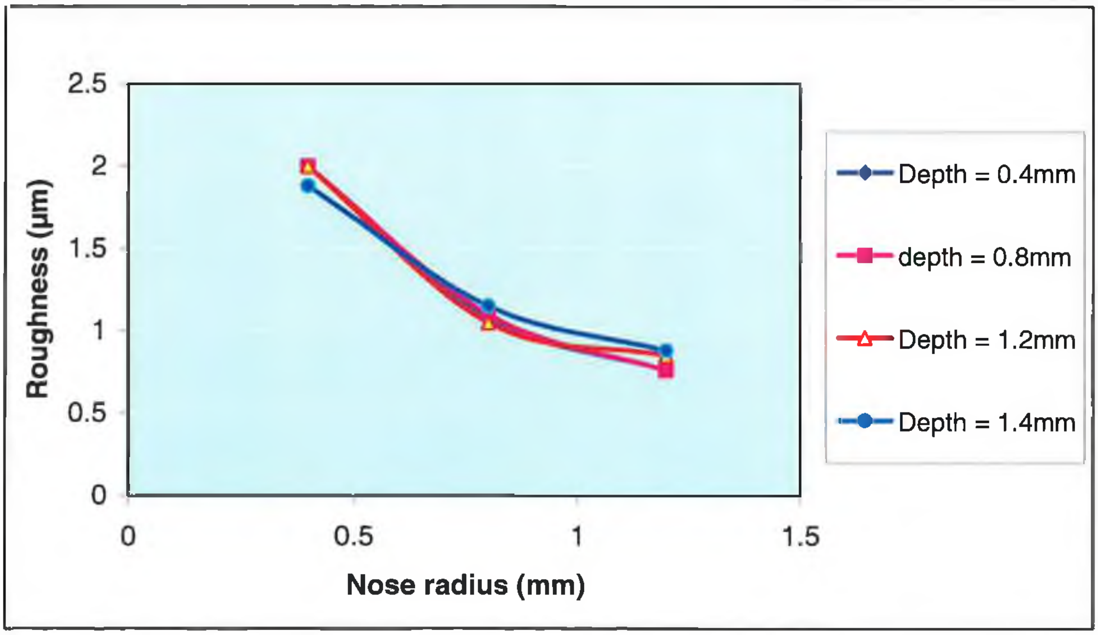

Figure 6.37 Shown the Relationship between Nose radius & Roughness at Feed 0.08 (mm/rev) and Speed 16 (m/min).

Figures; (6.36, 6.37) shows that the larger nose radius produces better surface finish.

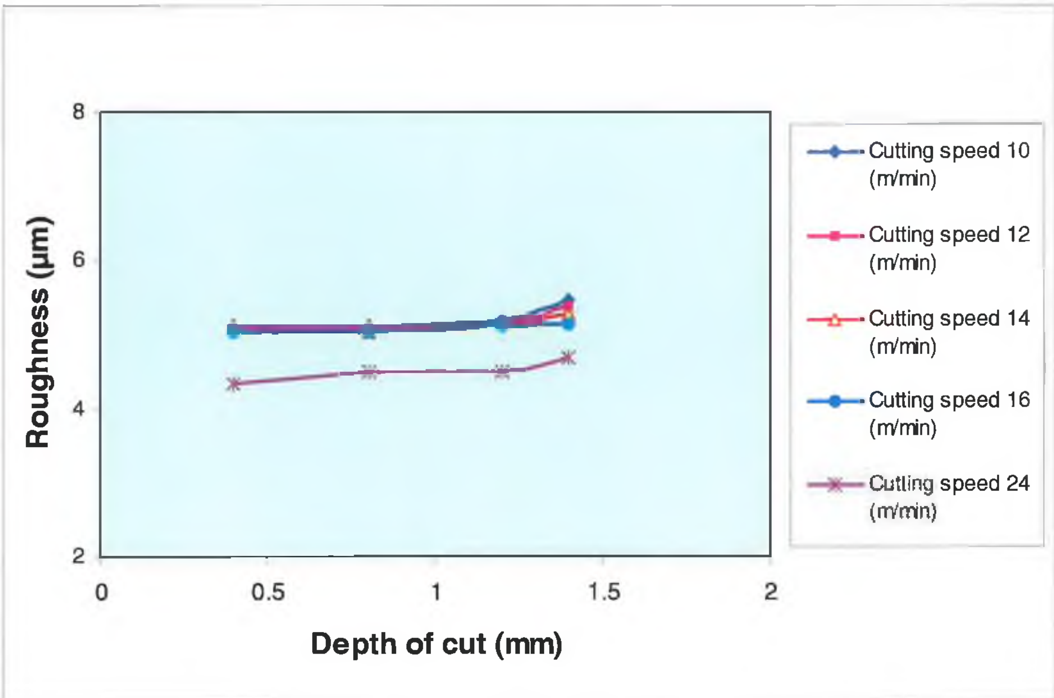

Figure 6.38 Relationship between Depth of cut & Roughness at Feed 0.25 (mm/rev)

Figures. (6.38) Shows that the machined average surface roughness (Ra) increases with increasing depth of cut.

Summary

The following conclusions are based on the results for turning tests with uncoated carbide tools under dry conditions. The effects of machining conditions namely feed rates, cutting speed, nose radius and depth of cut, on the average surface roughness (Ra) of machinable glass ceramic (Macor & Boron nitride) were studied during cutting operation. It was found that as feed rate increases the surface roughness value increase so the best surface finish was produced at less feed rate. It was also observed that the increase in cutting speed increases the quality of surface finish at constant feed and depth of cut. The effect of depth of cut on surface roughness (Ra) is shown that as the depth of cut increases the surface roughness (Ra) will increase. Also a large nose radius produces better surface finish. However increasing speed, feed, depth of cut and nose radius influence the surface finish. And also through the results the boron nitride is shown to be more machinable than Macor, because the hardness of Macor material is higher than boron nitride.

6.3 Tool Life

6.3.1 Factor affecting Tool Life

1. **Effect of Cutting speed on Tool life**

From the literature survey, cutting speed directly affects the tool wear, cutting forces, surface finish and the type of chip formed. At low speeds the material behaves in a brittle method, with discontinuous chips and low tool wear. However it also results in poor surface finish. High cutting speed results in continuous chips and better surface finish but the disadvantage causes an increase in cutting temperature, which leads to high tool wear and therefore the tool life is low. The major effect of cutting speed is on tool wear therefore efforts must be made to balance these factors to attain the most desired conditions [52].

2. **Effect of Feed rate on Tool life**

This is similar to cutting speed in that it influences tool wear, surface finish and cutting forces, but to a lesser extent. The effect of an increase in feed rate is an increase in the cutting force and temperature in the cutting zone, and also increase in cutting forces, and an increase in the likelihood of chipping of the cutting edge through mechanical shock. An increase in the feed rate also increases the tool wear and produces a poor surface finish [52].

3. **Effect of Depth of cut on the Tool life**

This has not good effect on the surface finish but has a significant effect on the cutting forces. A small increase in the depth of cut produce a significant increase in the cutting forces [52].

6.3.2 Tool Life Tests

The tool life experiments were carried out using uncoated carbide insert tool under dry conditions for both materials. Three sets of test runs were conducted. The first set of experiment was conducted by varying the cutting speed at a constant feed rate of 0.2 mm/rev, and depth of cut of 1.2 mm. In the second set of experimental runs, feed rate was varied while the cutting speed and depth of cut were kept constant of (60 m/min) and (1.2 mm) respectively. Finally for the third set of experiments the depth of cut was varied while the cutting speed and feed rate were kept constant of (60 m/min) and (0.2 mm/rev) respectively.

Tool wear values of both materials were measured using a Toolmakers microscope. The experimental conditions are shown in table (6.1).

Table 6.1. The experimental conditions to the tool life measurements.

Cutting speed (m/min)	Feed rate (mm/rev)	Depth of cut (mm)
20	0.08	0.8
40	0.12	1.2
60	0.2	1.4
80	0.25	1.6

During the study it has been noted that there is no change in the tool geometry, therefore no replacement and/ or maintenance for the tool during the total time of the cutting operation. The next paragraphs will explain the factors that affect the tool life and their relationship to my work.

a) The relationship between the tool life and temperature. It has been known for many years that as the tool temperature increases, the tool life reduces [39]. The relationship between the tool life and temperature is:

$$\theta T^{n} = C_3$$

Where θ is some measure of tool temperature; and n, C_3 are constants for the Tool-workpiece combination.

In this study since the cutting temperature is not expected to be high due to some parameters like the hardness of workpiece material. Therefore, no tool wears has achieved in the surface of the tool, for all the cutting conditions, which was used.

b) The rake angle effect on the tool life. It has been known that as the rake angle increases in the positive side the tool wear increases and consequently the tool life will be decrease. According to this and because in this work the rake angle was kept constant ($\gamma = 0$), so its effect will be slight on the tool life.

c) The affect of continuous chip on the tool life. Since the chip was discontinuous- it was like the powder- during the cutting operation of all the cutting conditions. So, no direct contact between the tool and the chip that led to no wear on the tool face due to the chip continuity.

d) The affect of tool hardness on the tool life and also the hardness of the materials itself.

In general the uncoated carbide tools gave higher tool life when machining ceramic materials.
The recommended cutting speed for machining ceramic materials using the uncoated carbide tools should be within 20-80 (m/min), feed rate should be 0.08-0.25 (mm/rev) and depth of cut should be 0.8-1.6 (mm).

6.4 Cutting Force

The metal cutting process is a result of two relative movements between the cutting tool and the work material, which has to be machined. The relative movements between the cutting edge and the work piece material results in an amount of metal corresponding to the depth of cut being separated from the workpiece material in the form of chips whilst the feed movement brings new material in front of the cutting edge after a particular cut has been finished.
A standard method of assessing the machinability of a material is to measure the cutting force components F_z, F_x, and F_y (tangential, axial, and radial), the tool holder was mounted on the kistler dynamometer connected to a PC based data acquisition system through the charge amplifiers. The Kistler piezoelectric dynamometer was mounted on the lathe. Chapter 5 describes the details of these instrumentations and equipments used.

In conducting the experiments, two of the machining parameters out of the three (cutting speed, feed rate and depth of cut) are kept constant. The third parameter was varied from one end of its operation range to the other, in order to observe its effect on the machining response (cutting force).

The cutting force tests were carried out for the both ceramic materials Macor and Boron nitride respectively using uncoated carbide tools under dry conditions to observe the effect of cutting speed, feed rate and depth of cut on the force produced. The purpose of these tests is to estimate the cutting forces and derive optimum cutting conditions to minimise the cutting forces produced.

The machining operation involved continuous turning at three different feed rates (1, 2, 3 mm/rev), and three different depths of cuts (0.5, 1, 1.5 mm) with the cutting speed varying from 15-45 (m/min).

Figures (6.39-6.41) and figures (6.52-6.54) shows the variation of tangential, axial and radial forces with cutting speed at a feed rate of 1, and depth of cuts of 0.5, 1, and 1.5 mm respectively. Similar plots of force speed variation at different feed rates of 2 and 3 (mm/rev) have been presented in figures (6.43-6.45), (6.56-6.58) and figures (6.47-6.49), (6.60-6.62) respectively.

All the figures for the Macor material (figures 6.39-6.51) depict that the tangential component of the cutting force F_z is the highest in magnitude followed by the feed F_x and radial F_y components.

Generally as the cutting speed increased the forces increased. The feed force was higher than the radial force at higher depth of cuts (1 and 1.5 mm).

While the Boron nitride all the figures depict that the feed force F_x is the highest of the three force present.

Figures (6.42, 6.46, 6.50) and (6.55, 6.59, 6.63) presents the variation of resultant cutting force with depth of cut at three different feed rate and constant cutting speed of 25 (m/min). The forces were found to increase linearly with the depth of cut. A similar trend was observed when the forces were plotted against different feed rate as shown in figures (6.51, 6.64). The cutting force was observed to increase linearly with the feed rate.

Results of Macor ceramic material

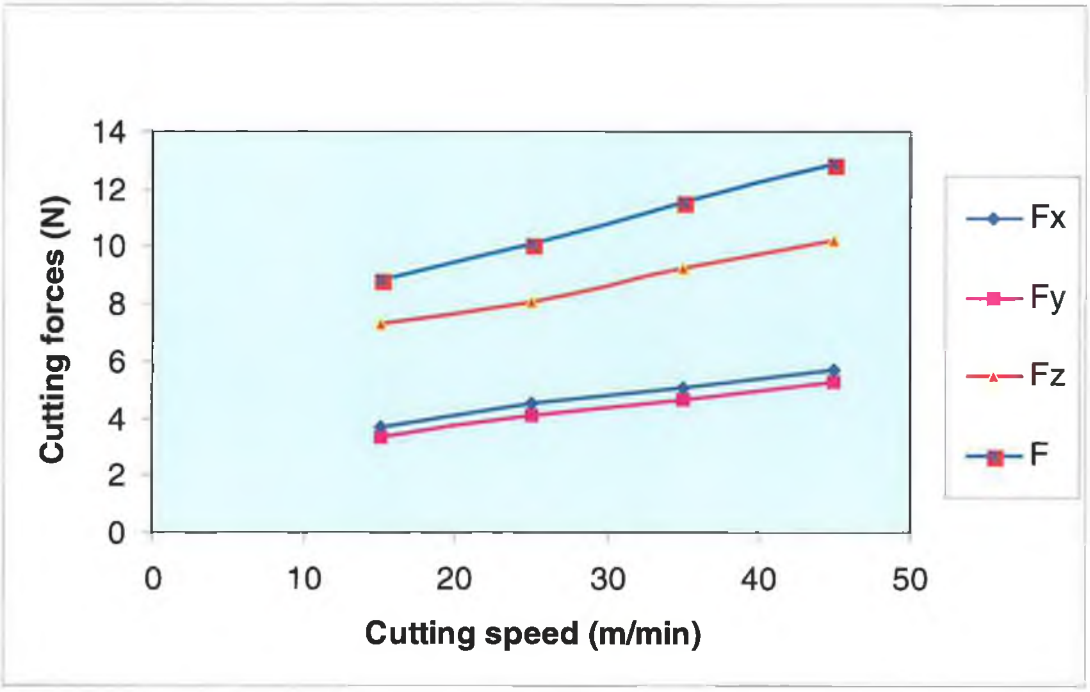

Figure 6.39 Relationship between Cutting forces & Cutting speed at Feed rate 1 (mm/rev) and Depth of cut 0.5 mm

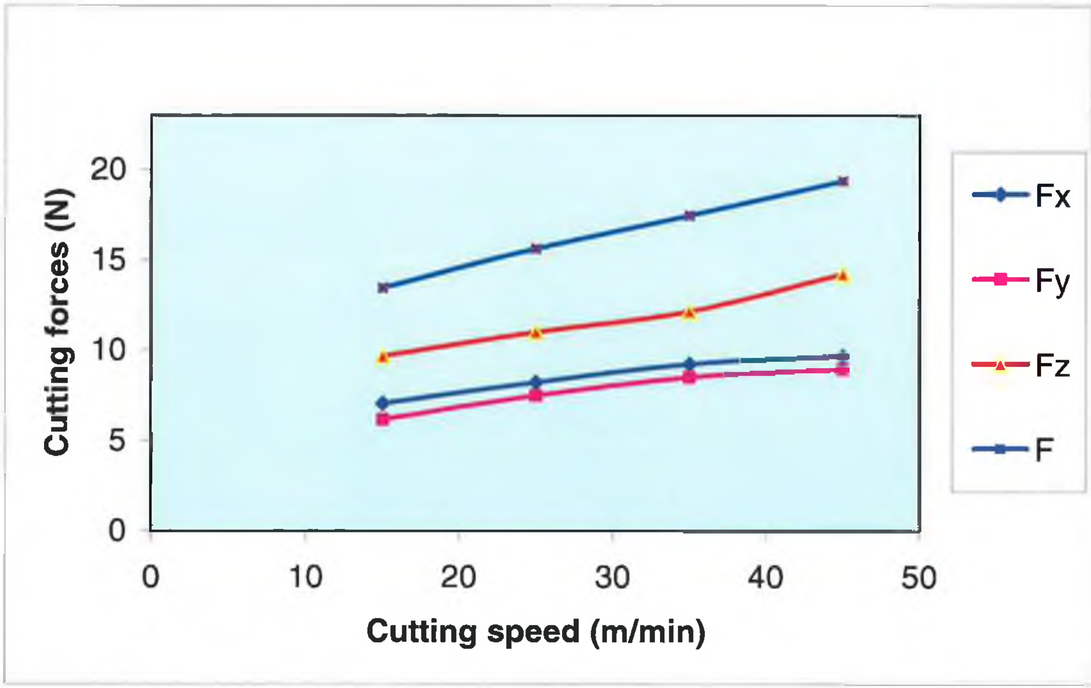

Figure 6.40 Relationship between Cutting forces & Cutting speed at Feed rate 1 (mm/rev) and Depth of cut 1 mm

Figures; (6.39, 6.40) shows that with the increases in cutting speed increase the cutting forces slightly.

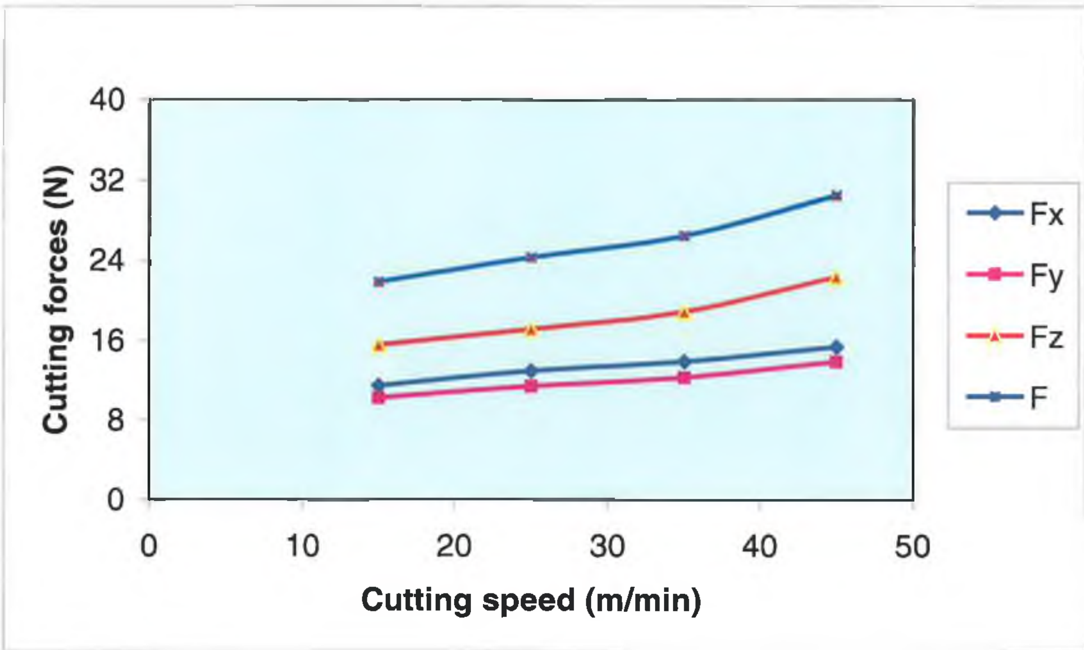

Figure 6.41 Relationship between Cutting forces & Cutting speed at Feed rate 1 (mm/rev) and Depth of cut 1.5 mm

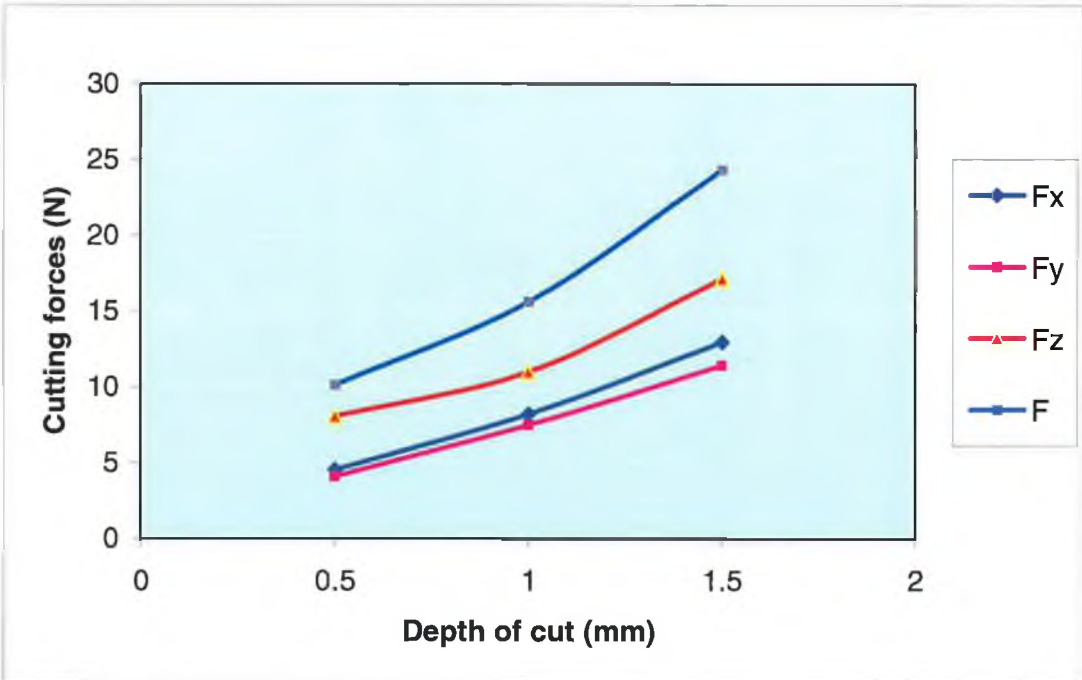

Figure 6.42 Relationship between Cutting forces & Depth of cut at Feed rate 1 (mm/rev) and Cutting speed 25 (mm/min)

Figure; (6.41, 6.42) shows that with the increase of depth of cut, cutting forces increase almost linearly.

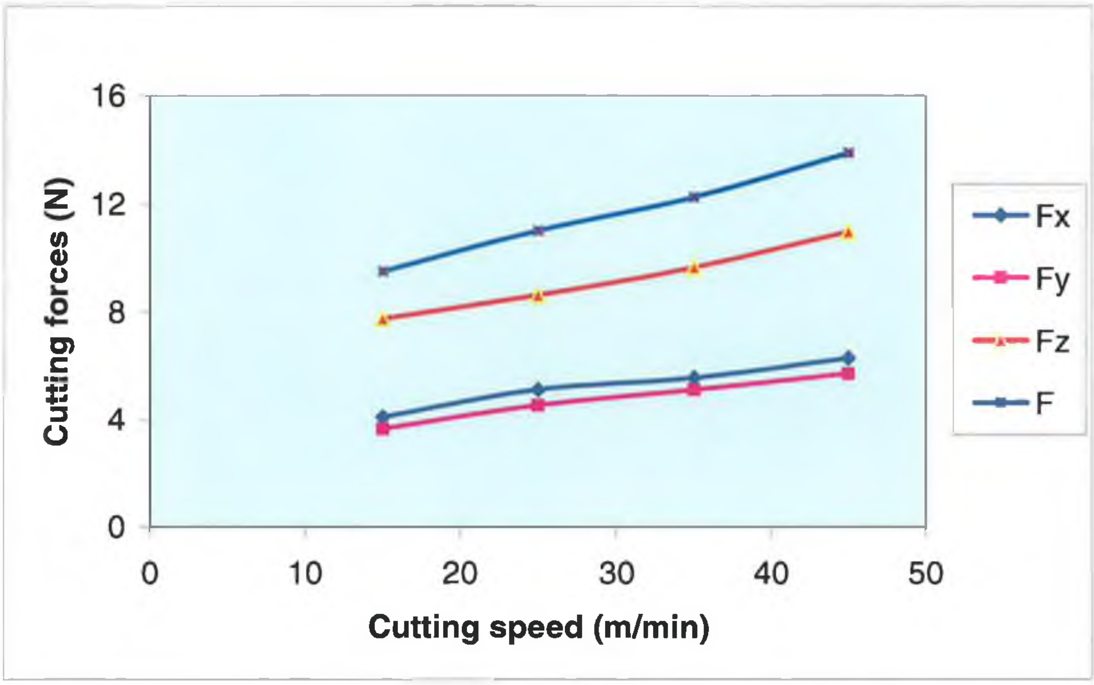

Figure 6.43 Relationship between Cutting forces & Cutting speed at Feed rate 2 (mm/rev) and Depth of cut 0.5 mm

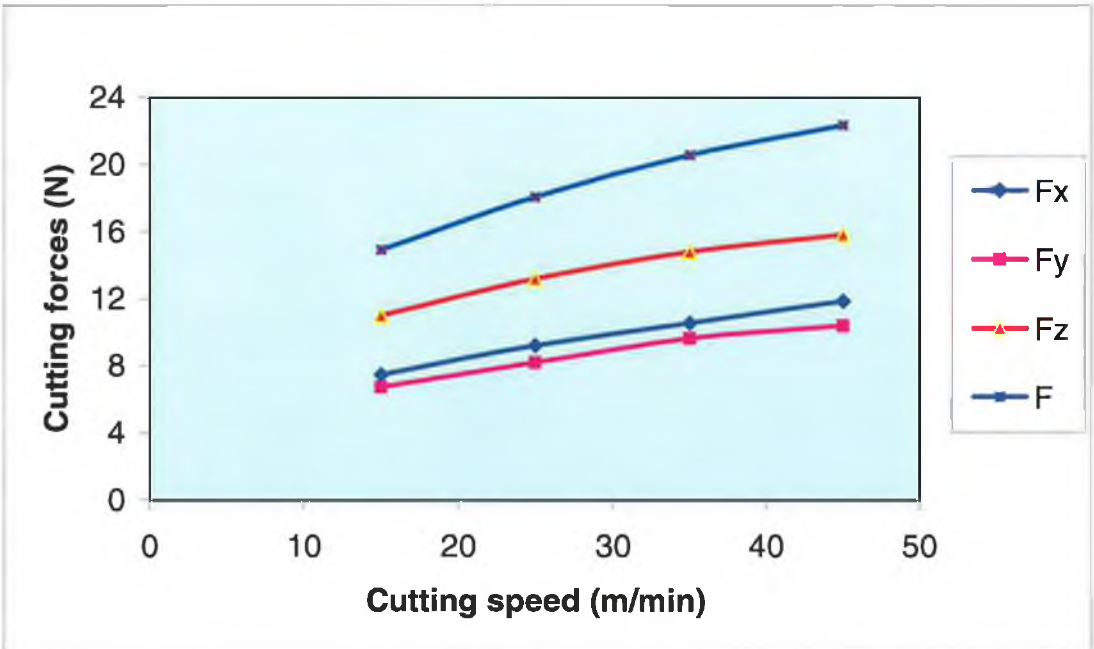

Figure 6.44 Relationship between Cutting forces & Cutting speed at Feed rate 2 (mm/rev) and Depth of cut 1 mm

Figures; (6.43, 6.44 and 6.45) shows that with the increases in cutting speed increase the cutting forces slightly.

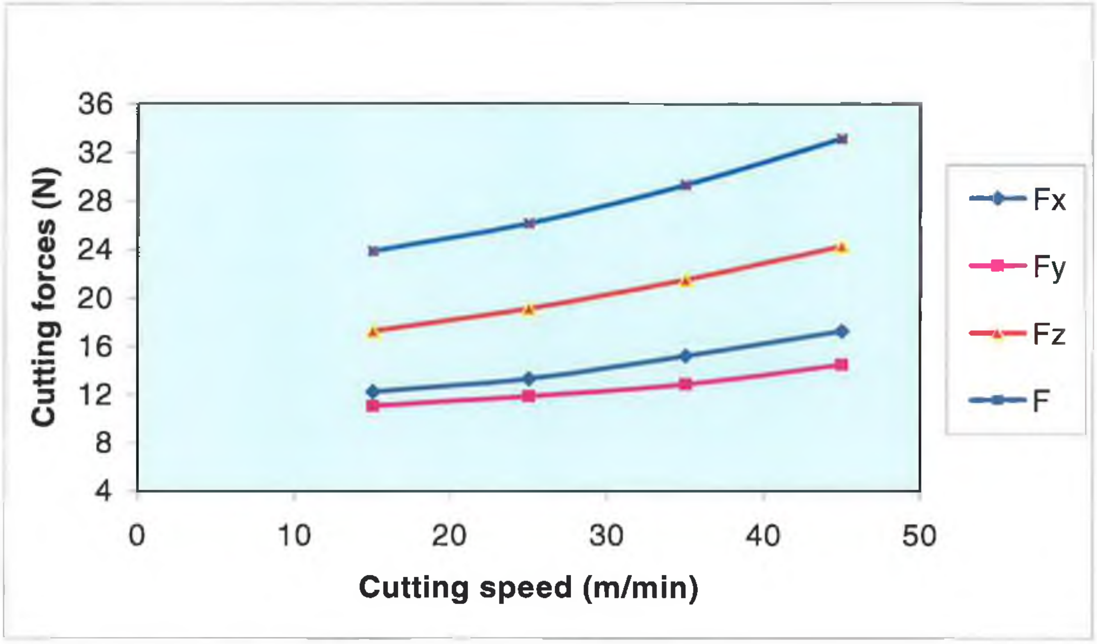

Figure 6.45 Relationship between Cutting forces & Cutting speed at Feed rate 2 (mm/rev) and Depth of cut 1.5 mm

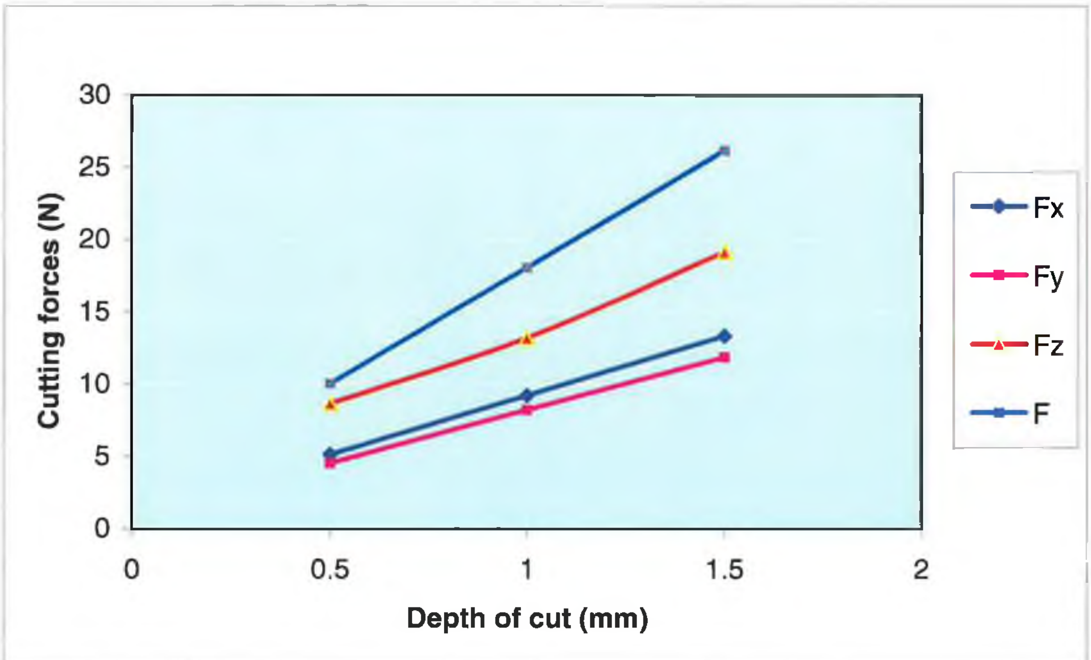

Figure 6.46 Relationship between Cutting forces & Depth of cut at Feed rate 2 (mm/rev) and Cutting speed 25 (mm/min)

Figure; 6.46 shows that with the increase of depth of cut, cutting forces increase almost linearly.

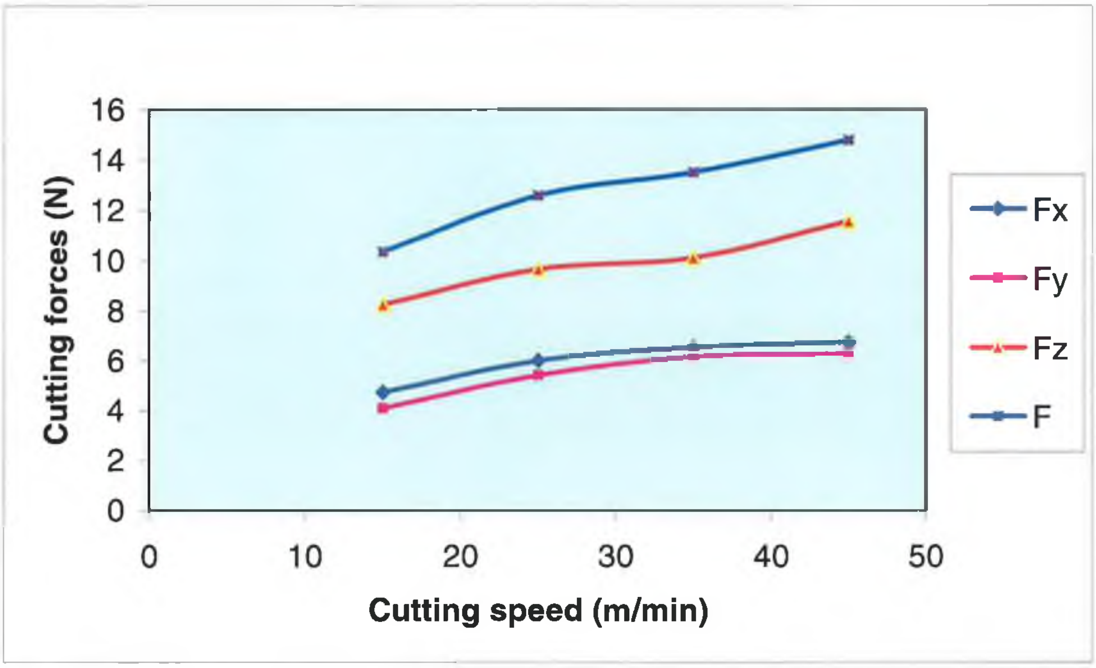

Figure 6.47 Relationship between Cutting forces & Cutting speed at Feed rate 3 (mm/rev) and Depth of cut 0.5 mm

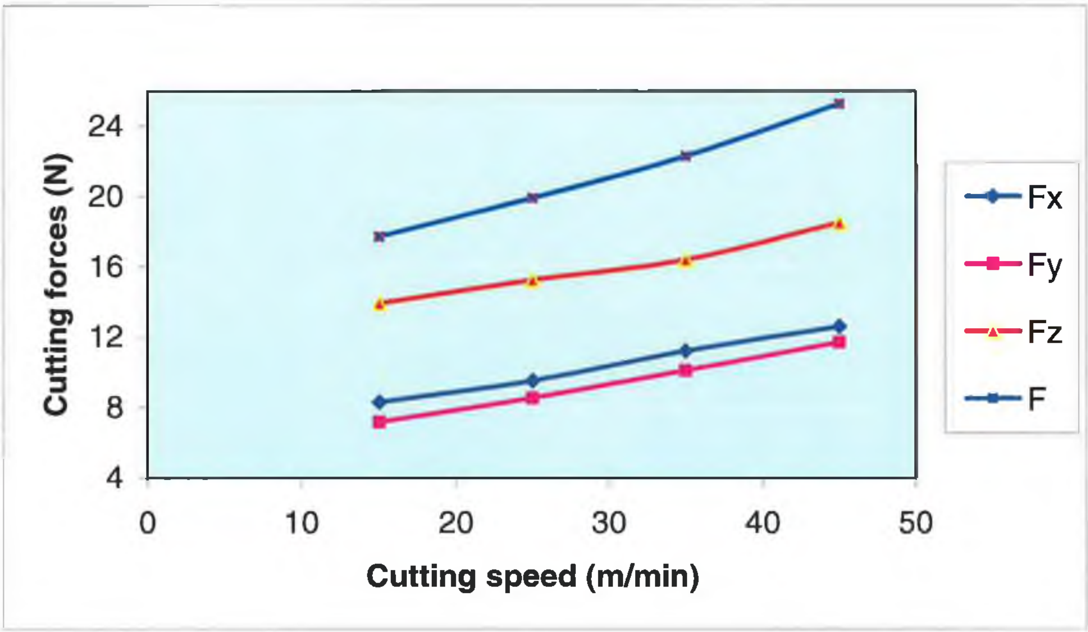

Figure 6.48 Relationship between Cutting forces & Cutting speed at Feed rate 3 (mm/rev) and Depth of cut 1 mm

Figures; (6.47, 6.48 and 6.49) shows that with the increases in cutting speed increase the cutting forces slightly.

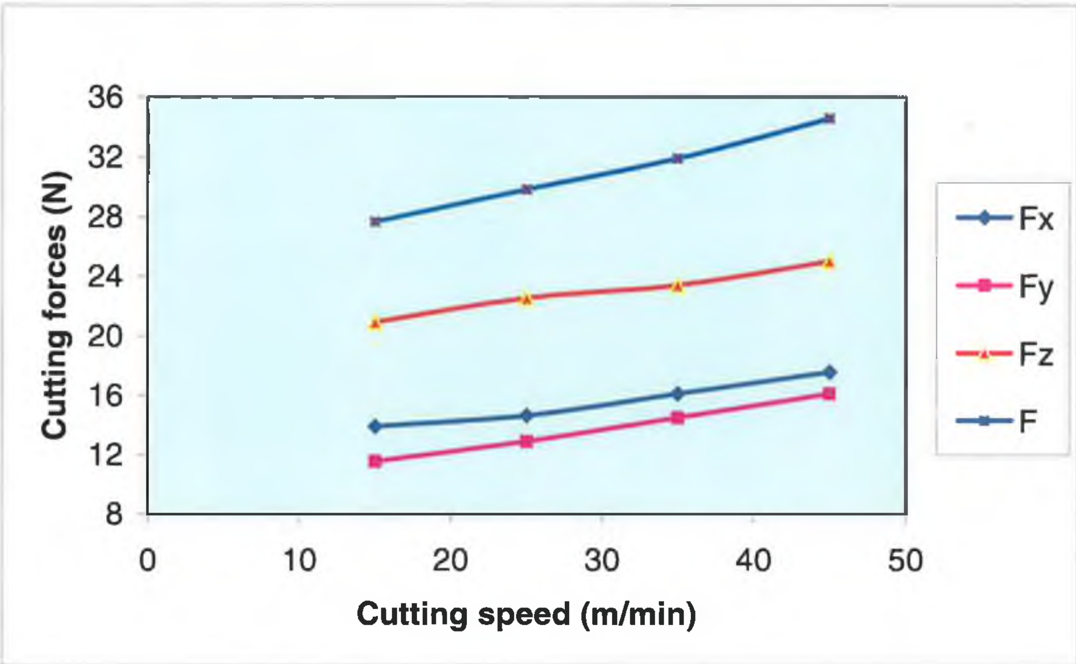

Figure 6.49 Relationship between Cutting forces & Cutting speed at Feed rate 3 (mm/rev) and Depth of cut 1.5 mm

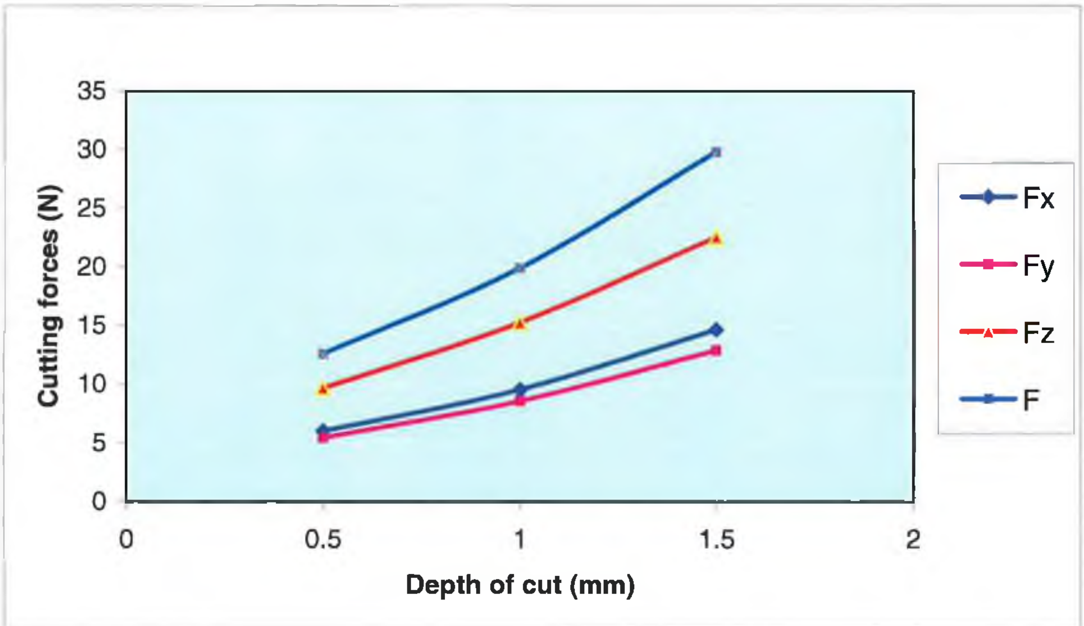

Figure 6.50 Relationship between Cutting forces & Depth of cut at Feed rate 3 (mm/rev) and Cutting speed 25 (mm/min)

Figure; 6.50 shows that with the increase of depth of cut, cutting forces increase almost linearly.

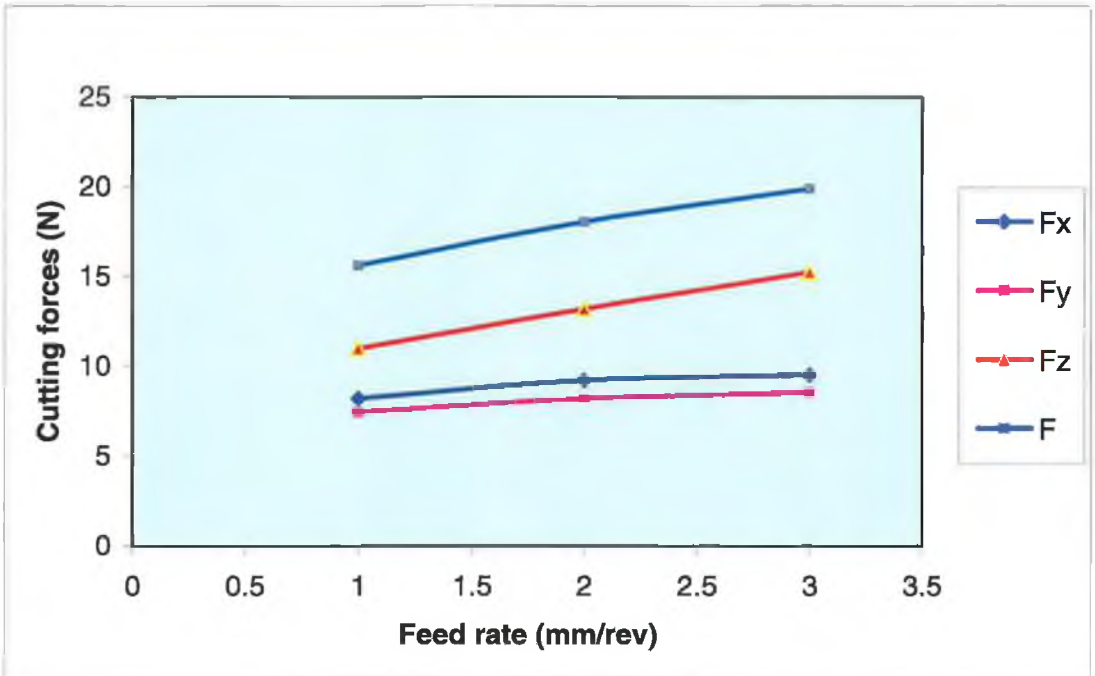

Figure 6.51 Relationship between Cutting forces & Feed rate at Depth of cut 1 mm and Cutting speed 25 (mm/min)

Figure; 6.51 shows that with the increase of feed rate, cutting forces increase almost linearly.

Results of Boron nitride ceramic material

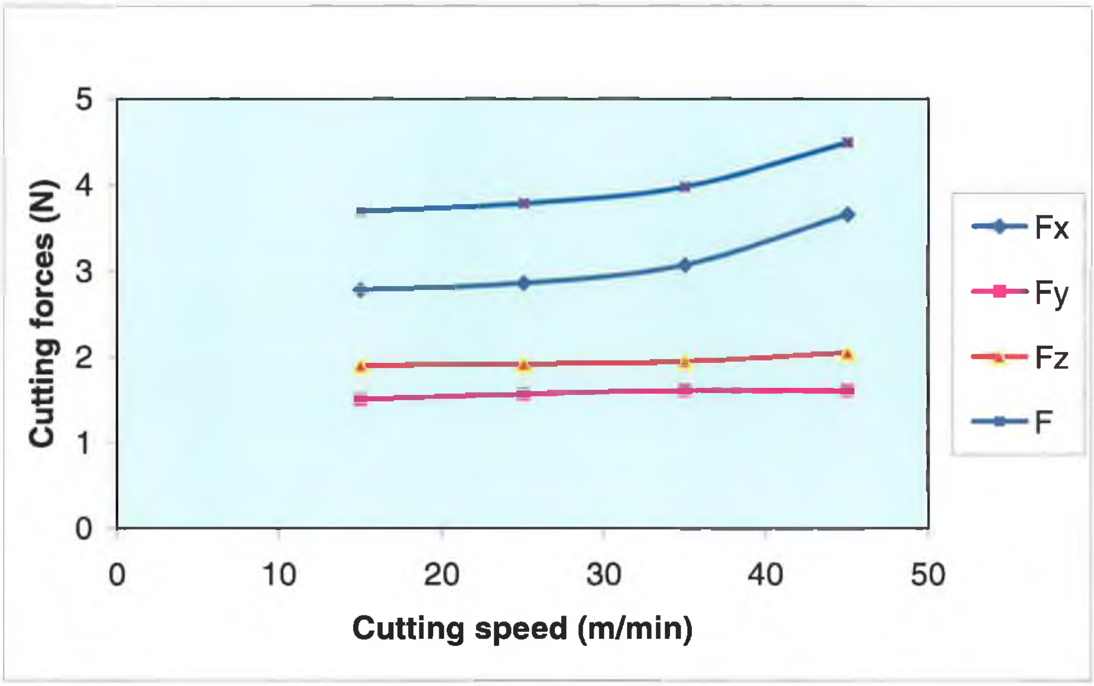

Figure 6.52 Relationship between Cutting forces & Cutting speed at Feed rate 1 (mm/rev) and Depth of cut 0.5 mm

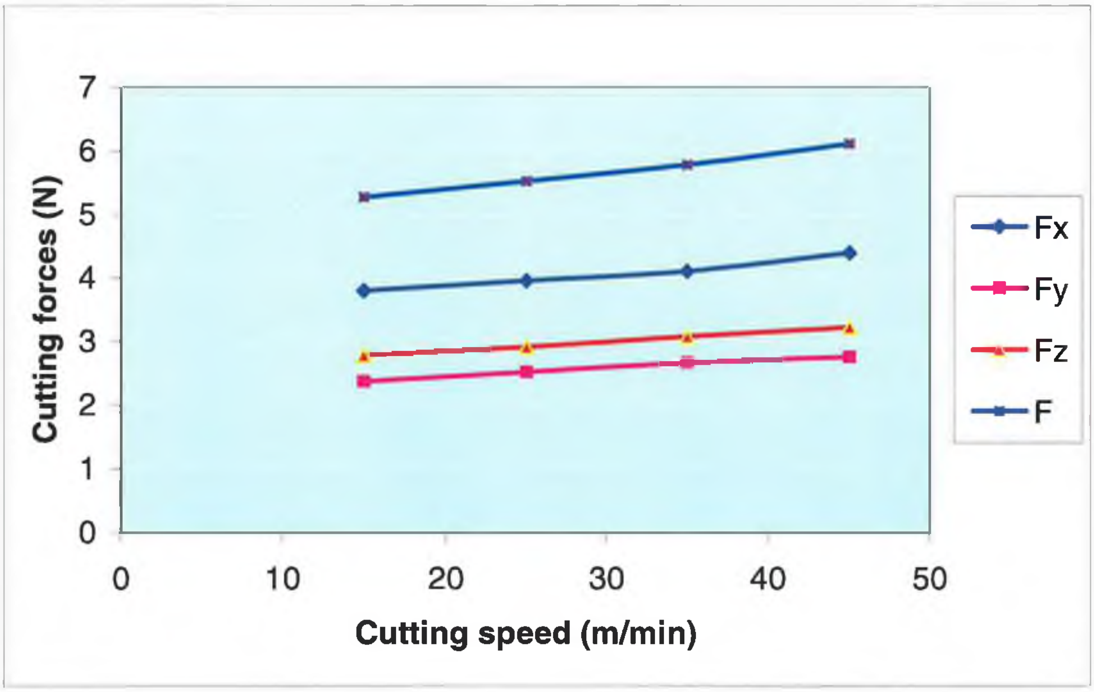

Figure 6.53 Relationship between Cutting forces & Cutting speed at Feed rate 1 (mm/rev) and Depth of cut 1 mm

Figures; (6.52, 6.53 and 6.54) shows that with the increases in cutting speed increase the cutting forces slightly.

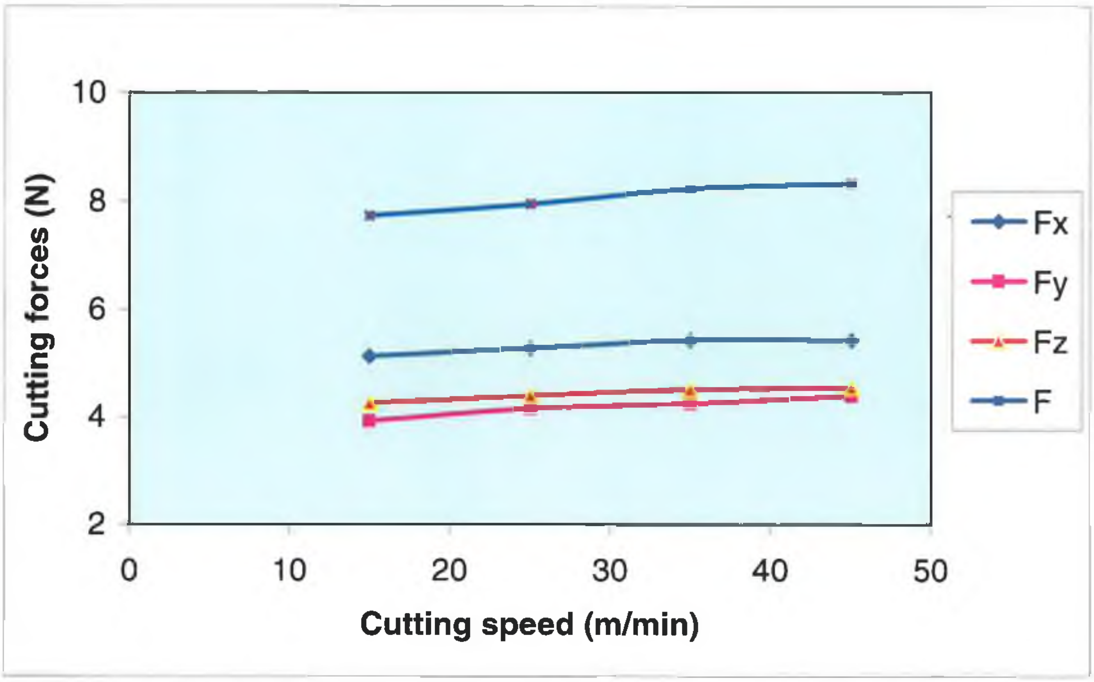

Figure 6.54 Relationship between Cutting forces & Cutting speed at Feed rate 1 (mm/rev) and Depth of cut 1.5 mm

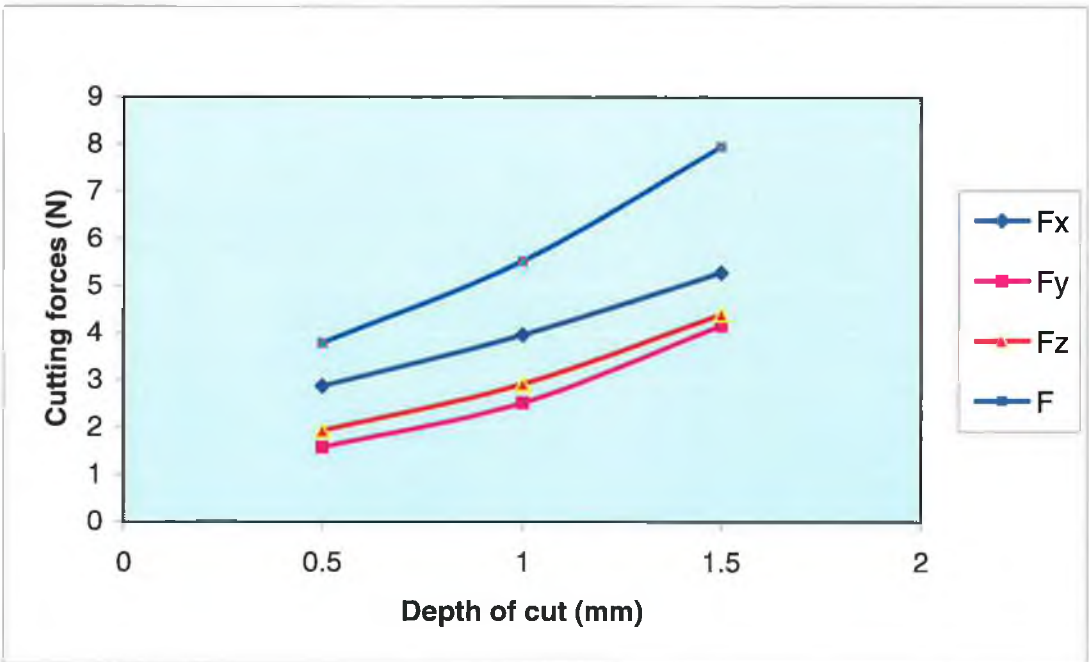

Figure 6.55 Relationship between Cutting forces & Depth of cut at Feed rate 1 (mm/rev) and Cutting speed 25 (m/min)

Figure; 6.55 shows that with the increase of depth of cut, cutting forces increase almost linearly.

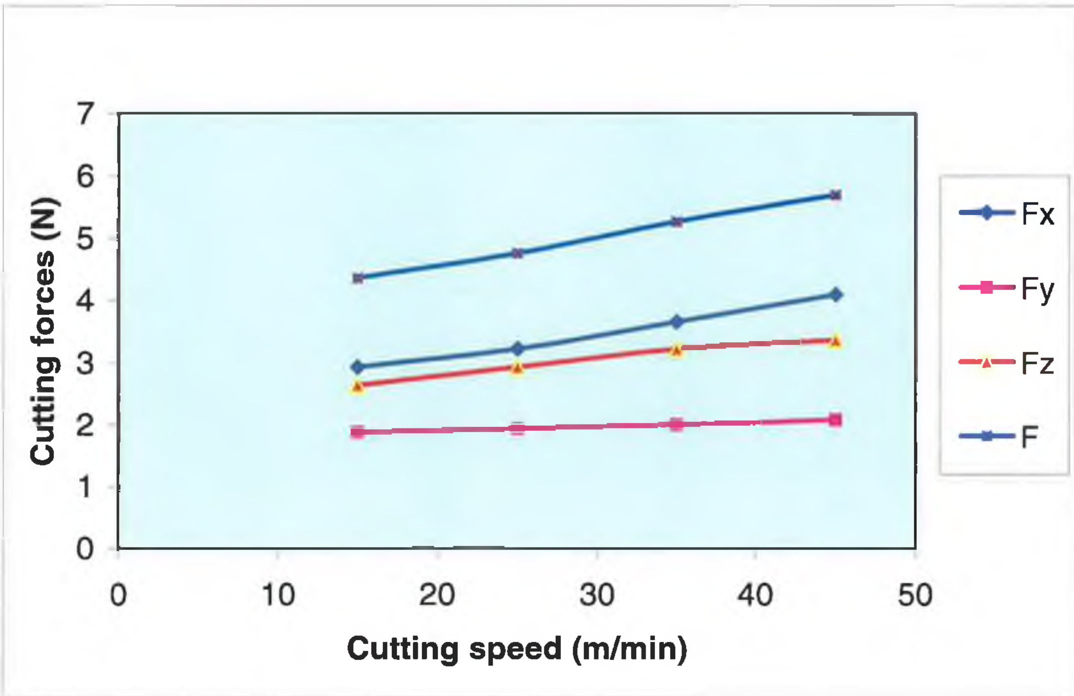

Figure 6.56 Relationship between Cutting forces & Cutting speed at Feed rate 2 (mm/rev) and Depth of cut 0.5 mm

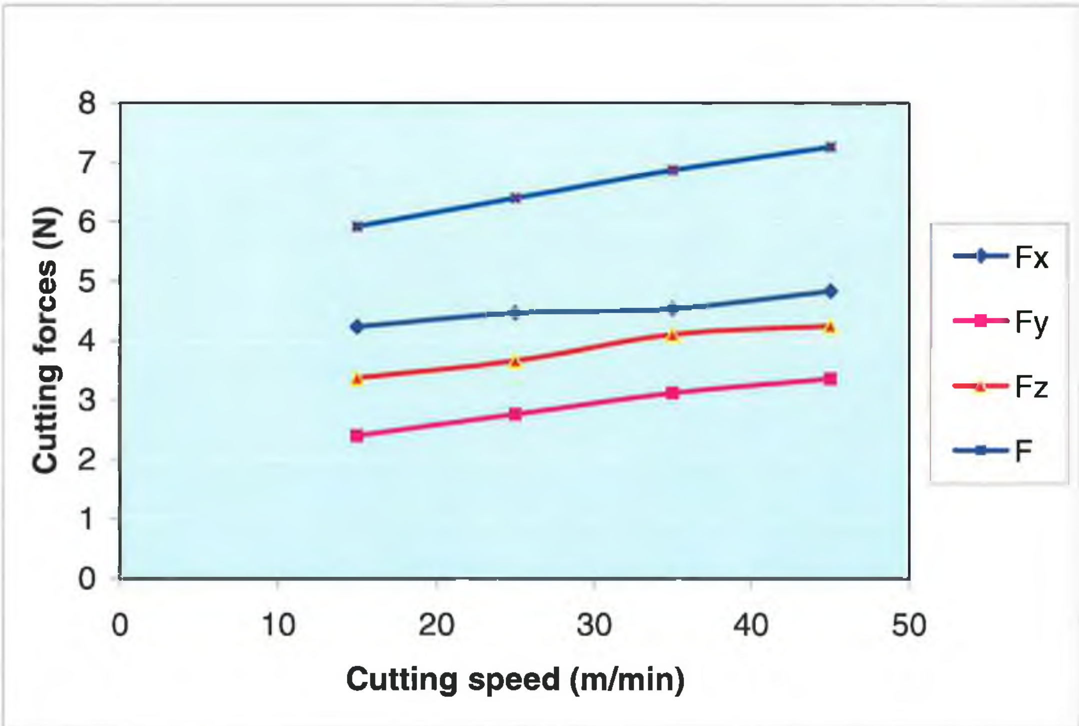

Figure 6.57 Relationship between Cutting forces & Cutting speed at Feed rate 2 (mm/rev) and Depth of cut 1 mm

Figures; (6.56, 6.57 and 6.58) shows that with the increases in cutting speed increase the cutting forces slightly.

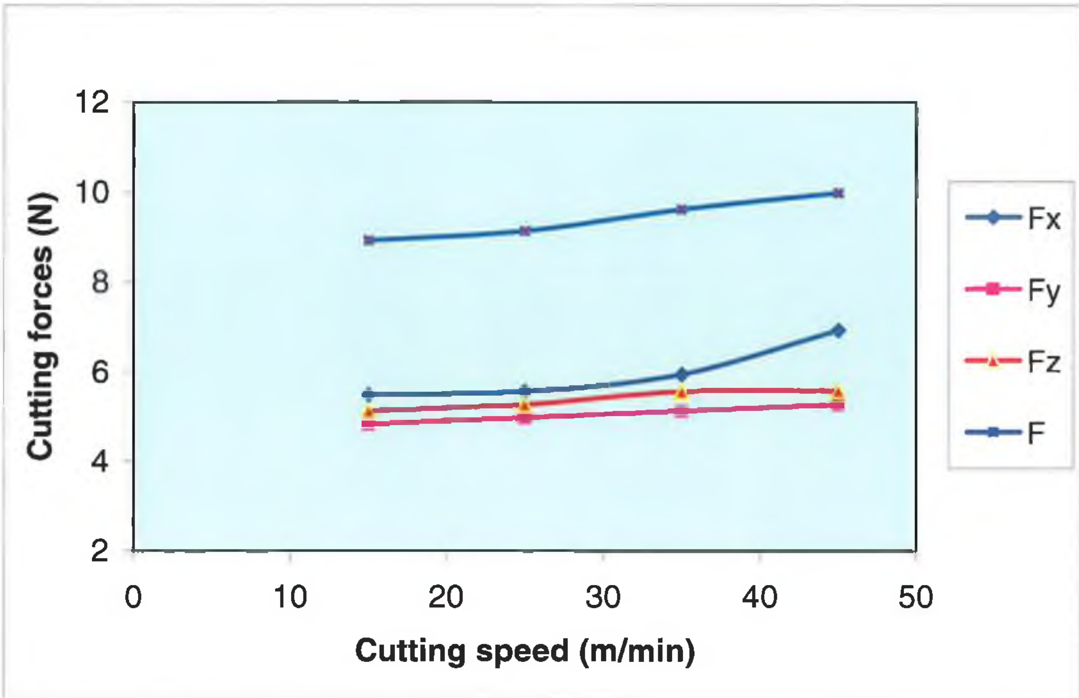

Figure 6.58 Relationship between Cutting forces & Cutting speed at Feed rate 2 (mm/rev) and Depth of cut 1.5 mm

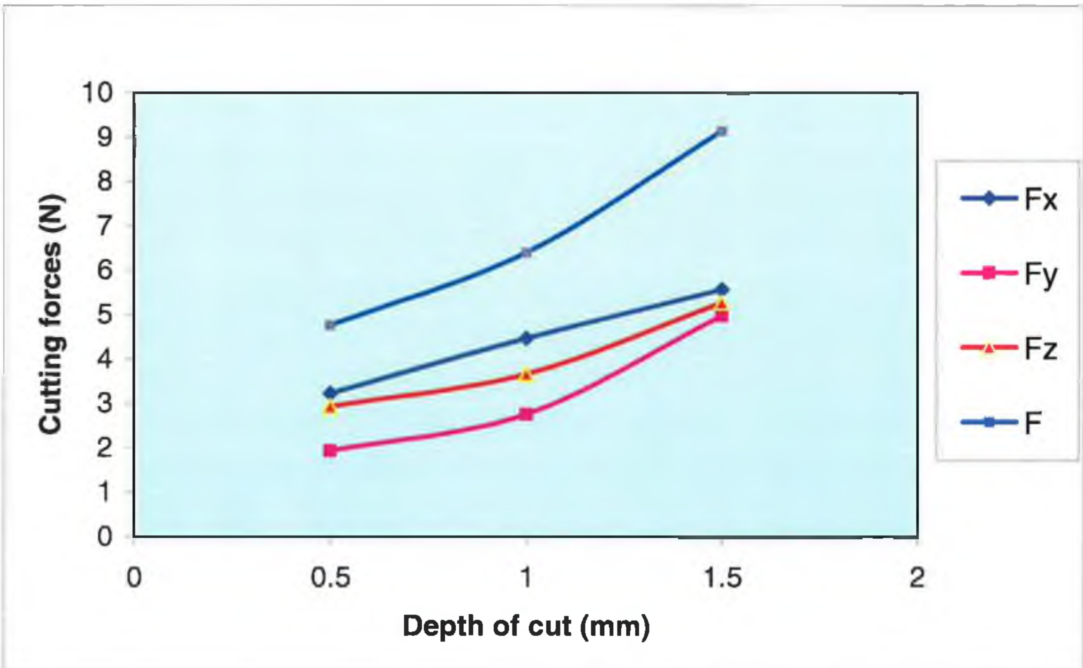

Figure 6.59 Relationship between Cutting forces & Depth of cut at Feed rate 2 (mm/rev) and Cutting speed 25 (m/min)

Figure; 6.59 shows that with the increase of depth of cut, cutting forces increase almost linearly.

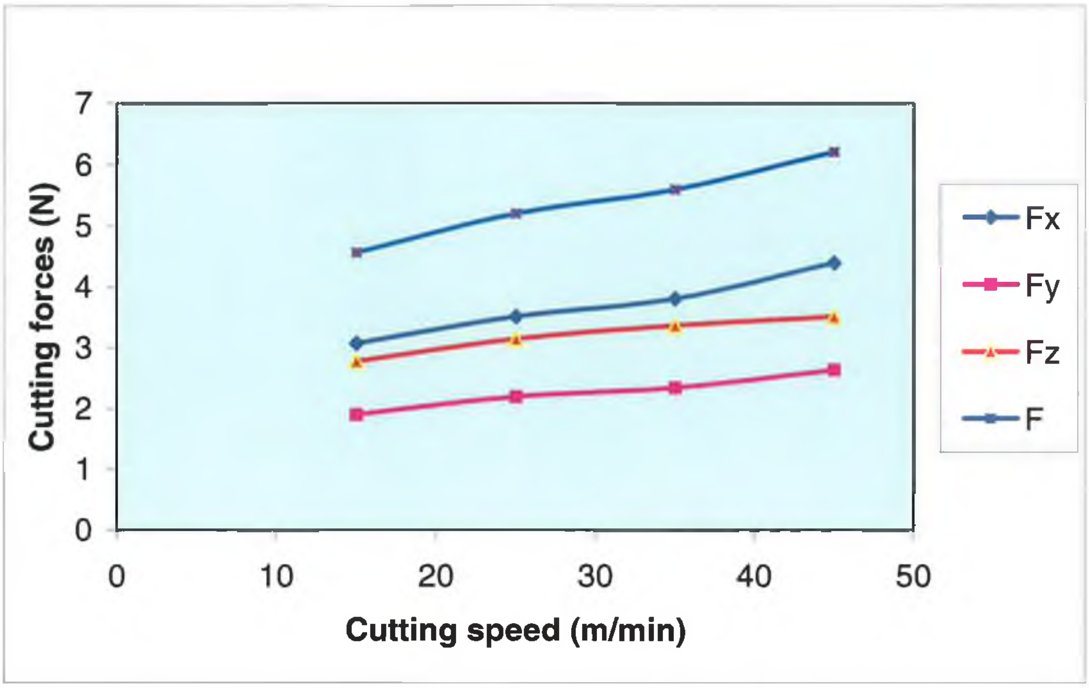

Figure 6.60 Relationship between Cutting forces & Cutting speed at Feed rate 3 (mm/rev) and Depth of cut 0.5 mm

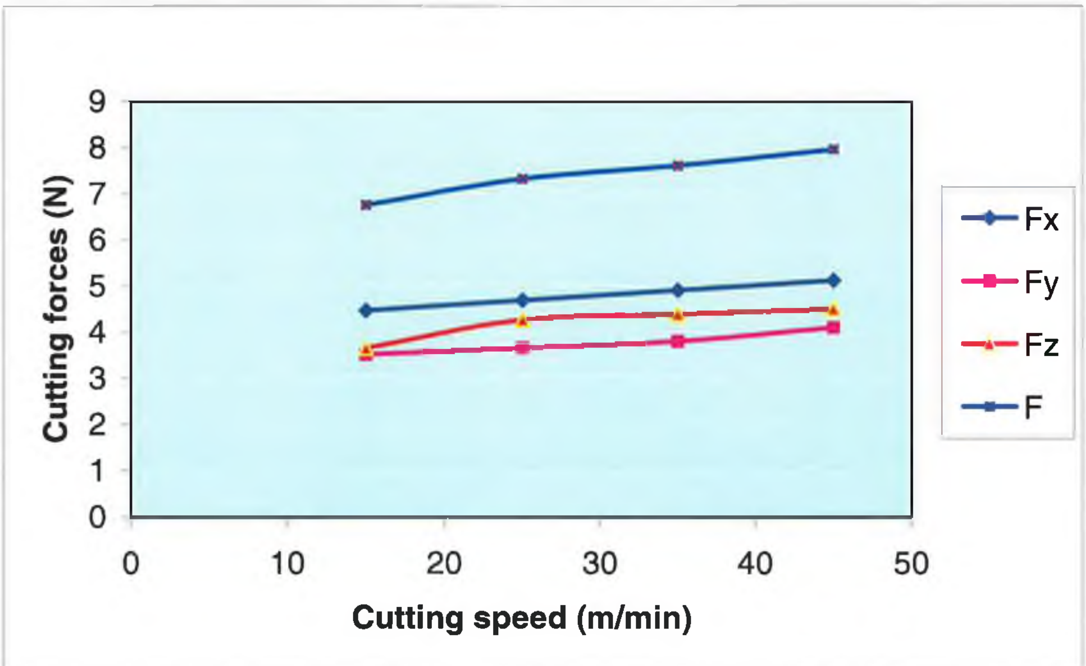

Figure 6.61 Relationship between Cutting forces & Cutting speed at Feed rate 3 (mm/rev) and Depth of cut 1 mm

Figures; (6.60, 6.61 and 6.62) shows that with the increases in cutting speed increase the cutting forces slightly.

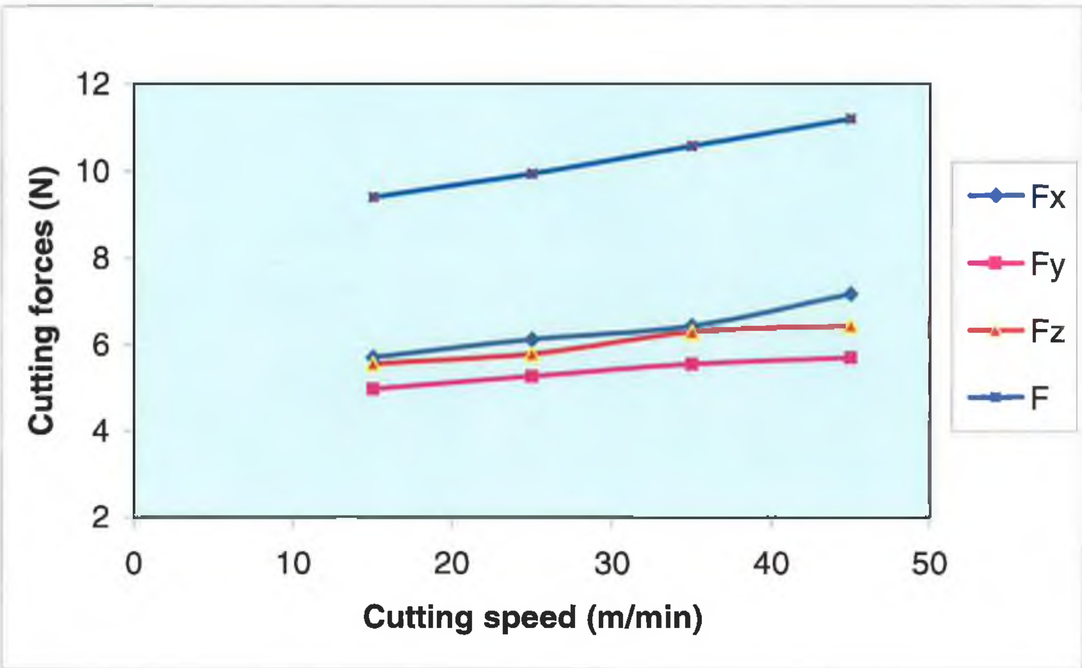

Figure 6.62 Relationship between Cutting forces & Cutting speed at Feed rate 3 (mm/rev) and Depth of cut 1.5 mm

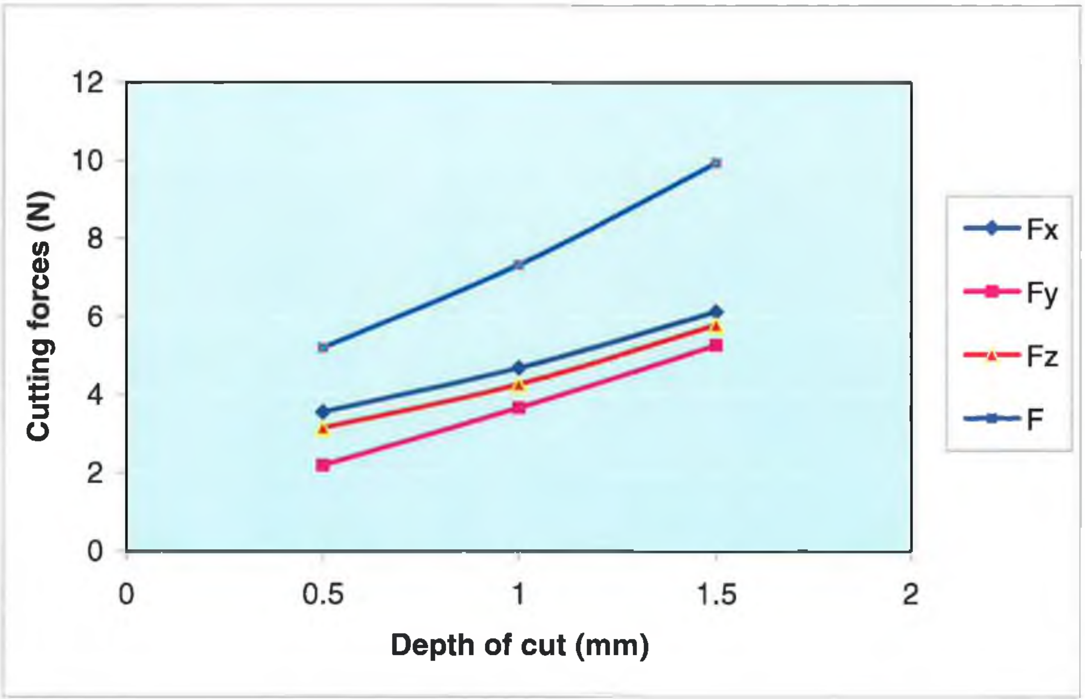

Figure 6.63 Relationship between Cutting forces & Depth of cut at Feed rate 3 (mm/rev) and Cutting speed 25 (m/min)

Figure; 6.63 shows that with the increase of depth of cut, cutting forces increase almost linearly.

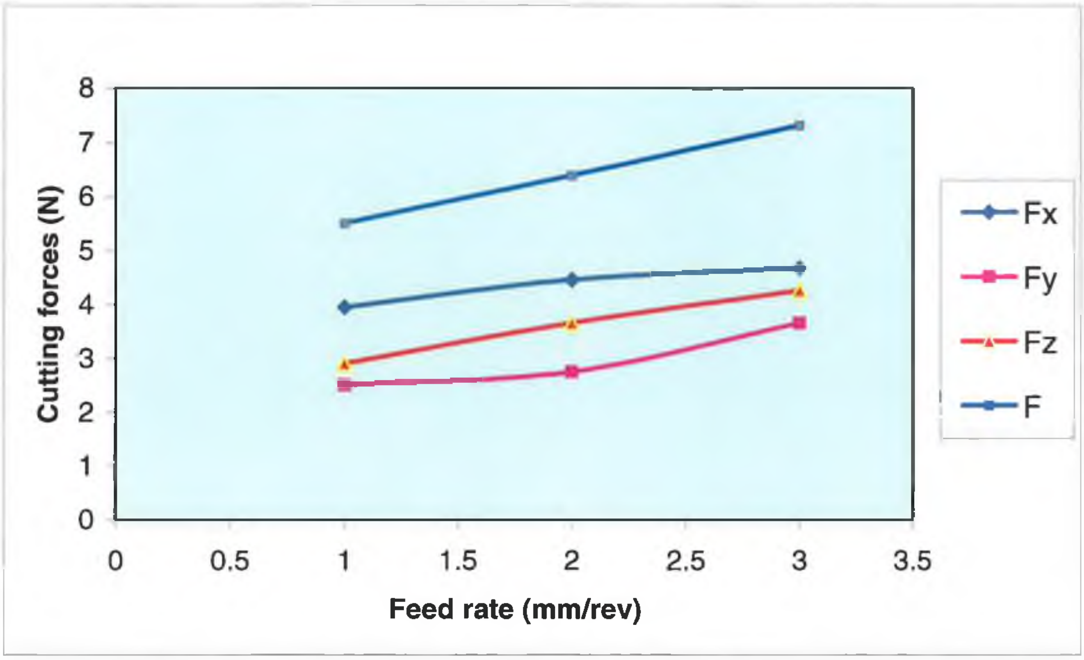

Figure 6.64 Relationship between Cutting forces & Feed rate at Depth of cut 1 mm and Cutting speed 25 (m/min)

Figure; 6.64 shows that with the increase of feed rate, cutting forces increase almost linearly.

Summary

For all conditions the results shows that as the feed rate increases the cutting forces and depth of cut increases linearly. Also with increase in the cutting speed the cutting forces will increase slightly. This may be because there is no built up edge (BUE) so there is no friction so the cutting force will increase slightly.

The tangential component of the cutting force F_z is the largest of the three cutting forces present for the Macor ceramic material.

The feed force F_x is the largest of the three cutting forces present for the Boron nitride ceramic material.

CHAPTER SEVEN:
DESIGN OF EXPERIMENTS RESULT AND DISCUSSIONS

7 DESIGN OF EXPERIMENT RESULTS AND DISCUSSIONS

7.1 Introduction

In this chapter experimental results and discussions for machinable ceramic materials, Macor and Boron Nitride are described. A design of experiment approach for surface roughness models is presented and developed. The experimental results and discussions together with the mathematical models on surface roughness for the both materials are described. The process utilized for the surface roughness study was a turning operation, the cutting tests were carried out using a carbide tools under dry conditions.

7.2 Design of Experiments

In order to establish an adequate functional relationship between the machining response (surface finish, tool life, and cutting force) and the cutting parameters (feed rate, nose radius, cutting speed, and depth of cut), a large number of cutting tests are required. It requires a separate set of tests for each and every combination of cutting tool and workpiece material. This increases the total number of tests and as a result experimentation cost also increases.

The experimental design takes into account the simultaneous variation of cutting speed, feed rate, and depth of cut, and predicts the response. This approach is known as response surface methodology where the response of the dependent variable (cutting force, surface finish, or tool life) is viewed as a surface and was first pioneered by Wu [53]. Factorial design is widely used in experiments involving several factors where it is necessary to study the combined effect of these factors on a response. The meaning of the factorial design is that each complete trial or replications of the all-possible combinations of the levels of the factors are investigated.

The functional relationship between the response (surface roughness) of the cutting operation and the investigated independent variables can be represented by the following equation:

$$R = \alpha (v, f, d) \qquad (7.1)$$

The response R could be tool life T in minutes, or surface roughness R_a in microns, or cutting forces F in Newton. However in this experiment R has been reported as surface roughness R_a. The equation results can be written in the following:

$$R_a = C\,V^k\,f^i\,d^m \qquad (7.2)$$

Where, R_a is the surface roughness (micrometers), while V, f and d are the cutting speed (m/min), feed rate (mm/rev) and depth of cut (mm) respectively. C, k, i and m are constant [31]. Equation (7.2) can be written as a linear combination of the logarithm of all the variables in the following form:

$$\ln R_a = \ln C + k \ln V + i \ln f + m \ln d \qquad (7.3)$$

Which may represent the following linear mathematical model:

$$y = b_0 x_0 + b_1 x_1 + b_2 x_2 + b_3 x_3 + \varepsilon \qquad (7.4)$$

Where y is the measured surface roughness on a logarithm scale, ε is the experimental error and, $x_0 = 1$, $x_1 = \ln V$, $x_2 = \ln f, x_3 = \ln d$, and b_0, b_1, b_2 and b_3 are the model parameters to be estimated. The a values are $b_0, b_1, b_2 \ldots$ etc, are to be estimated by the method of least squares. The basic formula is

$$b = (X^T X)^{-1} X^T y \qquad (7.5)$$

Where the calculation matrix is X and the variance matrix is $(X^T X)^{-1}$. b. Values for b are now calculated by using equation (7.5).

7.3 Surface Roughness Model For Macor Material

To develop the first-order model; a design consisting of twelve experiments has been used. Eight experiments represent a 2^3 factorial design with an added centre point being used to estimate pure error. Four experiments represent an added centre point to the cube, repeated four times to calculate pure error. The complete design consists of twelve experiments in two blocks, each block containing six experiments. The first block consisting of experiment numbers 1, 4, 6, 7, 9, and 10. Also the second block of six tests is 2, 3, 5, 8, 11, and 12, has been added for convenient identification and for easy calculation by taking into account the capacity of the lathe and limiting cutting conditions. The twelve experiments were performed in two blocks see Table (7.2). These two blocks were used to develop the first-order model. The central composite design with 12 experiments provided three levels for each independent variable, as shown in Table 7.1.

Table 7.1 Levels independent variables

	Low	Centre	High
Coding	-1	0	1
Cutting speed, v (mm/min)	15	30	60
Feed, f (mm/rev)	0.06	0.12	0.25
Depth of cut, d (mm)	0.4	0.8	1.6

The levels means:

(-1) Level = lowest level value of investigated variables.

(0) Level = centre level value of the investigated variables.

(1) Level = highest level value of the investigated variables.

The relationships between the code and independent variables is:

$$x_1 = \frac{\ln V - \ln(v)_{centre}}{\ln(v)_{high} - \ln(v)_{centre}}$$

$$x_2 = \frac{\ln F - \ln(f)_{centre}}{\ln(f)_{high} - \ln(f)_{centre}} \tag{7.6}$$

$$x_3 = \frac{\ln D - \ln(d)_{centre}}{\ln(d)_{high} - \ln(d)_{centre}}$$

The ratio between the high and centre values must be similar or close to the ratio between the centre and low values.

The matrix of independent variables X of twelve experiments given as follows:

$$X = \begin{array}{c} \begin{array}{cccc} X_0 & X_1 & X_2 & X_3 \end{array} \\ \left| \begin{array}{cccc} 1 & -1 & -1 & -1 \\ 1 & 1 & -1 & -1 \\ 1 & -1 & 1 & -1 \\ 1 & 1 & 1 & -1 \\ 1 & -1 & -1 & 1 \\ 1 & 1 & -1 & 1 \\ 1 & -1 & 1 & 1 \\ 1 & 1 & 1 & 1 \\ 1 & 0 & 0 & 0 \\ 1 & 0 & 0 & 0 \\ 1 & 0 & 0 & 0 \\ 1 & 0 & 0 & 0 \end{array} \right| \end{array}$$

Therefore,

$$(X^T X) = \left| \begin{array}{cccc} 12 & 0 & 0 & 0 \\ 0 & 8 & 0 & 0 \\ 0 & 0 & 8 & 0 \\ 0 & 0 & 0 & 8 \end{array} \right|$$

$$(X^T X)^{-1} = \left| \begin{array}{cccc} 1/12 & 0 & 0 & 0 \\ 0 & 1/8 & 0 & 0 \\ 0 & 0 & 1/8 & 0 \\ 0 & 0 & 0 & 1/8 \end{array} \right|$$

Table 7.2 Experiment conditions and results

Trial No.	Block No.	Speed (m/min)	Feed (mm/rev)	Depth (mm)	Coding			Surface roughness (μm)
					x_1	x_2	x_3	
1	1	15	0.06	0.4	-1	-1	-1	1.14
2	2	60	0.06	0.4	1	-1	-1	1.13
3	2	15	0.25	0.4	-1	1	-1	4.28
4	1	60	0.25	0.4	1	1	-1	4.42
5	2	15	0.06	1.6	-1	-1	1	1.28
6	1	60	0.06	1.6	1	-1	1	1.4
7	1	15	0.25	1.6	-1	1	1	5.82
8	2	60	0.25	1.6	1	1	1	4.84
9	1	30	0.12	0.8	0	0	0	1.58
10	1	30	0.12	0.8	0	0	0	1.5
11	2	30	0.12	0.8	0	0	0	1.58
12	2	30	0.12	0.8	0	0	0	1.5

The values of cutting speed, feed rate and depth of cut have been substituted into equation (7.6). As a result the equations are presented as follows:

$$x_1 = \frac{\ln V - \ln 30}{\ln 60 - \ln 30}$$

$$x_1 = \frac{\ln V - 3.40119)}{4.09434 - 3.40119}$$

$$x_1 = 1.442689 \ln V - 4.90686 \qquad (7.7)$$

$$x_2 = \frac{\ln f - \ln 0.12}{\ln 0.25 - \ln 0.12}$$

$$x_2 = \frac{\ln f - (-2.12026)}{(-1.38629) - (-2.12026)}$$

$$x_2 = 1.36245 \ln f + 2.88875 \qquad (7.8)$$

$$x_3 = \frac{\ln d - \ln 0.8}{\ln 1.6 - \ln 0.8}$$

$$x_3 = \frac{\ln d - (-0.22314)}{0.4700036 - (-0.22314)}$$

$$x_3 = 1.4459 \ln d + 0.3219 \qquad (7.9)$$

The block 1 of experiments includes numbers 1,4,6,7,9 and 10 calculations as follows:

$$X = \begin{array}{cc} \begin{array}{cccc} X_0 & X_1 & X_2 & X_3 \end{array} & \text{Trial number} \\ \left|\begin{array}{cccc} 1 & -1 & -1 & -1 \\ 1 & 1 & 1 & -1 \\ 1 & 1 & -1 & 1 \\ 1 & -1 & 1 & 1 \\ 1 & 0 & 0 & 0 \\ 1 & 0 & 0 & 0 \end{array}\right| & \begin{array}{c} 1 \\ 4 \\ 6 \\ 7 \\ 9 \\ 10 \end{array} \end{array}$$

From Equation (7.3) and (7.4), y = $\ln R_a$. Therefore:

$$y = \begin{array}{cc} \left|\begin{array}{c} \ln 1.14 \\ \ln 4.42 \\ \ln 1.4 \\ \ln 5.82 \\ \ln 1.58 \\ \ln 1.5 \end{array}\right| & \begin{array}{c} 1 \\ 4 \\ 6 \\ 7 \\ 9 \\ 10 \end{array} \end{array}$$

This can be computed to give:

$$y = \left|\begin{array}{c} 0.1310 \\ 1.4861 \\ 0.3364 \\ 1.7613 \\ 0.4574 \\ 0.4054 \end{array}\right|$$

To obtain the matrix used in Equation (7.5), the following matrix is calculated:

$$\left(X^T X\right) = \begin{vmatrix} 6 & 0 & 0 & 0 \\ 0 & 4 & 0 & 0 \\ 0 & 0 & 4 & 0 \\ 0 & 0 & 0 & 4 \end{vmatrix}$$

And

$$\left(X^T X\right)^{-1} = \begin{vmatrix} \frac{1}{6} & 0 & 0 & 0 \\ 0 & \frac{1}{4} & 0 & 0 \\ 0 & 0 & \frac{1}{4} & 0 \\ 0 & 0 & 0 & \frac{1}{4} \end{vmatrix}$$

$$(X^T X)^{-1}.X^T = \begin{vmatrix} \frac{1}{6} & 0 & 0 & 0 \\ 0 & \frac{1}{4} & 0 & 0 \\ 0 & 0 & \frac{1}{4} & 0 \\ 0 & 0 & 0 & \frac{1}{4} \end{vmatrix} \cdot \begin{vmatrix} 1 & 1 & 1 & 1 & 1 & 1 \\ -1 & 1 & 1 & -1 & 0 & 0 \\ -1 & 1 & -1 & 1 & 0 & 0 \\ -1 & -1 & 1 & 1 & 0 & 0 \end{vmatrix}$$

The following expressions are obtained:

$$b_0 = \frac{1}{6}(Y_1 + Y_4 + Y_6 + Y_7 + Y_9 + Y_{10})$$

$$b_1 = \frac{1}{4}(--Y_1 + Y_4 + Y_6 - Y_7)$$

$$b_2 = \frac{1}{4}(-Y_1 + Y_4 - Y_6 + Y_7)$$

$$b_3 = \frac{1}{4}(-Y_1 - Y_4 + Y_6 + Y_7)$$

Substituting in the values for Y_1, Y_4, Y_6, Y_7, Y_9, Y_{10}:

$$b_0 = \frac{1}{6}(0.1310 + 1.4861 + 0.33647 + 1.7613 + 0.4574 + 0.43178)$$

$$b_0 = 0.7673$$

$$b_1 = \frac{1}{4}(-0.1310 + 1.486 + 0.33647 - 1.7613)$$

$$b_1 = -0.0174575$$

$b_2 = \frac{1}{4}(-0.1310 + 1.486 - 0.33647 + 1.7613)$

$b_2 = 0.6949575$

$b_3 = \frac{1}{4}(-0.1310 - 1.486 + 0.33647 + 1.7613)$

$b_3 = 0.120175$

$y = b_0 x_0 + b_1 x_1 + b_2 x_2 + b_3 x_3$

$y' = 0.7673 - 0.017457 x_1 + 0.694957 x_2 + 0.12017 x_3$

Where y' is used to represent the function for block 1

The Block 2 calculations are as follows:

$$X = \begin{array}{c} \begin{array}{cccc} X_0 & X_1 & X_2 & X_3 \end{array} & \text{Trial number} \\ \left| \begin{array}{cccc} 1 & 1 & -1 & -1 \\ 1 & -1 & 1 & -1 \\ 1 & -1 & -1 & 1 \\ 1 & 1 & 1 & 1 \\ 1 & 0 & 0 & 0 \\ 1 & 0 & 0 & 0 \end{array} \right| & \begin{array}{c} 2 \\ 3 \\ 5 \\ 8 \\ 11 \\ 12 \end{array} \end{array}$$

Since $y = \ln R_a$:

$$y = \left| \begin{array}{c} \ln 1.13 \\ \ln 4.28 \\ \ln 1.28 \\ \ln 4.84 \\ \ln 1.58 \\ \ln 1.5 \end{array} \right| \begin{array}{c} 2 \\ 3 \\ 5 \\ 8 \\ 11 \\ 12 \end{array}$$

Which can be calculated as follows:

$$y = \begin{vmatrix} 0.1222 \\ 1.4539 \\ 0.2468 \\ 1.5769 \\ 0.4574 \\ 0.4054 \end{vmatrix}$$

To obtain the matrix used in Equation (7.5), the following matrix is calculated:

$$\left(X^T X\right) = \begin{vmatrix} 6 & 0 & 0 & 0 \\ 0 & 4 & 0 & 0 \\ 0 & 0 & 4 & 0 \\ 0 & 0 & 0 & 4 \end{vmatrix}$$

$$\left(X^T X\right)^{-1} = \begin{vmatrix} 1/6 & 0 & 0 & 0 \\ 0 & 1/4 & 0 & 0 \\ 0 & 0 & 1/4 & 0 \\ 0 & 0 & 0 & 1/4 \end{vmatrix}$$

The following expressions are obtained:

$$b_0 = 1/6\,(Y_2 + Y_3 + Y_5 + Y_8 + Y_{11} + Y_{12})$$

$$b_1 = 1/4\,(-Y_2 + Y_3 + Y_5 - Y_8)$$

$$b_2 = 1/4\,(-Y_2 + Y_3 - Y_5 + Y_8)$$

$$b_3 = 1/4\,(-Y_2 - Y_3 + Y_5 + Y_8)$$

Substituting in the values for Y_2, Y_3, Y_5, Y_8, Y_{11}, Y_{12}:

$$b_0 = 1/6\left(0.222 + 1.45395 + 0.24686 + 1.5769 + 0.4574 + 0.40546\right)$$

$$b_0 = 0.727095$$

$$b_1 = 1/4\left(-0.222 + 1.45395 + 0.24686 - 1.5769\right)$$

$$b_1 = -0.0245225$$

$$b_2 = \frac{1}{4}(-0.222 + 1.45395 - 0.24686 + 1.5769)$$

$$b_2 = 0.6403725$$

$$b_3 = \frac{1}{4}(-0.222 - 1.45395 + 0.24686 + 1.5769)$$

$$b_3 = 0.0368275$$

$y^{//}$ Denotes the response for the block 2 experiments:

$$y^{//} = b_0x_0 + b_1x_1 + b_2x_2 + b_3x_3$$

$$y^{//} = 0.727095 - 0.0245225x_1 + 0.6403725x_2 + 0.0368275x_3$$

Table 7.3 Analysis of variance for first block

Source	Sum of squares	DF	MS	F_{cal}	F_{lab}
Zero-order term	3.493	1	3.493		
First-order terms	1.990853	3	0.6636	12.773	
Lack of fit	0.27879	1	0.27879	5.366	161.4
Pure error	0.051955	1	0.051955		
Total	5.8146	6	0.9691		

Table 7.4 Analysis of variance for second block

Source	Sum of squares	DF	MS	F_{cal}	F_{lab}
Zero-order term	3.1720	1	3.1720		
First-order terms	1.7886	3	0.5962	11.475	
Lack of fit	0.071865	1	0.071865	1.383	161.4
Pure error	0.051955	1	0.051955		
Total	5.08442	6	0.8474		

The analysis of variance for the first and second blocks shows that the first order terms are adequate, since the F_{cal} = 12.773 and 11.475 respectively less than the F_{lab} = 161.4 as shown above in tables (7.3) and (7.4). As a result of the lack of fit test the lack of fit is not significant for the two blocks, which indicate that the developed model is adequately fits the data. The detailed formulae for the analysis of variance used in this investigation are shown in appendix B Table1,

The average of the two set results are as follows:

$$y = \frac{y^{/} + y^{//}}{2}$$

$$y = 0.7472 - 0.020989x_1 + 0.692664x_2 + 0.078498x_3 \qquad (7.10)$$

Substituting in for x_1, x_2 and x_3 which given in Equation (7.9), (7.10) and (7.11) in following Equation:

$$y = 0.747217 - 0.020989(1.442689\ln V - 4.90686) + 0.692664(1.36245\ln f + 2.88875) + 0.078498(1.4459\ln d + 0.3219)$$

$$y = 0.747217 - 0.03028\ln V + 0.10299 + 0.94372\ln f + 2.00093 + 0.1135\ln d + 0.025268$$

$$y = 2.8764 - 0.03028\ln V + 0.94372\ln f + 0.1135\ln d$$

$$y = \ln R_a = \ln C + k\ln V + i\ln f + m\ln d$$

$$\therefore C = e^{2.876405} = 17.75034$$

The values for k, i and m are:

$k = -0.03028, \quad i = 0.94372, \; and \quad m = 0.1135$

$$\therefore \qquad R_a = 17.750 \left(V^{-0.03028} f^{0.94372} d^{0.1135}\right) \qquad (7.11)$$

7.3.1 Result, Discussions, and Optimisation: First-Order Model

The equation (7.11) indicates that the surface finish deteriorates with the increase of feed rate or depth of cut while it improves with the increase of cutting speed.
The rate of metal removal Q (cm^3/min) is given by:

$$Q = dfV \qquad (7.12)$$

Where d is the depth of cut (mm), f is the feed rate (mm/rev) and V is the cutting speed (m/min), Equation (7.12) can be written as.

$$\ln Q = \ln d + \ln f + \ln V \qquad (7.13)$$

For a specific depth of cut $d = 0.8\,\text{mm}$, and using the transformation, equation (7.13) instead x_1, x_2, x_3 may be written as follows:

$\because \quad d = 0.8 \quad SO \quad \ln d = -0.2231435$

$$x_1 = \frac{\ln V - \ln 30}{\ln 60 - \ln 30}$$
$$x_1 = \frac{\ln V - 3.40119}{4.09434 - 3.40119}$$
$$x_1 = 1.442689 \ln V - 4.90686$$

$$\ln v = \frac{x_1 - 4.90686}{1.442689}$$
$$\ln v = 0.693150082 x_1 - 3.40119$$

$$x_2 = \frac{\ln f - \ln 0.12}{\ln 0.25 - \ln 0.12}$$
$$x_2 = \frac{\ln f - (-2.12026)}{(-1.38629) - (-2.12026)}$$
$$x_2 = 1.36245 \ln f + 2.88875$$

$$\ln f = \frac{x_2 + 2.88875}{1.36245}$$
$$\ln f = 0.73397188 x_2 + 2.12026129$$

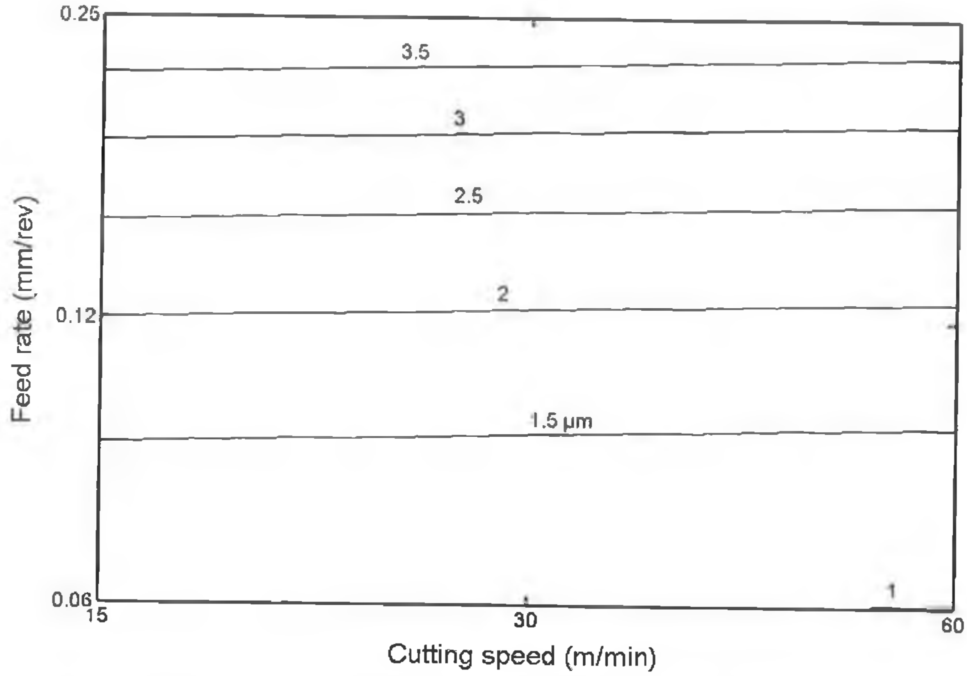

Figure.7.1 Surface roughness contours in cutting speed-feed planes at depth 0.4 mm

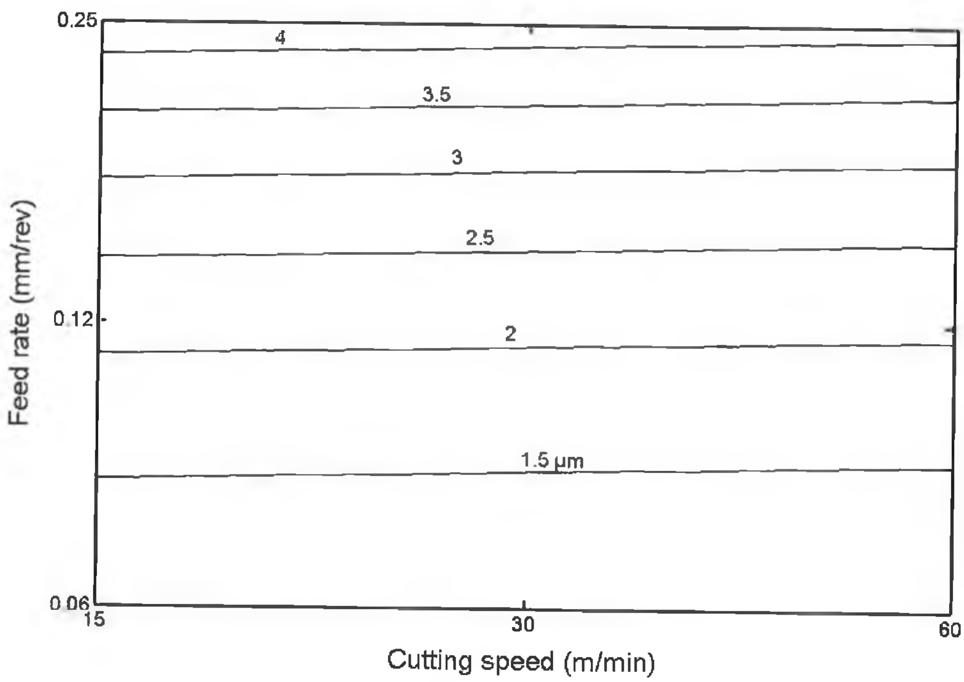

Figure.7.2 Surface roughness contours in cutting speed-feed planes at depth 0.8 mm

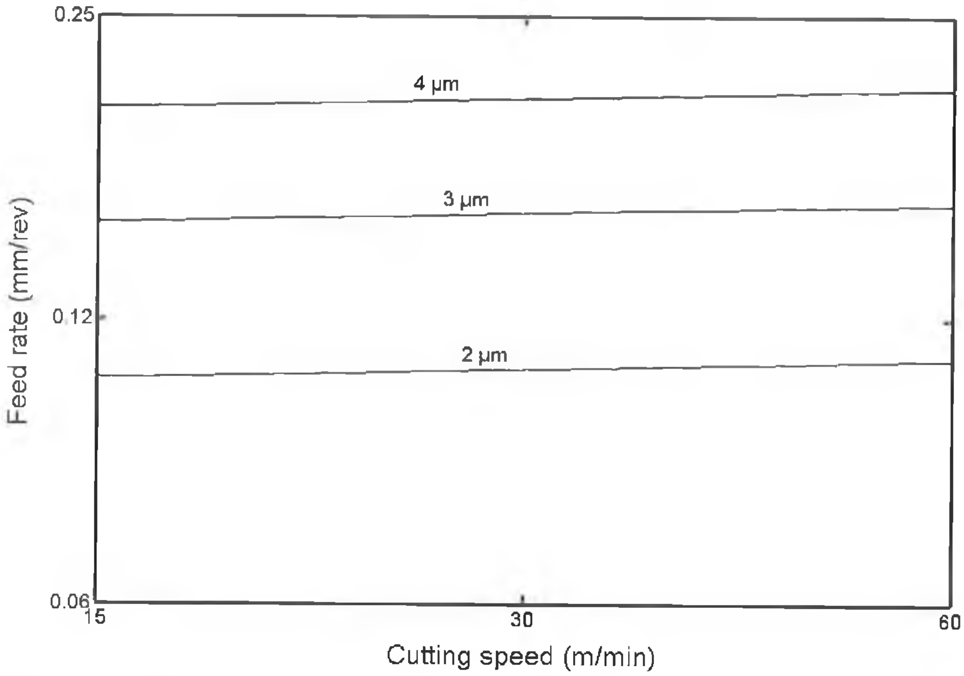

Figure.7.3 Surface roughness contours in cutting speed-feed planes at depth 1.6 mm

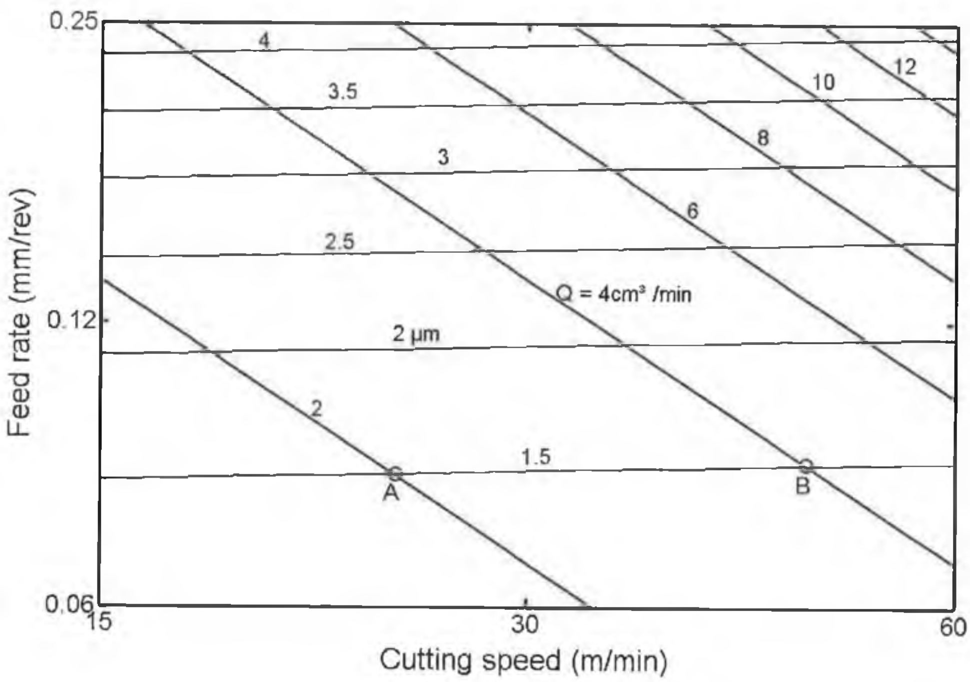

Figure.7.4 Response contours of surface roughness & metal removal at depth 0.8 mm

Figures; (7.1,7.2,7.3) shows that the increases in cutting speed increase the quality of surface finish while the surface finish decrease with increase of feed rate. Also it is shows in Figure 7.4; that the increase in material removal rate is obtained without any sacrifice in the quality of the produced surface.

Equation (7.13) can be presented as follows:

$$\ln Q = 1.057785571 + 0.69315x_1 + 0.73397x_2 \qquad (7.14)$$

Equation (7.11) has been plotted in Fig 7.1, 7.2, and 7.3 as contours for each of the response surface at three selected levels of depth of cut. These levels were chosen as low $(d = 0.4mm)$, centre $(d = 0.8mm)$, and high $(d = 1.6mm)$. It can be seen from Figures 7.1, 7.2, and 7.3 that the better surface finish was obtained at combination of high speed and low feed rate and depth of cut.

Figure 7.4 represents dual response contours of metal removal rate and surface roughness at depth of cut = 0.8 mm. However, cutting conditions that provide a higher rate of metal removal must be selected. It is shown in Fig 7.4 that the selection of cutting conditions represented by point B is better than which was selected by point A. this increase in material removal rate is obtained without any sacrifice in the quality of the produced surface.

7.3.2 Analysis of Results for Various Nose Radius of Macor Material

The design is obtained by 2^3 which, mean three factorial has been used at three level (v, f, r), cutting speed (m/min), feed rate (mm/rev), nose radius (mm).

The experiment has been carried out with three types of inserts having different nose radius these selected levels were chosen as low (r = 0.4 mm), centre (r = 0.8 mm), and high (r = 1.6 mm).

(-) Level = lowest level values of the investigated variables.

(+) Level = highest level value of the investigated variables.

(0) Level = centre level value of the investigated variables.

A design consisting of 12 experiments has been carried out to develop the first order model.

The relationships between the code and independent variables are as follows:

$$x_1 = \frac{\ln V - \ln(v)_{centre}}{\ln(v)_{high} - \ln(v)_{centre}}$$

$$x_2 = \frac{\ln F - \ln(f)_{centre}}{\ln(f)_{high} - \ln(f)_{centre}} \qquad (7.15)$$

$$x_3 = \frac{\ln(R) - \ln(r)_{centre}}{\ln(r)_{high} - \ln(r)_{centre}}$$

Table 7.5 Levels of independent variables

	Low	Centre	High
Coding	-1	0	1
Cutting speed, v (mm/min)	15	30	60
Feed, f (mm/rev)	0.06	0.12	0.25
Nose radius r (mm)	0.4	0.8	1.6

The ratio between the high and centre values must be similar to the ratio between the centre and low values for the all parameters as following:

Cutting speed (m/min) = $\frac{60}{30} = 2$ $\qquad \frac{30}{15} = 2$

Feed rate (mm/rev) $= \frac{0.25}{0.12} = 2$ $\qquad \frac{0.12}{0.06} = 2$

Nose radius (mm) $= \frac{1.6}{0.8} = 2$ $\qquad \frac{0.8}{0.4} = 2$

Table 7.6 Experiment conditions and results

Trial No.	Block No.	Speed v (m/min)	Feed f (mm/rev)	Nose radius r (mm)	Coding			Surface roughness (μm)
					x_1	x_2	x_3	
1	1	15	0.06	0.4	-1	-1	-1	1.3
2	2	60	0.06	0.4	1	-1	-1	1.25
3	2	15	0.25	0.4	-1	1	-1	6.85
4	1	60	0.25	0.4	1	1	-1	5.9
5	2	15	0.06	1.6	-1	-1	1	1.1
6	1	60	0.06	1.6	1	-1	1	1
7	1	15	0.25	1.6	-1	1	1	5.06
8	2	60	0.25	1.6	1	1	1	4.4
9	1	30	0.12	0.8	0	0	0	1.4
10	1	30	0.12	0.8	0	0	0	1.5
11	2	30	0.12	0.8	0	0	0	1.44
12	2	30	0.12	0.8	0	0	0	1.4

The independent variable which, exhibited in the equations (7.15) have been substituted by the values of cutting speed, feed rate and nose radius, as result the equations are presented as following:

$$x_1 = \frac{\ln V - \ln 30}{\ln 60 - \ln 30}$$

$$x_1 = \frac{\ln V - 3.40119}{4.09434 - 3.40119}$$

$$x_1 = 1.442689 \ln V - 4.90686$$

$$x_2 = \frac{\ln f - \ln 0.12}{\ln 0.25 - \ln 0.12}$$

$$x_2 = \frac{\ln f - (-2.12026)}{(-1.38629) - (-2.12026)}$$

$$x_2 = 1.362451 \ln f + 2.88875$$

$$x_3 = \frac{\ln r - \ln 0.8}{\ln 1.6 - \ln 0.8}$$
$$x_3 = \frac{\ln r - (-0.223143)}{0.470003 - (-0.223143)}$$

$$x_3 = 1.442695 \ln r + 0.32192809$$

The improvement of the first-order model used the central composite design with twelve experiments providing three levels for each independent variable as shown in Table 7.5. For the first-order model of the block 1 of six tests, the parameters in Table 7.6 were estimated, yielding the surface roughness predicting equation:

$$y = b_0 x_0 + b_1 x_1 + b_2 x_2 + b_3 x_3 \qquad (7.16)$$

The calculation has been done as Equation (7.16) for the first block six trails and the block 2 six trials. The results are listed in Table 7.6 The process of the analysis of the block 2 of six tests were similar to that of the block 1.

Combining the results of all 12 tests, the fitted surface predicting equation was as below:

$$y = 0.735602314 - 0.053096775 x_1 + 0.777817387 x_2 - 0.123155317 x_3 \qquad (7.17)$$

Substituting the values of x_1, x_2, x_3 in the Equation (7.21) gives:

$$y = 3.203413577 - 0.076602133 \ln v + 1.059737299 \ln f - 0.17767556 \ln r$$

$$y = \ln R_a = \ln C + k \ln V + i \ln f + m \ln r$$

$$\therefore C = e^{3.203413577} = 24.61641697$$

The values for k, i and m are:

$k = -0.076602133, \quad i = 1.059737299,$ *and* $\quad m = -0.17767556$

$$\therefore \quad R_a = 24.61641697 \left(V^{-0.076602133} f^{1.059737299} r^{-0.17767556}\right) \qquad (7.18)$$

The equation (7.18) has been plotted in Figure 7.5, 7.6 and 7.7 as contours for each of the response surfaces at three selected levels of nose radius These selected levels were chosen as low $(r = 0.4mm)$, centre $(r = 0.8mm)$, and high $(r = 1.6mm)$. The cutting speed V and the feed rate f were graphed utilizing the MATLAB computer package. It can be seen from Figures. 7.5, 7.6 and 7.7 that the surface finish improves with the increase of cutting speed and nose radius while it deteriorates with the increase of feed rate. However it was noticed that the nose radius has a significant effect on surface finish.

Figure 7.8 represents dual response contours of metal removal rate and surface roughness at depth of cut = 0.8 mm and nose radius = 0.8 mm. However, cutting conditions that provide a higher rate of metal removal must be selected. It is shown that the selections of cutting conditions represented by point B are better than those represented by point A. This increase in material removal rate is obtained without any sacrifice in the quality of the produced surface. This reduces the machining time, since the metal removal rate B is 50% greater than that of A. By this experiment the cutting conditions that give roughness as output were known clearly.

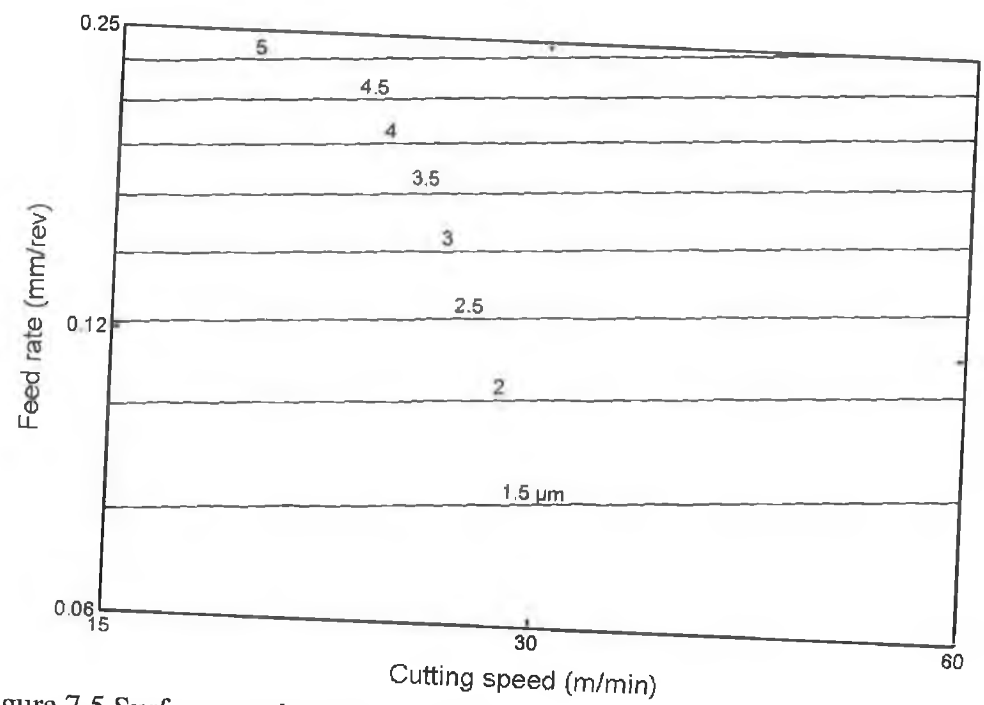

Figure.7.5 Surface roughness contours in speed-feed planes at nose radius 0.4 mm

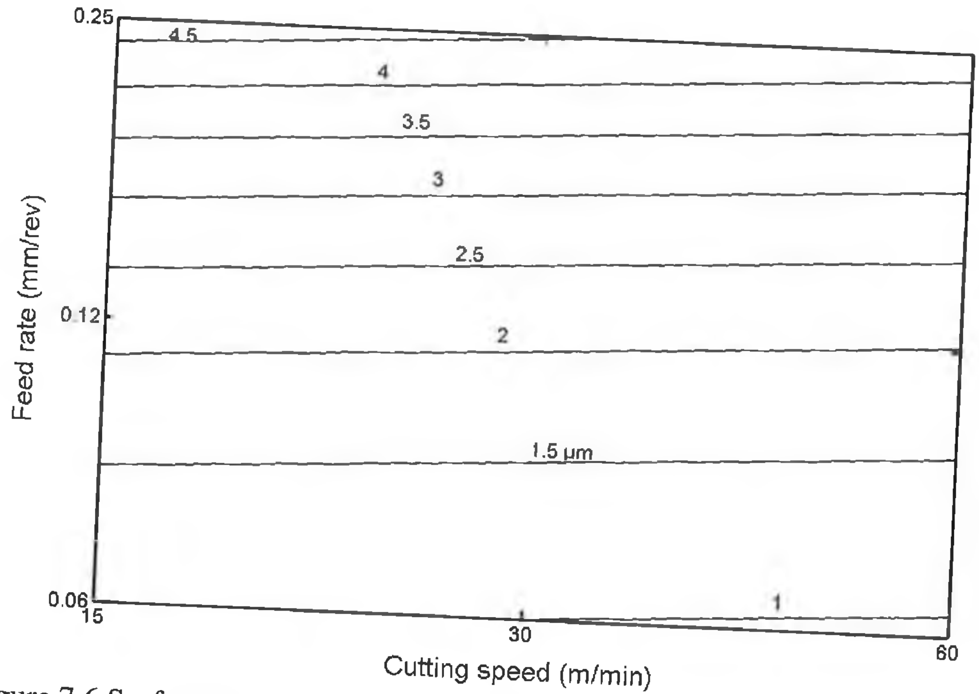

Figure.7.6 Surface roughness contours in speed-feed planes at nose radius 0.8 mm

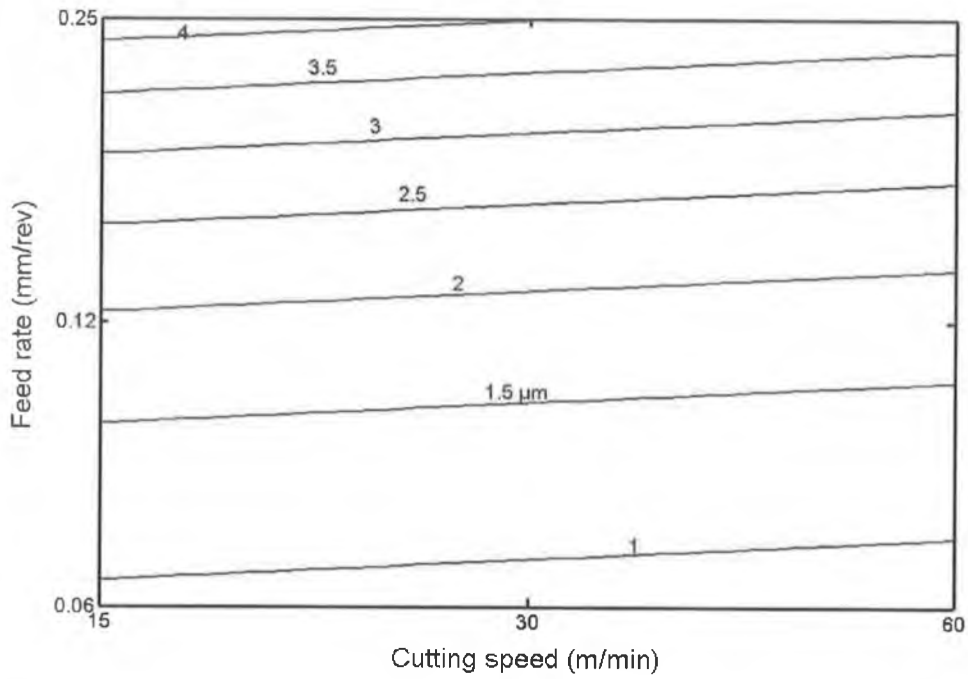

Figure.7.7 Surface roughness contours in speed-feed planes at nose radius 1.6 mm

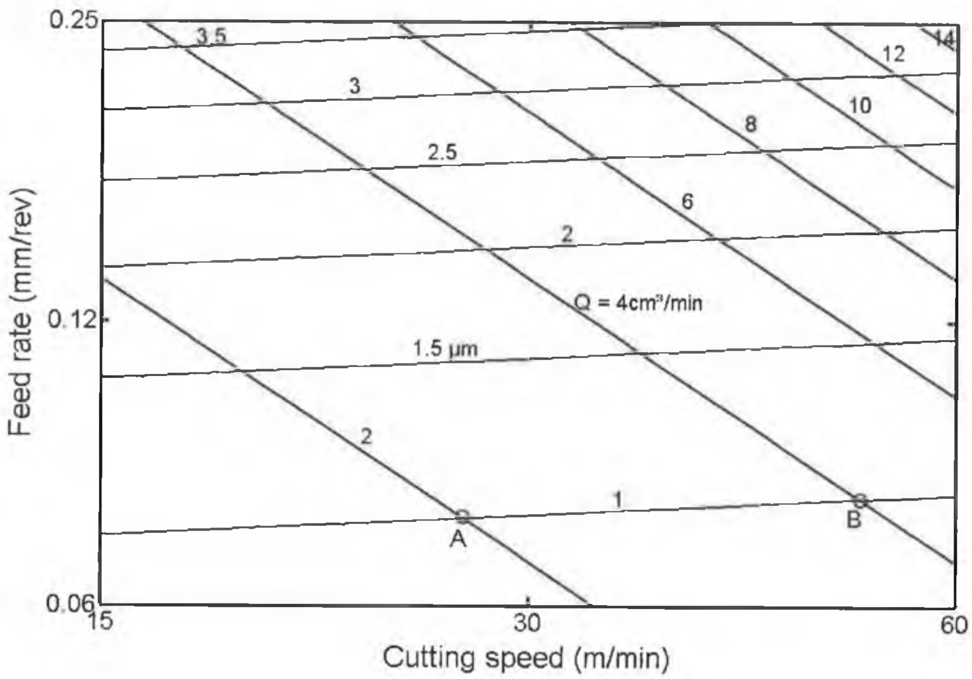

Figure.7.8 Response contours of surface roughness & metal removal at nose radius and depth of cut = 0.8 mm

Figures; (7.5,7.6,7.7) shows that the increases in cutting speed increase the quality of surface finish while the surface finish decrease with increase of feed rate. Also it is shows in Figure 7.8; that the increase in material removal rate is obtained without any sacrifice in the quality of the produced surface.

7.4 Surface Roughness Model For Boron Nitride Material

To develop the first-order model; a design consisting of 12 experiments has been used. 8 experiments represent a 2^3 factorial design with an added centre point being used to estimate pure error. 4 experiments represent an added centre point to the cube, repeated 4 times to calculate pure error. The complete design consists of 12 experiments in 2 blocks, each block containing 6 experiments. The first block consisting of experiment numbers 1, 4, 6, 7, 9, and 10. Also the second block of six tests is 2, 3, 5, 8, 11, and 12. Has been added for convenient identification and for easy calculation by taking into account the capacity of the lathe and limiting cutting conditions. The twelve experiments were preformed in two blocks see Table 7.7. These two blocks were used to develop the first-order model for Boron nitride.

Table 7.7 Experiment conditions and results

Trial No.	Block No.	Speed (m/min)	Feed (mm/rev)	Depth (mm)	Coding			Surface roughness (μm)
					x_1	x_2	x_3	
1	1	15	0.06	0.4	-1	-1	-1	0.64
2	2	60	0.06	0.4	1	-1	-1	0.62
3	2	15	0.25	0.4	-1	1	-1	2.78
4	1	60	0.25	0.4	1	1	-1	2.88
5	2	15	0.06	1.6	-1	-1	1	0.64
6	1	60	0.06	1.6	1	-1	1	0.625
7	1	15	0.25	1.6	-1	1	1	2.98
8	2	60	0.25	1.6	1	1	1	2.88
9	1	30	0.12	0.8	0	0	0	0.94
10	1	30	0.12	0.8	0	0	0	0.92
11	2	30	0.12	0.8	0	0	0	0.98
12	2	30	0.12	0.8	0	0	0	0.96

The central composite design with 12 experiments provided three levels for each independent variable, as shown in Table 7.8.

Table 7.8 Levels of independent variables

	Low	Centre	High
Coding	-1	0	1
Cutting speed, v (mm/min)	15	30	60
Feed, f (mm/rev)	0.06	0.12	0.25
Depth of cut, d (mm)	0.4	0.8	1.6

Table 7.9 Analysis of variance for first block

Source	**Sum of squares**	**DF**	**MS**	**F_{cal}**	**F_{lab}**
Zero-order term	2.350	1	2.350		
First-order terms	0.1975	3	0.0658	3.06	
Lack of fit	0.173	1	0.173	8.046	161.4
Pure error	0.0215	1	0.0215		
Total	2.742	6	0.457		

Table 7.10 Analysis of variance for second block

Source	**Sum of squares**	**DF**	**MS**	**F_{cal}**	**F_{lab}**
Zero-order term	2.2579	1	2.2579		
First-order terms	0.1998	3	0.0666	1.631	
Lack of fit	0.09553	1	0.09553	2.34	161.4
Pure error	0.04082	1	0.04082		
Total	2.594	6	0.4323		

The analysis of variance for the first and second blocks shows that the first order terms are adequate, since the F_{cal} = 3.06 and 1.631 respectively less than the

F_{lab} = 161.4 as shown above in tables (7.9) and (7.10). As a result of the lack of fit test the lack of fit is not significant for the two blocks, which indicate that the developed model is adequately fits the data. The detailed formulae for the analysis of variance used in this investigation are shown in appendix B Table1,

7.4.1 Result, Discussions, and Optimisation: First-Order Model

Using the technique in section 7.3, the results of the experiments can be transformed into an equation of surface finish under the conditions described earlier in this section. This equation is as follows:

$$\therefore \quad R_a = 11.26985 \left(V^{-0.01108} f^{1.03386} d^{0.014}\right) \qquad (7.19)$$

From the equation (7.19) it can be deduced that the surface finish improve with increase of cutting speed, while an increase in the feed rate or depth of cut results in an increase in the surface finish produced. Combining equation (7.6) and equation (7.13), the metal removal rate equation for a specific depth of cut (0.8 mm) could be written as equation (7.14).

$$\ln Q = 1.057785571 + 0.69315x_1 + 0.73397x_2$$

7.4.2 Analysis of Results for Various Nose Radius of Boron Nitride Material

The design is obtained by 2^3 which, mean three factorial has been used at three level (v, f, r), cutting speed (m/min), feed rate (mm/rev), nose radius (mm).

The experiment has been carried out with three types of inserts having different nose radius these selected levels were chosen as low (r = 0.4 mm), centre (r = 0.8 mm), and high (r = 1.6 mm).

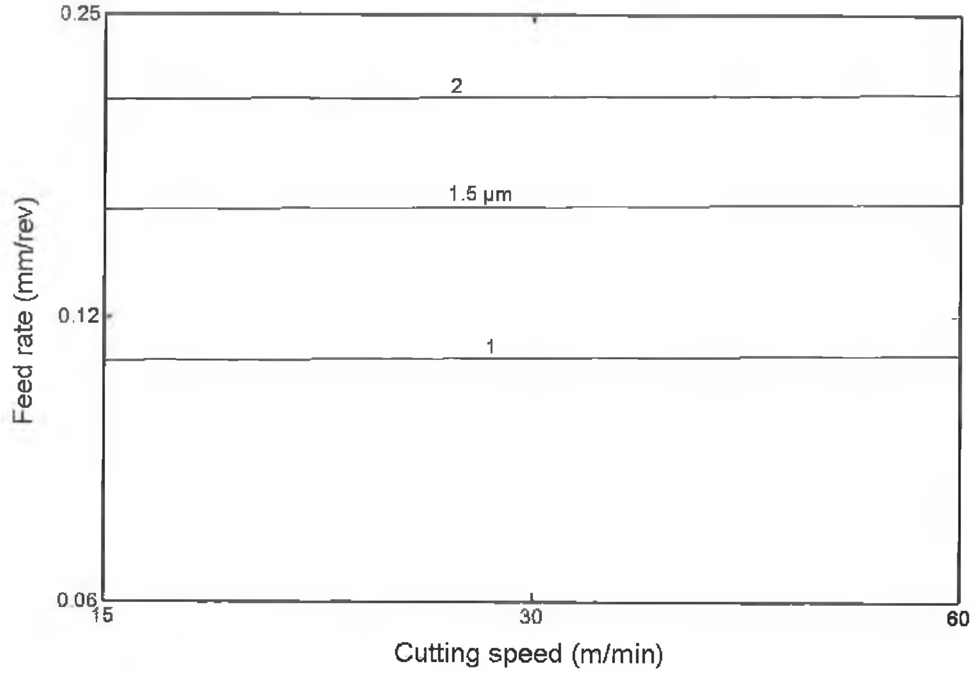

Figure.7.9 Surface roughness contours in cutting speed-feed planes at depth 0.4 mm

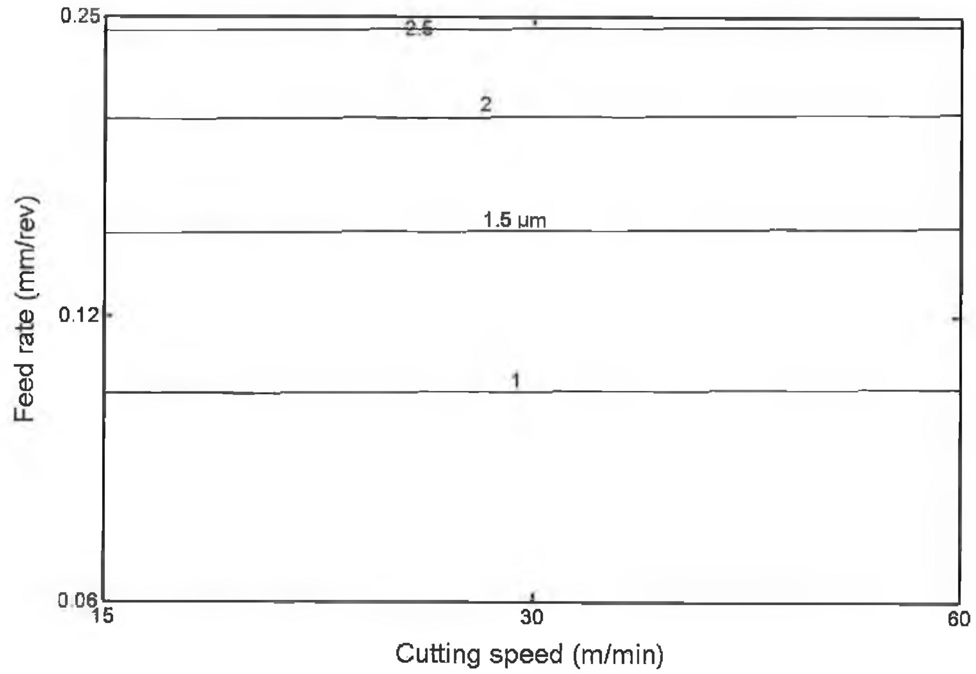

Figure.7.10 Surface roughness contours in cutting speed-feed planes at depth 0.8 mm

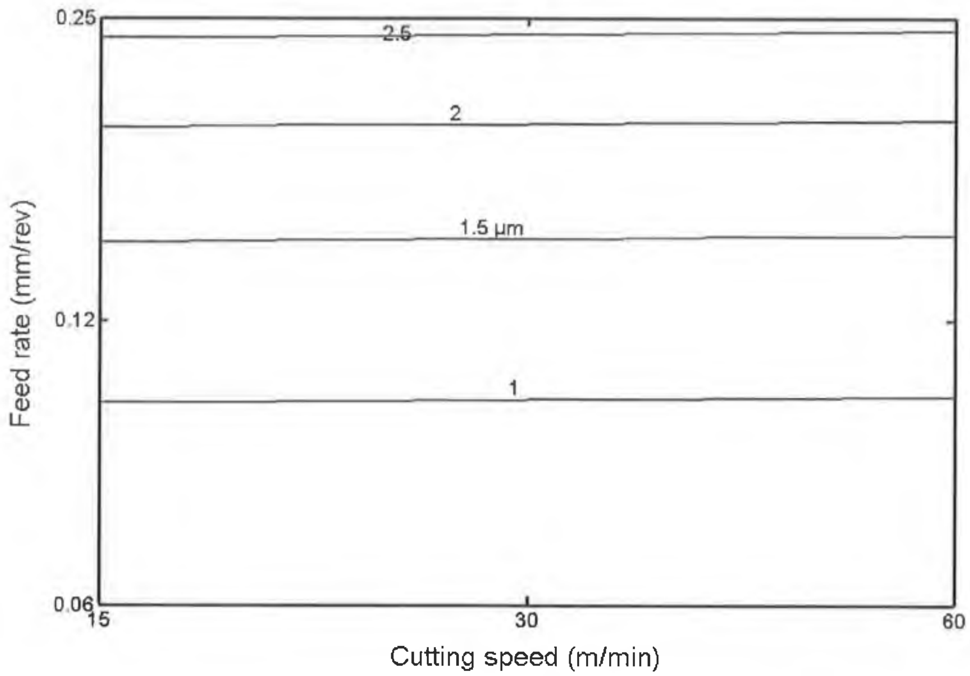

Figure.7.11 Surface roughness contours in cutting speed-feed planes at depth 1.6 mm

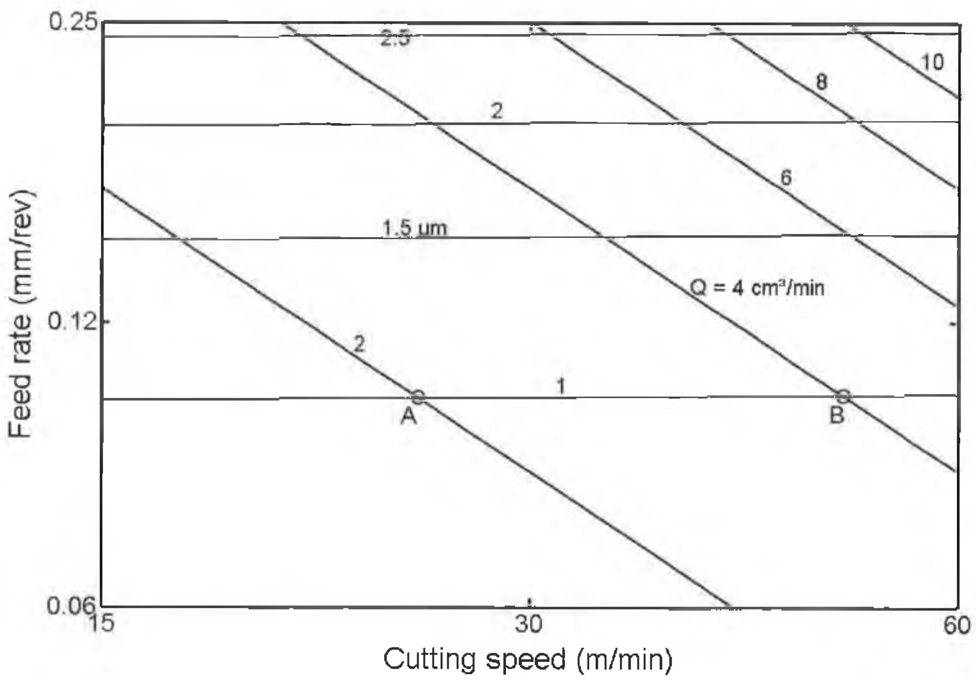

Figure.7.12 Response contours of surface roughness & metal removal at depth0.8mm

Figures; (7.9,7.10,7.11) shows that the increases in cutting speed increase the quality of surface finish while the surface finish decrease with increase of feed rate. Also it is shows in Figure 7.12; that the increase in material removal rate is obtained without any sacrifice in the quality of the produced surface.

Table 7.11 Experiment conditions and results

Trial No.	Block No.	Speed v (m/min)	Feed f (mm/rev)	Nose radius r (mm)	Coding			Surface roughness (μm)
					x_1	x_2	x_3	
1	1	15	0.06	0.4	-1	-1	-1	1.4
2	2	60	0.06	0.4	1	-1	-1	1.3
3	2	15	0.25	0.4	-1	1	-1	4.6
4	1	60	0.25	0.4	1	1	-1	4.5
5	2	15	0.06	1.6	-1	-1	1	0.48
6	1	60	0.06	1.6	1	-1	1	0.46
7	1	15	0.25	1.6	-1	1	1	1.6
8	2	60	0.25	1.6	1	1	1	1.54
9	1	30	0.12	0.8	0	0	0	0.74
10	1	30	0.12	0.8	0	0	0	0.72
11	2	30	0.12	0.8	0	0	0	0.74
12	2	30	0.12	0.8	0	0	0	0.76

Using the technique shown in section 7.3, the results of the experiments can be transformed into an equation of surface finish under the conditions described earlier in this section. This equation is as follows:

$$\therefore \quad R_a = 6.285216 \left(V^{-0.031895} f^{0.82489} r^{-0.76421}\right) \qquad (7.20)$$

The equation (7.20) has been plotted in Figure 7.13, 7.14, 7.15 as contours for each of the response surfaces at three selected levels of nose radius These selected levels were chosen as low $(r = 0.4mm)$, centre $(r = 0.8mm)$, and high $(r = 1.6mm)$. It can be deduced that the surface finish improve with increase of cutting speed and nose radius, while it deteriorates with the increase of feed rate. However it was noticed that the nose radius has a significant effect on surface finish.

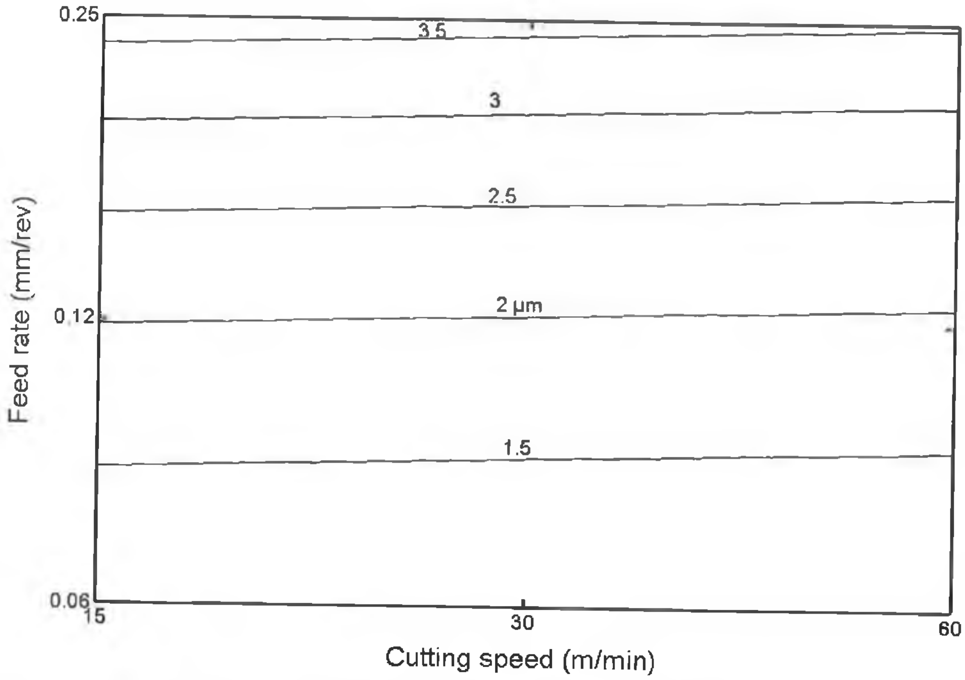

Figure.7.13 Surface roughness contours in speed-feed planes at nose radius 0.4 mm

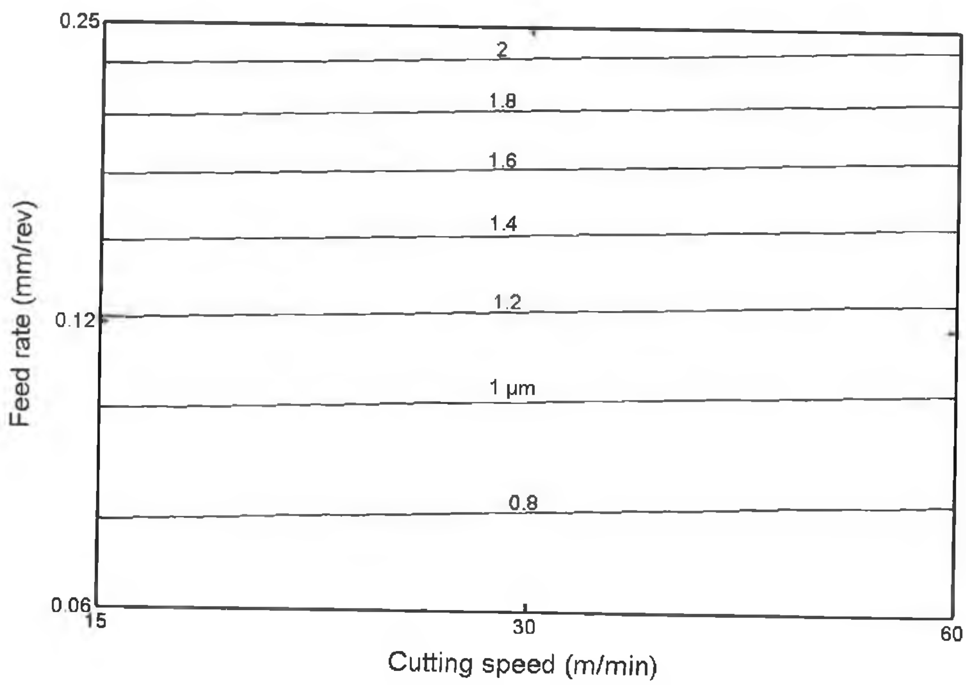

Figure.7.14 Surface roughness contours in speed-feed planes at nose radius 0.8 mm

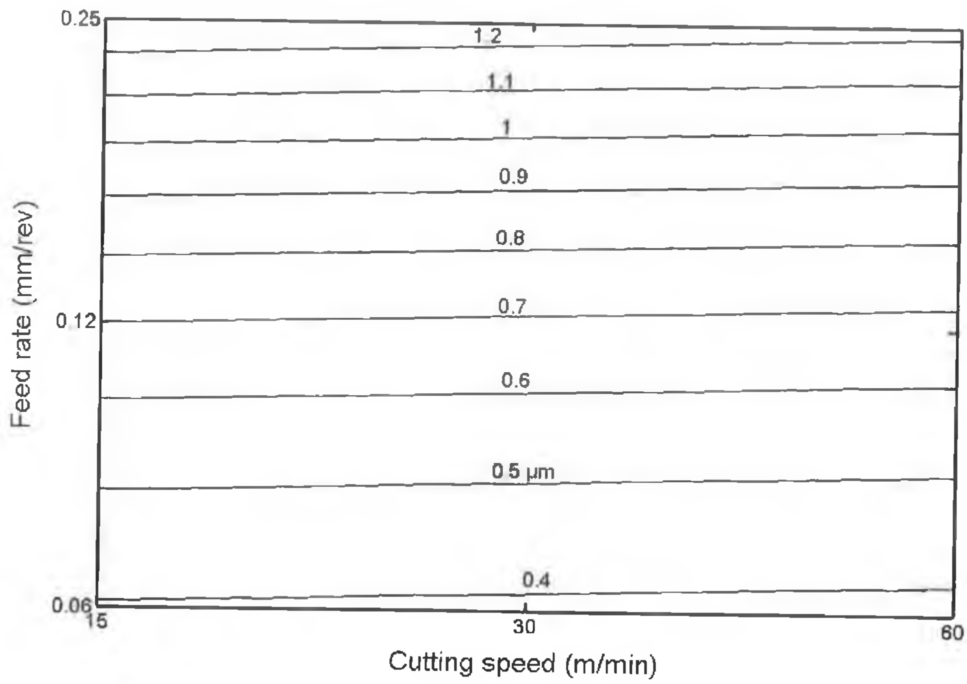

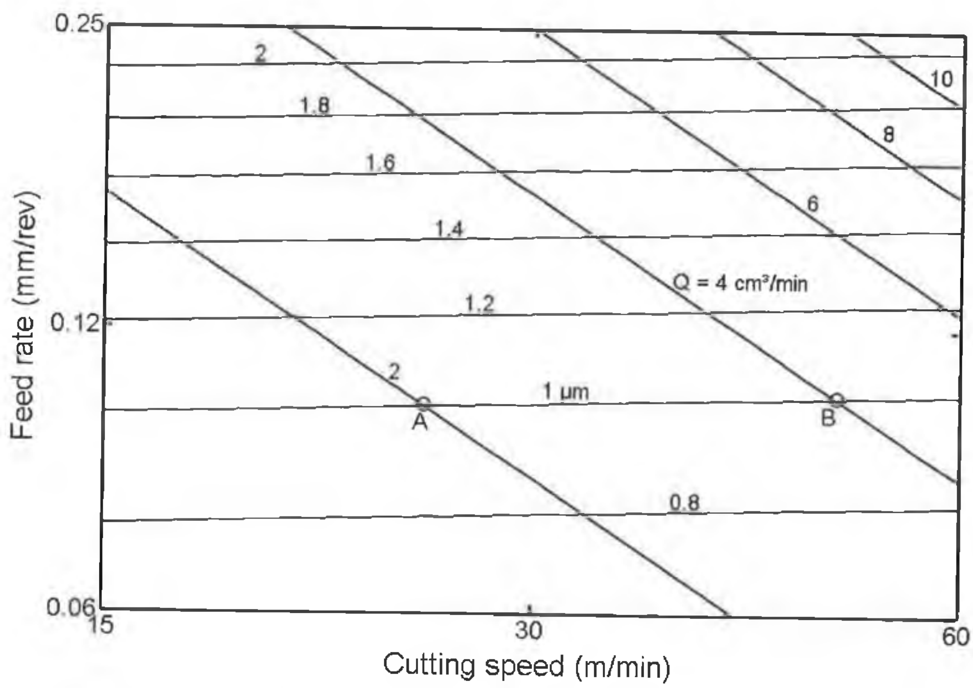

Figure.7.15 Surface roughness contours in speed-feed planes at nose radius 1.6 mm

Figure.7.16 Response contours of surface roughness & metal removal at nose radius and depth of cut = 0.8 mm.

Figures; (7.13,7.14,7.15) shows that the increases in cutting speed increase the quality of surface finish while the surface finish decrease with increase of feed rate.

Also it is shows in Figure 7.16; that the increase in material removal rate is obtained without any sacrifice in the quality of the produced surface.

Figure 7.16 represents dual response contours of metal removal rate and surface roughness at nose radius and depth of cut = 0.8 mm. However, cutting conditions that provide a higher rate of metal removal must be selected. It is shown that the selections of cutting conditions represented by point B are better than those represented by point A. This increase in material removal rate is obtained without any sacrifice in the quality of the produced surface. This reduces the machining time, since the metal removal rate B is 50% greater than that of A. By this experiment the cutting conditions that give roughness as output were known clearly.

Summary

- Observed that the increase in cutting speed increase the quality of surface finish at constant feed rate and depth of cut.
- An increase in the feed rate results in an increase in the surface finish.
- Surface roughness decrease with increase in the nose radius it was found that a large nose radius produces better surface finish.
- Surface finish increase with increase in the depth of cut.
- The increase in material removal rate is obtained without any sacrifice in the quality of the produced surface. This reduces the machining time, since the metal removal rate B is 50% greater than that of A.

It is clear from the graphs that surface finish improves with the increase of cutting speed and nose radius, however, it is decrease with increase of feed rate and depth of cut. However, although abetter surface is produced at low depths of cut, the increase in surface finish with increasing depth of cut is not very significant. Cutting speed and feed rate are the most significant factors affecting surface finish.

Response contours have been developed which relate surface roughness to cutting speed, feed rate, depth of cut and nose radius.

CHAPTER EIGHT:
CONCLUSION AND RECOMMENDATIONS

8 CONCLUSIONS AND RECOMMENDATIONS

8.1 Introduction

After the analysis of the test results, the conclusions and recommendations for both ceramic materials are presented in this chapter. A one variable at-a-time study and design of experiment approach are presented.

8.2 One variable at-a-time

8.2.1 Surface Finish

- The effect of feed rate on surface roughness is much more pronounced than the effect of cutting speed or depth of cut. As the feed rate increases the roughness values increases, so the best surface finish obtained at low feed rate.
- The increases in cutting speed increase the quality of surface finish at constant feed rate and depth of cut.
- The depth of cut effect on the surface roughness shows that as depth of cut increases the surface roughness will increases.
- The larger nose radius produces better surface finish.

8.2.2 Tool life

Experiments were conducted at variable cutting speed of 20-80 (m/min) and feed rate of 0.08, 0.12, 0.2 and 0.25 (mm/rev) and depth of cut of 0.8, 1.2, 1.4 and 1.6 (mm).
It was noted that there is no change in the tool wear, therefore no replacement and/ or maintenance for the tool, under the condition that was used and during the total time of the cutting operation.

8.2.3 Cutting Forces

- With the increase of feed rate or depth of cut, cutting forces increase almost linearly.
- The increases in cutting speed increase the cutting forces slightly.

These results are summarised in table 8.1.

Compression criteria	Component /cutting condition	Macor	Boron nitride
Cutting forces V = 15 (m/min) f = 1 (mm/rev), d = 0.5 (mm)	Fx	3.662 N	2.783 N The largest component
	Fy	3.321 N	1.509 N
	Fz	7.324 N The largest component	1.904 N
	F	8.836 N	3.694 N
Cutting forces V = 25 (m/min) f = 2 (mm/rev), d = 0.5 (mm)	Fx	5.127 N	3.223 N The largest component
	Fy	4.541 N	1.935 N
	Fz	8.643 N The largest component	2.930 N
	F	11.027 N	5.274 N
Cutting forces V = 45 (m/min) f = 3 (mm/rev), d = 0.5 (mm)	Fx	6.738 N	4.395 N The largest component
	Fy	6.299 N	2.637 N
	Fz	11.572 N The largest component	3.516 N
	F	14.798 N	6.215 N
Roughness (Ra) V = 10 (m/min), d = 1.4 (mm)	f = 0.08 (mm/rev)	1.775 μm	0.9 μm
	f = 0.2 (mm/rev)	7.88 μm	3.4 μm
	f = 0.25 (mm/rev)	9.46 μm	5.475 μm
Roughness (Ra) V = 14 (m/min), d = 1.4 (mm)	f = 0.08 (mm/rev)	1.7 μm	0.76 μm
	f = 0.2 (mm/rev)	7.46 μm	3.32 μm
	f = 0.25 (mm/rev)	8.72 μm	5.28 μm
Roughness (Ra) V = 24 (m/min), d = 1.4 (mm)	f = 0.08 (mm/rev)	1.4 μm	0.6 μm
	f = 0.2 (mm/rev)	4.4 μm	3 μm
	f = 0.25 (mm/rev)	6 μm	4.7 μm
Tool life	--	*No change	*No change
Hardness (Brinell)	--	154	108.5

Table 8.1 Shows the comparison between Macor and Boron nitride ceramics

* At all cutting conditions was use.

Figures; (8.1,8.2) Shows the comparison between Macor and Boron nitride ceramics in term of surface roughness.

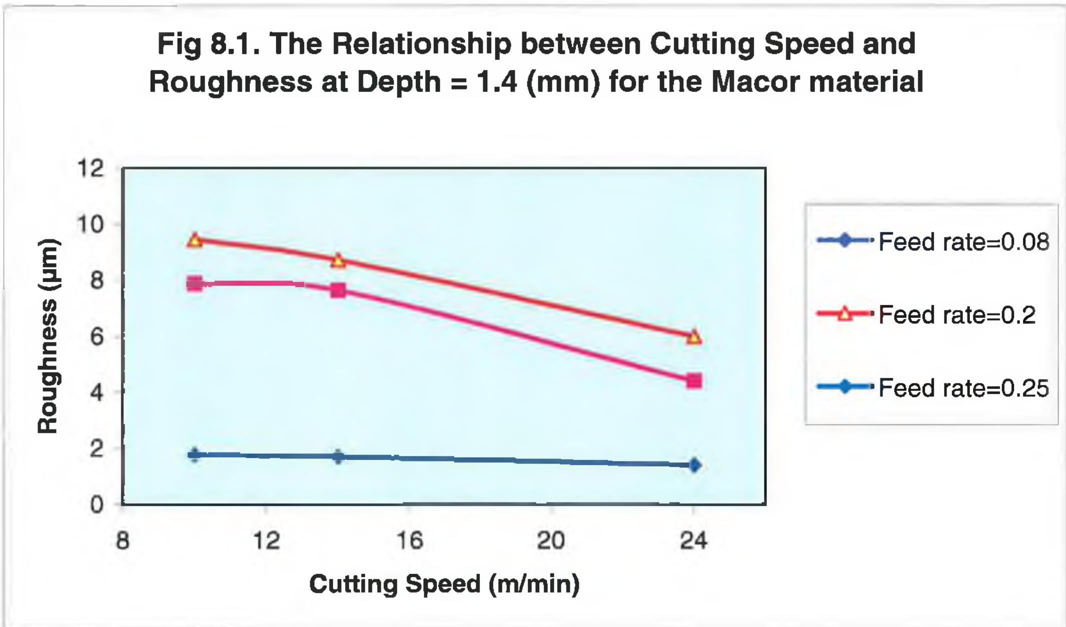

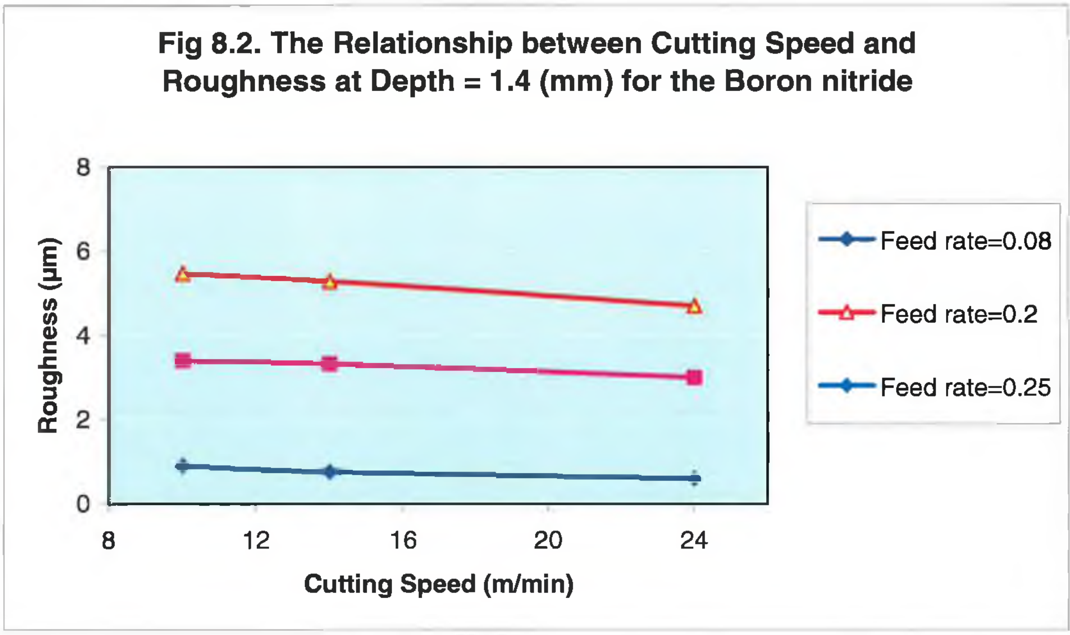

These figures shows that the Boron nitride material is more machinable than Macor material that because the hardness of Macor material higher than Boron nitride.

Figures; (8.3,8.4) Shows the comparison between Macor and Boron nitride ceramics in term of cutting forces.

Figure 8.3; Relationship between Cutting speed & Cutting forces at Feed rate 1 (mm/rev) and depth of cut 0.5 mm

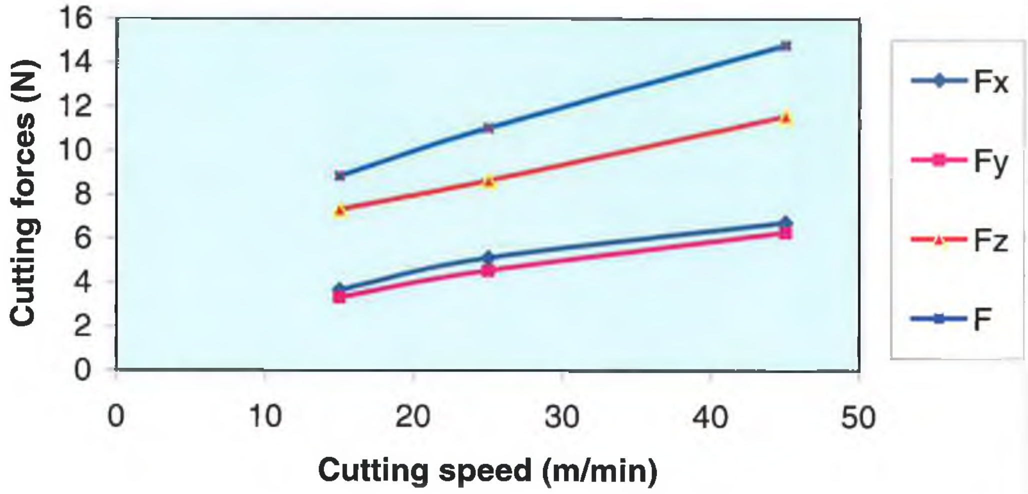

Figure 8.4; Relationship between Cutting speed & Cutting forces at Feed rate 1 (mm/rev) and depth of cut 0.5 mm

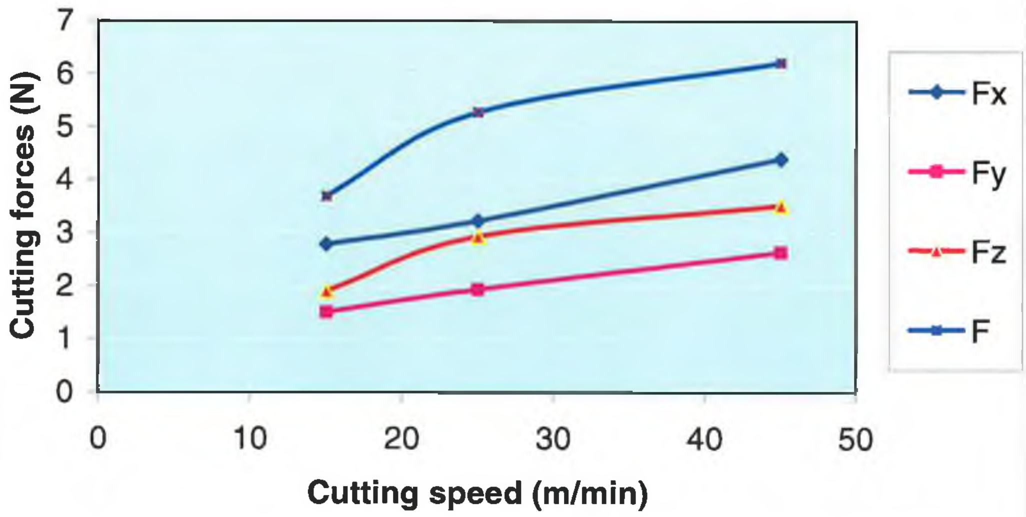

These figures show that the cutting forces of Boron nitride material are less than the cutting forces of Macor material. So Macor material requires more power than Boron nitride material.

8.3 Design of Experiments

- As the cutting speed increases, the surface finish improves.
- The roughness equation shows that the feed rate and nose radius are the main influencing factors on the surface finish followed by cutting speed and depth of cut.
- Response surface methodology provides a large amount of information with a small amount of experimentation.

8.4 Recommendations for the Further Work

- The use of various carbide tools for machining machinable ceramic materials should be made in testing machinability.
- With a view to developing a comprehensive computerized machinability data base systems using mathematical models, a large quantity of experimental data are required. These are necessary to validate the usefulness of a model.
- The use of different tool materials and geometries to machining ceramic materials may be useful to compare the variations in the surface roughness.
- It would be helpful to identify a model for a specific hardness group of materials and generalize it for that hardness range.

REFERENCE

1. Machining Data Centre, "Machining Data Handbook", 3rd Edition, Vol. 2, Metcut Research Associates Inc., Cincinnati, 1980.

2. H. Ernst., Physics of Metal Cutting, ASM, Cleveland, Ohio, 1938.

3. Boston, "Machinability of Ordnance Steels", Paper No. SP-123, Society of Automotive Engineers, 1958.

4. A.R. Boccaccini., "Machinability and Brittleness of Glass-Ceramics", Journal, Vol. 65, 1997.

5. D.S. Baik and J.S. Chun., "Effect of The Aspect Ratio of Mica Crystals and Crystallinity on The Microhardness and Machinability of Mica Glass-Ceramics", Journal, Vol. 67, 1997.

6. O.W. Reen., "Modern Developments in Powder Metallurgy", MPIF Publishers, Princetown, NJ, Vol. 10, PP. 431-451, 1977.

7. E.M. Trent., Metal Cutting, Butterworths London, 1977.

8. Sandvik, "Modern Metal Cutting", Sandvik Coromant, Sweden, 1994.

9. I.A. Choudhury and M.A.El-Baradie, "Machinability of Nickel-Base Super Alloys: a General Review", J. Vol. 77, 1998.

10. J.H. Song and J.R. Evans, "On the Machinability of Ceramic Compacts", 1997.

11. F.W. Boulger., "Machining Theory and Practice", Paper 69, Cleveland, Ohio, 1950.

12. Goodfeelow, Combridge Limited, England, Fax No: 0800 328 7689.

13. W. David, Richerson., "Ceramics Applications in Manufacturing", Handbook, 1988.

14. J Cherry., "Practical Investigations in Metal Cutting", The Production Engineering., Vol. 81, 1962.

15. Miltonc. Shaw., "Metal Cutting Principles", 1984.

16. N. Richards, D.A Spinwall, "Use of Ceramic Tools for Machining Nickel Based Alloys", Int, J, Mach., Vol. 29, 1996.

17. M.El-Baradie and M. Wilson, "Metal Cutting and Machinability", Engineering and Technology Series, National Board for Science and Technology, Vol. 6, 1983.

18. P. Mikell, Groover., "Fundamentals of Modern Manufacturing", handbook, 1996.

19. M. Rahman, S.Ramakrishna and Prakash, "Machinability study of Carbon Fiber Reinforced Composite", J, Vol. 89-90, 1999.

20. T.I.El-Wardany, M.A.Elbestawi, M.H.Attia and E.Mohamed., "Surface Finish in Turning of Hardened steel", PED-Vol. 62, 1992.

21. X.D. Fang and I. Jawahir., "Predicting Total Machining Performance in Finish Turning Using Integrated Fuzzy-Set Modles of The Machinability Parameters", Vol. 32, No. 4, 833-849, 1994.

22. C.H.Che. Haron., "Tool Life and surface Integrity in Turning Titanium Alloy", J. Vol.18, 2001.

23. J.T. Lin, D. Bhattacharyya and C. Lane., "Machinability of a Silicon Carbide Reinforced Aluminium Metal Matrix Composite", 1995.

24. I. Yellowley, G. Barrow., "The Assessment of Tool Life in Peripheral Milling", Proc. 19th International Matador Conference., Birmingham, PP.443-452, 1978.

25. T. Vorm, Koplev, Aa Lystup., "The Cutting Process, Chips and Cutting Force in Machining CFRP Composites", Vol. 14,(4), 371-376, 1983.

26. M.C. Shaw., "Metal Cutting Principles", Oxford University Press, New York, 1986.

27. C.H. Che Haron, A. Ginting, and J.H. Goh., "Wear of Coated and Uncoated Carbides in Turning Tool Steel", Vol. 116, 2001.

28. L. Moor., "Machine Tools Metals and Cutting Fluids", Handbook, 1972.

29. B.N. Colding., "Machinability of Metals and Machining Cost", Int, J, Vol. 1, PP. 220-248, 1961.

30. P. Magolderick and M.A.M. Hijazi., "The Use of Weighing Method to Determine a Tool Wear Algorithm for End Milling", Proc. 20th, Int, MTDR, Conference., Birmingham, PP. 345-349, 1979.

31. I.A. Choudhury and M.A. El-Baradie., "Machinability Assessment of Inconel 718 by Factorial Design of Experiment Coupled With Response Surface Methodology", J, Vol. 95, 1999.

32. I.A. Choudhury and M.A. El-Baradie., "Tool Life Prediction Model by Design of Experiments for Turning High Strength Steel", J, 319-326, 1998.

33. International Standard Organisation. 8688-2., "Tool Life Testing in Milling – Part 2: End Milling", 1989.

34. H. Wolforam and B. Georg., "Glass-Ceramic Technology", Handbook, 2002.

35. M.H. Lewis., "Classes and Glass-Ceramics", 1988.

36. http://www. Advanced ceramic materials. Com.

37. N. Fadi, and B. Mohamed., "High Performance Ceramics", The American University City in Cairo, 1998.

38. Machinability Data Center., "Machining Data Handbook", 3rd Edition, Vol. 2, 1980.

39. B. Mills and A.H. Redford., "Machinability of Engineering Materials", Handbook, University of Salford, UK, 1983.

40. H. Opitz, and W. Konic., "On The Wear of Cutting Tools", 8th. Jnt. MTDR. Conference, 173, 1967.

41. J. Ellis and G. Barrow., "The Failure of Carbide Tools When Machining High Strength Steels", 1967.

42. A.H. Redford., "The Effect on Cutting Tool Wear of Various Types of Chip Control Device", 1980.

43. F.W. Taylor., "On The Art of Cutting Metals", 1907.

44. Society Manufacturing Engineering., "Tool and Manufacturing Engineers", Handbook, Fourth Edition, Vol. 1, Machining, 1983.

45. M.O. Nicolls., "The Measurement of Surface Finish", De Beers Technical Service Centre, UK.

46. Surface Roughness Tester Operation Manual, Surftest 402 Series 178, Manual No: 4358, Mitutoyo Corporation.

47. Kistler Three Component Dynamometer Type 9265, Piezo-Instrumentation Kistler, Instruments Ltd.

48. Kistler Charge Amplifier Type 5011, Piezo-Instrumentation Kistler, Instruments Ltd.

49. National Instrument., "Data Acquisition (DAQ) Fundamentals", May 1996.

50. www.ceupenn.edu "Introduction to Data Acquisition Systems and Labview".

51. www.ccsi-inc.com "Technical Information".

52. B.L. Juneja., G.S. Sekhon., "Fundamentals of Metal Cutting and Machine Tools", John Wiley Inc. New York, 1987.

53. Wu. SM., "Tool Life Testing by Response Surface Methodology". Trans. ASME, Series B, Vol. 86, 105-116, 1964.

54. S.B. Rao., "Tool Wear Monitoring Through The Dynamics of Stable Turning", J. of Engineering for Industry, Vol. 108 (3), PP.183-190, 1986.

APPENDIX. A: TABLES OF ROUGHNESS AND CUTTING FORCE VALUES

Table 1 Shows values of roughness at depth of cut 0.4 mm

Cutting speed (m/min)	Roughness at feed rate, 0.08 (mm/rev)	Roughness at feed rate, 0.12 (mm/rev)	Roughness at feed rate, 0.2 (mm/rev)	Roughness at feed rate, 0.25 (mm/rev)
10	1.733	4.7	6.5125	8.7
11	1.725	4.64	6.5	8.5
12	1.68	4.6	6.24	8.3
13	1.642	4.52	6.2	8.2
14	1.633	4.5	6.2	8.2
15	1.62	4.22	6	8
24	1.33	2.5	4	5.2

Table 2 Shows values of roughness at depth of cut 0.8 mm

Cutting speed (m/min)	Roughness at feed rate, 0.08 (mm/rev)	Roughness at feed rate, 0.12 (mm/rev)	Roughness at feed rate, 0.2 (mm/rev)	Roughness at feed rate, 0.25 (mm/rev)
10	1.76	4.728	6.925	9.1
11	1.73	4.7	6.88	8.9
12	1.685	4.64	6.766	8.7
13	1.66	4.625	6.76	8.64
14	1.64	4.6	6.7	8.5
15	1.6	4.4	6.7	8.4
24	1.36	2.7	4.2	5.6

Table 3 Shows values of roughness at depth of cut 1.2 mm

Cutting speed (m/min)	Roughness at feed rate, 0.08 (mm/rev)	Roughness at feed rate, 0.12 (mm/rev)	Roughness at feed rate, 0.2 (mm/rev)	Roughness at feed rate, 0.25 (mm/rev)
10	1.76	4.83	7.6	9.3
11	1.733	4.787	7.425	9.1
12	1.71	4.75	7.34	8.85
13	1.685	4.7	7.3	8.7
14	1.67	4.7	7.24	8.6
15	1.64	4.45	6.88	8.56
24	1.4	2.7	4.2	5.96

Table 4 Shows values of roughness at depth of cut 1.4 mm

Cutting speed (m/min)	Roughness at feed rate, 0.08 (mm/rev)	Roughness at feed rate, 0.12 (mm/rev)	Roughness at feed rate, 0.2 (mm/rev)	Roughness at feed rate, 0.25 (mm/rev)
10	1.775	4.9	7.88	9.46
11	1.733	4.85	7.82	9.32
12	1.73	4.75	7.55	9.12
13	1.7	4.7	7.475	8.9
14	1.7	4.7	7.46	8.72
15	1.658	4.45	7.42	8.68
24	1.4	2.9	4.4	6

Table 5 Shows values of roughness at feed rate 0.08 (mm/rev)

Cutting speed (m/min)	Roughness at Depth 0.4 mm	Roughness at Depth 0.8 mm	Roughness at Depth 1.2 mm	Roughness at Depth 1.4 mm
10	1.733	1.76	1.76	1.775
11	1.725	1.73	1.733	1.733
12	1.68	1.685	1.71	1.73
13	1.642	1.66	1.685	1.7
14	1.633	1.64	1.67	1.7
15	1.62	1.6	1.64	1.658
24	1.33	1.36	1.4	1.4

Table 6 Shows values of roughness at feed rate 0.12 (mm/rev)

Cutting speed (m/min)	Roughness at Depth 0.4 mm	Roughness at Depth 0.8 mm	Roughness at Depth 1.2 mm	Roughness at Depth 1.4 mm
10	4.7	4.728	4.83	4.9
11	4.6	4.7	4.787	4.85
12	4.6	4.64	4.75	4.75
13	4.5	4.625	4.7	4.7
14	4.5	4.6	4.7	4.7
15	4.2	4.4	4.45	4.46
24	2.5	2.7	2.7	2.9

Table 7 Shows values of roughness at feed rate 0.2 (mm/rev)

Cutting speed (m/min)	Roughness at Depth 0.4 mm	Roughness at Depth 0.8 mm	Roughness at Depth 1.2 mm	Roughness at Depth 1.4 mm
10	6.5125	6.925	7.6	7.88
11	6.5	6.88	7.425	7.82
12	6.24	6.766	7.43	7.55
13	6.2	6.76	7.3	7.475
14	6.2	6.7	7.24	7.46
15	6	6.7	6.88	7.42
24	4	4.2	4.2	4.4

Table 8 Shows values of roughness at feed rate 0.25 (mm/rev)

Cutting speed (m/min)	Roughness at Depth 0.4 mm	Roughness at Depth 0.8 mm	Roughness at Depth 1.2 mm	Roughness at Depth 1.4 mm
10	8.7	9.1	9.3	9.46
11	8.5	8.9	9.1	9.2
12	8.3	8.7	8.85	9.12
13	8.2	8.64	8.7	8.9
14	8.2	8.5	8.6	8.72
15	8	8.4	8.56	8.68
24	5.2	5.6	5.96	6

Table 9 Shows values of roughness at cutting speed 10 (m/min) & constant feed rate

Nose radius (mm)	Roughness at Depth of cut 0.4 mm	Roughness at Depth of cut 0.8 mm	Roughness at Depth of cut 1.2 mm	Roughness at Depth of cut 1.4 mm
0.4	1.2	1.26	1.26	1.44
0.8	1.08	1.12	1.12	1.12
1.2	1.04	1	1.04	1.12

Table 10 Shows values of roughness at cutting speed 11(m/min) & constant feed rate

Nose Radius (mm)	Roughness at Depth of cut 0.4 mm	Roughness at Depth of cut 0.8 mm	Roughness at Depth of cut 1.2 mm	Roughness at Depth of cut 1.4 mm
0.4	1.12	1.12	1.15	1.2
0.8	1.08	1	1	1.12
1.2	1	1	0.94	1.04

Table 11 Shows values of roughness at cutting speed 12(m/min) & constant feed rate

Nose Radius (mm)	Roughness at Depth of cut 0.4 mm	Roughness at Depth of cut 0.8 mm	Roughness at Depth of cut 1.2 mm	Roughness at Depth of cut 1.4 mm
0.4	1.16	1.2	1.2	1.26
0.8	1.04	1.04	1.05	1.05
1.2	1	1	1.04	1.04

Table 12 Shows values of roughness at cutting speed 13(m/min) & constant feed rate

Nose Radius (mm)	Roughness at Depth of cut 0.4 mm	Roughness at Depth of cut 0.8 mm	Roughness at Depth of cut 1.2 mm	Roughness at Depth of cut 1.4 mm
0.4	1.38	1. 44	1.48	1.5
0.8	1.16	1.16	1.2	1.2
1.2	1.04	1.05	1.12	1.1

Table 13 Shows values of roughness at cutting speed 14(m/min) & constant feed rate

Nose Radius (mm)	Roughness at Depth of cut 0.4 mm	Roughness at Depth of cut 0.8 mm	Roughness at Depth of cut 1.2 mm	Roughness at Depth of cut 1.4 mm
0.4	1.38	1.425	1.44	1.44
0.8	1.04	1.04	1.08	1.1
1.2	1	1.02	1.04	1.08

Table 14 Shows values of roughness at cutting speed 15(m/min) & constant feed rate

Nose radius (mm)	Roughness at Depth of cut 0.4 mm	Roughness at Depth of cut 0.8 mm	Roughness at Depth of cut 1.2 mm	Roughness at Depth of cut 1.4 mm
0.4	1.35	1.38	1.425	1.44
0.8	1	1.04	1.08	1.08
1.2	1	1.04	1.08	1.05

Table 15 Shows values of roughness at feed rate 0.25 (mm/rev) to the Macor material

Depth of cut (mm)	Roughness at Speed 10 (m/min)	Roughness at Speed 11 (m/min)	Roughness at Speed 12 (m/min)	Roughness at Speed 13 (m/min)	Roughness at Speed 14 (m/min)	Roughness at Speed 15 (m/min)	Roughness At Speed 24 m/min
0.4	8.7	8.5	8.3	8.2	8.2	8	5.2
0.8	9.1	8.9	8.7	8.64	8.5	8.4	5.6
1.2	9.3	9.1	8.85	8.7	8.6	8.56	5.96
1.4	9.46	9.32	9.12	8.9	8.72	8.68	6

Table 16 Shows values of roughness at feed rate 0.25 (mm/rev) to the Boron nitride material

Depth of cut (mm)	Roughness at cutting speed 10 (m/min)	Roughness at cutting speed 12 (m/min)	Roughness at cutting speed 14 (m/min)	Roughness at cutting speed 16 (m/min)	Roughness at cutting speed 24(m/min)
0.4	5.12	5.1	5.1	5.05	4.35
0.8	5.12	5.1	5.05	5.04	4.5
1.2	5.2	5.15	5.14	5.133	4.5
1.4	5.475	5.38	5.28	5.14	4.7

Table 17 Shows values of roughness at depth of cut 0.4 mm

Cutting speed (m/min)	**Roughness at feed rate, 0.08 (mm/rev)**	**Roughness at feed rate, 0.12 (mm/rev)**	**Roughness at feed rate, 0.2 (mm/rev)**	**Roughness at feed rate, 0.25 (mm/rev)**
10	0.8	1.3	3.26	5.12
12	0.78	1.3	3.2	5.1
14	0.72	1.28	3.2	5.1
16	0.72	1.2	3.08	5.05
24	0.55	1	2.5	4.35

Table 18 Shows values of roughness at depth of cut 0.8 mm

Cutting speed (m/min)	**Roughness at feed rate, 0.08 (mm/rev)**	**Roughness at feed rate, 0.12 (mm/rev)**	**Roughness at feed rate, 0.2 (mm/rev)**	**Roughness at feed rate, 0.25 (mm/rev)**
10	0.8	1.4	3.275	5.12
12	0.76	1.38	3.2	5.1
14	0.74	1.4	3.1	5.05
16	0.74	1.32	3.1	5.04
24	0.575	1	2.7	4.5

Table 19 Shows values of roughness at depth of cut 1.2 mm

Cutting Speed (m/min)	Roughness at feed rate, 0.08 (mm/rev)	Roughness at feed rate, 0.12 (mm/rev)	Roughness at feed rate, 0.2 (mm/rev)	Roughness at feed rate, 0.25 (mm/rev)
10	0.83	1.42	3.32	5.2
12	0.76	1.5	3.3	5.15
14	0.82	1.375	3.24	5.14
16	0.76	1.35	3.15	5.133
24	0.6	1.1	2.7	4.5

Table 20 Shows values of roughness at depth of cut 1.4 mm

Cutting speed (m/min)	Roughness at feed rate, 0.08 (mm/rev)	Roughness at feed rate, 0.12 (mm/rev)	Roughness at feed rate, 0.2 (mm/rev)	Roughness at feed rate, 0.25 (mm/rev)
10	0.9	1.5	3.4	5.475
12	0.8	1.5	3.35	5.38
14	0.76	1.44	3.32	5.28
16	0.76	1.4	3.3	5.14
24	0.6	1.12	3	4.7

Table 21 Shows values of roughness at feed rate 0.08 (mm/rev)

Cutting speed (m/min)	**Roughness at Depth of cut 0.4 mm**	**Roughness at Depth of cut 0.8 mm**	**Roughness at Depth of cut 1.2 mm**	**Roughness at Depth of cut 1.4 mm**
10	0.8	0.8	0.83	0.9
12	0.78	0.76	0.76	0.8
14	0.72	0.75	0.8	0.76
16	0.72	0.74	0.76	0.76
24	0.55	0.575	0.6	0.6

Table 22 Shows values of roughness at feed rate 0.12 (mm/rev)

Cutting speed (m/min)	**Roughness at Depth of cut 0.4 mm**	**Roughness at Depth of cut 0.8 mm**	**Roughness at Depth of cut 1.2 mm**	**Roughness at Depth of cut 1.4 mm**
10	1.3	1.4	1.42	1.5
12	1.3	1.38	1.5	1.5
14	1.28	1.4	1.375	1.44
16	1.2	1.32	1.35	1.4
24	1	1	1.1	1.12

Table 23 Shows values of roughness at feed rate 0.2 (mm/rev)

Cutting speed (m/min)	**Roughness at Depth of cut 0.4 mm**	**Roughness at Depth of cut 0.8 mm**	**Roughness at Depth of cut 1.2 mm**	**Roughness at Depth of cut 1.4 mm**
10	3.26	3.275	3.32	3.4
12	3.2	3.2	3.3	3.35
14	3.2	3.1	3.24	3.32
16	3.08	3.1	3.15	3.3
24	2.5	2.7	2.7	3

Table 24 Shows values of roughness at feed rate 0.25 (mm/rev)

Cutting speed (m/min)	Roughness at Depth of cut 0.4 mm	Roughness at Depth of cut 0.8 mm	Roughness at Depth of cut 1.2 mm	Roughness at Depth of cut 1.4 mm
10	5.12	5.12	5.2	5.475
12	5.1	5.1	5.15	5.38
14	5.1	5.05	5.14	5.28
16	5.05	5.04	5.133	5.14
24	4.35	4.5	4.5	4.7

Table 25 Shows values of roughness at cutting speed 10(m/min) & constant feed rate

Nose Radius (mm)	Roughness at Depth of cut 0.4 mm	Roughness at Depth of cut 0.8 mm	Roughness at Depth of cut 1.2 mm	Roughness at Depth of cut 1.4 mm
0.4	1.94	1.94	2	2
0.8	1.1	1.16	1.2	1.2
1.2	0.76	0.76	1	0.85

Table 26 Shows values of roughness at cutting speed 12(m/min) & constant feed rate

Nose Radius (mm)	Roughness at Depth of cut 0.4 mm	Roughness at Depth of cut 0.8 mm	Roughness at Depth of cut 1.2 mm	Roughness at Depth of cut 1.4 mm
0.4	1.88	2	1.94	2
0.8	1.05	1.16	1.2	1.2
1.2	0.76	0.76	1	0.85

Table 27 Shows values of roughness at cutting speed 14(m/min) & constant feed rate

Nose Radius (mm)	Roughness at Depth of cut 0.4 mm	Roughness at Depth of cut 0.8 mm	Roughness at Depth of cut 1.2 mm	Roughness at Depth of cut 1.4 mm
0.4	1.94	2	1.94	1.94
0.8	1.12	1.16	1.2	1.2
1.2	0.76	0.76	1	0.88

Table 28 Shows values of roughness at cutting speed 16(m/min) & constant feed rate

Nose Radius (mm)	Roughness at Depth of cut 0.4 mm	Roughness at Depth of cut 0.8 mm	Roughness at Depth of cut 1.2 mm	Roughness at Depth of cut 1.4 mm
0.4	2	2	2	1.88
0.8	1.08	1.1	1.05	1.15
1.2	0.76	0.76	0.85	0.88

Table 29 Shows values of cutting forces at feed rat 1 (mm/rev) and depth 0.5 mm.

Cutting speed	Feed rate	Depth of cut	Cutting Forces (N)			
			Fx	Fy	Fz	F
15	1	0.5	3.662	3.321	7.324	8.836
25			4.541	4.102	8.057	10.117
35			5.102	4.687	9.229	11.540
45			5.713	5.273	10.254	12.868

Table 30 Shows values of cutting forces at feed rat 1 (mm/rev) and depth 1 mm.

Cutting speed	Feed rate	Depth of cut	Cutting Forces (N)			
			Fx	Fy	Fz	F
15	1	1	7.031	6.152	9.668	13.444
25			8.203	7.471	10.986	15.614
35			9.223	8.496	12.158	17.466
45			9.668	8.936	14.209	19.370

Table 31 Shows values of cutting forces at feed rat 1 (mm/rev) and depth 1.5 mm.

Cutting speed	Feed rate	Depth of cut	Cutting Forces (N)			
			Fx	Fy	Fz	F
15	1	1.5	11.484	10.254	15.578	21.902
25			12.964	11.426	17.139	24.338
35			13.916	12.305	18.896	26.497
45			15.381	13.916	22.412	30.537

Table 32 Shows values of cutting forces at feed rat 1 (mm/rev) & speed 25 (m/min).

Depth of cut	Feed rate	Cutting speed	Cutting Forces (N)			
			Fx	Fy	Fz	F
0.5	1	25	4.541	4.102	8.057	10.117
1			8.203	7.471	10.986	15.614
1.5			12.964	11.426	17.139	24.338

Table 33 Shows values of cutting forces at feed rat 2 (mm/rev) and depth 0.5 mm.

Cutting speed	Feed rate	Depth of cut	Cutting Forces (N)			
			Fx	Fy	Fz	F
15	2	0.5	4.102	3.662	7.764	9.514
25			5.127	4.541	8.643	11.027
35			5.566	5.127	9.668	12.277
45			6.299	5.728	10.986	13.898

Table 34 Shows values of cutting forces at feed rat 2 (mm/rev) and depth 1 mm.

Cutting speed	Feed rate	Depth of cut	Cutting Forces (N)			
			Fx	Fy	Fz	F
15	2	1	7.471	6.738	11.012	14.915
25			9.211	8.203	13.184	18.054
35			10.547	9.643	14.795	20.569
45			11.865	10.400	15.820	22.343

Table 35 Shows values of cutting forces at feed rat 2 (mm/rev) and depth 1.5 mm.

Cutting speed	Feed rate	Depth of cut	Cutting Forces (N)			
			Fx	Fy	Fz	F
15	2	1.5	12.251	11.066	17.285	23.902
25			13.330	11.865	19.148	26.174
35			15.234	12.891	21.533	29.358
45			17.285	14.502	24.316	33.171

Table 36 Shows values of cutting forces at feed rat 2 (mm/rev) & speed 25 (m/min).

Depth of cut	Feed rate	Cutting speed	Cutting Forces (N)			
			Fx	Fy	Fz	F
0.5	2	25	5.127	4.541	8.643	10.027
1			9.211	8.203	13.184	18.054
1.5			13.330	11.865	19.148	26.174

Table 37 Shows values of cutting forces at feed rat 3 (mm/rev) and depth 0.5 mm.

Cutting speed	Feed rate	Depth of cut	Cutting Forces (N)			
			Fx	Fy	Fz	F
15	3	0.5	4.738	4.102	8.247	10.357
25			6.006	5.420	9.651	12.593
35			6.541	6.152	10.107	13.519
45			6.738	6.299	11.572	14.798

Table 38 Shows values of cutting forces at feed rat 3 (mm/rev) and depth 1 mm.

Cutting speed	Feed rate	Depth of cut	Cutting Forces (N)			
			Fx	Fy	Fz	F
15	3	1	8.302	7.178	13.916	17.722
25			9.521	8.542	15.247	19.901
35			11.220	10.107	16.406	22.297
45			12.598	11.719	18.508	25.270

Table 39 Shows values of cutting forces at feed rat 3 (mm/rev) and depth 1.5 mm.

Cutting speed	Feed rate	Depth of cut	Cutting Forces (N)			
			Fx	Fy	Fz	F
15	3	1.5	13.916	11.572	20.947	27.682
25			14.648	12.891	22.553	29.822
35			16.113	14.502	23.437	31.925
45			17.578	16.113	25.049	34.584

Table 40 Shows values of cutting forces at feed rat 3 (mm/rev) & speed 25 (m/min).

Depth of cut	Feed rate	Cutting speed	Cutting Forces (N)			
			Fx	Fy	Fz	F
0.5	3	25	6.006	5.420	9.651	12.593
1			9.521	8.542	15.247	19.901
1.5			14.648	12.891	22.553	29.822

Table 41 Shows values of cutting forces at depth 1 mm and speed 25 (m/min).

Feed rate	Depth of cut	Cutting speed	Cutting Forces (N)			
			Fx	Fy	Fz	F
1	1	25	8.203	7.471	10.986	15.614
2			9.211	8.203	13.184	18.054
3			9.521	8.542	15.247	19.901

Table 42 Shows values of cutting forces at feed rat 1 (mm/rev) and depth 0.5 mm.

Cutting speed	Feed rate	Depth of cut	Cutting Forces (N)			
			Fx	Fy	Fz	F
15	1	0.5	2.783	1.509	1.904	3.694
25			2.864	1.570	1.920	3.788
35			3.076	1.611	1.950	3.982
45			3.662	1.611	2.051	4.495

Table 43 Shows values of cutting forces at feed rat 1 (mm/rev) and depth 1 mm.

Cutting speed	Feed rate	Depth of cut	Cutting Forces (N)			
			Fx	Fy	Fz	F
15	1	1	3.796	2.373	2.783	5.271
25			3.955	2.516	2.912	5.518
35			4.102	2.666	3.076	5.778
45			4.395	2.758	3.223	6.108

Table 44 Shows values of cutting forces at feed rat 1 (mm/rev) and depth 1.5 mm.

Cutting speed	**Feed rate**	**Depth of cut**	**Cutting Forces (N)**			
			Fx	**Fy**	**Fz**	**F**
15	1	1.5	5.127	3.927	4.248	7.730
25			5.273	4.158	4.395	7.946
35			5.420	4.248	4.509	8.231
45			5.420	4.395	4.541	8.325

Table 45 Shows values of cutting forces at feed rat 1 (mm/rev) & speed 25 (m/min).

Depth of cut	**Feed rate**	**Cutting speed**	**Cutting Forces (N)**			
			Fx	**Fy**	**Fz**	**F**
0.5	1	25	2.864	1.570	1.920	3.788
1			3.955	2.516	2.912	5.518
1.5			5.273	4.158	4.395	7.946

Table 46 Shows values of cutting forces at feed rat 2 (mm/rev) and depth 0.5 mm.

Cutting speed	**Feed rate**	**Depth of cut**	**Cutting Forces (N)**			
			Fx	**Fy**	**Fz**	**F**
15	2	0.5	2.930	1.881	2.636	4.367
25			3.223	1.935	2.930	4.766
35			3.662	2.006	3.223	5.274
45			4.102	2.083	3.369	5.702

Table 47 Shows values of cutting forces at feed rat 2 (mm/rev) and depth 1 mm.

Cutting speed	Feed rate	Depth of cut	Cutting Forces (N)			
			Fx	Fy	Fz	F
15	2	1	4.233	2.402	3.369	5.919
25			4.466	2.759	3.662	6.400
35			4.541	3.116	4.102	6.867
45			4.834	3.358	4.248	7.258

Table 48 Shows values of cutting forces at feed rat 2 (mm/rev) and depth 1.5 mm.

Cutting speed	Feed rate	Depth of cut	Cutting Forces (N)			
			Fx	Fy	Fz	F
15	2	1.5	5.493	4.834	5.127	8.934
25			5.566	4.980	5.273	9.142
35			5.950	5.127	5.566	9.626
45			6.930	5.273	5.574	9.985

Table 49 Shows values of cutting forces at feed rat 2 (mm/rev) & speed 25 (m/min).

Depth of cut	Feed rate	Cutting speed	Cutting Forces (N)			
			Fx	Fy	Fz	F
0.5	2	25	3.223	1.935	2.930	4.766
1			4.466	2.759	3.662	6.400
1.5			5.566	4.980	5.273	9.142

Table 50 Shows values of cutting forces at feed rat 3 (mm/rev) and depth 0.5 mm.

Cutting speed	Feed rate	Depth of cut	Cutting Forces (N)			
			Fx	Fy	Fz	F
15	3	0.5	3.076	1.904	2.783	4.564
25			3.516	2.197	3.149	5.206
35			3.809	2.344	3.369	5.599
45			4.395	2.637	3.516	6.215

Table 51 Shows values of cutting forces at feed rat 3 (mm/rev) and depth 1 mm.

Cutting speed	Feed rate	Depth of cut	Cutting Forces (N)			
			Fx	Fy	Fz	F
15	3	1	4.466	3.516	3.658	6.759
25			4.687	3.662	4.272	7.323
35			4.913	3.809	4.395	7.613
45			5.126	4.102	4.511	7.965

Table 52 Shows values of cutting forces at feed rat 3 (mm/rev) and depth 1.5 mm.

Cutting speed	Feed rate	Depth of cut	Cutting Forces (N)			
			Fx	Fy	Fz	F
15	3	1.5	5.713	4.980	5.566	9.403
25			6.125	5.273	5.791	9.942
35			6.445	5.566	6.299	10.592
45			7.178	5.713	6.445	11.211

Table 53 Shows values of cutting forces at feed rat 3 (mm/rev) & speed 25 (m/min).

Depth of cut	**Feed rate**	**Cutting speed**	**Cutting Forces (N)**			
			Fx	**Fy**	**Fz**	**F**
0.5	3	25	3.516	2.197	3.149	5.206
1			4.687	3.662	4.272	7.323
1.5			6.125	5.273	5.791	9.942

Table 54 Shows values of cutting forces at depth 1 mm and speed 25 (m/min).

Feed rate	**Depth of cut**	**Cutting speed**	**Cutting Forces (N)**			
			Fx	**Fy**	**Fz**	**F**
1	1	25	3.955	2.516	2.912	5.518
2			4.466	2.759	3.662	6.400
3			4.687	3.662	4.272	7.323

APPENDIX. B: FORMULAE FOR ANALYSIS OF VARIANCE

Table 1. Formulae for analysis of variance

Source	Sum of squares (SS)	Degrees of freedom (DF)
Zero-order term	$\left(\sum_{i=1}^{N} yi\right)^2 \Big/ N$	1
First-order terms	$\sum_{i=1}^{k} bi(iy)$	k
Lack of fit	By subtraction	$n_c - k$
Pure error	$\sum_{i=1}^{no} (y_{ni} - y_0)^2$	$n_0 - 1$
Total	$\sum_{i=1}^{N} y_i^2$	N

The detailed formulae for the analysis of variance used in this investigation are shown in Table 1. Where n_0 is the number of central points, n_c the number of corner points, N the total number of experimental points, k the dimension of the design, y_{ni} the logarithm of observed responses at the central point with mean $\bar{y}_0$ and (iy) the sums of cross-products of columns in the X matrix with the column y of observation.

APPENDIX. C: PUBLICATIONS

1. Mohamed A.Dabnun, and M.A.El-Baradie, "Machinability assessment of machinable Glass-ceramic", Proceeding of MDP-8, Cairo University Conference on Mechanical Design and Production Cairo, Egypt, January 4-6, 2004.
2. Mohamed A. Dabnun, M.S.J. Hashmi, and M.A. El-Baradie, "Machinability Study of Macor Ceramic" submitted to Journal of material Processing technology. 2004.
3. Mohamed A. Dabnun, M.A. El-Baradie and M.S.J. Hashmi, "Machinability of Glass ceramic", Materials Processing Research centre. "Poster", 2004.